12-2021

Investigating Depth Estimation to Archaeological Magnetic Source Bodies

Jeremy G. Menzer
University of Arkansas, Fayetteville

Investigating Depth Estimation to Archaeological Magnetic Source Bodies

A dissertation submitted in partial fulfillment
of the requirements for the degree of
Doctor of Philosophy in Environmental Dynamics

by

Jeremy G. Menzer
Edinboro University of Pennsylvania
Bachelor of Science in Geology, 2012
East Tennessee State University
Master of Science in Geosciences, 2015

December 2021
University of Arkansas

This dissertation is approved for recommendation to the Graduate Council.

_____
Kenneth L. Kvamme, Ph.D.
Dissertation Director

_____
Christopher L. Liner, Ph.D.
Committee Member

_____
Benjamin R. Vining Ph.D.
Committee Member

Abstract

Magnetometry is the most widely applied archaeo-geophysical technique. Current practice standards employ the technique to map only in a two-dimensional plan view fashion, but in deep geologic studies depth estimators are routinely applied to magnetic datasets. These estimators provide three-dimensional information to magnetic source-bodies. There are many different depth estimators employed in geologic study that all require various degrees of processing complexity. This study investigates two mathematically simple techniques, half-width rules and multi-height methods. Half-width rules are likely the oldest depth estimators within the field while multi-height techniques are but a minor footnote in the literature. The applicability of these methods is first examined through computer modeling. This process involves creating simple geometric source-bodies and modeling the resultant theoretical magnetic maps. The depth estimation techniques are then evaluated in this model environment. Next, the proposed depth estimators are tested at a modern constructed test site in Illinois and three real-world archaeology sites throughout Arkansas and Tennessee. Multiple archaeological feature types are surveyed with a focus on point-source like bodies (e.g. hearths and small pits). The estimator's accuracy is evaluated with proxy depth to source information via down-hole magnetic susceptibility logs collected at each magnetic feature. This allows a direct comparison without the need for costly excavations. Through half-width and multi-height techniques, this study aims to move archaeo-geophysical applications of magnetometry from simple plan view based survey towards true three-dimensional mapping.

Acknowledgments

There are surely many individuals to thank for the success and completion of this project. In that respect there are likely too many to name, so if you are left out of this list—I apologize. I would like to first thank my committee members: Drs. Kenneth Kvamme, Christopher Liner, and Benjamin Vining. Ken many thanks go to you for all your assistance over the years, the wealth of knowledge you have passed along to me, your library and most importantly sticking with me while moving into retirement. Thank you. Many thanks to my committee for all the mentor-ship and classes over the years. This dissertation would not have been possible without a grant from the National Council for Preservation Technology and Training, a subdivision of the National Park Service. Also, many thanks to Gorden Konieczek and the entire SENSYS team for providing much needed equipment. In that regard, I must also give thanks the Center for Advanced Spatial Technologies for providing additional survey equipment. Thanks to Jami Lockhart, Tim Mulvihill, Carol Swboni, and the Arkansas Archeology Survey and National Forest Service for all things at the Woolsey Site. Additional thanks to Carey Baxter, Michael Hargrave, and the Construction Engineering Research Laboratory for providing the records and access to CATS. Many thanks to Dr. Eileen Ernenwein for setting up access to Runion and your guidance throughout the years. I would like to thank the other gracious landowners, the Brannon and Runion families, for allowing access and continued archaeological work on their land. Additionally, thanks to Pickett State Park, Tennessee for providing housing while working at Pile Mound. I would like to thank Jo Ann Kvamme for all of her help throughout the years. Thanks to Carl Williford for help in the field and all the discussions over the years. Also thanks to Dr. Dylan aka “Stumbles” Young, for his continued double checking of my poor math skills. Finally, I want to thank my family for all their support over the years to finish this.

Table of Contents

List of Tables

List of Figures

Chapter 1: Introduction to Project, General Archaeo-magnetics, Research Questions, Field Study Sites, Instrumentation and Equipment

Introduction

Magnetometry is the most widely used geophysical technique in archaeology because of its ability to successfully map subsurface archaeological features in most environmental settings. This has led to it being termed "nature's gift to archaeology" (Kvamme 2006). In modern archaeo-geophysical practice, depth information is not commonly attained, yielding only two-dimensional (2D) plan maps without a vertical dimension. Accurate depth estimates to magnetic targets can be obtained in geophysics using down-hole methods, but this information is only obtainable at the site of a single core-hole, something not easily done over large regions. In wide-area surveys, accurate depth information is currently obtainable only through ground-penetrating radar (GPR) surveys, while less accuracy is achievable through electrical resistivity and electromagnetic induction (EMI) methods. GPR tends to be a slower method of survey using pedestrian methods, it is not as commonly used, and cannot easily cover areas as large as magnetometry. Yet, deep-earth geologic applications of magnetometry commonly derive depth information. This project aims to move magnetometry surveys in archaeology beyond a simple 2D prospection method by permitting three-dimensional (3D) estimates to subsurface targets, and by allowing hypotheses about site content to be tested while decreasing excavation and survey costs. This is accomplished through use of several theoretical approaches pertaining to the behavior of magnetism, a series of computer modeling simulations, and real-world testing at a controlled site and three archaeological sites.

There are many acronyms used throughout this document. In order to minimize confusion a list of acronyms and their respective meanings is provided in appendix A.

This chapter provides a brief introduction to archaeo-magnetic research and surveys. It overviews the basics of the technique, and how it is employed globally and specifically within the United States. It also discusses the specific research questions of this project relating to two types of depth estimation, half-width (HW) rules and multi-height surveys (Weymouth 1976; Witten 2006). Background information about the four field study sites is also presented. They include the Controlled Archaeological Test Site (CATS; Isaacson et al. 1999) and three real-world archaeological sites: Woolsey (3FR46), Pile Mound (40FN180), and Runion (40WG20), the first located in Arkansas and the remainder in Tennessee (Menzer 2015; Mulvihill et al. 2019; Shreve et al. 2020). This project employs multiple types of magnetometers, each measuring different aspects of the Earth's magnetic field. A brief background on magnetometers in general and specifics about each instrument is provided. This is followed by a description of all other technical equipment employed in the project including a down-hole magnetic susceptibility (MS) meter, a Global Navigation Satellite System (GNSS), and a push-style soil-probe.

Chapter 2 explains the theoretical background behind the advanced processing and specific depth estimation techniques examined in this project. Many of these specialized magnetic topics are outside the usual archaeo-geophysical community's purview. They include such topics as "Reduction to the Pole" (RTP) processing and an in-depth review of the nature of what is known as the "Structural Index" (SI) and how it relates to depth estimation techniques (Reid et al. 2014; Tabbagh et al. 1997). This is followed by the theoretical background for the two depth estimation techniques employed in this project, HW rules and multi-height surveys.

Chapter 3 provides a brief theoretical explanation of the modeling environment used to simulate the effects of magnetic source bodies (e.g. archaeological features) in the near-surface. A variety of source body models are developed to represent real-world archaeological features. Magnetic models are then derived from these source bodies which HW and multi-height depth

estimation techniques are then tested on in a noiseless environment. The results of these tests are then examined and details are discussed regarding the accuracy and effectiveness of the depth estimation techniques.

Chapter 4 presents the field methods employed by the project. It begins with standard field practices pertaining to survey design and the use of each instrument. This involves setting up or using existing grid systems at the sites and placing grid blocks over the features of interest. Surveys are then conducted using either guide tapes marked in meters or through GNSS. The use of magnetic base stations is also discussed as they are not commonly employed in archaeo-magnetic surveys. An account of the procedure for doing multi-height surveys over the same piece of ground is provided, because this technique is not part of standard field practice and has not been widely employed (however, seeWeymouth 1976, 2000). Procedures for down-hole MS surveys are described, a necessary tool in this project to validate depth estimates. Finally, the data processing scheme and algorithms are discussed.

Chapter 5 presents the magnetic maps from each field location with the down-hole magnetic susceptibility (DHMS) core locations. Magnetic data and core location quality is evaluated and any errors or noise is discussed. The magnetic susceptibility logs are presented and their overall quality and trends are discussed. Finally, the intricacies of individual magnetic anomalies, and MS logs are discussed in correspondence with depth estimates. Depth estimation error is graphically shown for each feature of interest. These data are then aggregated and summarized focusing on overall depth estimation accuracy.

Chapter 6 provides a brief review of the document up to that point and then begins discussion of the errors and areas that can be improved upon in this study. The modeling and field results are discussed separately and methods of potential improvement to the depth

estimation techniques are suggested. The general results of the depth estimation techniques are discussed as a whole and future areas of improvement to this study are addressed.

Chapter 7 provides concluding remarks on the project. It summarizes the project as a whole and how this may be employed in the archaeological community.

Archaeo-magnetics

Magnetic investigations have been used in mineral and ore exploration since the seventeenth century in Scandinavia (Aspinall et al. 2008). Developments in the early twentieth century have led to an explosion of their use in both geology and archaeology. In the latter, the first features to be surveyed with a magnetometer were kilns in England (Aitken 1958). Since then, magnetometry has become the most commonly used geophysical method in archaeological prospection (Gaffney 2008).

Two primary magnetic methods are employed, passive magnetometry and active electromagnetic induction (EMI). Magnetometers measure a combination of permanent and induced magnetism, while EMI devices measure local induced magnetism. The most prevalent permanent magnet is the Earth's geomagnetic field, which is created by the convection and rotation of its liquid outer core (Reynolds 2011). Stated simply, the liquid core acts like a bar magnet with a North and South pole, a dipole, and lines of magnetic flux connecting the two poles. These lines of magnetic flux represent the strength and direction of the magnetic field (Aspinall et al. 2008). A magnetic field's strength increases the closer it gets to a magnetic pole (Witten 2006). The strength of the Earth's field also changes temporally, due to the Earth's daily rotation and solar winds caused by the Sun (Aspinall et al. 2008; Witten 2006). These variations can be exacerbated by solar storms that can cause rapid changes, within minutes, to the ambient magnetic field (Kvamme 2006).

Without the Earth's constant magnetic field, few materials would possess their own permanent magnetic field—otherwise known as a remanent field (Kvamme 2006). The most common type of remanent magnetism in archaeological contexts is thermoremanence, which is created through heating of a material. Any heating increases the strength of magnetism; however, it is most effective when materials are heated past the Curie point, approximately 600 degrees Celsius (Tite 1972). Reaching the Curie point breaks the bonds controlling the alignment of magnetic material. Upon cooling, all of the magnetic material will re-align to the present magnetic field, commonly the Earth's (Aspinall et al. 2008). This is often observed in igneous rocks, smelted iron rich metals, and fired clay. Other types of remanence exist, but they occur less commonly and usually do not produce a large magnetic effect.

Induced magnetism occurs when an active magnetic field induces magnetically susceptible material. This causes such materials to become magnetized and produce their own secondary magnetic field, which can then be measured. Common active magnetic fields include the Earth's geomagnetic field, which is omnipresent, and local electromagnetically induced fields created by EMI instruments. EMI instruments are able to make a direct measurement of magnetic susceptibility by exploiting the ratio between the level of magnetization in a material and the strength of the magnetizing field produced by the machine (Aspinall et al. 2008; Dalan 2006). The measure of a material's ability to become magnetized is directly related to the minerals present in a material (Dalan 2006; Kvamme 2006).This is a dimensionless unit commonly measured in parts per thousand (ppt).

MS increases in soil or other materials occur in a variety of ways. Topsoil is magnetically enhanced through natural or anthropogenically caused fires, certain forms of bacteria, and sediment accumulation. Fires lead to the magnetic enhancement of soil through the "Le Borgne effect," where hematite converts to magnetite and then maghemite (Aspinall et al. 2008; Le

Borgne 1955, 1960). Various forms of bacteria move magnetic particles upwards and concentrate them. They especially thrive in waste piles such as pits and middens. Additionally, fine-grained magnetite and maghemite tend to migrate upwards and accumulate in top soil (Dalan 2006; Evans and Heller 2003). Therefore, the addition or removal of topsoil is commonly detected with magnetic instruments. The inclusion of fired ceramics, brick, and ferrous metals further enhances the magnetism of archaeological soil (Aspinall et al. 2008; Weston 2002).

When performing geophysical surveys, certain areas or points of interest are commonly designated as "anomalies". In a geophysical context, an anomaly is a measurement that is greatly different, contrasting with the natural background soil matrix. They can occur as individual point-sources or as broad areas. Magnetic anomalies can be assigned to two main categories, dipolar or monopolar. Dipolar anomalies exhibit both positive and negative magnetism within the survey. Common anomalies that exhibit dipoles arise from materials associated with remanent magnetism (e.g. metal, igneous rock, fired clay, kilns) or areas of paired soil accumulation and removal (e.g. ditch and embankments). Monopoles, theoretically cannot exist, but in practice they occur as local sources of either positive or negative magnetism within the survey. For monopoles, the theoretical opposite pole is located some large distance away and therefore is not measurable in the survey area. Common monopolar anomalies typically represent areas exposed to fire (e.g. hearths, burnt structures) and areas of soil accumulation or removal (e.g. pits, ditches, embankments). Areas of increased magnetism (in contrast to the background matrix) are referred to as positive anomalies while areas of decreased magnetism are termed negative anomalies. Robust positive anomalies can be created where soil removal is paired with in-filling, such as a pit filled with magnetically enhanced refuse. Additionally, overall magnetic enrichment, beyond that of typical topsoil, occurs as a result of human occupations. This is due to the general inclusion of waste materials and moving or mounding of soil. For these reasons,

magnetic techniques work well for discovering evidence left by past peoples in their traces of occupation and modifications of the local environment.

The workhorse of current archaeo-geophysics world-wide is the Bartington Grad 601-dual fluxgate magnetometer. This dual gradiometer system is carried by the user and data are aligned to real-world locations by aligning measurements with survey guide lines. Increasingly, surveys with cart systems (unmotorized and motorized) are being employed that drastically increase survey speed and even data density. These systems are more limited by ground conditions and costs than carried systems. They are most commonly employed in European nations. Surveys with either of these systems almost exclusively produce a 2D plan view map of the data. This allows for precise Cartesian coordinates of potential anomalies, but lacks any depth information of the sources. However, magnetometry does have the capability to yield depth information, a third dimension, which would allow the data to be visualized in 2.5 or 3D. This topic will be addressed more thoroughly throughout this dissertation.

Research Questions

This project aims to answer a series of research questions pertaining to depth estimation using magnetic data.

1. How well do half-width rules work in a modeling environment? The usefulness of half-width (HW) rules in archaeo-geophysics is investigated using a variety of magnetic data models. HW rules are the most basic form of depth-estimation in magnetometry, but are rarely used in archaeological contexts. When they are employed in archaeology, only a single aspect of the rule, “full-width half-maximum”, is utilized. However, this rule is only theoretically applicable to a specific data context, whereas the entire suite of HW rules could potentially be suitable for a broader range of archaeological data. Some prior work has been done in this area, but with little success (Weymouth 2000; Witten 2006).

Additionally, the various HW rules estimate depth to different locations within a source body (top, center, bottom) depending on the source body's type and the rule applied. This project tests the applicability of HW rules in a modeling environment and aims to better delineate the locations within source bodies at which depth is being estimated.

2. Can half-width rules provide adequate depth-estimations to actual archaeological features? The success of HW rules in a theoretical modeling environment may not translate to real-world application of the techniques owing to soil variations and changes as well as general environmental "noise." For this reason, data were collected at multiple field sites in different environments to assess the accuracy of the HW rules at real archaeological sites. This allows the practical accuracy of the techniques to be determined.
3. Do multi-height techniques work in a modeling environment? Multi-height techniques are a brief footnote in the archaeo-geophysical community and therefore have not been properly investigated (Weymouth 1976). A modeling environment is used to determine the applicability, if any, that multi-height techniques have on determining depth to magnetic source bodies. By using a modeling environment the technique can be tested on a variety of source body types, as it is currently unclear how accurately this method will estimate depth to various types of sources.
4. Can multi-height techniques provide adequate depth-estimations to actual archaeological features? Multi-height techniques have not been tested on real-world archaeological sites and therefore their applicability is unknown. This study assesses the suitability and accuracy of multi-height techniques in archaeological applications.
5. Do the half-width and multi-height techniques provide a consistent minimum or maximum estimate to points of interest? Ideally, both techniques will provide accurate

depth-estimations to archaeological targets. However, if they do not they may provide consistent over- or underestimates to source bodies. If this occurs the consistent information may be "corrected" through modeling to guide excavations or to answer anthropological questions.

Study Sites

This project tests the proposed methods at four field sites, a constructed site for testing geophysical instruments and survey methods and three archaeological sites (Figure 1.1). These sites were chosen based on multiple criteria. The Controlled Archaeological Test Site (CATS), located in Champaign, Illinois, was selected because this facility offers multiple archaeological feature types commonly encountered in North American Archaeology. They have been accurately mapped for comparison against geophysical survey results. CATS is located relatively close to the author's university in northwest Arkansas (Isaacson et al. 1999). One other such test site is easily accessible in the United States, the Hazardous Materials Management and Emergency Response Training Facility (HAMMER) near Richland, Washington (Conyers 2013). However, this location would have required much more travel and funds to investigate.

Three prehistoric Native American sites, Woolsey (3FR46), Pile Mound (40FN180), and Runion (40WG20), were investigated to test magnetic depth estimation in real-world applications (Menzer 2015; Mulvihill et al. 2019; Shreve et al. 2020). These sites were chosen based on four main criteria: 1) magnetometry data had been previously collected at these sites revealing excellent magnetic anomalies that likely point to archaeological features, 2) the sites had been subject to excavations, providing information about soils and confirming that archaeological features were present, 3) the sites contained a variety of archaeological feature types—structures, pits, hearths, etc.—permitting assessments of the methods developed against a

broader archaeological background, and 4) the sites were located within a reasonable distance from northwest Arkansas.

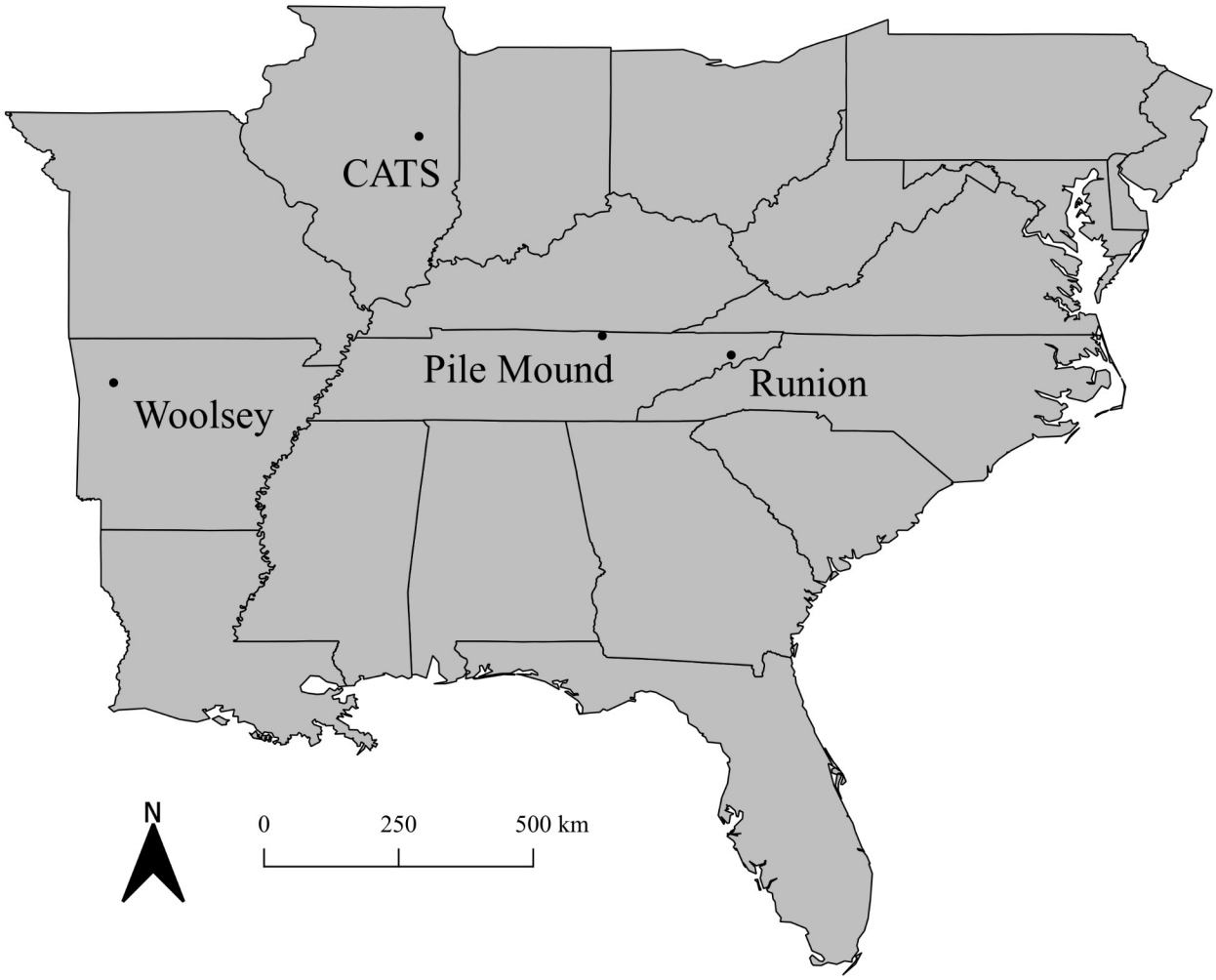

Figure 1.1. Study Sites.

Constructed Test Site: CATS

CATS was built in the summer of 1997 at the U.S. Army Construction Engineering Research Laboratory (CERL) in Champaign, Illinois. It encompasses a well-groomed 2500 sq m area that is almost perfectly level with the exception of constructed mounds and a ditch and embankment structure. The site is demarcated by a small buffer area surrounded by four by four inch posts (Figure 1.2). The background soil matrix is Drummer silty clay loam and Catlin silt loam with a general profile of a 36 cm thick A horizon and an 84 cm thick B horizon (Isaacson et

al. 1999). The site was surveyed prior to feature construction and was deemed void of disturbance other than previous farming and is located away from general traffic and utility lines. The site (Figure 1.3) contains multiple feature types including a ditch and embankment complex, palisade, roasting pit, mound, isolated burial, house complex, midden, historical cellar, limestone piers and brick sidewalk, brick matrix, and a matrix of wood and metal objects (Isaacson et al. 1999).

Since its construction the site has gone through minor damage and change (Personal communication, CERL staff). Accidental damage occurred to the southeastern portion of the ditch and embankment complex and two more mounds were constructed. The damage was somewhat mitigated and notes along with communication with staff provide an estimated area of effect. Details regarding the construction of the additional mounds are lacking. It was hoped that the area would be completely devoid of intrusive metal scatter from recent activity, but my surveys show at least some more recent undocumented disturbance to the site and deviations from the published plan map, (see Chapter 5).

Figure 1.2. Aerial view of CATS. Boundary posts demarcate the test site area. Labeled areas correspond to the layout in Figure 1.3. A) Ditch and embankment; D) mound with burial; F) house complex; K) wood and metal objects. Additionally, two undocumented mounds were added after initial construction. Image, Google Earth.

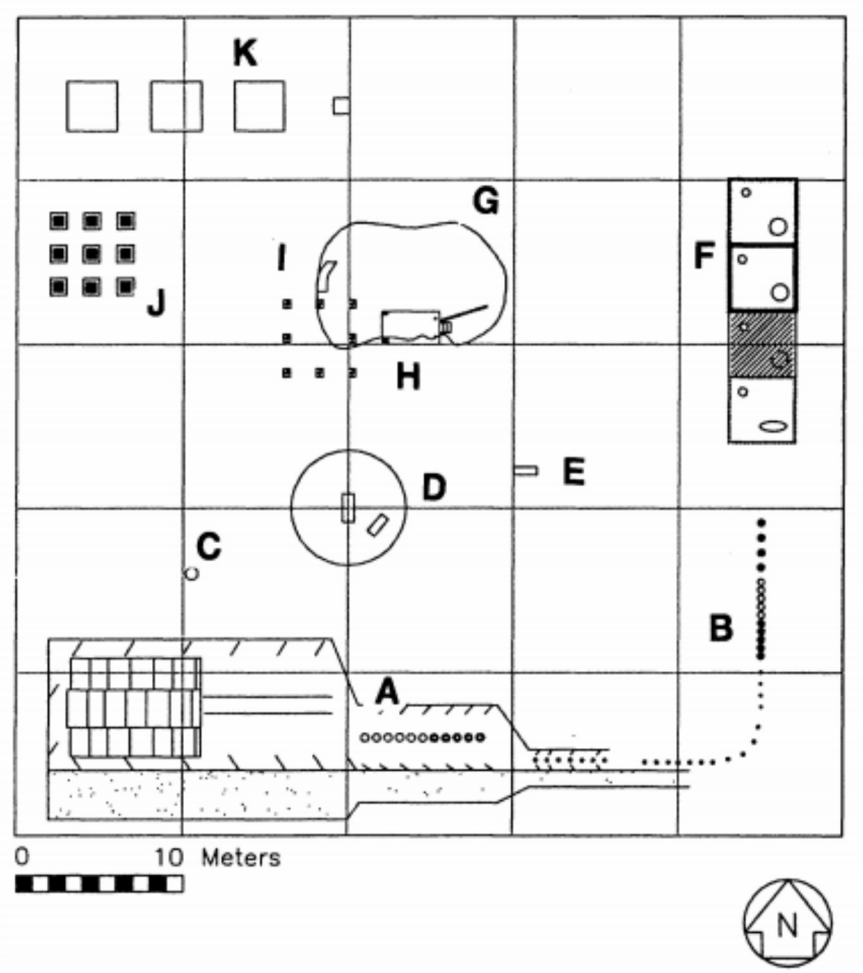

Figure 1.3. CATS Map. Original building plan for CATS site. This area sits within the boundary posts marked in figure 1.2. A) ditch and embankment; B) a palisade; C) roasting pit; D) mound with burial; E) individual burial; F) houses with pits and hearths, shaded house was burnt; G) a broad midden; H) historical cellar; I) limestone pillars and a brick sidewalk; J) a matrix of brick; K) wood and metal objects (CERL, USA 2018).

Archaeological Site: Woolsey

The Woolsey site (3FR46) is located in northwest Arkansas, near the town of Cass along the Mulberry river. The area exists in a flat lying flood plain planted with a rotating crop selection (Figure 1.4). The site is located on National Forest Service land and was originally recorded in 1972 (House 1972). In 2017 the Arkansas Archeological Survey (ARAS) and Arkansas Archeological Society planned their yearly training program at the site. Prior to the program, a magnetic gradiometry survey was conducted by ARAS covering roughly 2.25 ha of

the site to identify potential features of interest. Two exploratory backhoe trenches and test units were excavated to confirm potential features. During the training program, 18 two by two m units were excavated to determine the sources of several magnetic anomalies. Of those potential magnetic anomalies, at least two were found to be well preserved storage pits. They allowed correlation of magnetic anomaly types with potential archaeological feature types, which informed my subsequent field testing in this project. The site contains Late Archaic through Mississippian period artifacts. Materials recovered from the two well-defined pits date to the Mississippian period, ranging from approximately 1160-1282 C.E. A subset of the gradiometer survey (Figure 1.5) was used to plan this project. From these data two small areas were selected that contain plausible pit-like anomalies, an archaeological target of interest.

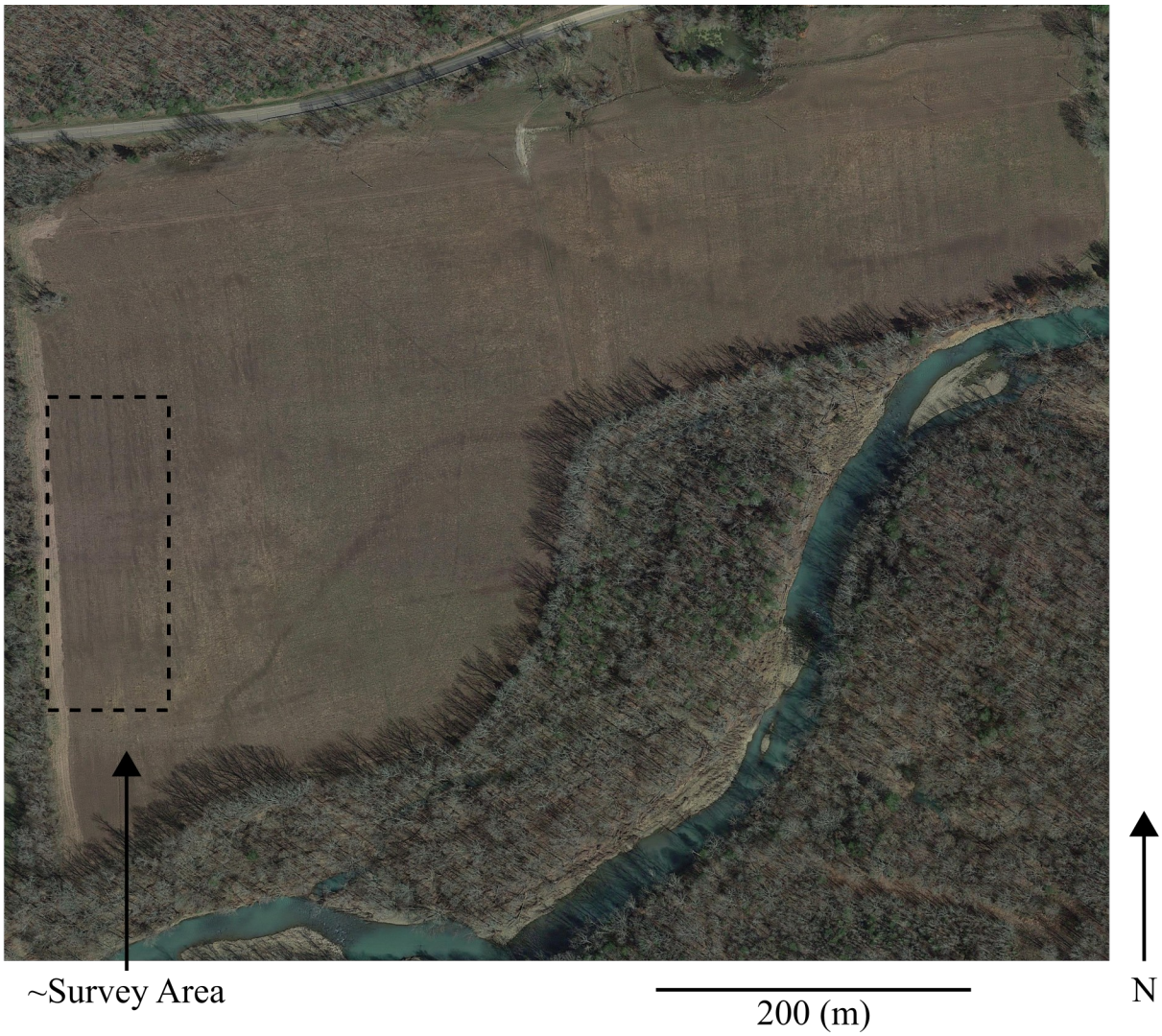

Figure 1.4. Aerial view of Woolsey. Survey area located in southwest of field. Mulberry river located to the south of the field. Image source, Google.

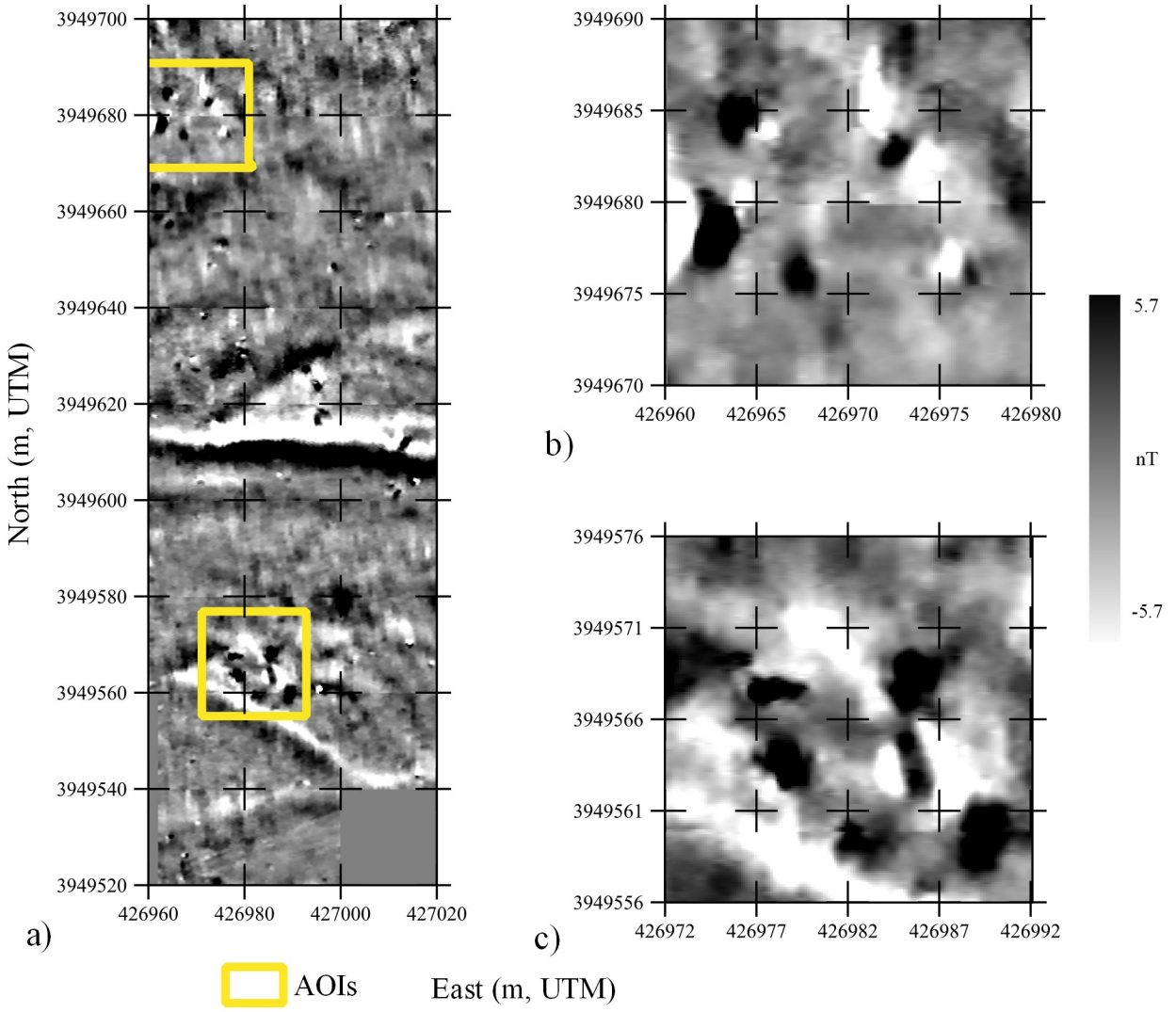

Figure 1.5. Woolsey Magnetic Gradiometry. a) A subset of the gradiometry data, showing two areas of interest (AOIs) with potential pit like features. b) Northern AOI (G2) containing principal magnetic anomalies of interest. c) Southern AOI (G1) containing principal magnetic anomalies of interest. Data courtesy Dr. Jami Lockhart, ARAS.

Archaeological Site: Pile Mound

Pile Mound (40FN180) is a Mississippian mound site located just off the western edge of the Upper Cumberland Plateau (UCP) in north-central Tennessee. The site is relatively flat with small undulations throughout the area. It sits within the Wolf River flood plain and is currently used for pasture or hay (Figure 1.6). Current dates place the site between roughly 1050 and 1300 C.E. The site was originally recorded by Myer (1924) as a mound 30.5 m in diameter and 1.5 m

high. The mound sat untested by excavation, until a small pit was dug in 1996 by Alexander Archaeological Consultants. Since 2014 the site has been subjected to extensive archaeo-geophysical survey and excavations by the author and colleagues (Menzer 2015). It is culturally important due to the general lack of knowledge about Mississippian mounds in the surrounding 75 km region. To date, over eight hectares of magnetometry (Figure 1.7), GPR, EMI, and electrical resistivity data have been collected along with information gained from numerous test excavations. The site contains at least four structures and multiple stone features, pits, hearths, and unidentified features. The five areas of interest for this study center over likely pit and hearth features and two large features of unknown origin. Of all the sites surveyed, the quality of magnetic survey results was the lowest at this site. It was therefore used as a test case in a difficult magnetic environment.

Figure 1.6. Aerial view of the Pile Mound site. Photograph, Jeremy Menzer

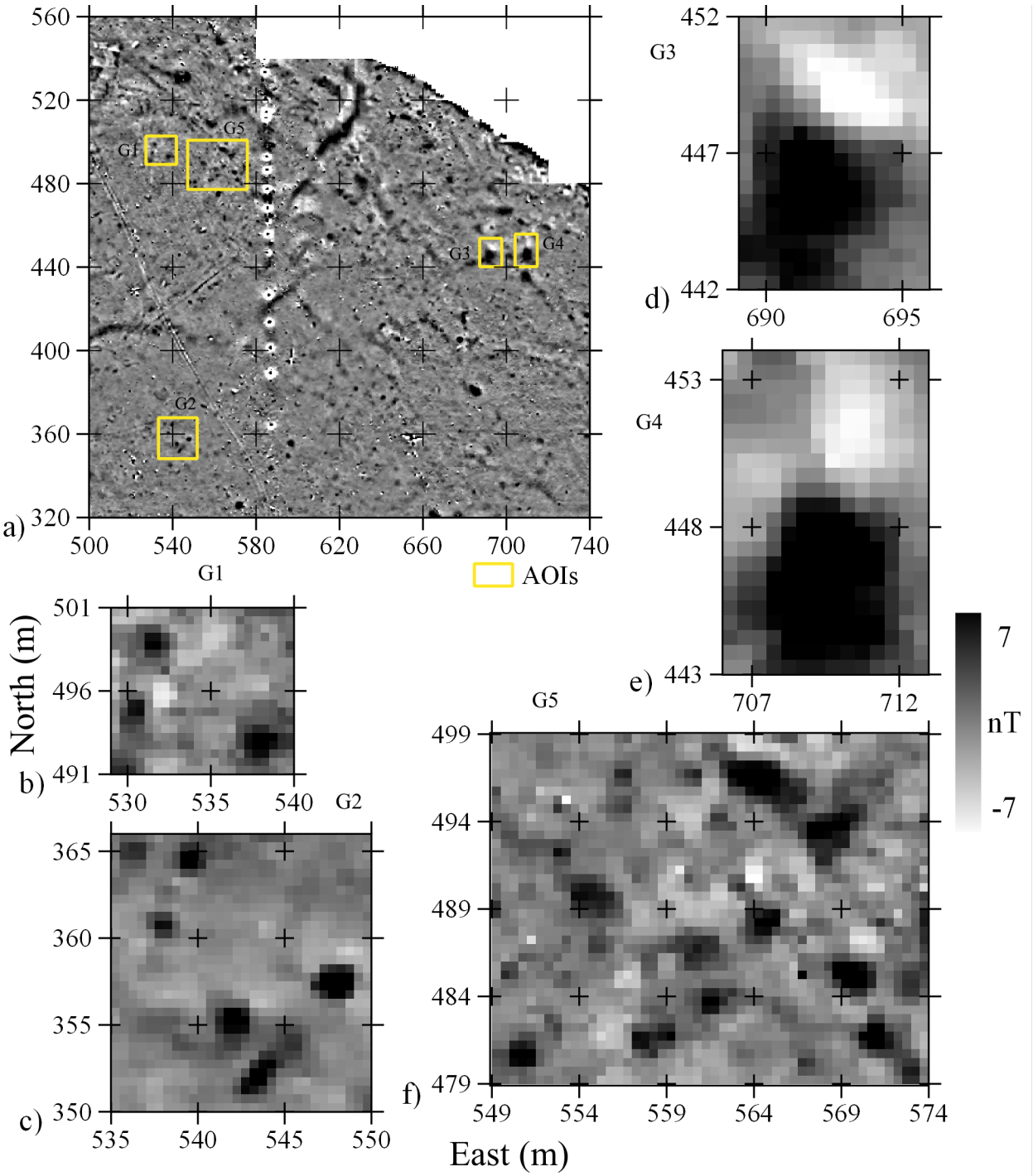

Figure 1.7. Pile Mound Magnetic Gradiometry. a) subset of the gradiometry data extent showing multiple potential archaeological features and five AOIs for this study, b) subset of data for AOI G1, b) subset of data for AOI G2, d) subset of data for AOI G3, e) subset of data for AOI G4, f) subset of data for AOI G5.

Archaeological Site: Runion

The Runion site (40WG20) is located in Upper East Tennessee, on the flood plain of the Nolichucky river. The site is nearly flat and is currently used as pasture (Figure 1.8). It was first investigated with archaeo-geophysics in 2017 by Dr. Eileen G. Ernenwein of East Tennessee State University. Her team surveyed 6 ha with magnetic gradiometry (Figure 1.9) which identified 21 possible structures and various other features of interest (Ernenwein and Franklin 2017). Further geophysical investigations and other techniques complement and expand this data set. Excavations followed in 2018 to test potential features of interest confirming two structures at the site. Materials recovered provide potential dates for the site which place it roughly between 1570 and 1650 C.E. (Franklin 2018). The previous gradiometry data were used to place three areas of interest for the current study. Two are located over potential structures and one is a larger area encompassing many possible pit or hearth-like features.

Figure 1.8. Aerial view of Runion. Nolichucky River to the East. Image source, Google.

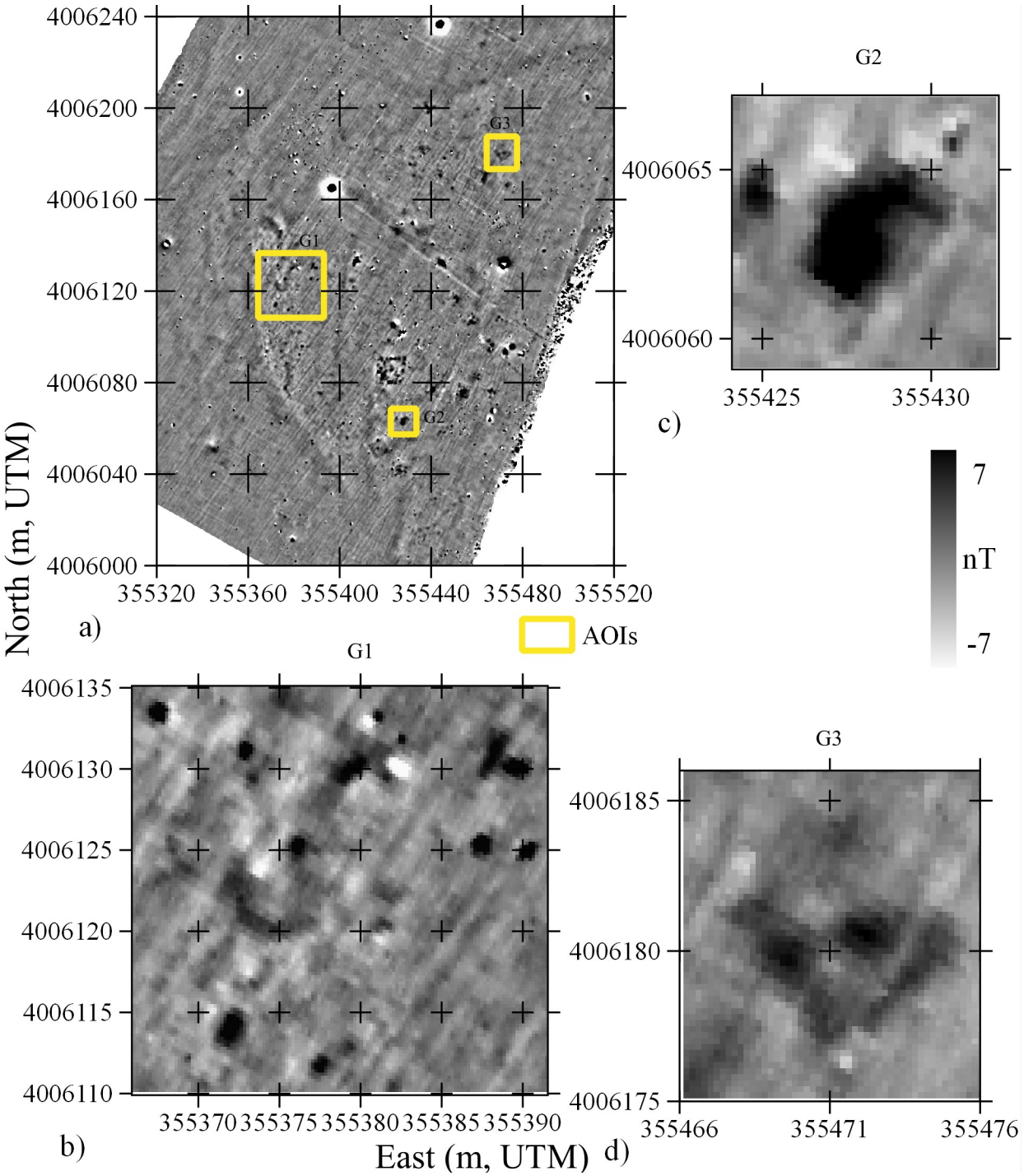

Figure 1.9. Runion Magnetic Gradiometry. a) Data showing numerous archaeological and geological anomalies and AOIs, b) data subset of AOI G1, b) data subset of AOI G2, c) subset of AOI G3.Data courtesy of Dr. Eileen Ernenwein.

Instrumentation Background Review

Various equipment was employed in this study, including multiple magnetometers of different types, a down-hole magnetic susceptibility meter, a push-style soil probe, and a real-time kinematic GNSS. The general background on these instrument types and the specific details of each instrument are discussed in more detail below.

Magnetometers

There are multiple types of magnetometers in use in archaeology, geology, and other related fields. The most commonly used in archaeology are proton precession, fluxgate, Overhauser, optically-pumped alkali-vapor, and cryogenic superconducting quantum interference devices (Aspinall et al. 2008). These devices can vary in what they measure, either the ambient total field (a scalar) or a component of the total field in a particular direction (a vector). Component measurements are most common in the vertical direction, but can be in any direction.

Additionally, these instruments can be used in varying manners, either to measure the changing magnetic field over an area, an areal survey, or to measure diurnal variations and the constant background field as a base station. They can also be configured to give the output of individual sensors or the gradient output, which is the difference between two sensors over some distance. Although all the instruments measure the total field or some part of it, how they record the data can have profound effects on what can be done with the recorded information, particularly in the multi-height depth estimation technique. Only those used in this study will be describe in greater detail below.

Proton precession magnetometers are the oldest instrument type used in archaeology (Aspinall et al. 2008). These instruments have the lowest cost and the slowest speed. They are composed of an encased hydrogen rich fluid surrounded by a wire coil. A large magnetic field, on the order of mega-Teslas, is induced via the coil, causing the hydrogen atoms to align in the

direction of the induced field—this process takes a few seconds. Once the induced field is removed, the hydrogen atoms spin (precess) back to alignment with the ambient field. At this moment, they produce a current in the coil proportional to the ambient field (Witten 2006). Given more time the atoms randomize due to thermal effects and no longer are collectively oriented with the ambient field, therefore no longer providing an accurate measurement of the ambient field (Aspinall et al. 2008). Due to this process, measurements take three or more seconds which makes this technique extremely slow compared to others.

Optically-pumped alkali-vapor instruments are much more complex and expensive. These instruments employ an alkali-metal (sodium, potassium, rubidium, or cesium) in vapor form (Aspinall et al. 2008). In this state the optical transparency of the vapor changes relative to the exposed magnetic field. Polarized light is passed through the vapor and the measured intensity of this light can be used to determine the magnitude of the ambient magnetic field (Witten 2006). With this increased complexity comes a few benefits. The instruments are much more sensitive than proton instruments and can measure almost immediately, with common instruments measuring at least 10 readings per second. However, they require large batteries and are prone to dead zones, where sensor orientation can cause no effects from the ambient magnetic field to be measured (Aspinall et al. 2008). This can be accounted for with proper survey design.

Fluxgate magnetometers are the most commonly employed instrument type in archaeo-geophysics. This is due to their relative low-cost and high collection speed. This instrument works by wrapping a coil of wire around a ferromagnetic metal, specifically an alloy called mu metal. When this rod is exposed to an external magnetic field, a dipole moment is created in the rod. This new field created in the rod then produces an electrical current in the coil wrapped around the rod which is proportional to the external magnetic field (Witten 2006). Due to the

induction occurring in the direction of the rod, the instrument only measures the component of the total field in that direction, therefore making the measurement yield a vector measurement. Three fluxgates can be oriented in the three principle directions and upon combining their respective measurements the total field can be estimated. These measurements are sensitive to any angle changes or tilt in the rod—requiring the instrument to be kept at a constant facing. These instruments are generally placed in a vertical gradient configuration (Aspinall et al. 2008).

Terms

Several definitions are needed to differentiate between a total field measurement, a fixed differential measurement, a gradient, and a component measurement.

- A *total field measurement* is simply the measure of the ambient field with one sensor at any location.
- A *fixed differential measurement* is performed with a stationary base station and a roving sensor. The difference in measurement between these two instruments provides a measurement that eliminates time variations and the regional background level of magnetism.
- A *gradient measurement* is calculated between two sensors at a short, fixed distance. In a vertical alignment the higher sensor is subtracted from the lower sensor and then divided by the distance between the sensors, which yields the gradient measurement located at the midpoint of the two sensors (Breiner 1999). Gradient measurements are used to eliminate time variations, regional fields, and can minimize the effects of local disturbing fields (e.g. power lines).
- A *component measurement* is made in a single principal direction of the magnetic field which can be combined with two other orthogonal measurements to form a total field measurement. In a three dimensional Cartesian coordinate system, these are the x, y, and

z planes, with z describing the vertical dimension. Furthermore, a vertical gradient measurement acts as a high-pass filter that accentuates shallow anomalies while better resolving complex anomalies (Aspinall et al. 2008; Breiner 1999). This is further accentuated by using only the vertical component.

Magnetic Susceptibility Meters

MS meters differ from magnetometers in that they only measure an induced magnetic field and are not affected by remanent fields. They are active prospecting instruments, unlike magnetometers which are passive. A local primary electromagnetic field is generated which then induces a secondary magnetic field in a material. The ratio of the effects of the primary and secondary fields to the known primary field is the MS, commonly expressed as susceptibility per unit volume (κ). In the International System of Units (SI), it is dimensionless unit (Dalan 2006). There are two general categories of MS meters, single- and dual-coil (slingram). Single-coil instruments use the same electromagnetic coil to transmit and then receive the induced signal. Their effective prospecting depth is related to the diameter of the coil (Dalan 2006). They usually have effective depths of 1-10 cm and are only capable of making single point measurements. This makes them much slower with a maximum speed of roughly a reading per second. Dual-coil instruments contain a separate transmitter and receiver where the effective depth is a function of the distance between the coils. They can commonly sample at much higher frequencies, making them more fitting for large areal surveys. Only one instrument was employed in this study, the single-coil Bartington MS2 with the H sensor (a down-hole instrument). This instrument was used to evaluate the depth estimation techniques by determining actual depths to targets.

Instrumentation Used in This Project

Geometrics G-857

The G-857 proton-precession style magnetometer is an older low-cost instrument compared to the others used in this survey (Figure 1.10). This instrument measures the Earth's total magnetic field with a resolution to 0.1 nT at a rate of one reading per three seconds or more (Geometrics, Inc. 2015). It is capable of collecting data at a faster rate, but in doing so it sacrifices data sensitivity. This type of instrument can be configured for single sensor or gradiometer areal surveys or as a stationary base station. In this project it was employed as a single-sensor base station. Individual total field measurements are stored internally.

Figure 1.10. Base Stations. Both magnetic base stations G-857 (left) and MagBase (right).

Geomtrics G-858

The G-858 is an alkali-vapor (cesium) style magnetometer that can also be used for areal surveys and as a base station (Figure 1.11). This instrument differs from proton magnetometers with sensitivity between 0.05 to 0.01 nT, depending on the data collection rate which ranges between 0.1 to 1 second, respectively (Geometrics, Inc. 2001). This instrument is able to collect data at much higher sensitivities and speeds. The G-858 also has a more modern control unit,

allowing simpler navigation and easier configuration of two sensors. This instrument stores individual and gradient total field measurements.

a)  b) 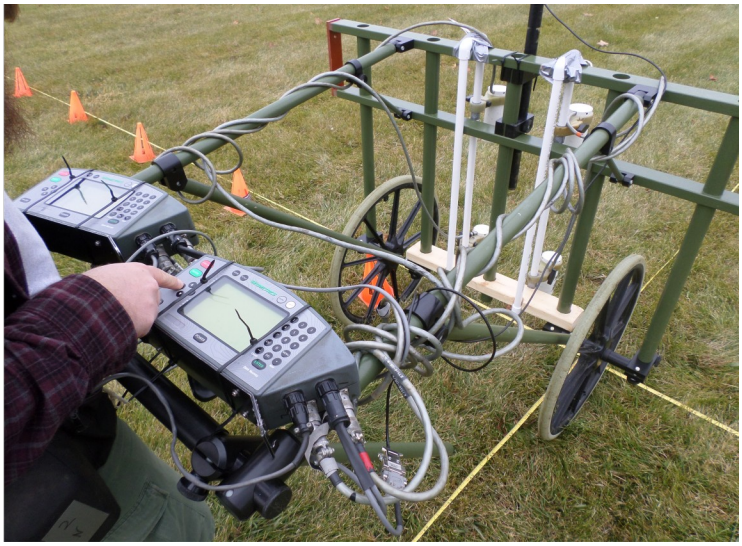

Figure 1.11. G-858 Setup. a) front view of non-magnetic cart with four G-858 sensors and Leica GNSS receiver, b) rear view of non-magnetic cart showing two G-858 control units.

SENSYS MagBase

The MagBase employs a single FGM3D/75 fluxgate 3-axis magnetometer for the collection of data in three principle directions which can be used individually, or combined together to form a total field value (Figure 1.10). The device records all three magnetic axes at a constant 200 readings per second with a resolution of less than 0.3 nT (SENSYS 2018). In addition to the magnetic readings, the instrument has built in accelerometers and a GNSS, allowing the device to shut off if it is moved during data collection. It also records the GNSS time stamp in Coordinated Universal Time (UTC) allowing for data integration with other instruments. This instrument stores three individual component measurements.

SENSYS Prototype

A prototype magnetometer provided by SENSYS contained nine FGM3D/75 three axis fluxgate sensors mounted on a non-magnetic cart system (Figure 1.12). The sensors were spaced at a constant 0.2 m in the x direction, and their vertical height above the ground surface could be

altered. All readings were recorded at the same resolution and sampling rate as the MagBase, at less than 0.3 nT and with 200 readings per second. This device interfaced with an external GNSS allowing for precise measurement locations and for those measurements to be associated with UTC time stamps. Due to the nature of the device, a prototype, a laptop computer was used to run data logging software (MonMX lite 4.0) and store all measurements. This allowed for the collection of all three axes of each sensor, 27 individual measurements, at 200 readings per second. These measurements can be used individually or combined to form the total field.

a)  b) 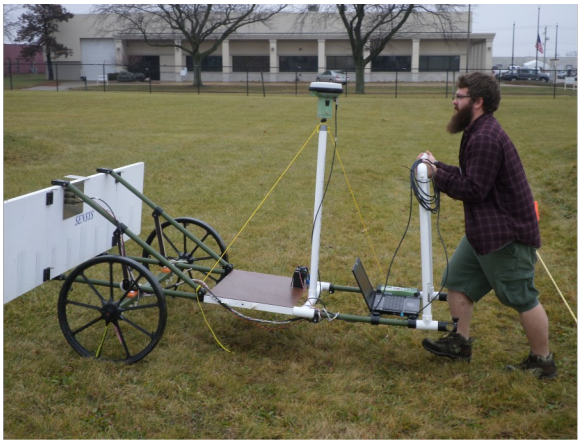

Figure 1.12. SENSYS Prototype. a) designed prototype setup at lower sensor heights, b) modified set up at higher sensor heights.

SENSYS MAGNETO MXPDA

This device is a non-magnetic cart based system which employs up to five vertical component fluxgate sensors with horizontal (x) spacing of 0.25 or 0.5 m (Figure 1.13a). It can employ either FGM650/10 or FGM650/3 vertical component gradiometers (vertical spacing of 0.65 m). The FGM650/3 sensors were used in this study, which have a resolution of less than 0.2 nT with a sampling rate of 20 or 100 readings per second (SENSYS 2017). Location data can be acquired via an external GNSS or with an odometer. The gradiometers come factory tuned and therefore require no further field adjustments. This device stores the vertical component magnetic gradient of each sensor.

Bartington Grad601

This instrument is presently considered the workhorse in archaeo-geophysics. In the dual configuration it consists of two vertical component fluxgate gradiometers with 1 m vertical spacing at 1 m horizontal separation (Figure 1.13b). It has an effective data resolution of 0.03 nT and can record data in increments of 1 to 4 per meter in the horizontal (x) and up to 8 in the vertical (y) direction (Bartington Instruments 2014). Additionally, this system requires an in-field tuning procedure prior to survey. The system is carried by an operator which requires guide lines to be placed on the ground to line up sensor readings with real-world locations. It stores the vertical component magnetic gradient of each sensor.

a)  b) 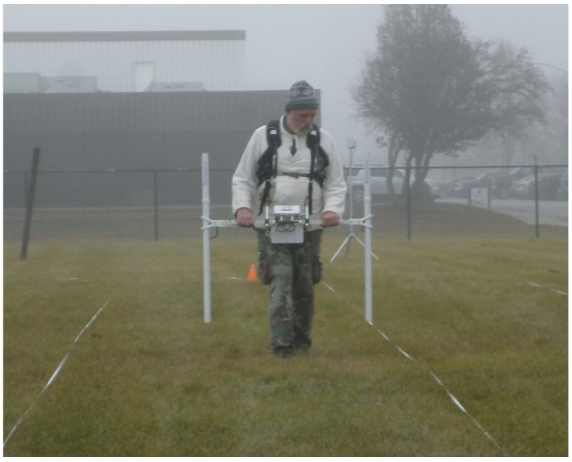

Figure 1.13. SENSYS MXPDA and Bartington Grad601. a) SENSYS MXPDA with 5 sensors at 0.25 cm horizontal separation and Leica GNSS receiver, b) Bartington dual Grad601 with 2 sensors at 1 m horizontal separation.

Bartington MS2 with H Sensor

The MS2 single-coil magnetic susceptibility meter is a portable system that employs the MS2 control unit and a variety of sensor heads, depending on the task (Figure 1.14). The system generates a low intensity alternating magnetic field in a sensor coil. When placed near a material the frequency of the field will change in proportion to the material's magnetic susceptibility (Dalan 2006). It can measure in either SI or CGS units at an acquisition sensitivity of either 1 or

0.1—the latter requiring a 10 times increase in collection time (Bartington Instruments 2010). For volume susceptibilities it has a data resolution of 10^{-5} SI. For this study only the MS2H, a down-hole sensor, was employed which is designed for use in a 22-25.4 mm diameter hole up to 100 m deep. Scaling factors are used to adjust measurements depending on hole diameter. The sensor probe is attached to aluminum tube sections which are used to lower the sensor into a hole at desired depth intervals, minimum vertical resolution being 1.25 cm and maximum speed is one reading per 0.95 second. The horizontal depth penetration, or sensitivity, falls-off rapidly being 50% at 2 mm, 10% at 5.5 mm and 1% at 13 mm from the sensor (Bartington Instruments 2010). This means that in practice it is only measuring the effects of the soil it is touching or in immediate proximity. When using a computer with the "Multisus" data logging software (provided by Bartington), readings are automatically recorded and drift correction can be automatically applied if zeroing is performed at the beginning and end of data collection at a core hole.

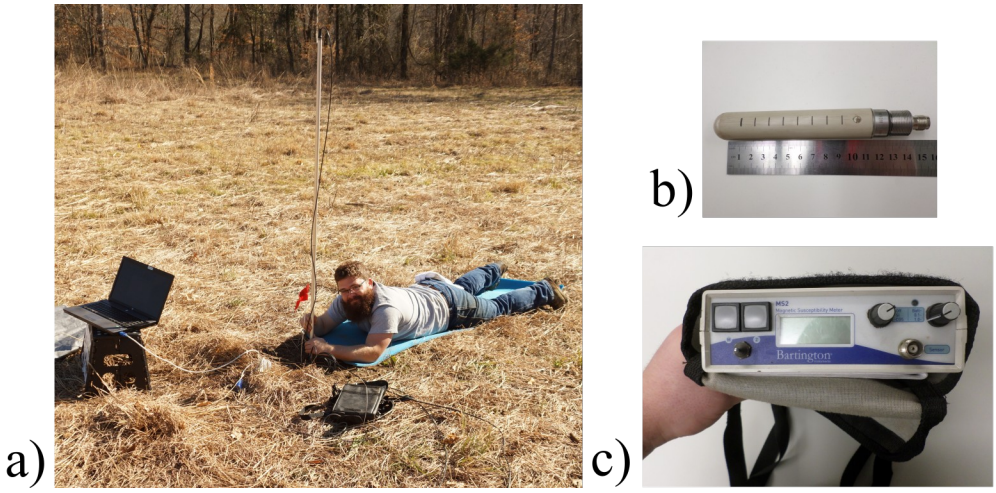

Figure 1.14. Down-hole MS. a) down-hole MS system in use at Woolsey, b) close up of MS2H sensor, c) close up of MS2 control unit.

Additional Equipment

In addition to the geophysical equipment used throughout the project, two extremely important instruments were also employed. A GNSS in the form of a Leica GS/CS15 real-time-kinematic (RTK) base station and receiver system was integral to the success of the project. It was used for determining the location of all survey areas, placement of down-hole soil probe locations, and allowed direct location recording and navigation of all magnetometer cart systems. A soil-probe system, JMC Backsaver, was used to create the appropriate holes for the down-hole MS system and also allowed visual examinations of soils and sediments.

Leica RTK

The Leica GS15 GNSS receiver and CS15 controller were employed throughout the study for navigational purposes (Figure 1.15). In a RTK configuration two GNSS receivers are used, one as a base station and the other as a roving unit. The base station is set up either over a known or unknown location; in this project all base station locations were known. This allows the base station to send a correction signal to the rover, which can be employed in real-time or in post processing. Depending on ground conditions (e.g. tree cover, buildings) and atmospheric conditions, this type of survey permits centimeter level accuracy, with a maximum accuracy of 1 cm horizontal and 2 cm vertical (Leica Geosystems 2012).

a)  b) 

Figure 1.15. Leica GNSS. a) Leica GS15 receiver set up as a RTK base station, b) close up of CS15 control unit.

JMC Backsaver

This device is a soil sampling probe, which is designed to use the operator's body weight to force the probe into the ground and when the operator retrieves the probe (Figure 1.16a). The sampling depth can be increased by adding extension rods to the system for sampling up to approximately 10 m below the ground. JMC offers various soil probe diameters ranging from 0.56 to 1.2 inches, depending on the soil environment and application. Both wet and dry probes were used in this study, which are 0.688 and 0.75 inch diameters respectively. The 18 inch open face soil probe was used, which allows immediate manual interpretation of soil during survey (Figure 1.16b).

a)  b) 

Figure 1.16. Soil Probe. a) JMC Backsave being inserted into a hole, b) 18 inch open-face soil-probe allowing soil analysis.

Chapter 2: Magnetics: Theoretical Background

Much of the theoretical knowledge this project employs is not commonly addressed by the archaeo-geophysical community. For this reason, an in depth look at the theory behind depth estimation techniques, half-width rules and multi-height techniques, is necessary. This project also employs a specialized magnetic processing technique, "reduction to the pole" and the topic of the "Structural Index". Although commonly employed and discussed within the geological community and literature, the lack of their use and discussion within the archaeo-geophysical community warrants an in-depth review here. As these topics are pertinent to the understanding of the depth estimation techniques, they are addressed first.

Specialized Magnetics Knowledge

Reduction to the Pole

Reduction to the pole (RTP) is a well-known magnetic processing method, first developed by Baranov (1957), which adjusts magnetic data to make them appear as if they were located and collected at a magnetic pole (Figure 2.1). This is performed because, due to magnetic field inclination and declination changes at different latitudes, magnetic anomalies do not directly correspond with the locations of their source bodies (Baranov 1957; Bhattacharyya 1965). The process of reducing magnetic data to the pole has gone through multiple changes in computation since its inception. Original Fourier methods were performed in the frequency domain and perform poorly at low magnetic latitudes, below 15 degrees (Baranov 1957; Baranov and Naudy 1964; Bhattacharyya 1965; Silva 1986). Kanasewich and Agarwal (1970) took advantage of the Fast Fourier Transform (FFT) to speed up the computation, but this method is still unstable at low latitudes. Gunn (1975) addressed the problem in the space or wavenumber domain showing that the method can be a linear transformation applied to the original data.

Pearson and Skinner's (1982) method is also performed in the wavenumber domain, but in an attempt to

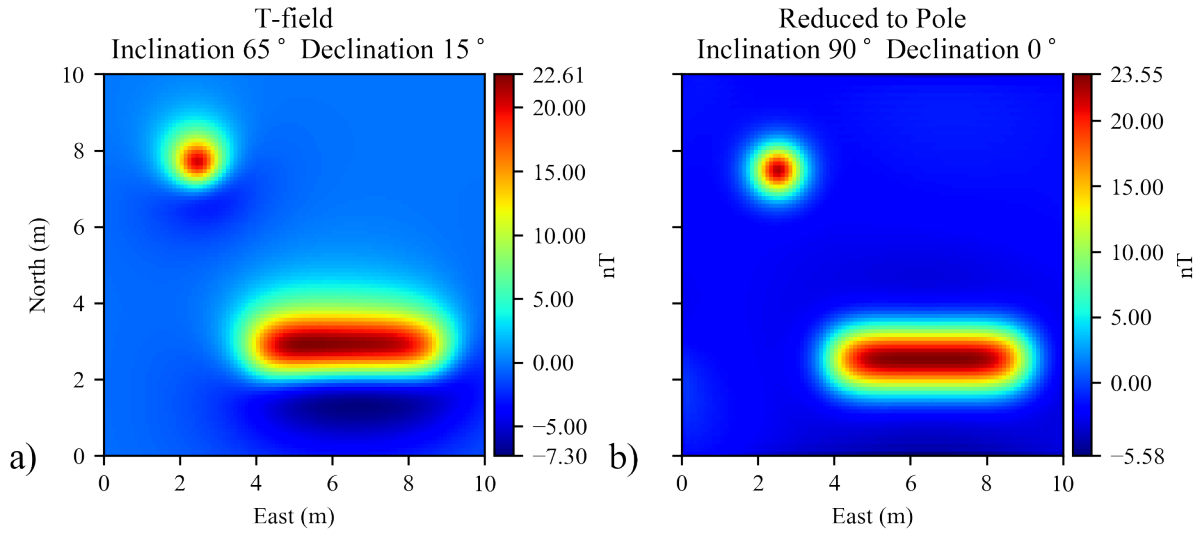

Figure 2.1. Reduction to the Pole Example. Model data of a sphere and a wall. a) Total field data located at 65 and 15 degrees inclination and declination, respectively, showing asymmetry. b) Total field data after reduction to the pole corresponding to 90 and 0 degrees inclination and declination, respectively, showing perfect symmetry.

modify the method to work better at low latitudes, they proposed that the data be spectrally whitened. This requires a priori knowledge and only reduces some noise from the data, any noise left after filtering is enhanced through the reduction process, therefore it is not an optimal technique (Silva 1986). Silva (1986) suggests a new method for reduction to the pole through inversion and not FFT. This method performs well at low latitudes, but is computationally more intensive.

By reducing magnetic data to the pole, one alters the magnetic data so that it appears as if the source body is located at a magnetic pole and that the data would have been collected there. The primary result is that that magnetization becomes vertical (Baranov 1957; Baranov and Naudy 1964; Bhattacharyya 1965; Von Frese 1984). Reduction to the pole therefore achieves multiple goals. Reduced anomalies are centered over their causative bodies, and therefore, appear more symmetrical and are easier to interpret. Moreover, induced dipoles often appear as

monopoles, because the opposite pole is now obscured beneath the near pole. Quantitative analysis, including depth estimation, is more reliable (Baranov 1957; Baranov and Naudy 1964; Salem et al. 2007; Von Frese 1984). Some drawbacks to the method derive from remanent magnetization. Baranov and Naudy (1964) note that the presence of remanence could be problematic, but it is not as big a problem as originally suspected. However, it has been shown that remanence can cause a shift in magnetic data away from its correct location through the reduction technique (Bhattacharyya 1965; Salem et al. 2007; Von Frese 1984). Von Frese (1984) suggests that this could assist interpretation of archaeological features. Additionally, one assumption of the above methods is that the regional magnetic fields have constant direction, which does not hold when looking at regional-scale (e.g. many kilometers) surveys. Arkani-Hamed (1988) modifies the technique in the spectral domain to account for declination and inclination changes across large areas. However, this method is unnecessary for small area surveys, and therefore is not applicable to archaeological data.

The above techniques are all usually only applied to total field data, but vertical component gradiometers are the most commonly used instruments in archaeology. Tabbagh et al. (1997) address these issues and provide an equivalent RTP solution for vertical component gradient data. Tabbagh et al. (1997) state that like many of the above methods theirs too performs poorly in low latitudes and fails in the presence of remanence. Nevertheless, they suggest two analytic signal moduli which effectively reduce the data to the pole and are not adversely affected by remanence.

Structural Index

The Structural Index (SI) is fundamental to potential-field (e.g. magnetic and gravity) depth estimates (Reid and Thurston 2014). It is a factor that simultaneously accounts for the geometry and fall-off rate of subsurface sources (Breiner 1999; Mushayandebvu et al. 2001; Reid

and Thurston 2014; Witten 2006). Such factors are extremely difficult to calculate and therefore have only been offered for simple geometric objects (Witten 2006). The SI is apparent, implicitly or explicitly, in all depth estimates, because it inherently accounts for the geometric nature and field curvature of what is being measured (Reid and Thurston 2014). This allows for the distance to be calculated from source bodies to the measurement location (Breiner 1999). The SI can be related to geologic or archaeological feature types through simplified models. In magnetics, a spherical dipole model is the most basic and commonly used for point source objects. This model has a fall-off rate of the inverse cube of distance, while a spherical monopole has a fall-off rate of the inverse square (Aspinall et al. 2008; Breiner 1999; Witten 2006). Breiner (1999 fig. 34) shows multiple graphic examples and their corresponding SI.

Table 2.1. Structural Indices. Simple geometries and their respective indices.

Geometry	Structural Index (n)	Fall-off rate
Sphere (Dipole)	3	$\frac{1}{\text{Distance}^3}$
Vertical Cylinder (Monopole)	2	$\frac{1}{\text{Distance}^2}$
Edge of Narrow Dike (Line of Monopoles)	1	$\frac{1}{\text{Distance}^1}$

In both simple (HW and multi-height) and more complex depth estimation techniques, the correct SI is needed to produce accurate results (Barbosa et al. 1999; Desvignes et al. 1999; Mushayandebvu et al. 2001; Reid and Thurston 2014). In other words, in order to undertake depth estimation to a source body, one must be willing to assign a particular geometry to that body as well as an SI value. Desivgnes at al. (1999) have suggested that although many archaeological features are small and clustered they are limited in their thickness and the tops are commonly larger than their bottoms, so a spherical model does not work well. They state SI=2 is more appropriate. Due to the difficulty in qualitatively determining the correct SI, many authors,

including Barbosa et al. (1999), have created algorithms that automatically estimate SI. These estimates are usually based on a least-squares fitting technique.

Depth Estimation Techniques

Various depth estimation techniques require a range of pre-processing to be performed to the data before the depth estimation can be performed. In most cases, this may simply include the standard set of processes used for data cleanup and visual enhancement. In almost all cases, HW rules are performed on data without any advanced processing (e.g. reduction to the pole). Although many authors use these rules without RTP, all data for this project have been reduced before depth estimation (Aspinall et al. 2008; Tite 1972; Weymouth 2000; Witten 2006). Prior use of the techniques have almost always been done at high magnetic latitudes, where RTP has little visual effect on the data and is not a common archaeo-geophysical processing technique. Even at high magnetic latitudes, RTP does change depth estimation results and RTP is essential to proper estimation at lower latitudes. More surveys are being performed globally where this is an issue. RTP changes the depth estimation by allowing equal measurements on both sides of an anomaly curve. Prior to RTP the curves would be skewed, where after RTP they would be normal. Without RTP, measurements at different radial angles would differ. Performing RTP centers the anomaly increasing accuracy of measurements in all directions.

Although little prior research has been performed on multi-height techniques, in theory the measurements for the depth estimation process should be performed at the center of the anomalous source (Breiner 1999; Weymouth 1976, 2000). For this reason, all multi-height depth estimates are also performed on reduced data.

Half-width rules

The half-width (HW) or full-width half-maximum (FWHM) rule is a graphical depth estimation technique (Aitken 1961; Aspinall et al. 2008; Breiner 1999). It has been in use since at

least the 1950's (Smellie 1956) and is the most well-known simple estimation technique (Aitken 1961; Aspinall et al. 2008; Bevan 1998; Breiner 1999; Desvignes et al. 1999; Oh et al. 2008; Reynolds 2011; Tite 1972; Weymouth 2000; Witten 2006). The method can be applied directly to 2D magnetic profiles and gridded or contoured plan-view data. The premise of the rule is that causative body depth is equivalent to the linear distance between two points that equal half of the maximum anomaly strength (Figure 2.2) (Breiner 1999; Reynolds 2011). This is for a spherical dipole and other calculations are more suitable for sources of different polarity and geometry (Aitken 1961; Breiner 1999). The following equations are taken from Breiner (1999:30) where Z is the depth to the source body below the ground surface, h is the height of the sensor above ground, and $X_{(1/2)}$ is the distance between the maximum and half-maximum:

For dipoles

$$Z = (2 * X_{(1/2)}) - h$$

Equation 2.1

For a single monopole

$$Z = (1.3 * X_{(1/2)}) - h$$

Equation 2.2

For a line of monopoles

$$Z = X_{(1/2)} - h$$

Equation 2.3

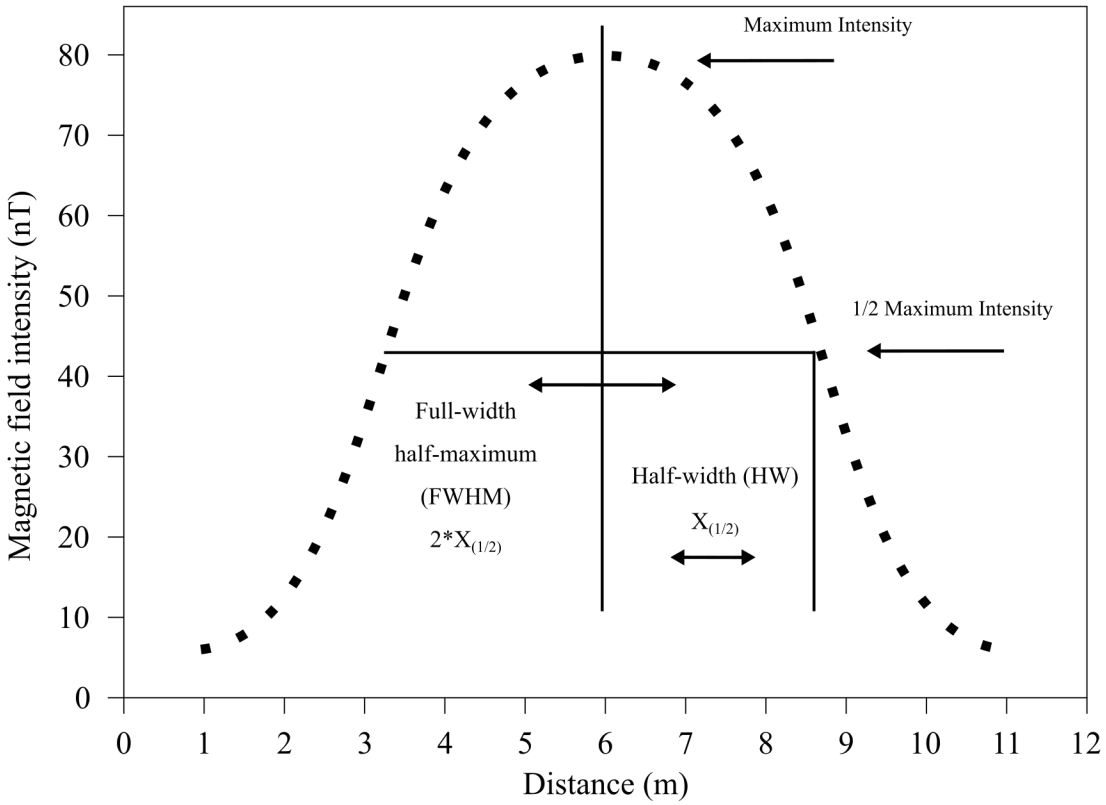

Figure 2.2. Graphic representation of the half-width rules on a magnetic profile.

Worked Example 1.

Assuming the source body is a sphere for the magnetic profile in the above Figure 2.2. We employ Eq.1. for a spherical dipole, where Z is the depth to source, $X_{(1/2)}$ is the half-width, and h is the height of the sensor above ground.

$X_{(1/2)} = 2.8$ m, h = 0.5

$Z = (2*2.8)-0.5$

$Z = 5.1$ m

The center of the anomalous source is 5.1 m below ground.

Many authors provide slight variations to and considerations for the use of the FWHM rule. Bevan (1998) suggests when using contour data that the depth is equal to the average diameter around an anomaly peak. Aitken (1961) and Tite (1972) both note that the measured distance is equal to the depth or the width of the anomalous source, whichever is greater. Additionally, other authors note that the measurement should be made in the magnetic N-S direction, as this corresponds to the source's component that is measured when using a total field sensor (Breiner 1999; Smellie 1956; Weymouth 2000). If data has been reduced to the pole, different statistical measurements can be used (e.g. min, max, median, mean) as all measurements are in the N-S direction. This may assist in better estimates for source bodies that are not perfectly spherical. It also appears that depending on the source body geometry, either a sphere or line, the method will estimate depth to the center or top of the source, respectively (Reynolds 2011; Smellie 1956). Furthermore, the anomaly width is also related to the sensor used. A vertical component fluxgate sensor will produce a smaller width than a total field sensor and therefore the FWHM is likely to be more accurately applied to total field data (Aspinall et al. 2008; Weymouth 2000). Again, if data are first reduced to the pole, there should be no difference between vertical component and total field data.

Studies by Weymouth (2000) and Witten (2006) both analyze the HW rules in an archaeological context using models of simple dipole features. The studies vary in design, testing features at multiple depths and at different magnetic inclinations and declinations and also comparing total field and vertical component measurements. They both conclude with errors ranging from 1 to ~20 percent of the depth to the source with error generally decreasing with increased depth to source, and Weymouth (2000) suggests better results may be acquired with a finer measurement grid.

It should be noted that although in much of the literature it appears that HW rules are an independent method, they are in fact derived from the same equations as the multi-height techniques discussed below (Breiner 1999). This can be seen as Equation 2.5 is actually a simplification of the following when measurements are directly above the source. This includes the total field measurement (ΔF), the magnetic moment (M), the volume of the source (V) the angle between the vertical field at the source and the point of measurement (θ), the depth below surface to the source (Z), the height of the measurement above ground (h), and the fall-off rate or SI (n):

$$\Delta F = \frac{2MV * \cos^2\theta - MV * \sin\theta}{(Z+h)^n}$$

Equation 2.4

Multi-height

Multi-height surveys involve two or more magnetic sensors fashioned in a linear series (most often vertically above the ground surface) and in some cases a stationary base sensor. To the author's knowledge, the only theoretical application in archaeology of a non-gradient multi-height survey to estimate depth was outlined by Weymouth (1976).

In principle, the relationship between a measured magnetic force and its causative body can be made which includes the force (ΔF) or measured field intensity, magnetic moment (M), the volume of the source (V), the depth below surface to the source (Z), the height of the measurement above ground (h), and the fall-off rate also known as the Structural Index (n). This is described in slightly different forms by many authors (Aitken 1970; Aspinall et al. 2008; Breiner 1999; Weymouth 1976) and is likely found in many introductory physics texts.

$$\Delta F = \frac{2MV}{(Z+h)^n}$$

Equation 2.5

As we can see, the field intensity (or magnetic measurement) is inversely related to the distance of a source body dependent upon its fall-off rate—which is commonly three or two for dipoles and monopoles, respectively (Table 2.1; Breiner 1999). Weymouth (1976) utilized this relationship to estimate depths to multiple archaeological features by acquiring multiple differential magnetic measurements at various heights. Multiple measurements allow for difficult to attain magnetic properties, such as magnetic moment and dimensionality (M and V, respectively), to be algebraically removed from the equation. The ratio of these measurements can then be used to approximate the depth to anomaly sources by making use of the magnetic fall-off rate or SI (n), which depends on the assumed geometry of the source body. This was performed by manipulating Equation 2.5 for two measurements (F_1 and F_2) at two heights (h_1 and h_2) and solving for the depth (Z):

$$\text{a.}\quad F_1 = \frac{2MV}{(Z+h_1)^n} \qquad \text{b.}\quad F_2 = \frac{2MV}{(Z+h_2)^n}$$

Equation 2.6. a. and b.

Algebraically combining equations 6a and 6b and solving for d yields:

$$Z = \frac{(h_2 - h_1 * (F_1/F_2)^{1/n})}{((F_1/F_2)^{1/n} - 1)}$$

Equation 2.7

No conclusive field evidence is provided for the method (Weymouth 1976) and it appears the technique was not used by others in archaeology. Weymouth (2000) references the above method as a possible technique for depth estimation, however, no further use of the technique has been conducted which may be attributed to the decreased use of total field sensors in archaeological applications. A similar equation is presented by Breiner (1999), but similarly there is little evidence of its use in the literature.

Worked Example 2.

Assume the source body is a sphere for the magnetic profiles in Figure 2.3 below. We employ Equation 2.7 for a spherical dipole where h_1 and h_2 are the measurement heights, F_1 and F_2 are the maximum field intensities, Z is the depth below ground surface, and we use an SI of n=3.

$h_1 = 0.3$

$h_2 = 1.3$

$F_1 = 80$

$F_2 = 30$

$n = 3$

$$Z = \frac{\left(1.3 - 0.3 * \left(80/30\right)^{1/3}\right)}{\left(\left(80/30\right)^{1/3} - 1\right)}$$

The depth to the center of the anomalous source from the ground surface is 2.29 m.

Other Depth Estimation Techniques

It should be noted there are various other magnetic depth estimation techniques employed in deep geologic applications (Blakely 1996; Reid et al. 1990; Reynolds 2011). Although beyond the scope of this project, at a minimum they warrant being listed here. There are various other graphical methods similar to half-width rules, generally termed slope-methods. These techniques are easy to apply, but lack concrete theoretical bases, and are usually thought of as "rules-of-thumb" (Åm 1972; Blakely 1996; Peters 1949; Reynolds 2011). More mathematically complicated methods include, Euler Deconvolution, Center of Mass Estimation, Spectral Analysis, Werner Deconvolution, Dipole Fitting, and Inversion techniques, to name a majority, although others exist (Blakely 1996; Helbig 1963; Reynolds 2011). These methods all have

specific and broad applications depending on the background soil matrix and the magnetic target. Many require more intricate mathematics. Some have been briefly tested in the archaeological world with inconclusive results, but they may provide adequate results in the future.

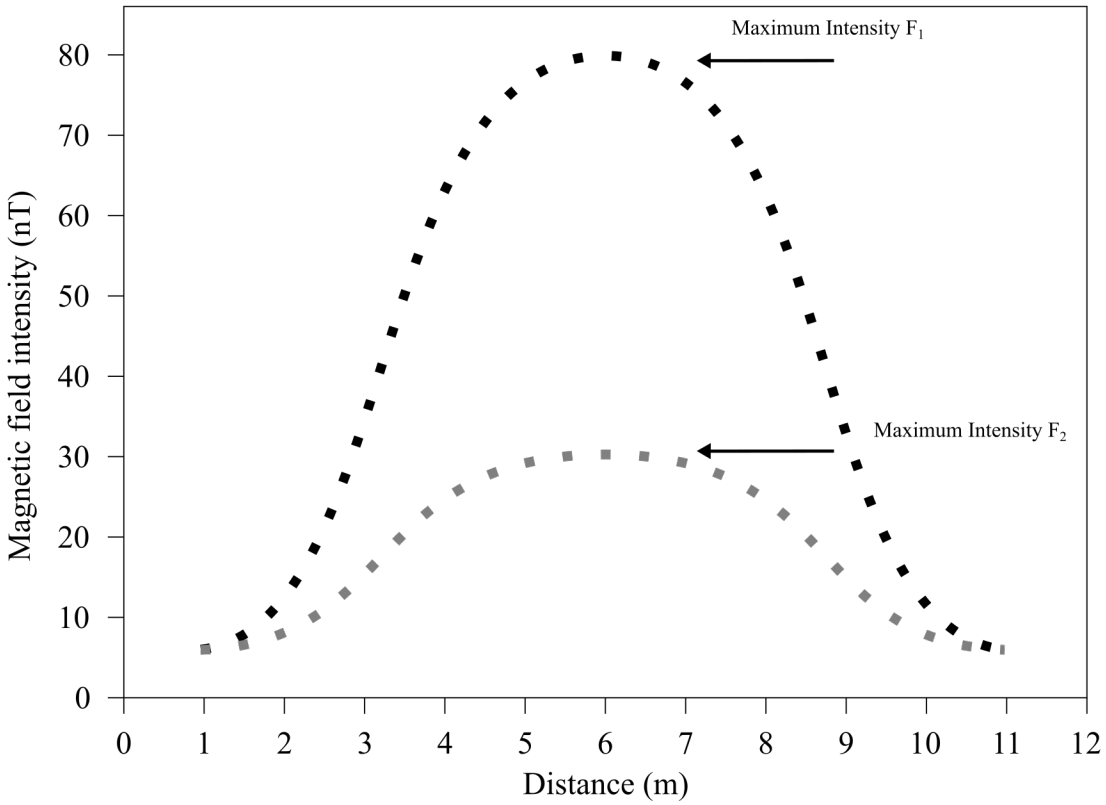

Figure 2.3. Multi-height example. The magnetic response from the same source body measured at two different sensor heights, lower (black) and higher (gray).

Chapter 3: Magnetic Modeling

This project uses a combination of magnetic models with targets varying in size, shape, and depth to better understand and evaluate the magnetic depth estimation techniques described above. Modeling the magnetic field response of magnetic source bodies is widespread in geology but is less commonly applied in archaeo-geophysical studies (Blakely 1996; Breiner 1999; Burger et al. 2006; Eder-Hinterleitner and Neubauer 2001; Neubauer and Eder-Hinterleitner 1997; Neubauer 2001; Scollar 1969; Witten 2006). In general, magnetic modeling is performed by creating a model magnetic source body and then mathematically estimating the theoretical magnetic field response created by the magnetic source body given its parameters. In this study, models are broken into two categories, simple and complex. Archaeological features are modeled by simple geometric objects, spheres or rectangular prisms, and more complex geometric constructions of small prisms. Simple magnetic models are used to represent point-sources, pits, hearths, walls, and floors. More complex magnetic models include un-layered concave half-spheres, representing hearths and shallowly shaped pits. These various models are used to better understand the types of magnetic anomalies produced by archaeological features and to test the magnetic depth estimation techniques.

Magnetic Modeling Background

Due to mathematical complexity, and the desire to not re-invent the wheel, the open-source Python library "fatiando a terra" was used to create all the magnetic models in this study (Uieda et al. 2013). For additional information on this Python library see Appendix E. This library houses functions to create magnetic models with different modeling techniques depending on their shape. This study employs the use of models derived from spherical bodies (Blakely 1996), prismatic bodies (Bhattacharyya 1964), and polygonal prisms (Plouff 1976). These techniques work in a similar fashion, where a single object is created (e.g. a large sphere) and the

parameters of magnetization are defined for this object. The parameters include: magnetic intensity of induced and/or remanent magnetism, the intensities' corresponding directions (via the background and potential remanent field's inclinations and declinations), and the volume of the source body. Given that all models in this study use only induced magnetism at the pole (90 degrees inclination, 0 degrees declination), parameters greatly simplify. From these variables, the principal component (x, y, z) and total magnetic fields are estimated. Additionally, techniques may also use multiple small objects (e.g. small spheres or prisms), where results for each object are calculated and summed to produce the overall effect. Using small objects allows greater variability in the shape of source bodies and potential inter-source variability to be modeled. In all cases, these models are created within a non-magnetic background matrix.

Model Design Scheme

A straight forward testing scheme was employed for each depth estimation technique. All models were created with only induced magnetization at 90 degrees inclination and 0 degrees declination. These are the parameters for data that have been reduced to the pole, assuming no effects from remanent magnetization. Prior testing by the author confirmed no difference in the model environment between modeled data at the pole and data reduced to the pole. Additional model parameters included size, depth, and magnetic intensity. These parameters were varied in an attempt to produce "archaeological like" anomalies. Sizes of source bodies depended on the type of feature (e.g. pit, wall, floor). They were confined to reasonable archaeological feature sizes. Depths to the top of source bodies ranged from 0.1 to 3.0 m below the ground surface, as anomalies deeper than this are not regularly encountered in archaeology or by magnetic survey. Magnetic intensity was varied from 0.01 to 100 ampere per meter (A/m). Due to size and depth parameters, some of these intensities were not appropriate for realistic archaeological features.

Therefore, models were limited to those where anomalies produced a maximum total field between 0.05 and 50 nT measured at 0.3 m above the ground surface.

The magnetic field was sampled on a 0.1 by 0.1 m grid. This is a denser sampling than the current standard field data density of 0.5 by 0.125 m. This was done to address any potential differences in successful depth estimation from a failure in technique versus limited sampling density, as techniques may require denser data sampling to perform properly (Weymouth 2000). Model total field magnetic data were rounded to three decimal places, as this is about the highest resolution any commercial systems achieve. Most systems achieve accuracy closer to a half of one decimal place. Models are evaluated with no noise to further examine proof of the modeling concepts.

Simple Geometries: Sphere

Spherical models are the most basic. They represent point source bodies and this geometry is a dipole with SI=3. This geometry was iterated from top depths of 0.1 to 3.0 m and radii of 0.05 to 0.5 m. Examples are shown in Figure 3.1. These models were further cycled through magnetic intensities of 0.01 to 100 A/m. This created a total of 1500 iterations. Data were filtered based on a lower sensor height of 0.3 m above the ground for magnetic total field values between 0.5 of 50 nT resulting in the evaluation of 566 magnetic models. This geometry creates a dipolar magnetic field, but when the magnetic field is induced at or reduced to the magnetic pole it is observed as a monopole. The resulting field is a circular anomaly whose diameter varies due to magnetic intensity, diameter, and depth of the source body. An example magnetic field from a sphere with a radius of 0.25 m and a top depth of 0.75 m and a magnetic intensity of 1.0 A/m is found in Figure 3.2.

Simple Geometries: Wall

Wall models use a single rectangular prism as their geometric base. They represent narrow linear source bodies and this geometry relates to SI=2. This geometry was iterated from top depths of 0.1 to 3.0 m and widths from 0.1 to 1.5 m with the thickness ranging from 0.1 to 2.0 m. Examples are shown in Figure 3.3. They were further cycled through magnetic intensities of 0.01 to 100. This created a total of 45,000 iterations. Data were filtered based on a lower sensor height of 0.3 m above the ground for magnetic total field values between 0.5 of 50 nT resulting in the evaluation of 18,001 magnetic models. This geometry creates a dipolar magnetic field, when the magnetic field is induced at or reduced to the magnetic pole it is observed as a monopole. The resulting field is a rounded rectangular anomaly whose width varies due to width, magnetic intensity, depth, and thickness of the source body. An example magnetic field from a wall is found in Figure 3.4 with a width of 1.0 m, top depth of 0.75 m, thickness of 0.25 m, magnetic intensity of 1.0 A/m, and magnetic inclination and declination of 90 and 0 degrees respectively.

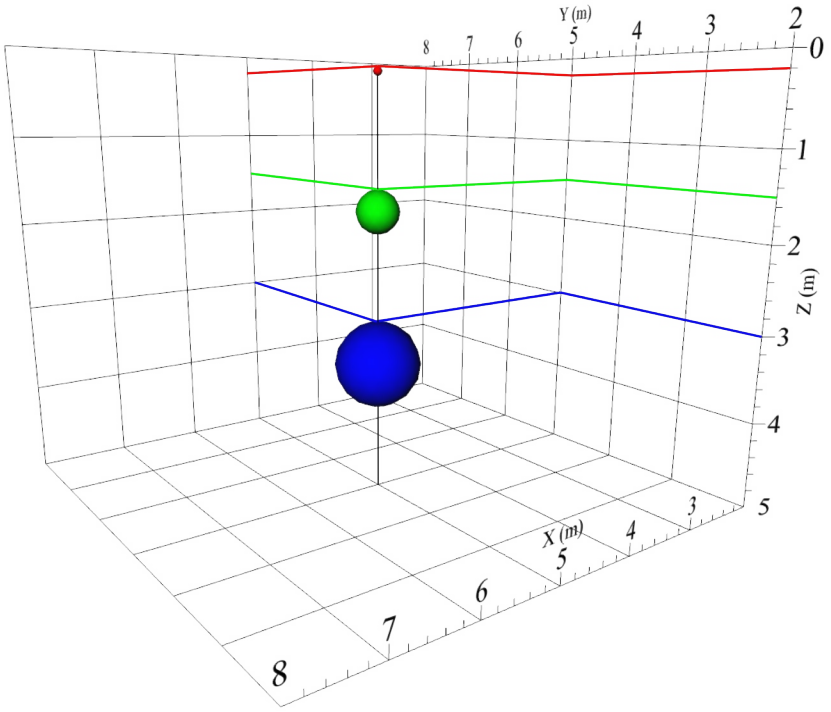

Figure 3.1: Model Spheres. Three spherical models with radii of 0.15, 0.3, 0.5 m and top depths from 0.1 to 3.0 m, red, green, blue respectively.

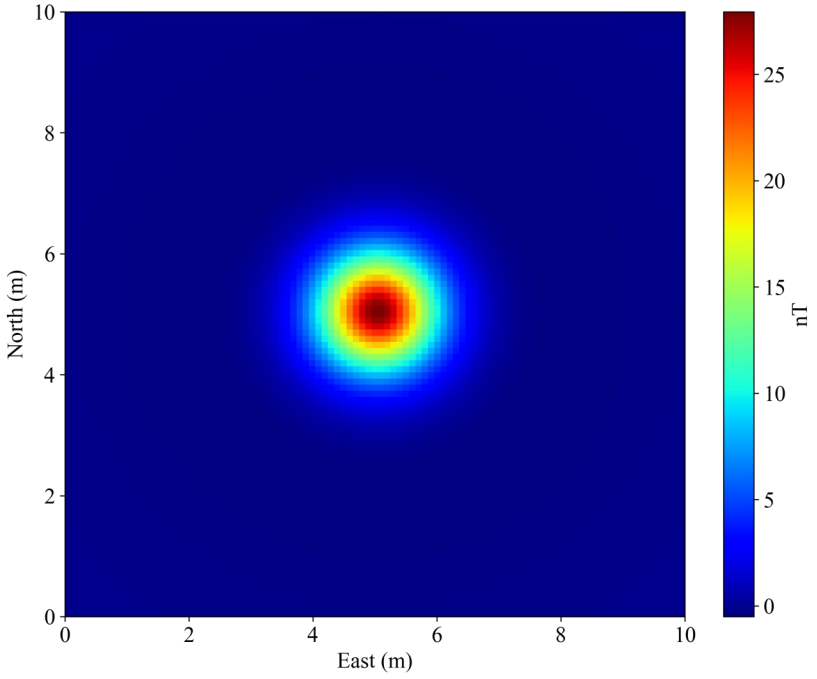

Figure 3.2: Magnetic Field – Sphere. Example sphere with radius 0.5 m, top depth 0.75 m, magnetic intensity 1.0 A/m, sensor height at 0.3 m above ground surface, magnetic inclination and declination at 90 and 0 degrees respectively.

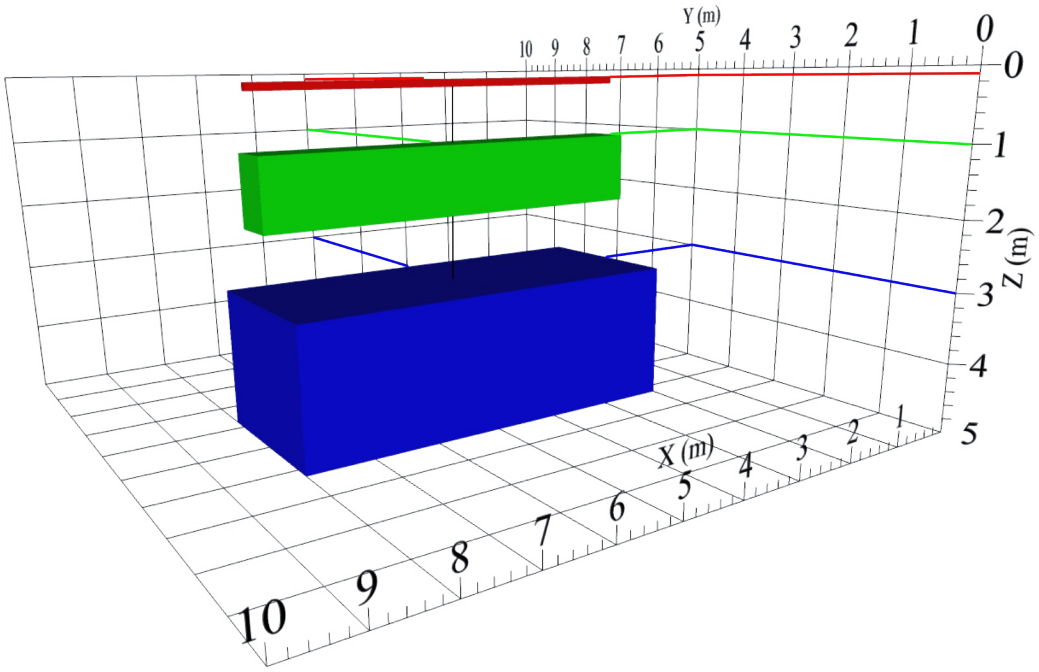

Figure 3.3: Model Walls. Three rectangular models with dimensions (L, W, H) of (6, 0.1, 0.1), (6, 0.7, 1), (6, 2.5, 2) m and top depths from 0.1 to 3.0 m, red, green, blue respectively.

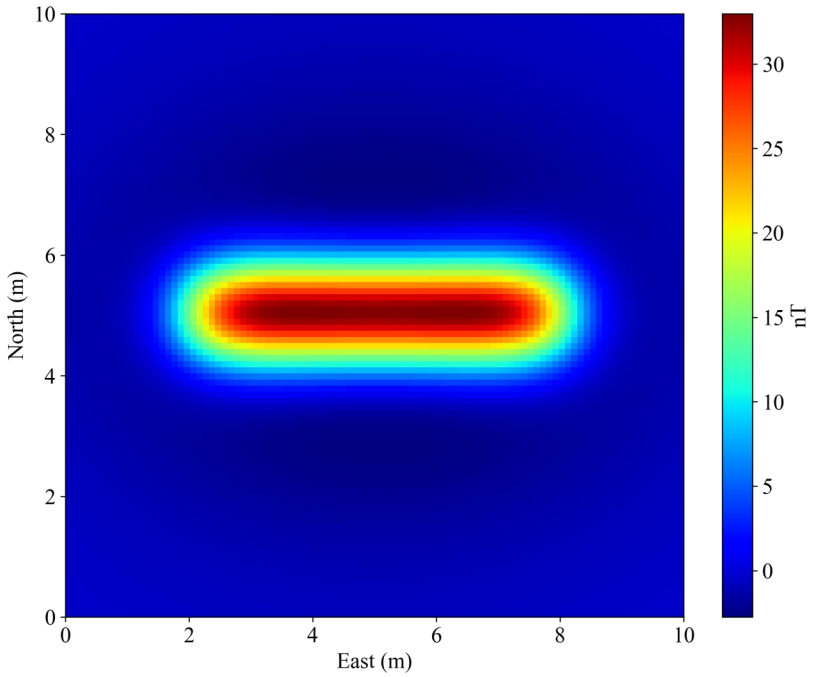

Figure 3.4: Magnetic Field – Wall. Example wall with length 6 m, width 1.0 m, top depth 0.75 m, thickness 0.25 m, magnetic intensity 1.0 A/m, sensor height at 0.3 m above ground surface, magnetic inclination and declination at 90 and 0 degrees respectively.

Simple Geometries: Floor

Floor models use a single rectangular prism as their geometric base. They represent very thin wide linear source bodies. This geometry relates to SI=1. This geometry was iterated from top depths of 0.1 to 3.0 m and widths from 4.0 to 6.5 m with the thickness ranging from 0.05 to 0.5 m. Examples are shown in Figure 3.5. They were further cycled through magnetic intensities of 0.01 to 100. This created a total of 9,000 iterations. Data were filtered based on a lower sensor height of 0.3 m above the ground for magnetic total field values between 0.5 of 50 nT resulting in the evaluation of 3,600 magnetic models. This geometry creates a dipolar magnetic field, but when the magnetic field is induced at or reduced to the magnetic pole it is observed as a monopole. The resulting field is a rectangular anomaly whose width varies due to width, magnetic intensity, depth, and thickness of the source body. Additionally, higher magnetism can be observed above the four outer corners of the source body. This is due to the singular large prism being used in the model environment. This effect is reduced with decreased magnetic intensity and deeper depths. An example magnetic field from a floor is found in Figure 3.6 with parameters: width of 6.0 m, top depth of 0.75 m, thickness of 0.25 m, with a magnetic intensity of 1.0 A/m, and magnetic inclination and declination of 90 and 0 degrees respectively.

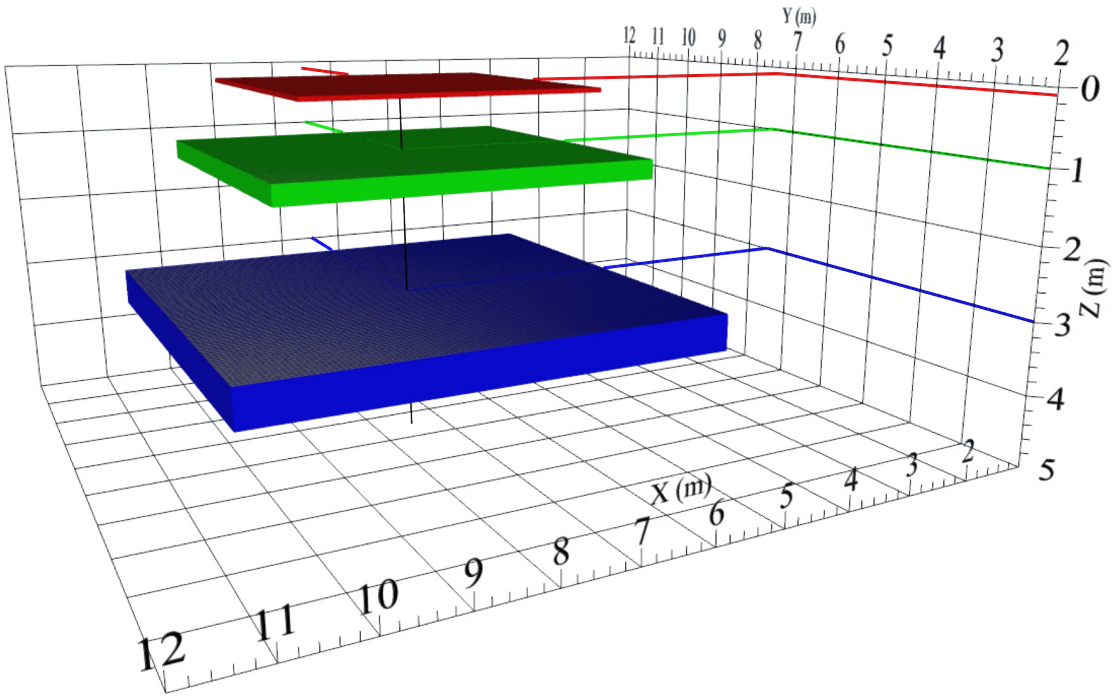

Figure 3.5: Model Floors. Three rectangular models with dimensions (L, W, H) of (4, 4, 0.05), (5, 5, 0.25), (6.5, 6.5, 0.5) m and top depths from 0.1 to 3.0 m, red, green, blue respectively.

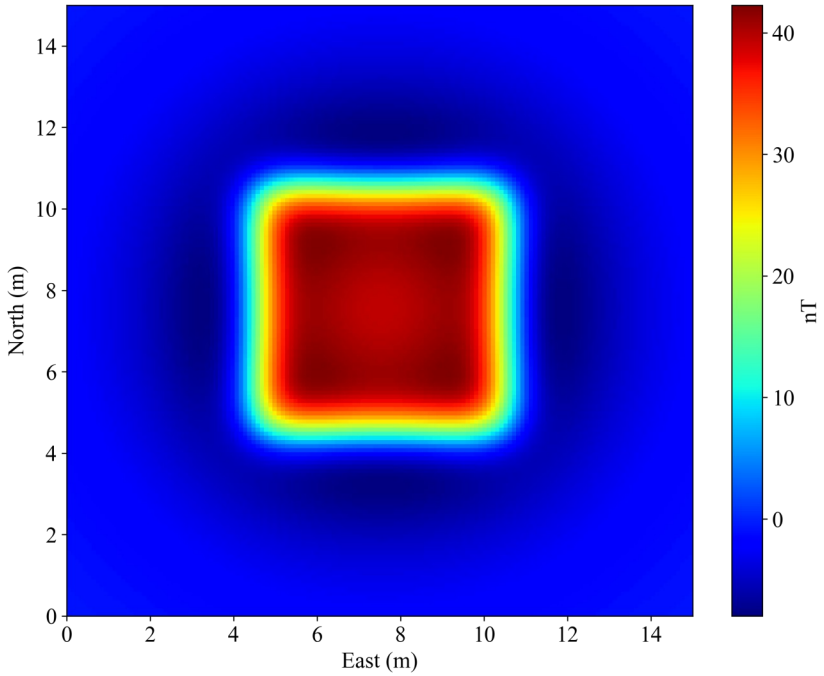

Figure 3.6: Magnetic Field – Floor. Example floor with length and width of 6 m, top depth 0.75 m, thickness 0.25 m, magnetic intensity 1.0 A/m, sensor height at 0.3 m above ground surface, magnetic inclination and declination at 90 and 0 degrees respectively.

Complex Geometry: Half-sphere

Half-sphere models use a series of small rectangular prisms to construct the desired half-sphere shape. Individual prisms ranged in size depending on the half-sphere radius, in order to lessen computation time on larger half-spheres. Models with radii 0.35 m or larger used prisms of 0.05m. Models with radii between 0.2 and 0.35 m used prisms of 0.025 m. Models with radii smaller than 0.2 used prisms of 0.01 m. Half-sphere models represent point-like sources, most similar to a hearth or potential pit structure. There is no defined SI for this shape, but given its similarity to a sphere, it is likely between 3 and 2. An SI=3 was employed in this study. This geometry was iterated from top depths of 0.1 to 3.0 m and radii of 0.05 to 0.5. Examples are shown in Figure 3.7. They were further cycled through magnetic intensities of 0.01 to 100 that created a total of 1500 iterations. Data were filtered based on a lower sensor height of 0.3 m above the ground for magnetic total field values between 0.5 of 50 nT resulting in the evaluation of 539 magnetic models. This geometry creates a dipolar magnetic field, but when induced at or reduced to the pole only the positive polarity is observed. The resulting field is a circular anomaly whose diameter varies due to magnetic intensity, diameter, and depth of the source body. An example magnetic field from a half-sphere with a radius of 0.5 m and a top depth of 0.75 m and a magnetic intensity of 1.0 A/m is found in Figure 3.8.

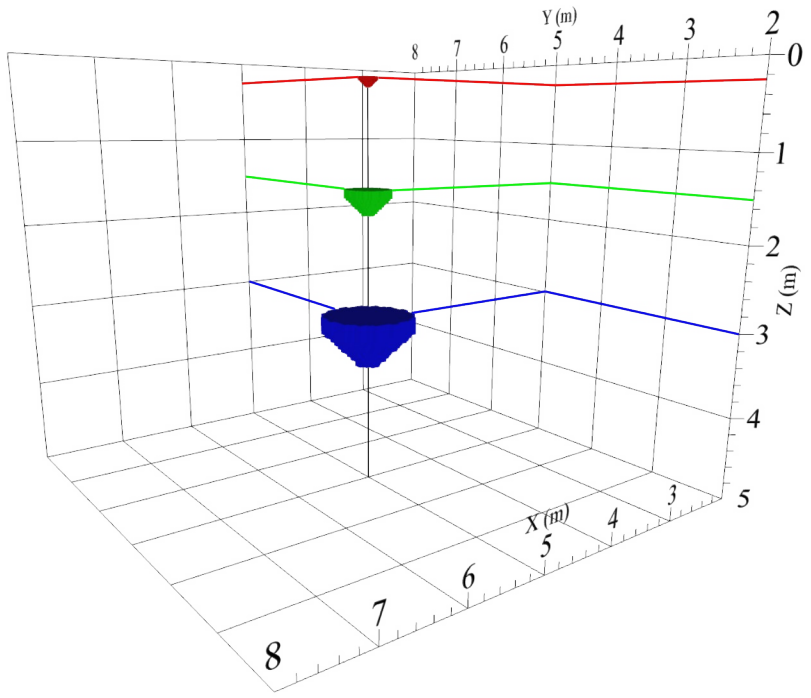

Figure 3.7: Model Half-spheres. Three half-sphere models with radii of 0.1, 0.2, 0.5 m and top depths from 0.25 to 3.0 m, red, green, blue respectively.

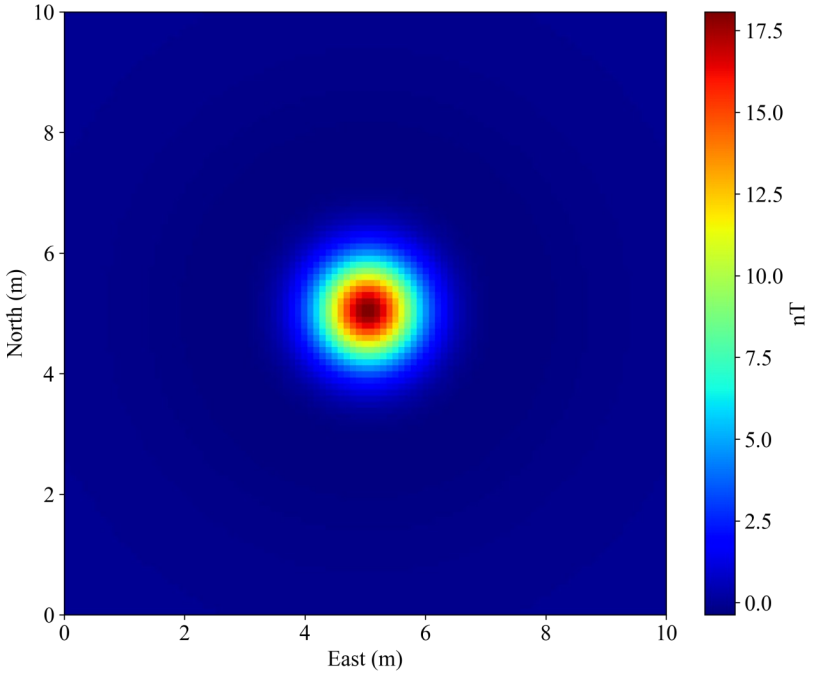

Figure 3.8: Magnetic Field – Half-sphere. Example half-sphere with radius 0.5 m, top depth 0.75 m, magnetic intensity 1.0 A/m, sensor height at 0.3 m above ground surface, magnetic inclination and declination at 90 and 0 degrees respectively.

Modeling Results

Model results were interpreted and evaluated in the Python programming environment. Depth estimates were plotted against the true model depths to determine errors between the depth techniques' estimates and the true depths to the top, center, and bottom of source bodies. Overestimates are represented by negative errors and underestimates are represented by positive errors. The modeling results are represented in the figures below which show significant over-plotting of results. Over-plotting is when two or more data points occur at the same location obscuring the visualization of data points. This is due to approximately 500 to 18,000 data points being plotted with some occurring in the identical locations because the depth of source bodies is consistent with varying source body geometries (e.g. there are multiple data points at every depth, one for each radius, width, or thickness). In these cases, the property represented by the color ramp is not the only size of that property at any one location on the graphic. It is simply the last to be plotted. Where discrepancies may arise due to over-plotting, data were visualized in other ways in the Python environment. However, due to limitations in graphic displays in a report, they are not included here.

Half-width Rules

The theoretical background for the half-width rules suggest the technique is most applicable for spherical point sources, although the method can be applied to non-spherical sources (Breiner 1999). Various authors note the method will provide an estimate of the depth or width of the source, whichever is greater (Aspinall et al. 2008; Tite 1972). Depending on the SI of the object, the technique may estimate the depth to the top, center, or bottom of the source body. For those reasons, the method was evaluated for all model source geometries to better understand how the technique performs in all situations. The technique was implemented on magnetic profile data. When source body geometries are not uniform, the shortest distance was

used for measurement (e.g. the width of a wall not the length). The technique could be implemented on 2D plan view data, either rasterized or contoured, however, higher data resolution is achieved via magnetic profiles. Spatial accuracy of the implemented technique is plus or minus 0.02 m. Furthermore, the technique was evaluated with sensor height at both 0.3 and 1.3 m above the ground.

Sphere. The half-width technique designated for spheres, FWHM, works extremely well in the model environment. Figure 3.9. shows the FWHM results at both 0.3 and 1.3 m sensor heights. The FWHM matches almost perfectly with the distance to the center of the respective source body. Minor deviations can be seen in the difference between the estimate distance and the true distance to the center of the source bodies, however, at the lower sensor height this error is under 0.02 m—the limit of the implementation. At the higher sensor, the majority of the data falls near the 0.02 m difference range, but error of up to 0.08 m is seen. The highest error is seen in cases of extremely low nT values (less than 0.05 nT). The excellent results further suggest the applicability of the technique for spherical source bodies. However, models indicate the FWHM performs poorly when estimating depths to the tops or bottoms of spherical bodies. Given the excellent performance of the method for sphere center-points, the top and bottom estimates are not presented as a viable depth estimator exists.

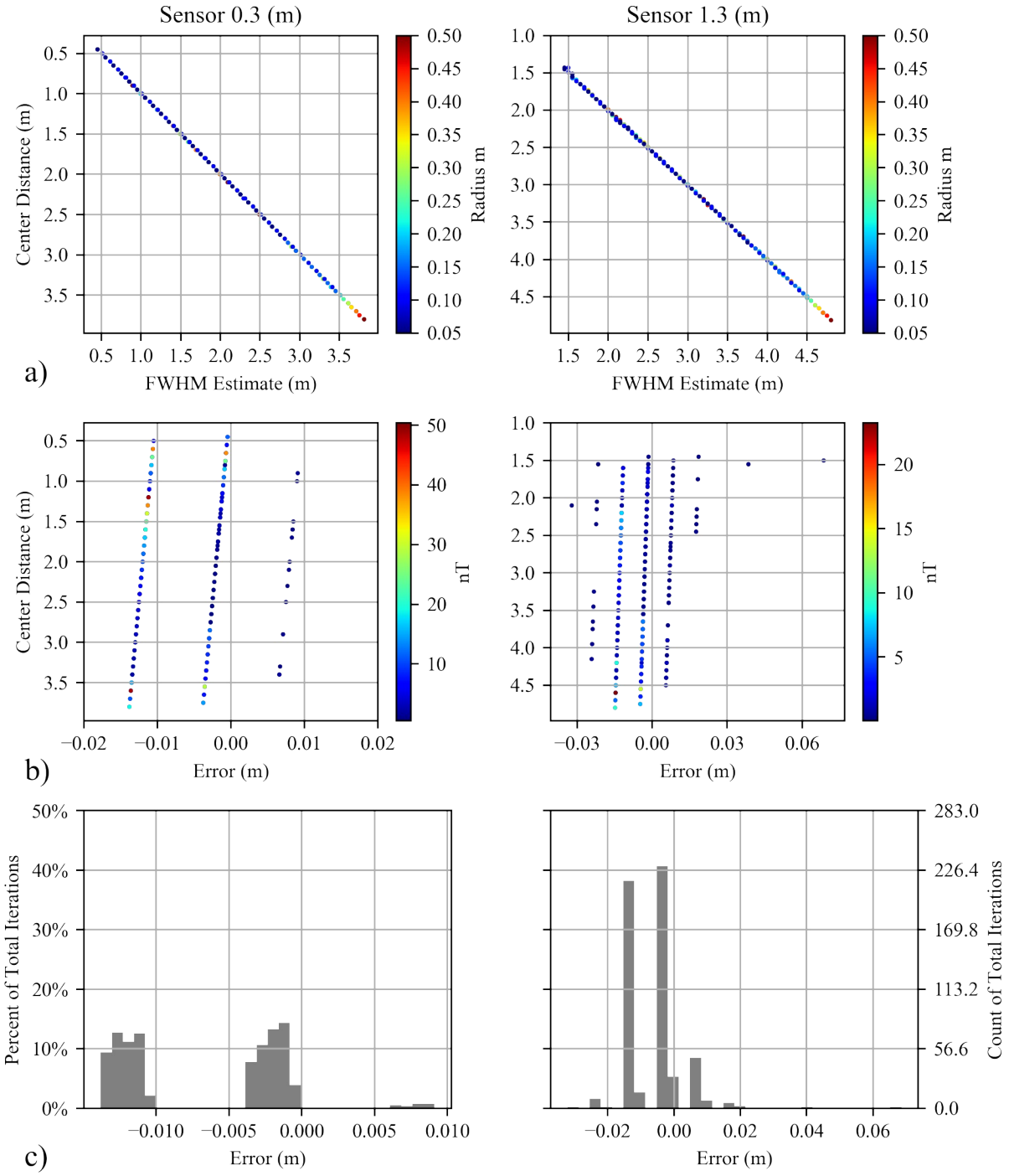

Figure 3.9. Full-width Half-maximum for spheres. a) Plots of the true center distance versus the FWHM estimated distance. b) Plots of the true center distance versus the error in the estimated distance. c) Histograms of error results. Note data over plotting in a and b of 566 data points.

Wall. One would expect that the half-width rule with SI=2 would be the most appropriate for the wall model. The models show a fairly linear relationship with the distance to the top and

center of source bodies, but the estimates range greatly, over approximately 1.5 m from their true values (Figures 3.10 and 3.11.). The error range does appear to lessen with greater depth. Given the mediocre results, SI=1 and SI=3 were also investigated. An SI=1 had worse results. Implementing SI=3 (FWHM) on rectilinear source bodies is less accurate than with spherical bodies with three trends evident in the results.

The FWHM roughly estimates the center distance of a source body with a significant amount of error ranging between plus or minus 0.35 and 0.23 m from the mean for lower heights and -0.005 and -0.08 m for higher heights (2 standard deviations), respectively (Figures 3.12c and 3.13c). The areas of largest error are seen at center distances less than 2 m. This result is more accurate and precise than SI=2.

Interestingly, the technique consistently overestimates the distance to the top of the source body (Figures 3.12 and 3.13). The error ranges from negligible to slightly over 1 m. The estimates are always more than the actual distance. Although there is a consistent over-estimation, this circumstance can be employed to estimate a maximum distance to the top of a source body. The FWHM estimate for linear bodies is always more than the distance to the top of the body by up to roughly 1 m. Despite the foregoing if the width of the body can be estimated, or constrained to some degree by a priori knowledge, one could better determine the exact distances to the top of the source body by adding approximately one half of the width to the distance estimate.

The FWHM technique does not appear to have any meaningful relationship with the bottoms of the source bodies.

There are approximately linear trends in the modeled data that may result because in the model all features are dipolar, whereas SI=2 is directly related to monopoles. In real-world data, walls commonly yield monopolar anomalies.

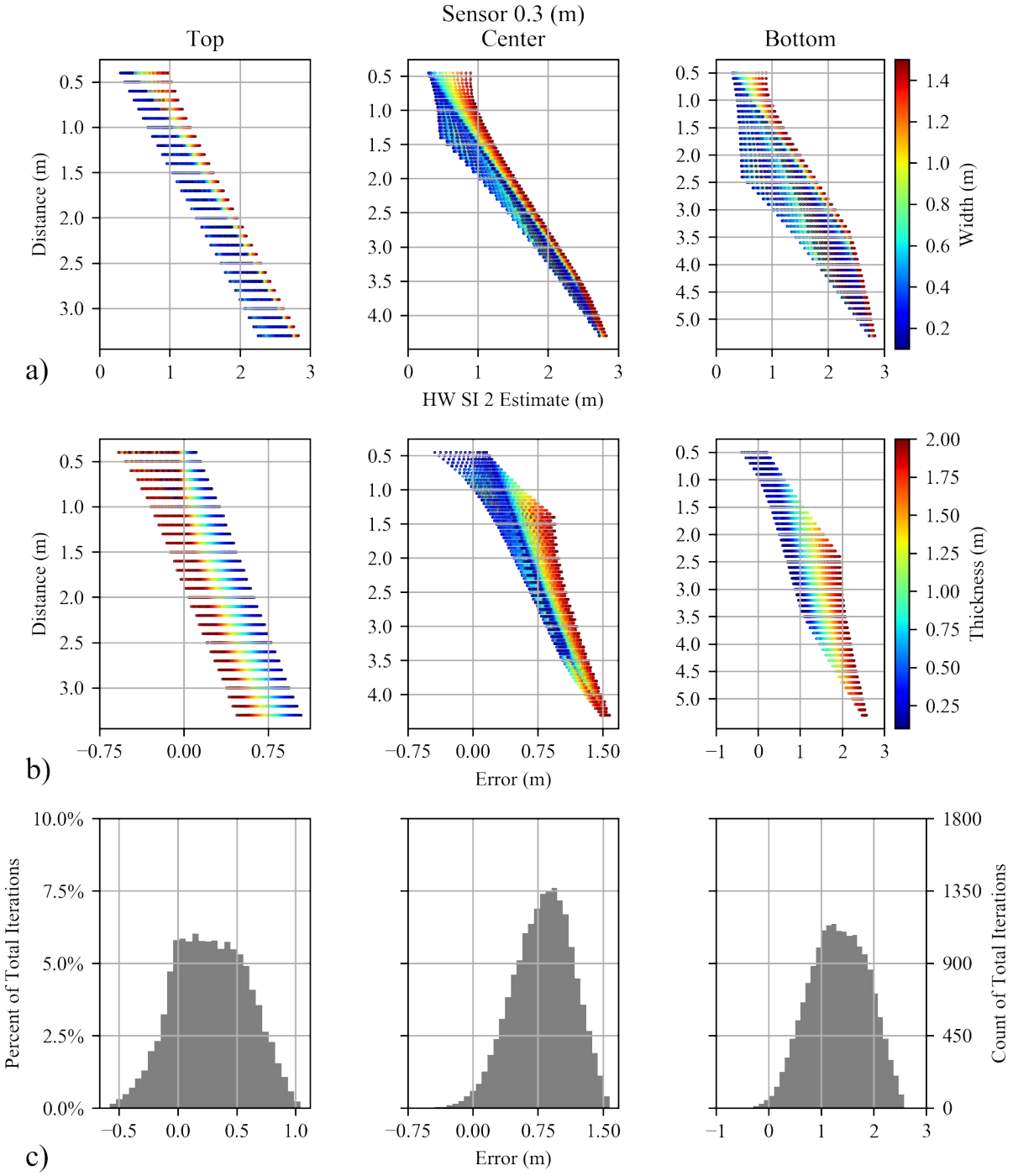

Figure 3.10. Half-width for walls with SI=2 and sensor height at 0.3 m. a) Plots of the true distance versus the HW estimated distance, b) Plots of the true distance versus the error in the estimated distance. c) Histograms of error results showing distinct positive biases (underestimated of depths). Note data over plotting in a and b of the 18,001 data points which causes obscuring of some widths and thicknesses.

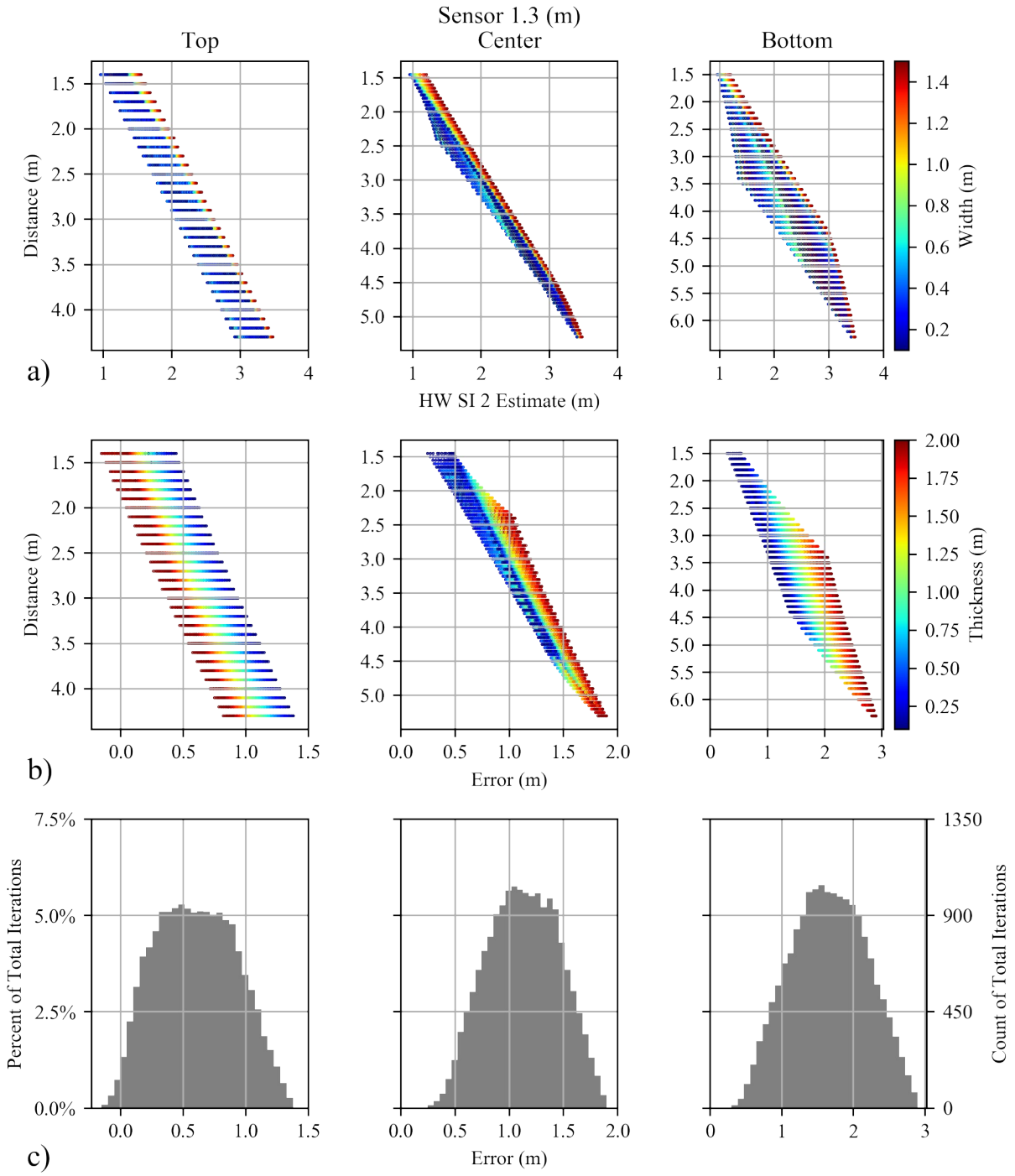

Figure 3.11. Half-width for walls with SI=2 and sensor height at 1.3m. a) Plots of the true distance versus the HW estimated distance. b) Plots of the true distance versus the error in the estimated distance. c) Histograms of error results showing distinct positive biases (underestimates of depth). Note data over plotting in a and b of the 18,001 data points which causes obscuring of some widths and thicknesses.

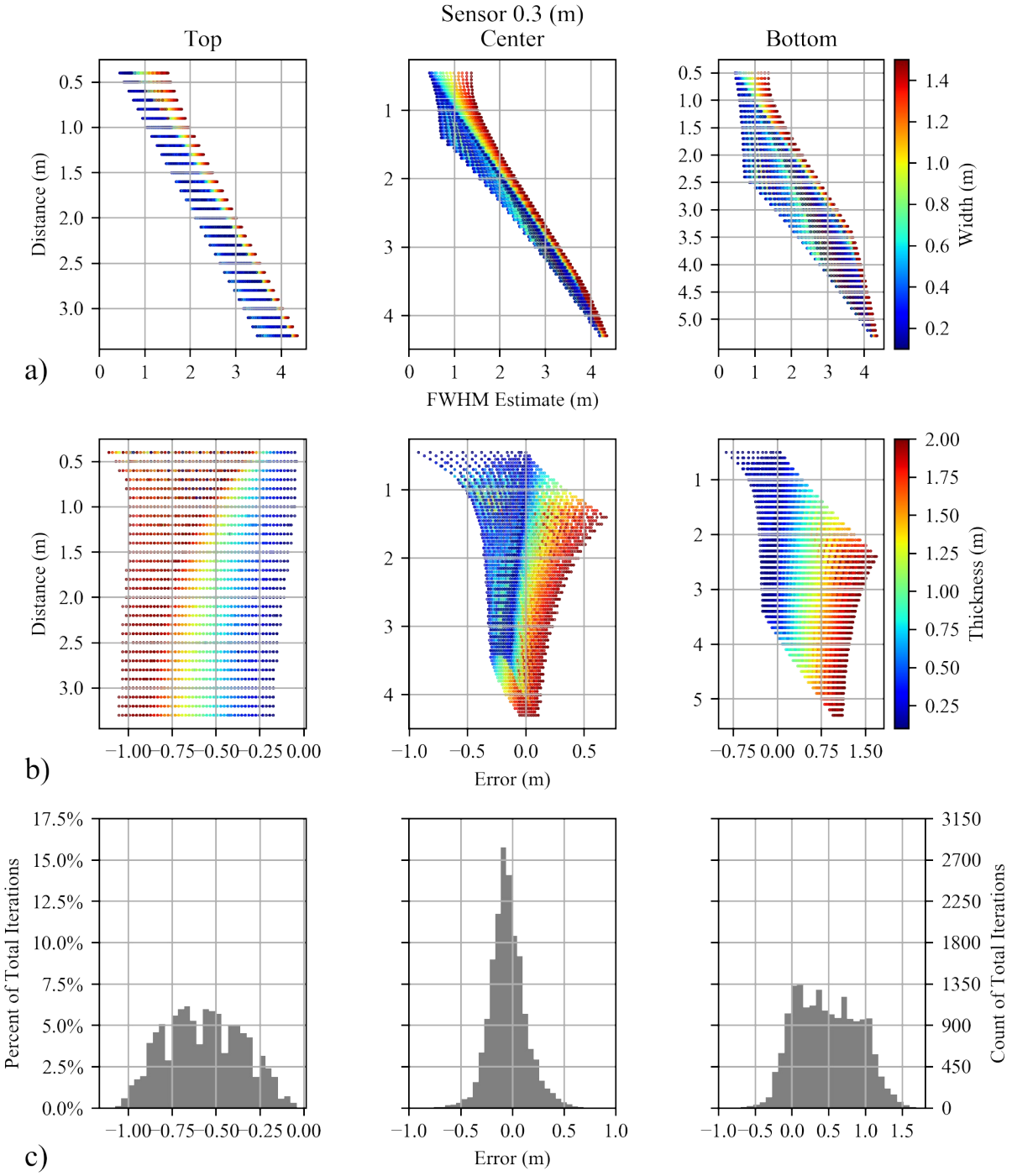

Figure 3.12. Full-width Half-maximum for walls with sensor height at 0.3 m. a) Plots of the true distance versus the FWHM estimated distance. b) Plots of the true distance versus the error in the estimated distance. c) Histograms of error results showing distinct positive biases for top depth (overestimated of depths). Note data over plotting in a and b of the 18,001 data points which causes obscuring of some widths and thicknesses.

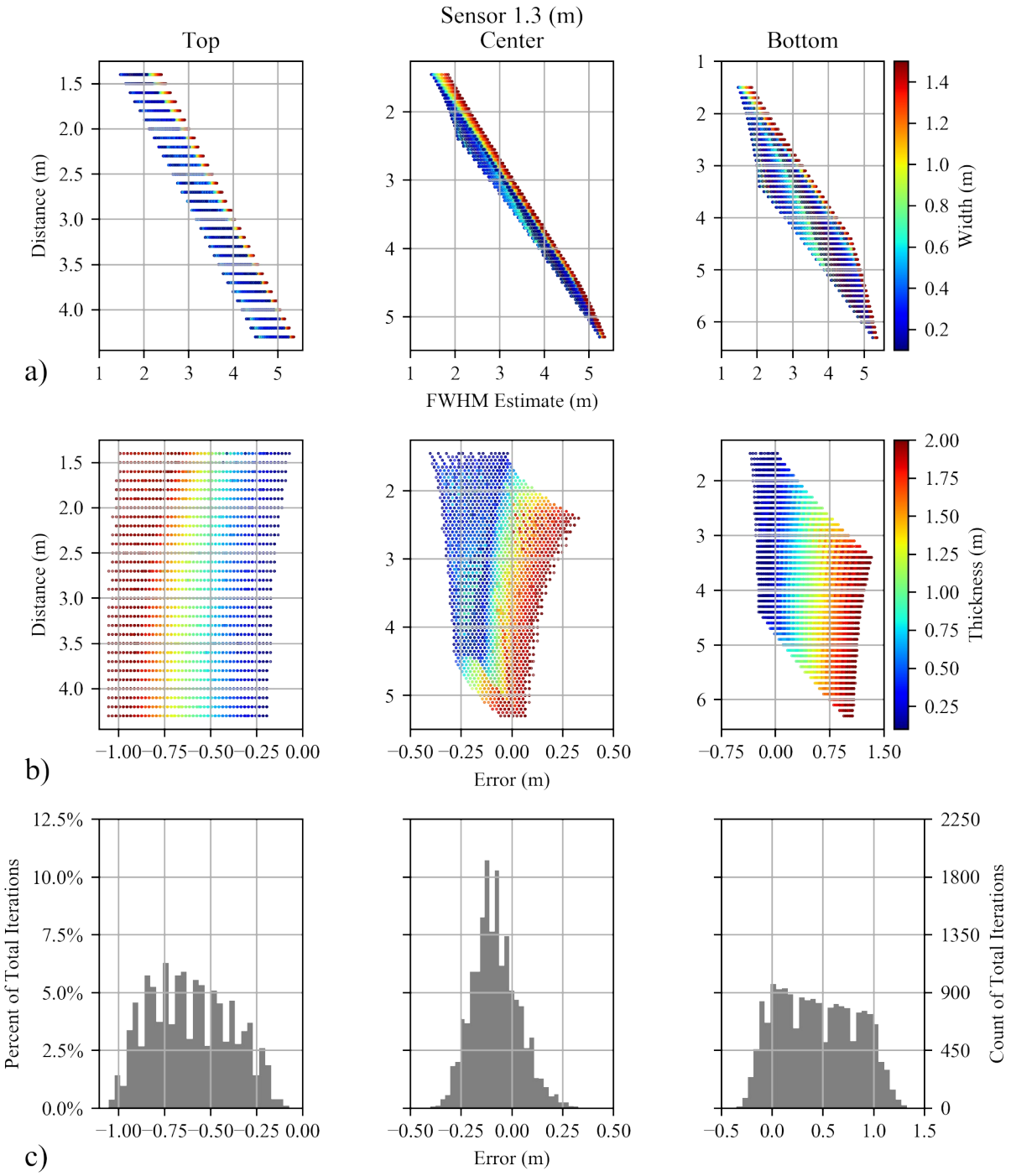

Figure 3.13. Full-width Half-maximum for walls with sensor height at 1.3m. a) Plots of the true distance versus the FWHM estimated distance. b) Plots of the true distance versus the error in the estimated distance. c) Histograms of error results showing distinct positive biases for top distance (underestimates of depth). Note data over plotting in a and b of the 18,001 data points which causes obscuring of some widths and thicknesses.

Floor. In theory one would expect floors to commonly be represented by single monopolar anomalies corresponding with SI=1. Yet, in the modeling outcome they are represented by either multiple (the corners) or a single (the middle) dipolar anomalies. This discrepancy, similar to that with the wall model, is likely an avenue of error when estimating depths. To provide a means to move forward and to remove data that could be problematic to the multi-height models, the floor models with multiple dipolar anomalies were filtered from the original data-set. Based on this filtering scheme, shallow data with smaller widths were removed. Additionally, it is clear that any HW rule will be affected by any long distances across an anomaly. This is evident in figures 3.14 and 3.15 as depth estimation error scales with the width of source bodies. An SI=1 gives the most consistent data, centered on 0 m error, but with an error range of 4 m. An SI=2 and SI=3 were also examined and results were considerably worse.

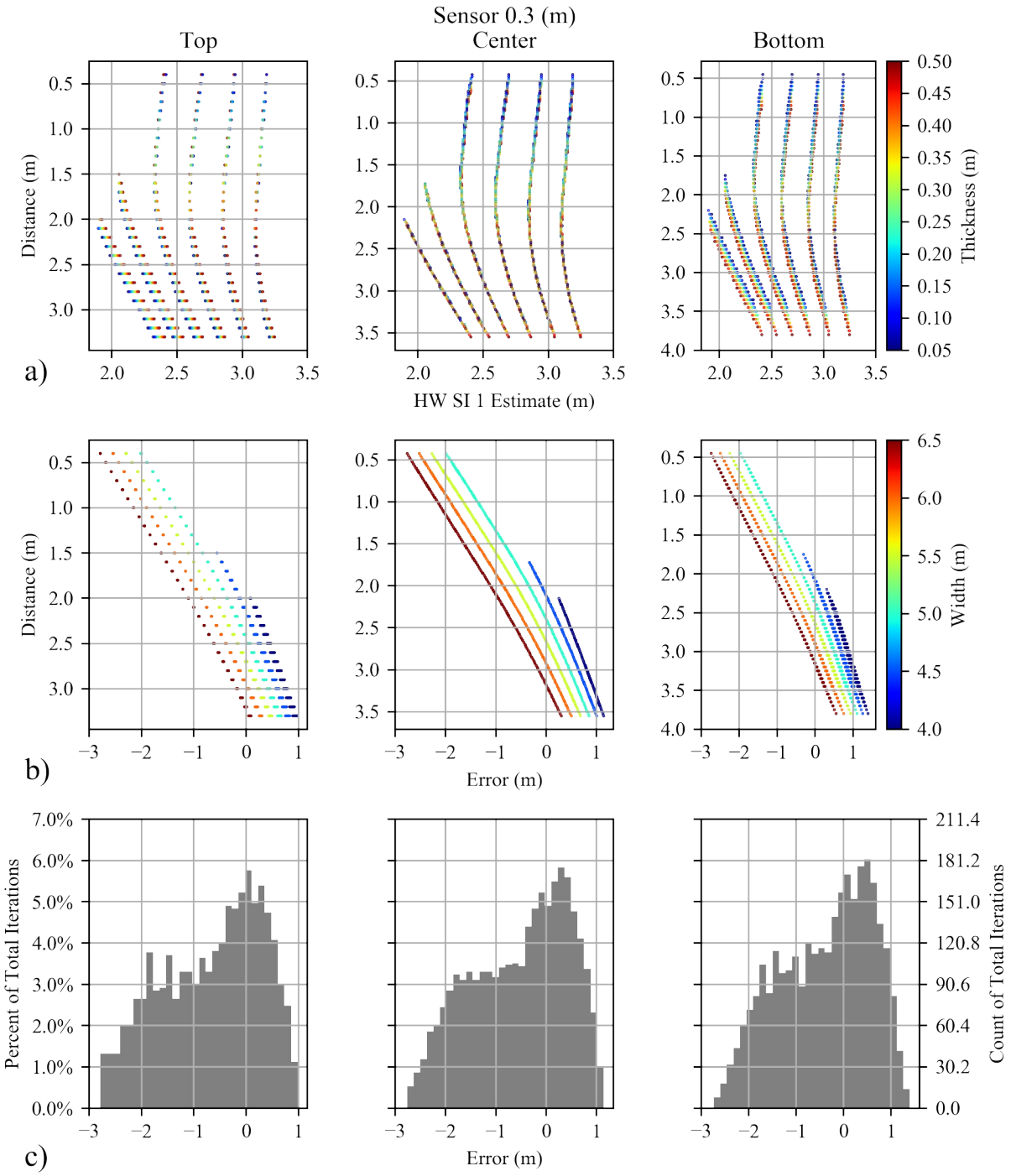

Figure 3.14. Half-width for floors with SI=1 and sensor height at 0.3 (m). a) Plots of the true distance versus the HW estimated distance. b) Plots of the true distance versus the error in the estimated distance. c) Histograms of error results. Note data over plotting in a and b of 3,020 data points.

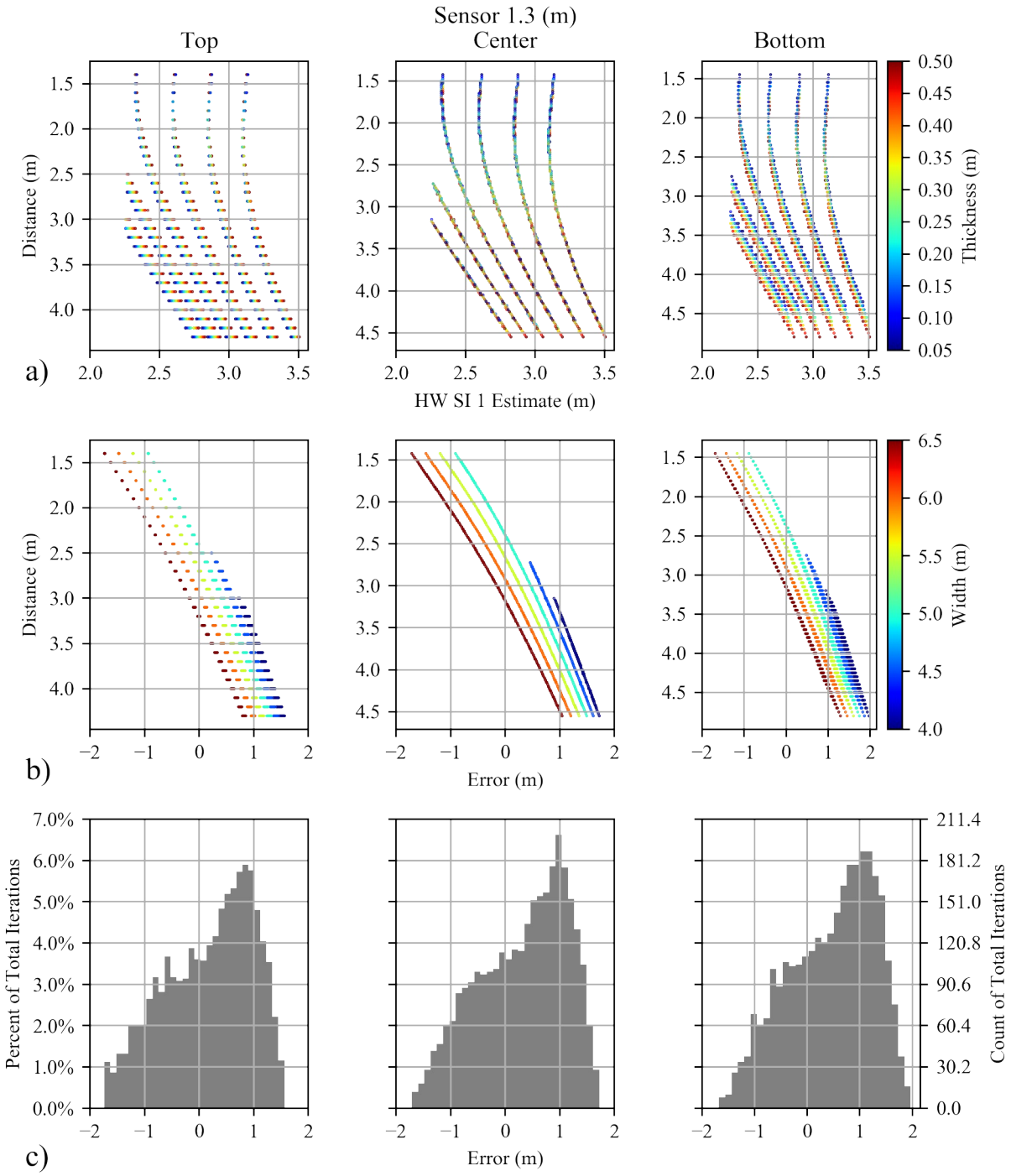

Figure 3.15. Half-width for floors with SI=1 and sensor height at 1.3 (m). a) Plots of the true distance versus the HW estimated distance. b) Plots of the true distance versus the error in the estimated distance. c) Histograms of error results. Note data over plotting in a and b of 3,020 data points.

Half-sphere. The half-width technique designated for spheres, FWHM, works extremely well on half-sphere models in the modeling environment. Figure 3.16 shows the FWHM results at both 0.3 and 1.3 m sensor heights. The FWHM matches almost perfectly with the distance to the center of the respective source body in most cases. Major deviations occur when the diameter of the half-sphere is greater than the distance to the center of the source body, while moderate deviations occur when the diameter of the half-sphere is greater than the distance to the top of the source body. When the diameter is smaller than the distance to the center of the source body only minor deviations occur. At both sensor heights, the majority of the data are overestimated by greater than 0.0 m and less than 0.06 m. The results further suggest the applicability of the technique for half-sphere source bodies and warrant no further investigation into other HW rules or potential estimations to the top or bottom of source bodies.

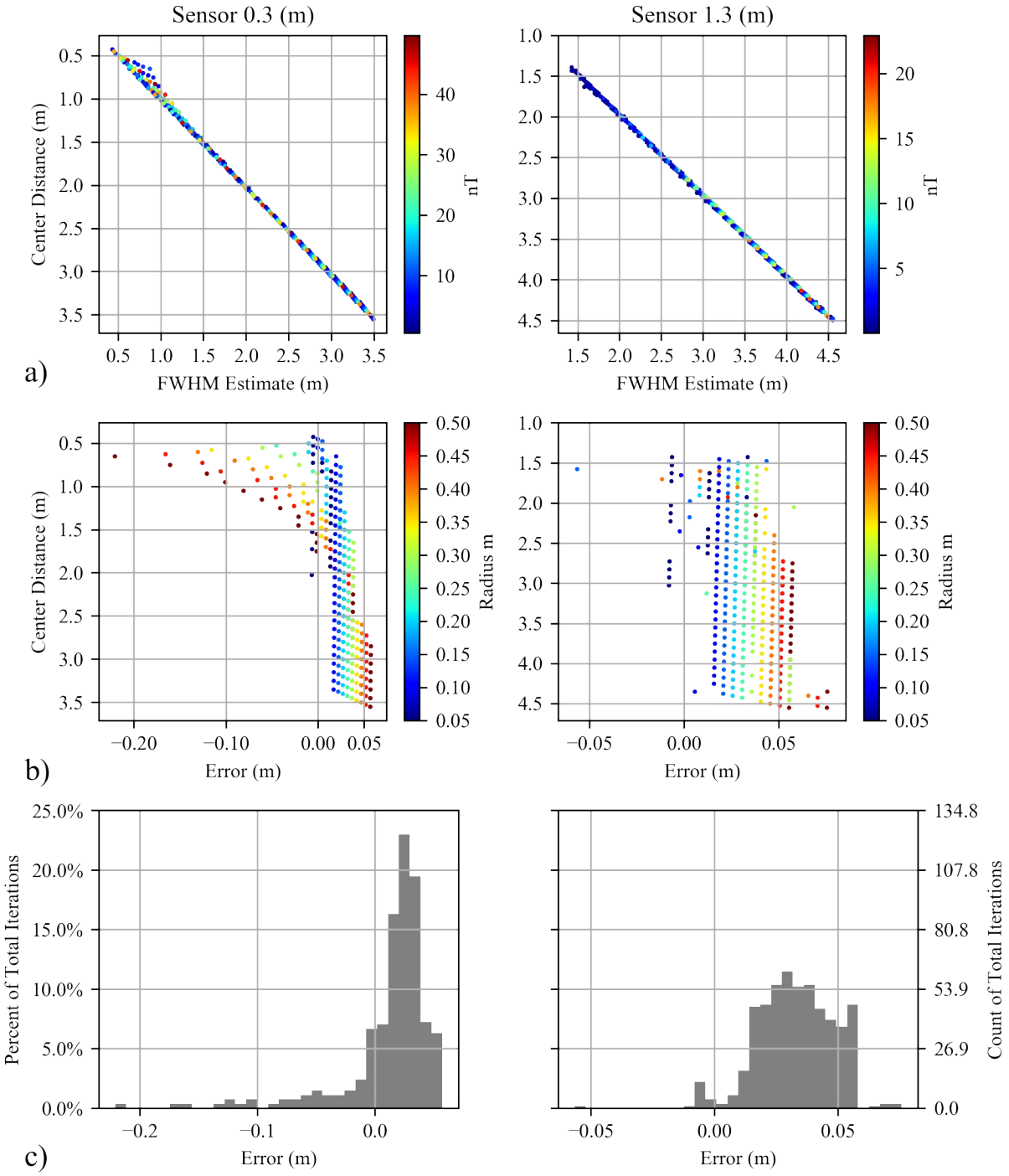

Figure 3.16. Full-width Half-maximum for half-spheres at sensor heights of 0.3 and 1.3 m. a) Plots of the true center distance versus the FWHM estimated distance. b) Plots of the true center distance versus the error in the estimated distance. c) Histograms of error results. Note data over plotting in a and b of 539 data points.

Multi-height

Although there is little information on applications of multi-height techniques in the literature, given the mathematical relationships it holds with other depth estimation techniques, it follows that the technique should work and vary with SIs and their respective source body geometries (Breiner 1999; Weymouth 1976, 2000). It is also unclear whether the technique will estimate the distance to the top, center, or bottom of the source body. Given this knowledge gap, the method was evaluated for all the prior source model geometries, to better understand how the technique performs in these situations. The technique was implemented on magnetic profile data. The technique could be implemented on rasterized 2D plan view data, but higher data resolution is achieved via magnetic profiles. Spatial accuracy of the implemented technique is +/- 0.02 m. Furthermore, the technique was evaluated with sensor heights at 0.3 and 1.3 m above the ground.

Sphere. Model data confirms the applicability of using the multi-height technique to estimate the distance to spherical bodies. When SI=3 is used, the technique properly estimates the distance to the center of the source bodies within 0.02 m—the limit of the implementation (Figure 3.17). Given the excellent performance of the method for sphere center-points, model results for other SIs are not presented as a viable depth estimator exists.

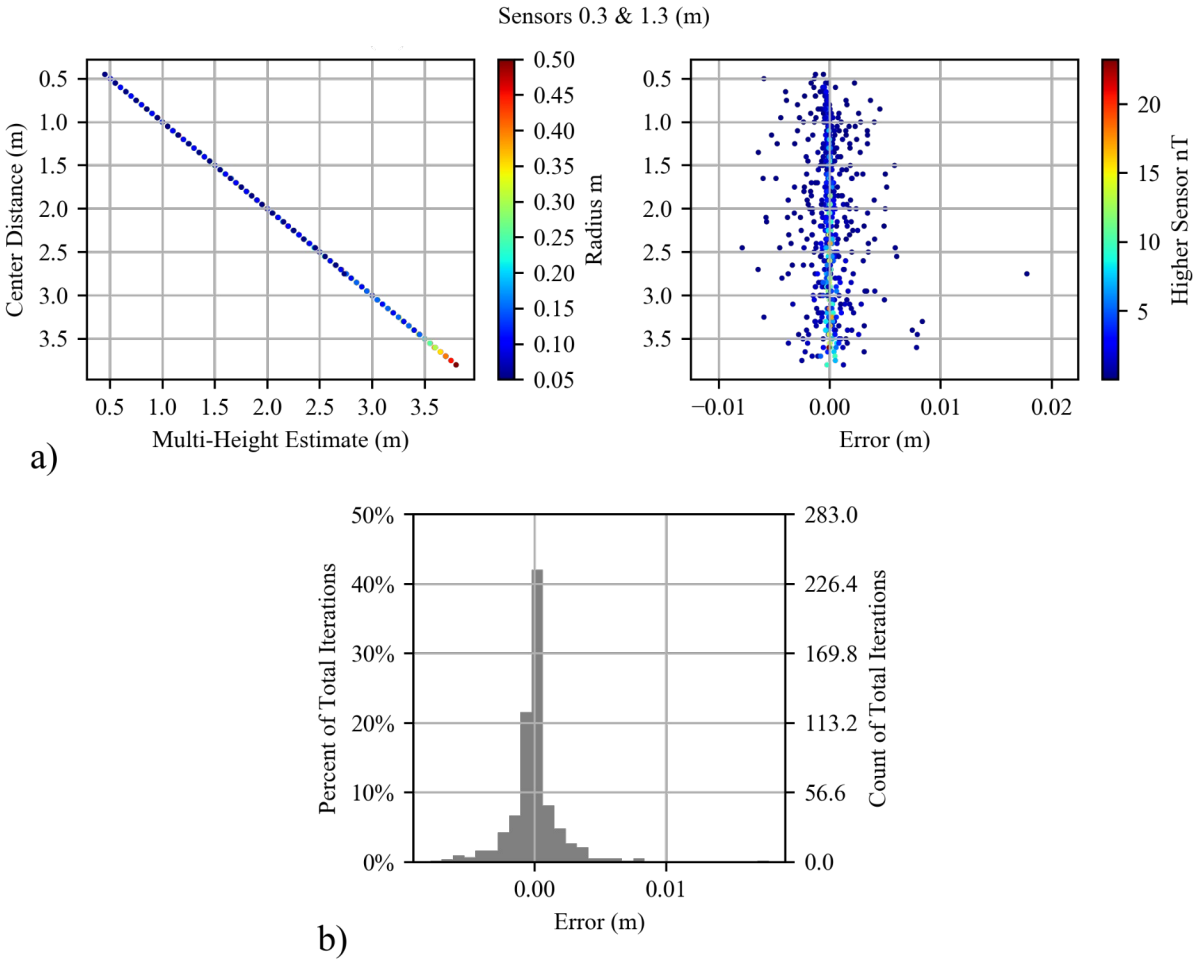

Figure 3.17. Multi-height for spheres with an SI= 3. Plots of the true center distance versus the multi-height estimated distance and versus the error in the estimated distance. b) Histograms of error results. Note data over plotting in a of 566 data points.

Wall. Again, one would expect that SI=2 would be the most appropriate for the wall model. This model shows a somewhat linear trend converging at depth for estimation to source body tops and centers, but estimates range greatly, over approximately 1.5 m (Figure 3.18). The error range does appear to lessen with depth. The SI=2 does not appear to have a meaningful relationship with the bottom of source bodies. Given the mediocre results, SI=1 and three were also investigated. An SI=1 had worse results. Similar to the half-width methods, the SI=3 on rectilinear source bodies is less accurate than with spherical bodies, but does have a substantial linear trend to the center of source bodies (Figure 3.19). The technique consistently

overestimates the center distance by approximately 1 m. The greatest variance is seen at depths above 2 m and lessens with increased depth. Similar to the FWHM, but less distinct, a relationship is seen between the multi-height estimate and the top distance to source bodies. A similar scheme may be applied here to give estimates of maximum depths to source bodies. Again, there are approximate linear trends in the modeled data that may result because in the model all features are dipolar, whereas the SI=2 is directly related to real-world monopoles.

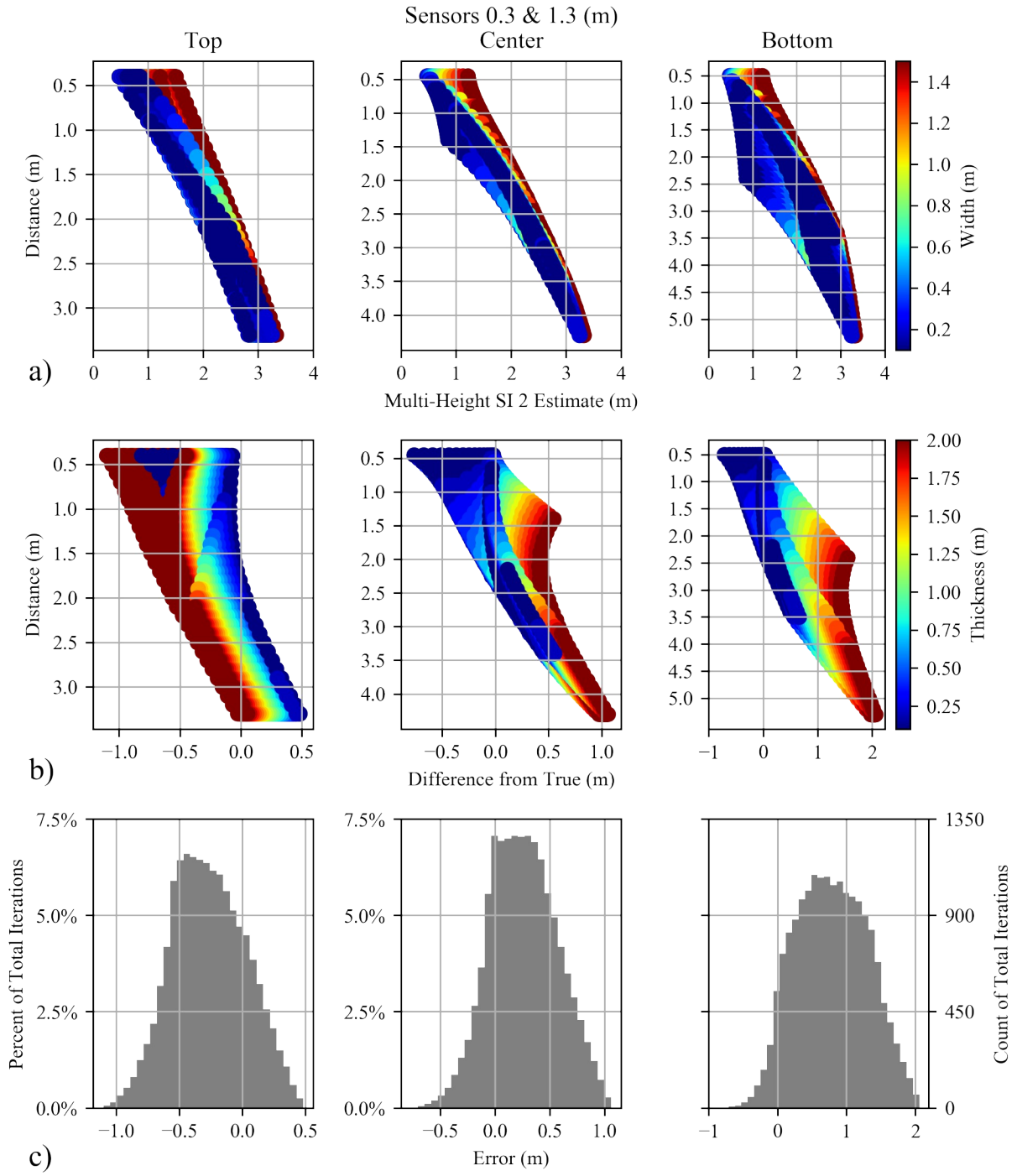

Figure 3.18. Multi-height for walls with an SI=2. a) Plots of the true distance versus the multi-height estimated distance. b) Plots of the true distance versus the error in the estimated distance. c) Histograms of error results showing distinct positive biases for top distance (overestimates of depth). Note data over plotting in a and b of the 18,001 data points which causes obscuring of some widths and thicknesses.

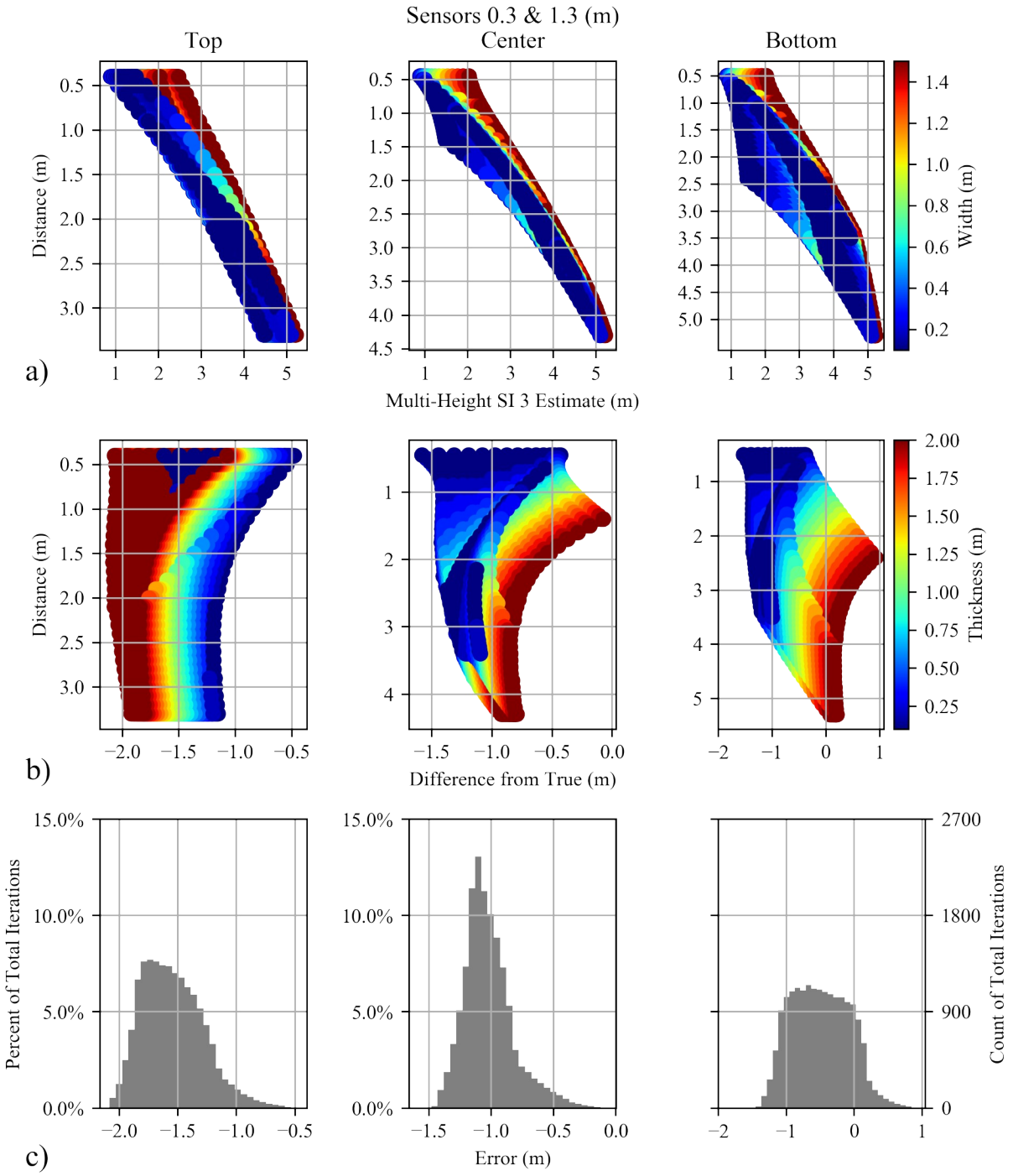

Figure 3.19. Multi-height for walls with an SI=3. a) Plots of the true distance versus the multi-height estimated distance. b) Plots of the true distance versus the error in the estimated distance. c) Histograms of error results showing distinct positive biases for top and center distance (overestimates of depth). Note data over plotting in a and b of the 18,001 data points which causes obscuring of some widths and thicknesses.

Floor. Given the multi-height data has been similar to the HW rules for other source bodies, it follows that the multi-height data for floors would be similar. However, multi-height data are not effected in the same way by the increased width of source bodies. The best results are for SI=1 (Figure 3.20). Although the range of error is large (3 m), when the model floors are constrained to widths of 5.5-6.5 m above a 2 m top depth (e.g. large floors at shallow depths), the data shows little error (plus or minus 0.25 m) to the top of the source body. Additionally, with these constraints, the data shows consistent under-estimation of the center depth by approximately 0.25 m. Although the technique does show applicability under these conditions, unfortunately the results are not more consistent for other source body geometries. Models using larger SIs yielded enormous errors with little trend, and therefore are not shown here.

Half-sphere. Model data confirms the applicability of using the multi-height technique to estimate the distance to half-spherical bodies (Figure 3.21). Similarly to the FWHM rule, major deviations occur when the diameter of the half-sphere is greater than the distance to the center of the source body, while moderate deviations occur when the diameter of the half-sphere is greater than the distance to the top of the source body. When the diameter is smaller than the distance to the center of the source body only minor deviations from true depths occur. The majority of the data are underestimated by less than 0.06 m. The results further suggest the applicability of the technique for half-sphere source bodies and warrant no further investigation into potential estimations to the top or bottom of source bodies.

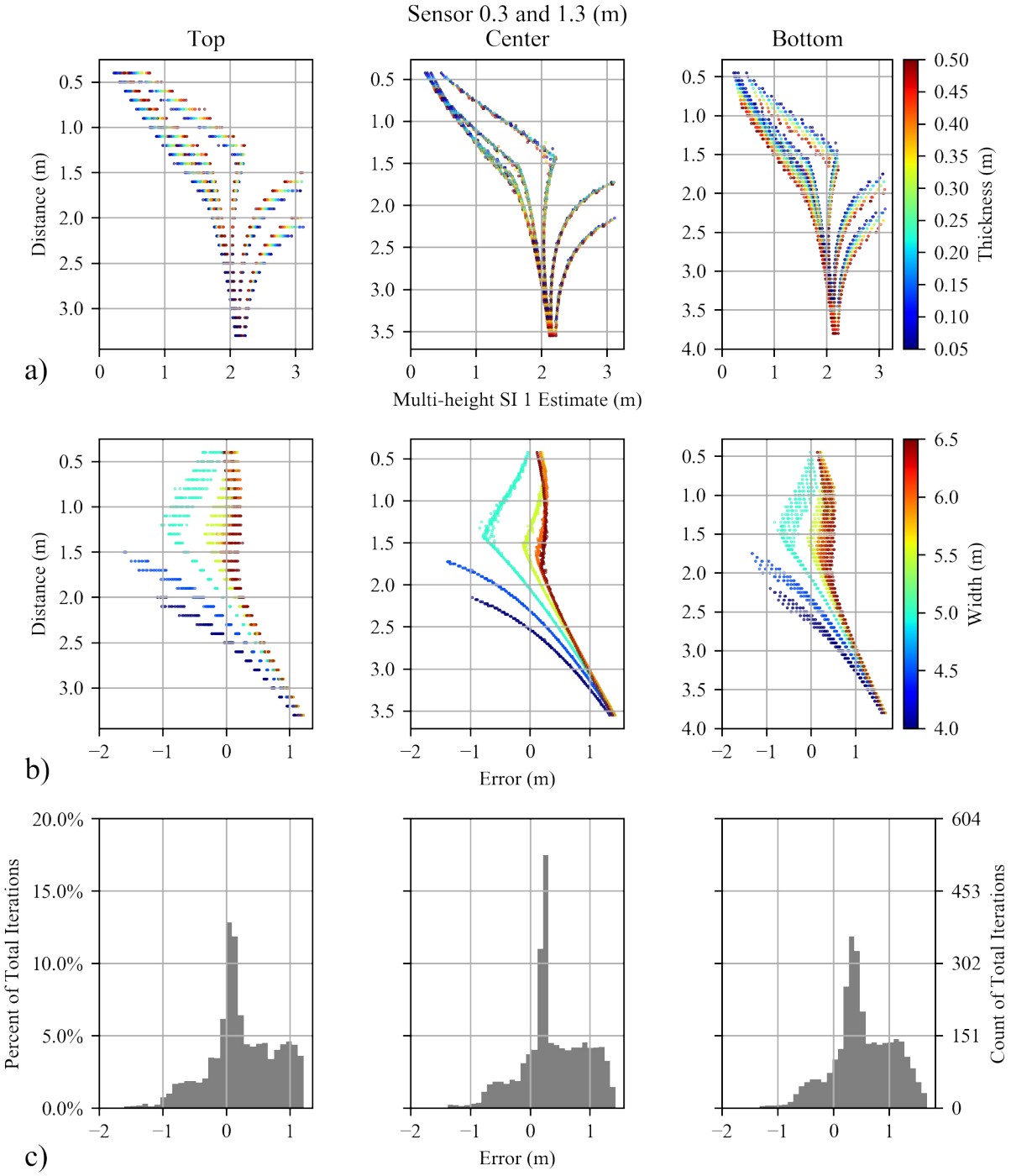

Figure 3.20. Multi-height for floors with an SI=1. a) Plots of the true distance versus the multi-height estimated distance. b) Plots of the true distance versus the error in the estimated distance. c) Histograms of error results. Note data over plotting in a and b of 3,020 data points.

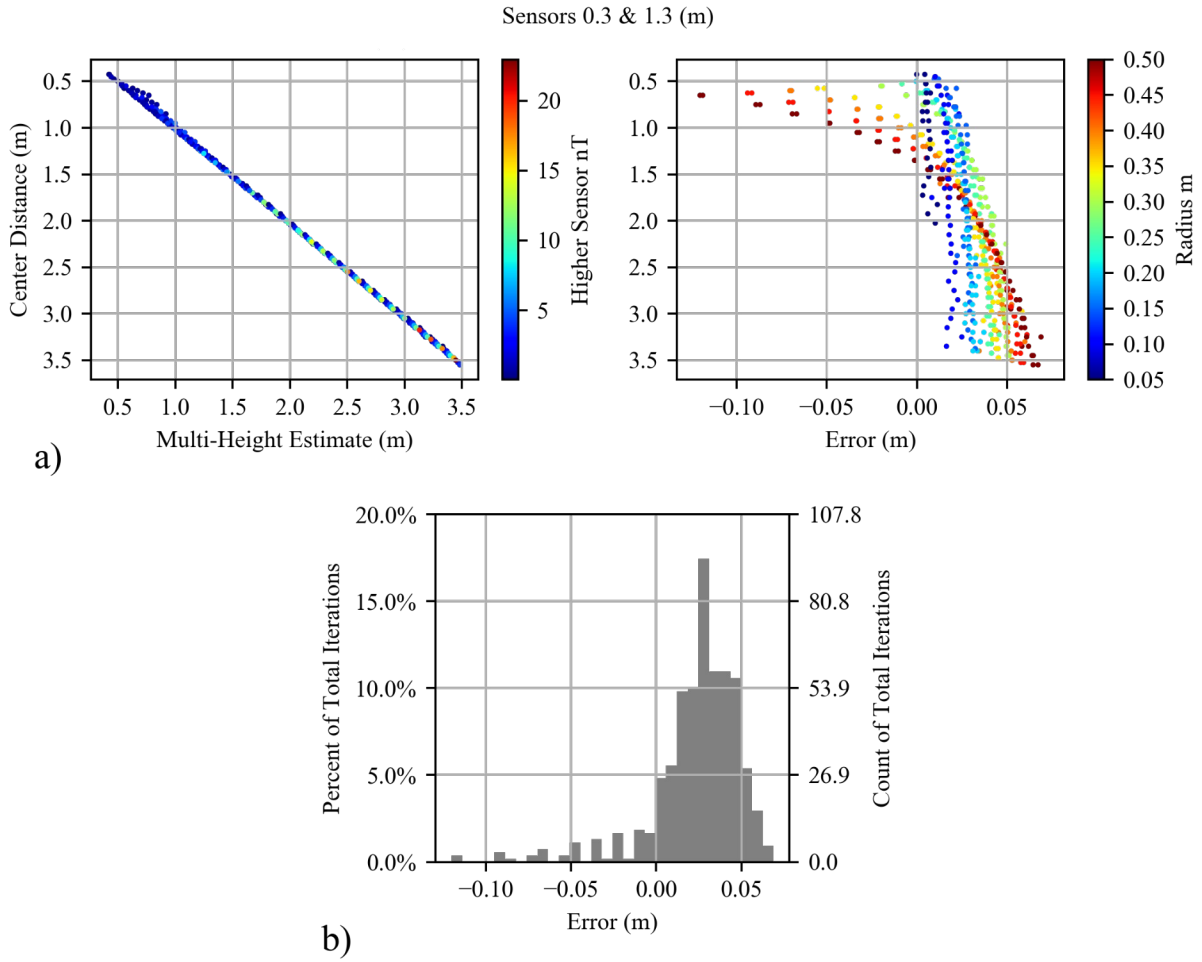

Figure 3.21. Multi-height for half-spheres with an SI=3. Plots of the true center distance versus the multi-height estimated distance and versus the error in the estimated distance. b) Histograms of error results. Note data over plotting in a of 539 data points.

Summary

Model results for sphere and half-spheres were very accurate for both FWHM and multi-height with SI=3. Error is introduced for half-spheres if source bodies are wider than they are deep. This follows as other authors suggest that FWHM should estimate to depth or width, whichever is larger (Aspinall et al. 2008; Tite 1972). However, when this occurs an accurate width is not estimated. Results for walls were more accurate and more precise with increased depth, but were especially inaccurate at shallow depths. This suggests the depth estimation techniques are only somewhat useful, but may be more applicable to other near-surface geophysics disciplines (e.g. environmental remediation, or shallow ore bodies) than archaeology.

Model floor results were most accurate at short distances (less than 2 m) to source bodies and with widths greater than 5.5 m.

Both wall and floor model results could have suffered from errors in modeling these source body types with single source geometries (e.g. one large rectangular prism) which resulted in single or multiple dipolar anomalies. Using multiple smaller rectangular prisms may reduce this affect and create anomalies more similar to observed monopoles. This would likely produce more realistic and accurate results.

Wall model results did provide an interesting avenue of further research. FWHM and to a lesser degree multi-height with SI=3 results suggest the maximum top distance can be estimated and constrained, which is extremely useful information when excavating or making relationships between features of different depths across an archaeological site.

Additionally, as linear trends are evident in many of the results, through further modeling, "correction factors" could potentially be created. Better results may potentially be gained by fitting trend lines to the model data and then correcting depth estimates based on these.

Foremost, modeling results show that the proposed multi-height technique is a viable and accurate technique for depth estimation to dipolar point source anomalies. This includes archaeological features like pits and hearths and non-archaeological targets found in environmental remediation and unexploded ordnance detection. It also provides moderate results for floor and wall like anomalies.

Chapter 4: Field Methods and Data Processing

Archaeo-geophysics Field Methods

Typical archaeo-geophysical surveys involve setting up a site grid system, composed of square blocks, with a total-station or GNSS system. During survey, stakes are placed at grid block corners and base lines are laid between them. Guide lines are laid between base lines to assist the surveyor walking in a straight line and on pace (Figure 4.1). Many handheld systems

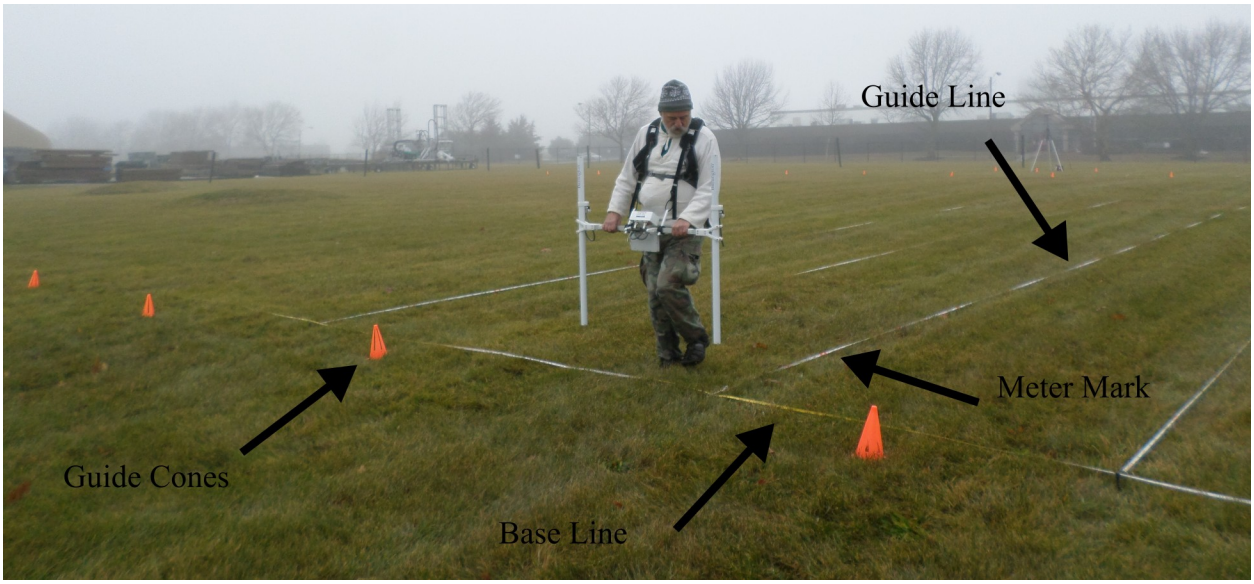

Figure 4.1. Field Survey. Surveying with a Bartington Grad601 and using base lines to demarcate grid boundaries, guide lines to survey straight and align pace with meter marks. Guide cones are in place for additional survey with a cart system.

use a metronome to relate readings to spatial location by requiring a surveyor to walk at a constant pace so that measurement locations can be aligned to real world locations. Some cart systems eliminate the need of the metronome by using a survey wheel to measure distance. This still requires the surveyor to walk in straight lines, so often guide lines or guide cones are used. Other cart systems use GNSS to log the precise location of all data points, and although this partially negates the use of guides, it is beneficial to data quality to still walk in extremely straight lines in order to avoid data gaps. Thus guide cones are commonly used for these surveys as well.

Project Specific Field Methods

Magnetometry

Due to prior work at all sites, a known GNSS datum was located upon arrival. This greatly facilitated the establishment or reestablishment of grid systems at each site and allowed for onsite "areas of interest" (AOIs) containing significant magnetic features to be targeted prior to arrival. This allowed surveys to be performed over smaller concentrated areas with features of interest instead of over broad swaths of area with few or no features of interest. Due to the small size of CATS and its concentration of features, the entire site was surveyed as one grid block.

At each site a Geometrics G-857 and a SENSYS MagBase were used as base stations 1.7 m above the ground (Figure 1.10). The G-857 collected readings at 3/second, the highest speed possible at the highest data resolution of 0.1 nT. The MagBase collected readings at 200/second with data resolution of less than 0.3 nT. Because of prior magnetometry or the known location of features at CATS, the base stations were placed in magnetically quite locations and separated by at least 10 m to avoid any electronic interference between the two instrument. At the beginning of each survey the G-857 clock was reset to UTC, due to minor clock drift.

Four cesium vapor sensors were mounted to a non-magnetic cart system at 0.25 m (x) and 0.5 m (z) spacing (Figure 1.11). This placed the sensors at 0.35 and 0.85 m above ground. The cart design allowed for a single survey to acquire data at two different heights. This helps to reduce the noise between data sets as all sensors are subjected to the same errors from cart vibration and ground conditions. One control unit was required for each pair of sensors. These units were then daisy-chained together with a cable so that the GNSS information and starting and stopping of lines were all synced together. Both instruments were set to the lowest sensitivity (0.05 nT) and highest rate of collection 10/second—unbeknownst to the author during data collection, one control unit was faulty and was unable to collect data at the highest rate of

collection, this caused one data set to be acquired at 5/second causing unfortunate data resolution discrepancies. At the beginning of each survey each control unit clock was reset to UTC, due to minor clock drift.

The SENSYS prototype had to be configured in two ways to acquire data at distinctly different heights (Figure 1.12). This required each grid block to be surveyed at one height, then the instrument to be reconfigured to the second height before the second survey could be performed. These different surveys certainly increased error between data sets. The cart system was subjected to different vibrations and movement during the surveys and minor variations in data locations were unavoidable. Additionally, in the lowest setting the sensor housing sat less than 10 cm off the ground, this caused increased error due to it hitting high grass and slightly raised areas of ground. The two configurations placed the sensors at approximately 0.0845 and 0.3845 m above the ground. Nine sensors were placed 0.2 m (x) apart and sensors collected readings at 200/second at less than 0.3 nT.

Because magnetic gradiometer data were previously acquired at the three real-world sites, it only needed to be collected at CATS. Both the SENSYS MXPDA and Bartington Grad601 were used to collect data at 0.25 m horizontal spacing. The SENSYS instrument allowed for full GNSS navigation. The Bartington instrument was not used in conjunction with GNSS, and therefore required grid blocks to be set up with baselines and guide lines.

Although GNSS was used to acquire data location and could be used for navigation on the SENSYS equipment, tape measures were set out as grid block baselines to better ensure data quality. At the end of each baseline plastic cones were placed to mark the center location of each cart swath (Figure 4.1). The purpose was two-fold—it allowed the surveyor to sight on a mark facilitating movement in straighter lines and provided an easy way to keep track of which lines were surveyed. This was especially helpful if GNSS data quality dropped below centimeter

accuracy—forcing the survey to stop in the middle of a survey line. The line start location could easily be relocated via the placement of the survey cones. Snow actually aided data collection at Runion, because the cart wheel tracks could simply be followed for the second survey.

Down-hole MS

Down-hole MS was performed at the three real-world sites. It was not performed at CATS because source body parameters are known and ground disturbances would damage the integrity of the site. After magnetometry survey, the JMC soil-probe was used to create a hole at each anomaly of interest. These were placed as close to the center or location of peak magnetism for each anomaly. In the case of larger broad anomalies, multiple holes were placed throughout the anomaly at localized maximums and dispersed for good coverage of the anomaly source. If rocks or impenetrable ground were encountered the probe was moved 15-25 cm away in cardinal directions until a suitable hole was made. In some instances punching a hole was not possible and those locations were abandoned. Holes were made between 1 and 2 m deep, as prior excavation information allowed the author to roughly calculate a likely maximum depth to potential archaeological features. The H sensor was zeroed at the beginning and end of each core hole in order to account for thermal drift. Data were collected at 0.02 m vertical spacing. Additionally, all soil probes were documented and soil was analyzed in the field for indications of an archaeological feature or geologic reason for increased magnetism (Figure 1.16 b).

Data Processing

This project employed a variety of data processing techniques in multiple software and custom scripts developed in the Python programming language. These included multiple equipment specific software needed to properly format and in some cases pre-process the data. These included MagMap (Geometrics), MagDrone and MonMx (SENSYS), Grad601 and Multisus (Bartington). Additionally, geophysics processing software (ArchaeoFusion) was

employed for some basic processes to Bartington gradiometer data. Geographic Information Systems (GIS) software in the form of QGIS was employed for data management and visualization. Finally, *fatiando a terra* and custom scripts developed in Python 2.7 and 3.8 were employed to perform some data pre-processing and all of the depth estimation techniques, as no current commercially or freely available software have the capabilities to perform all of these tasks. A combination of Voxler (Golden Software) and Python scripts were used to process, analyze, and visualize the down-hole MS data.

A minimalist approach was taken towards data processing. Although additional processing may produce a "better looking" image, the data values would be further affected by these processes and potentially skew depth estimation results. Data were processed as little as possible while still removing major noise and error from instrumentation. Pre-processing of the G-858 GNSS data included data filtering of erroneous locations and line smoothing. The SENSYS MXPDA system did not require GNSS processing. The SENSYS prototype GNSS data underwent line smoothing.

Magnetometry data underwent this general processing scheme:

60 Hz Filter – Most of the sensors (Bartington, Geometrics, and SENSYS MXPDA) undergo this filtering in the field through the data logging equipment, however, the SENSYS MagBase and prototype systems required this filtering post data acquisition. This filtering is performed to remove effects from ambient electromagnetic fields caused by overhead power lines.

Hampel Filter – The SENSYS MagBase system required further noise and spike reduction which was achieved through a Hampel filter. A Hampel filter is a moving window median absolute deviation (MAD) filter. The MAD is calculated by first finding the median of a data window. This first median is subtracted from the data within the

window and the absolute value of the new data is found. Next, the new median value is determined for this absolute data. This data is used to determine outliers. These outliers are then replaced with the median data value.

Differential Correction – Differential correction is performed by subtracting base station data from survey data. This simultaneously eliminates diurnal effects in the Earth's background magnetic field and regional deep geologic magnetic fields.

Zero Median Traverse (ZMT) – Due to directionality effects from surveys being performed in a zig-zag manner and minor differences between sensors, individual data lines could be drastically different from their neighbor, causing striping. A ZMT minimizes these effects by subtracting the median value of an entire line of data from each point within that line. This helps to balance the difference between different sensors and to reduce the effects of directionality.

Median Decimation – Given the high data sampling rate of the SENSYS prototype in one direction, these data were decimated in the in-line direction to remove any aliasing effects. This was achieved by performing a 20 sample moving window median filter. The median of 20 data points was taken and used as a new data point. This effectively resampled data to 20 samples per 0.1 m.

Interpolation with IDW – A standard inverse distance weight squared interpolation was used to produce a regular grid of data from the GNSS collected points. This interpolation technique weights data closer to the point of interpolation higher than those further away. This follows as data closer to the point should be more alike to that point than those further away. An elliptical search window, where the x radius was larger than the y radius, was used to further localize which raw data points were used in the interpolation.

Mean Profile Filter (MPF) – In the special case of extremely 'stripey' data a further destriping process was applied to the data. This is achieved by using a low-pass filter in the direction of stripes, to enhance them, then applying a high-pass filter perpendicular to the stripes to highlight them, creating a dataset of only stripes. This stripe data is then subtracted from the original dataset.

Reduction to the Pole (RTP) – Data were reduced to the pole to estimate as if the survey was performed at the pole. This processes simultaneously rectifies the data to be centered on the anomalous source body and adjust its magnitude to that if only vertical magnetization occurred.

Custom functions and scripts were created to perform depth estimation procedures in Python, see Appendix E. The half-width techniques were performed by locating the maximum data point within a data window. A line is then passed through this maximum point to determine the full-width at half-maximum. The line is rotated every one degree for a total of 180 lines covering 360 degrees. If the line does not pass through the half-maximum on both sides of the maximum point, it is discarded from evaluation. The multi-height technique was performed by locating the maximum data point of a lower height data window. The location of this maximum point is then used for the higher data set. The two data values and their respective heights above the ground surface are then used in Equation 2.7 and a result is returned with a desired SI value.

Magnetic Susceptibility data required little processing. They were multiplied by a constant factor of (1.739) to assist in correcting for sensitivity differences due to hole size, but otherwise underwent no further data processing (Bartington Instruments 2010).

Chapter 5: Field Results

The field results are first presented by field site and then combined to show overall trends within the data set. For each of the four field sites, CATS, Woolsey, Pile Mound, and Runion, an overview of the survey parameters and any field condition issues are discussed. A complete magnetic map is presented from the most representative survey with the location of down-hole MS cores, where applicable. Additional magnetic surveys and more detailed maps of individual features can be found in Appendix (B). Magnetic susceptibility core locations, the respective depth and maximum MS values, and the corresponding maximum magnetometry values can be found in Appendix (D). A description of each features' magnetic anomalies, their corresponding down-hole MS data, and the depth estimates are presented. The effectiveness of the depth estimation is discussed in regards to the field data. These individual and site level results are then aggregated and presented as a whole in the summary.

In total, six depth estimates were made for every structural index that was chosen to be investigated. The combined use of each sensor type's (SENSYS and G-858) lower and higher surveys were evaluated by equation 2.7 with SI=3 and SI=2 which created two MH estimates per SI. Although HW minimum, median, and maximum estimates were calculated for all anomalies, this research has shown the minimum estimate to be the most accurate (see Appendix B), and therefore, others are not shown. This makes four HW estimates per feature, where applicable. The HW minimum was taken for the SENSYS lower (0.0845 m) and higher (0.3845 m) surveys and the G-858 lower (0.35 m) and higher (0.85 m) surveys. SI=3 and SI=2 were analyzed as previous modeling data show SI=3 should be the most accurate for point-sources, but other researchers have suggested SI=2 for archaeological features (Desvignes et al. 1999).

A continued pattern throughout the results is that magnetic anomalies are wider than the distance from the source-body center to the magnetic sensor. This is important because the

computer modeling data show when a point-source is wider than the distance from the source-body center to the sensor, an overestimation of the distance will occur. So although modeling data show good results for the sphere and half-sphere models, real-world parameters may make them unreliable in practice. In the model data, this more greatly effects the HW rule than the MH technique.

CATS

Results include only a description of the magnetometry surveys and of the depth estimation model, as no down-hole MS was performed to get at depths to anomalous bodies in order to preserve the integrity of the test facility. Four different magnetometer systems were used at CATS. Gradiometer surveys were not used for depth estimation. Due to the low height of the SENSYS prototype error was introduced while surveying over the mound. This occurred because the cart design has a solid sensor housing 1.8 m wide with a wheel span of approximately 0.8 m centered on the cart. When moving the cart near the edge of the mound, sides of the cart would dig into the ground. When the cart was atop the mound center, the sensors were actually different distances from the ground surface due to the rigidness of the sensor housing. Otherwise, field conditions presented no impediments to data quality.

Magnetometry

No prior magnetometry data were available for the site, so in addition to the total field surveys, two vertical component gradient surveys were performed for comparison. A known GNSS datum was put in place at the site prior to arrival, but it did not coincide with the original datum at the site. This created some minor discrepancies when aligning the new data to the original site layout (Figure 1.3), but correspondence between the two datasets is clear. The published layout (Figure 1.3) has obvious errors in relation to where features were originally placed and no updated map with the additional mounds and ditch complex modifications has

been published. Feature E is interpreted in the magnetic maps from internal CERL documents, but it is in a different location than the published map.

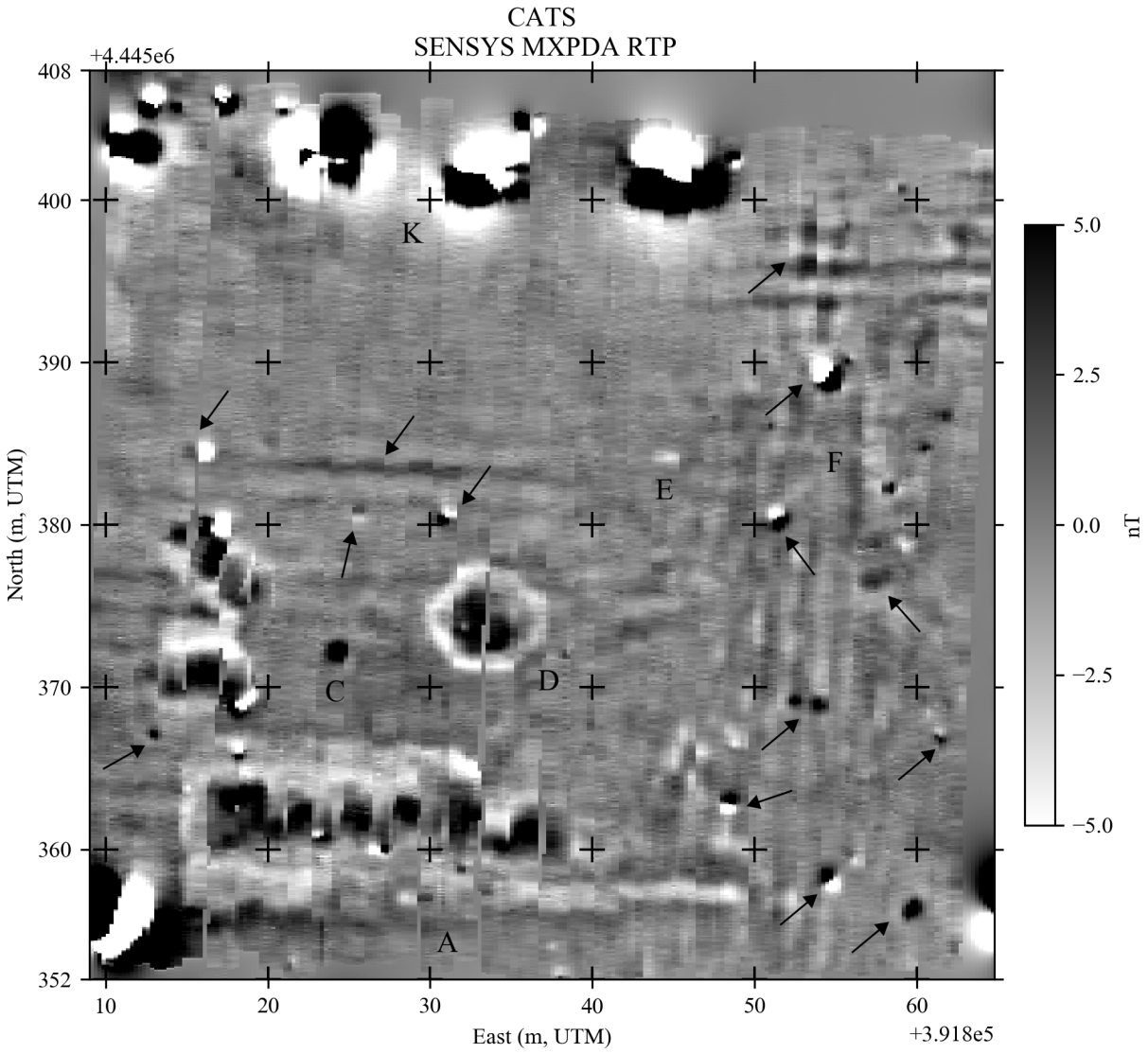

Figure 5.1. CATS SENSYS MXPDA. Processed MXPDA data in UTM coordinates. Detected known features are labeled A-K. Unknown features are highlighted with arrows.

An approximately 55 x 55 m area was surveyed with the SENSYS MXPDA at 0.25 x 0.1 m resolution (Figure 5.1). This area encompassed the inside of the wood posts demarcating the site (Figure 1.2). The outline of features A and D are clearly visible along with some internal components. Features C and E are clearly defined. The outline of feature F is faint along with

some clear internal features, however, these internal features do not clearly align with the location of known internal features (Figure 1.1). Feature K is present in the data, however not in the locations designated (Figure 1.1). No indication of features B, G, H, I, or J are visible, but should be found within the survey area. The two undocumented mounds and potential internal features are clearly defined in the data. Multiple undefined anomalies are present in the data.

A subset of this area, approximately 40 x 30 m, was surveyed with the Bartington Grad601, SENSYS prototype, and G-858. Both total field instruments were used to survey at lower and higher heights. All additional surveys delineated the same magnetic features as figure 5.1.

Depth Estimation of Features

The author hoped to have full records of all the "archaeological" features constructed at the site, but some features were either never fully recorded or records have been lost. Unfortunately, this is the case for the two usable features (C and E). Feature C is a roasting pit while E is a pig burial. Depth estimates for features were performed on the prototype and G-858 datasets. Due to equipment malfunction, feature C is not present in the G-858 higher survey, limiting some depth estimates. Two photographs of feature C during construction are available (Figure 5.2). No clear record of feature E is available. The following depth estimation tables are labeled as follows: SI (Structural Index), HW (half-width), MH (multi-height), min (minimum), med (median), max (maximum).

Feature C is defined as a clear circular anomaly approximately 1 m in diameter in the SENSYS data. The G-858 lower data show a somewhat offset anomaly approximately 1.5 m in diameter. From the photographs in the CERL archive, the author places reasonable feature dimensions to around 1 m diameter and slightly less than 1 m, perhaps 0.6-0.7 m to the burnt material in the pit, the anomalous source (Figure 5.2). Depth estimates are similar from both

datasets and fairly consistent estimates are produced between the HW minimum, median, and maximum (Table 5.1). The SI=3 half-width minimum and multi-height depth estimates in table 5.1 appear reasonable. As expected the estimates decrease in size when using a smaller SI, see table 2.1. Additionally, the HW median value falls between the HW minimum and HW maximum estimates. Generally speaking, the lower the survey height the larger the minimum depth estimate while higher surveys produce large maximum estimates. Without further details, no definitive accuracy assessment can be made.

a)  b) 

Figure 5.2. Construction Photographs of CATS Feature C. a) Top down view of pit. b) Oblique view of pit. Images courtesy of CERL, USA 2018.

Table 5.1. CATS Feature C Depth Estimates.

Survey	SI	HW Min	HW Med	HW Max	MH
SENSYS Lower	3	0.90	0.97	1.09	
SENSYS Higher	3	0.77	1.04	1.27	
SENSYS Both	3				0.78
G-858 Lower	3	0.83	0.95	1.17	
G-858 Higher	3	N/A	N/A	N/A	
G-858 Both	3				N/A
SENSYS Lower	2	0.55	0.60	0.68	
SENSYS Higher	2	0.36	0.54	0.69	
SENSYS Both	2				0.45
G-858 Lower	2	0.42	0.50	0.64	
G-858 Higher	2	N/A	N/A	N/A	
G-858 Both	2				N/A

The lower prototype data around feature E show a clear elliptical, but negative anomaly approximately 0.5 x 2 m while the higher data are extremely dispersed. The G-858 data around feature E show a clear anomaly of amorphous shape approximately 1 x 1.5 m. Feature E is a negative anomaly so, depth estimates were performed on the minimum instead of maximum data. Depth estimates are not similar between both datasets (Table 5.2). This is likely due to the dispersed nature of the anomaly in both higher height surveys as they are barely detectable and scrambled. Given the low nT values and non-definitive anomalies in both higher height surveys, the author suspects feature E is rather shallow. Additionally, given the oblong nature of the anomaly an appropriate depth estimation is likely made from the minimum HW estimate. For the prototype and G-858 lower survey these seem reasonable, but without further details no definitive accuracy assessment can be made. The negative depth estimates for the higher surveys make sense given their poor quality and low nT values. Assuming a true SI=3 for the feature and

its likely shallow depth, using lower SIs would produce erroneous results as mathematically the estimate must decrease with a smaller SI.

Table 5.2. CATS Feature E Depth Estimates.

Survey	SI	HW Min	HW Med	HW Max	MH
SENSYS Lower	3	0.38	0.59	1.21	
SENSYS Higher	3	0.25	0.36	0.85	
SENSYS Both	3				0.71
G-858 Lower	3	0.39	0.53	0.77	
G-858 Higher	3	-0.22	-0.14	0.39	
G-858 Both	3				0.10
SENSYS Lower	2	0.22	0.35	0.75	
SENSYS Higher	2	0.03	0.10	0.42	
SENSYS Both	2				0.40
G-858 Lower	2	0.13	0.22	0.38	
G-858 Higher	2	-0.44	-0.39	-0.04	
G-858 Both	2				-0.11

Site Summary

Unfortunately, due to the lack of firm depth information for the features tested more cannot be done with data. The depth estimates from the site seem reasonable, but it appears the work at this site was unsuccessful in regards to studying depth estimation. Future researchers may benefit from the multiple magnetic maps of the site.

Woolsey

Results for this site includes magnetometry surveys, down-hole MS for determination of actual depths to anomalous bodies, and depth estimation through modeling. Two different magnetometer systems were used at Woolsey, the Geometrics G-858 and SENSYS prototype. Due to instrument error, the G-857 base station was used to differentially correct both the G-858 and prototype data. Two 20 x 20 m grid blocks were selected for survey encompassing nine

magnetic anomalies of interest. The vegetation in the survey area was cut immediately prior to survey. This created a fairly smooth area, but the prototype at the lowest setting did snag on vegetation in some areas likely introducing minor error. Nine down-hole MS logs were taken, denoted as A-I. Prior gradiometry survey data were used to guide data collection. A known GNSS datum was in place at the site before survey began. This allowed alignment between a prior gradiometer survey and the current survey.

Magnetometry

Grid blocks one and two (G1 and G2) each encompass a 20 x 20 m area surveyed at 0.2 x 0.1 m and 0.25 x 0.1 m resolution for prototype and G-858 data, respectively. G1 prototype data overall appear of good quality with little to no data defects (Figure 5.3a). All five features (A-E) are well-defined in both lower and higher datasets. The G1 G-858 data were extremely stripey and underwent further data processing with a MPF. Even with this process, data appear somewhat 'speckled' with possible high frequency noise (see Appendix). All features are distinguishable with similar dimensions to the prototype counterparts. In the G-858 data features C, D, and especially E are near or encompassed by noise. This degrades how well they are defined, which may result in poor depth estimates.

Overall G2 prototype data are of good quality with little noise (Figure 5.3b). All four features are well-defined in datasets from both lower and higher instrument configurations. The G2 G-858 data again had severe striping and underwent MPF (see Appendix). Some minor high frequency noise is seen in the lower dataset. All four features (F-I) are present in both datasets but are not as well-defined as the prototype data.

Down-hole MS

Nine magnetic anomalies were chosen for depth estimation testing, A-I, (Figures 5.4 and 5.5). The location of MS cores was based on the previously collected gradiometry data. The

location of all G1 cores appear well-centered with the exception of feature E in the G-858 data (see Appendix). Anomaly F is most certainly dipolar and so the MS core may be ill placed as it is centered in the positive portion of the anomaly while the actual locus of it is likely between the two poles (Figure 5.3b). Two G2 MS cores (G and I) are on the edge of anomalies and are not ideally located for best results. No other issues are present with the down-hole MS data. The MS data can be categorized into two types at this site: a well-defined single peak or a larger area of higher MS.

Four of the logs (A-D) show clear data peaks and well-defined magnetic features more similar to point-sources. In these cases, the MS maximum locations are likely good proxies for the center depth of the magnetic features (Figure 5.4). This is because the areas of up and down-slope leading to the peaks are approximately the same distance. Feature D does have a slightly longer up-slope than down, but given the much higher MS at the peak, the deeper center depth is likely warranted.

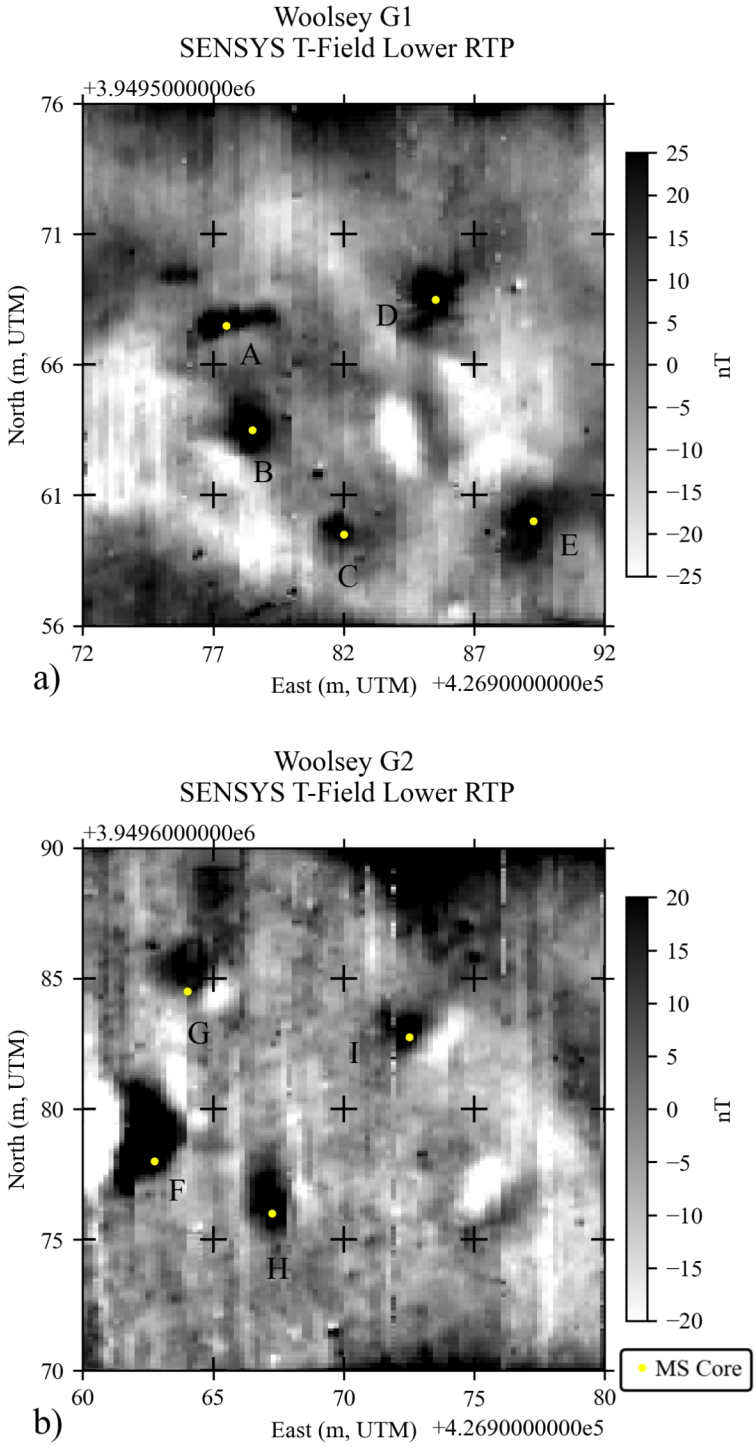

Figure 5.3. Woolsey G1 and G2 SENSYS Lower Surveys. Processed SENSYS lower data, G1 (a) and G2 (b), in UTM coordinates. Labels of features A-I with corresponding MS core locations in yellow.

The other five logs (E-I) do not clearly show a single small magnetic feature, e.g. a point-source. Log E shows a small area (approximately 0.4 m) of increased MS and the MS decreases. The contrast between the areas of high and low MS are much smaller than other logs at the site however. Given the potential poor placement of core E, the depth of the maximum MS is likely moderately accurate, but is lacking clear definition as it is laterally out of place (Figure 5.4). The other four logs (F-I) have a steep increase in MS through the top 0.1 to 0.15 m, which corresponds with the plow zone and an A soil horizon and is expected to have higher MS (Figure 5.5). Then, the MS continues to increase until leveling off, generally at a shallow depth, where it continues at a very high MS for a significant portion of the log. The MS may or may not begin to decrease at deeper depths. In these cases, the MS maximum depth is usually shallow compared to the overall area of increased MS. This pattern more likely reflects an archaeological 'pit' structure and so the shallower MS maximum is likely not the center of the total magnetic source-body. An adjusted center location is likely more accurate, but requires interpretation from the author to select the beginning and end of the magnetic body. Once done, a simple mathematical calculation to the center is possible. In these cases, using SI=3 is likely not appropriate as it does not fit a point-source model. Computer models were not directly tested for this type of feature, but borrowing from a geologic equivalent model, a vertical cylinder, SI=2 is more appropriate (Table 2.1). It is likely in the cases of pit features that the depth estimation will have more variability and decreased accuracy as the pit is an amalgamation of areas more magnetic material.

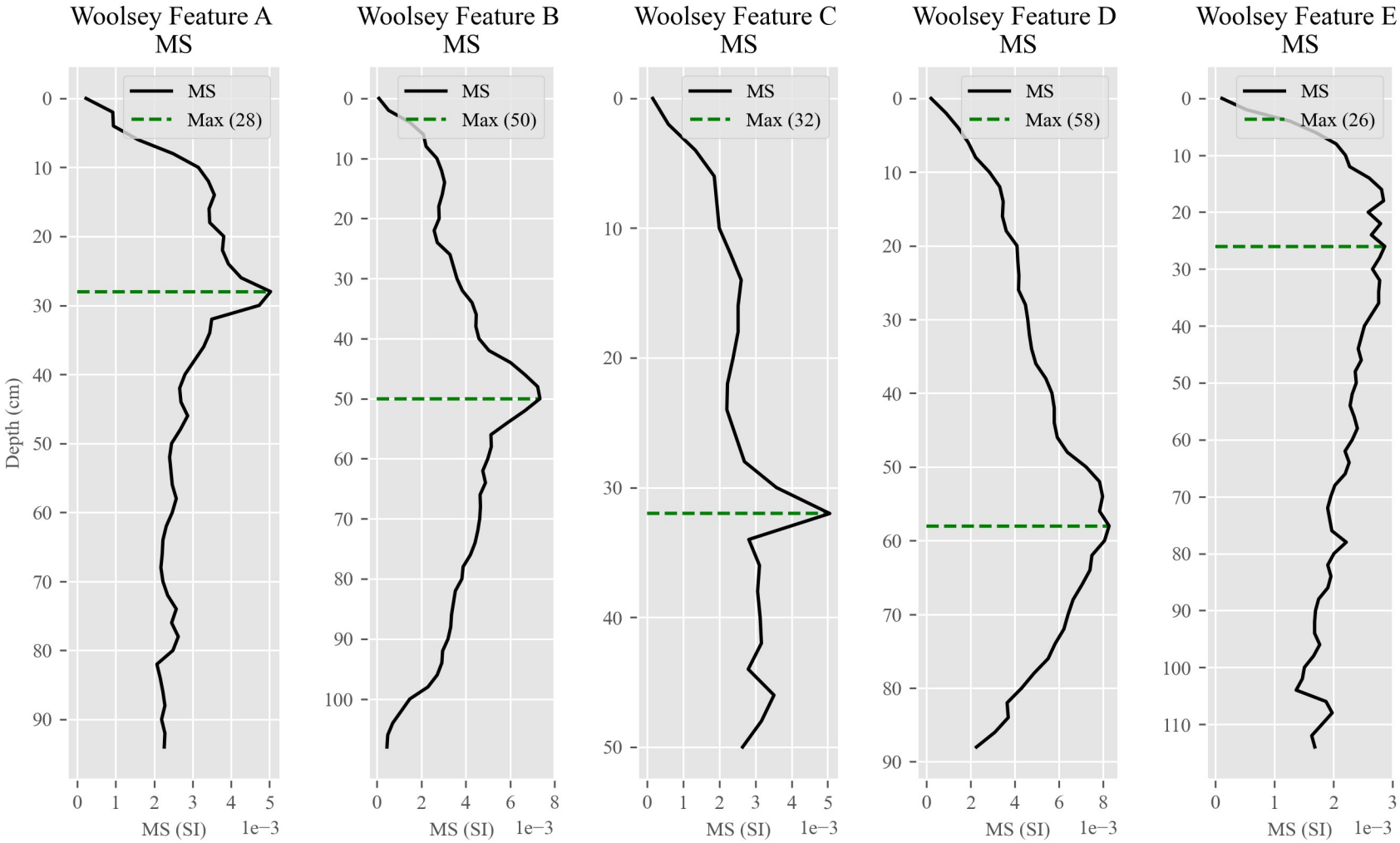

Figure 5.4. Woolsey DHMS Logs of Features A-E. MS logs of features A-E with MS in the dimensionless SI units and log depth in cm below surface. Logs A-C show clear well-defined single peaks. Log D shows a moderate single peak while log E is non-descript.

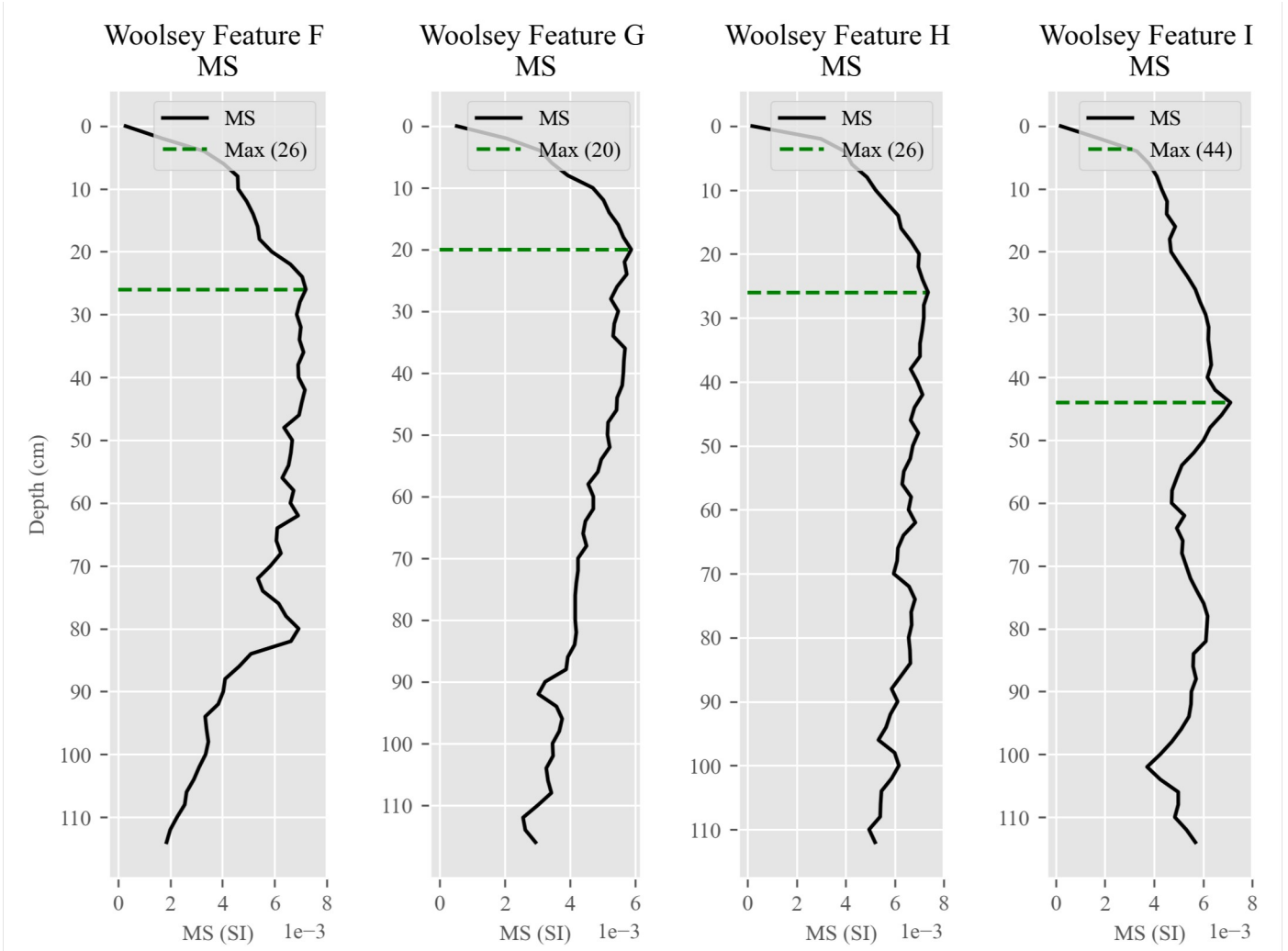

Figure 5.5. Woolsey DHMS Logs of Features F-I. MS logs of features F-I with MS in the dimensionless SI units and log depth in cm below surface. Logs F-I all fit an archaeological pit model and are likely not good point-source models.

Depth Estimation of Features

Depth is estimated for all features at the site using each magnetic survey. This results in individual HW estimates for every magnetic survey and a MH estimate for each sensor type (Figures 5.6 and 5.7). For all depth analyses, consistency is defined as agreeing with or being extremely similar to each other. Estimates of the same sensor type may be consistent, a difference in the estimates of say 0.1 m, but not be particularly accurate to the depth of the feature.

A) Feature A is a linear magnetic anomaly measuring approximately 1 x 3 m (Appendix B.1). The MS log shows a moderately defined peak with a maximum strength at 0.28 m below the surface (BS) and the feature likely ranging from approximately 0.22 to 0.32 m BS, although the top could be as shallow as 0.1 m BS (Figure 5.4). Manual core interpretation showed charcoal between 0.24 and 0.28 m BS, a good correspondence with the MS log. The magnetic anomaly is wider than the distance to the MS peak from both lower height surveys. These combined data suggest the magnetic source-body is likely not a point-source and a wall model would therefore better fit this feature. Given all magnetic data sets clearly show the anomaly (Appendix B.1) and a good MS log was acquired, this anomaly is a good candidate for depth analysis. HW depth estimates are consistent between the SENSYS surveys but not as consistent between the G-858 surveys (the two SENSYS results are overplotted at the same point in Figure 5.6). This is likely due to the lower quality of the G-858 lower survey where the data maximum is located on the very western edge of the anomaly, thus skewing estimates (Appendix B.1). MH SI of two estimates appear to closely estimate the depth (Figure 5.7). Using SI=2 appears the most accurate overall.

B) Feature B is a well-defined circular magnetic anomaly measuring approximately 2 m in diameter. Feature B offers a moderately good MS log showing a maximum peak strength at 0.5

m BS with the feature likely ranging from approximately 0.4 to 0.56 m BS (Figure 5.4). Additionally, a slight increase and decrease in MS on either side of the feature can be observed from 0.22 to 0.98 m suggesting a possible larger feature. These parameters make it a good candidate for analysis. The anomaly diameter is larger than the depth to the feature, but it likely can be considered a point-source. Depth estimates are consistent between survey heights and fairly consistent between instrument types (Figures 5.6 and 5.7). All techniques overestimate the depth to the feature, but using SI=2 appears to be most accurate. The higher surveys provide the most accurate assessments. This supports the idea that this feature is wider than the distance to the sensor for all surveys. When the distance to the sensor increases which occurs with the higher the survey height, error in the depth estimate should decrease. This is what is observed.

C) Feature C is a fairly defined circular magnetic anomaly measuring approximately 1.5 m in diameter. Feature C's MS core was moved 0.15 m to the right of center due to a reddish sandstone rock at 0.33 m BS. In the second core, a well-defined maximum MS peak at 0.32 m BS is observed. The obstruction is possibly fire cracked rock (FCR) and is likely in part the cause of the MS anomaly. The feature appears to range from 0.28 to 0.34 m BS (Figure 5.4). This down-hole log was stopped at 0.5 m BS due to a rock. So, it is possible that a deeper magnetic source is present at the location. Based on these results, feature C is likely a good candidate for depth analysis. Depth estimates between the sensors are consistent except the higher G-858 for the HW method (Figures 5.6 and 5.7). This is potentially due to the more linear representation of the anomaly in that magnetic dataset (Appendix B.1). This is also the likely cause for the drastically different MH estimates for the low and high G-858. An SI of three consistenly overestimate the feature depth while SI=2 is a fair estimator. This anomaly is wider than its depth in all surveys.

D) Feature D is a fairly circular magnetic anomaly measuring approximately 2.2 m in diameter. Feature D shows a gradual peak throughout the entire log from 0 to 0.88 m with a maximum centered at 0.58 m BS (Figure 5.4). The greatest MS strength occurs from 0.48 to 0.62 m BS in the log. Given the high MS throughout, this suggests a possibly elongated source (deep pit) with the most magnetically susceptible material occurring at 0.48 to 0.62 m BS. These parameters make the feature a good candidate for depth estimation. Depth estimates appear consistent and accuracy increases with the height of the sensor (Figures 5.6 and 5.7). All depth estimates overestimate, but SI=2 is the most accurate. The magnetic anomalies from all surveys are much wider than the depth to the MS maximum. This suggests the feature is wider than its distance to sensors and depth estimation accuracy increases with distance, which is expected in this condition.

E) Feature E is a slightly elliptical magnetic anomaly measuring approximately 2 x 2.5 m. The G-858 datasets are of poorer quality while the SENSYS data is also only fair (see Appendix B.1). The MS log for feature E is not well placed and the log does not show a defined peak or anomaly (Figure 5.4). MS increases from the surface to 0.18 m BS reaching a maximum at 0.26 m and then slowly drops with depth. Given the non-descript MS log and that its placement is in question for the G-858 anomalies, it is likely this log has missed the majority of the magnetic source. This feature is not a good candidate for depth estimation. The HW estimates vary greatly compared to the MH estimates, which is to be expected given the magnetic survey quality (Figures 5.6 and 5.7). Given the non-descript MS log, it is difficult to estimate a feature depth. However, given the consistent large estimates from the better-quality magnetic data and the larger size of the magnetic anomalies, it is likely this feature is wider than the distance to sensors, making depth estimation unreliable by these methods.

F) Feature F is a slightly elliptical anomaly and is distinctly bipolar, although a portion of the negative side is not encompassed by the survey. The positive portion of the anomaly measures approximately 2 x 2.8 m. In addition to the clear dipolar nature, the lowest survey anomalies exhibit extreme nT values over 200 nT. This would suggest a possible metal object. The MS log does not show a well-defined singular peak (Figure 5.5). The maximum value is located at 0.26 m BS and a minor peak is centered at 0.8 m BS, although the MS values are fairly consistent between these points on the log. Given the dipolar nature of the anomaly it is likely the MS core could have been more accurately placed. Without further details this is likely not a good candidate for analysis. Depth estimates are fairly consistent between all instruments and survey heights (Figure 5.6 and 5.7). If the magnetic source body is located near the peak MS depth, the depth is severely overestimated with SI=3. If the source body is located near the minor peak, the depth is only slightly overestimated with this SI. Using SI=2 produces fairly consistent and accurate results to the peak MS depth. Given the high nT values and dipolar nature of the anomaly this suggests a smaller point-source, potentially shallow. Without a more properly placed MS core it is difficult to assign great confidence in the depth estimates accuracy.

G) Feature G is a circular anomaly measuring approximately 2 m in diameter. It is possibly dipolar in nature. Unfortunately, the MS core location for feature G appears to be ill placed at the southern edge of the anomaly (Figure 5.3b). The MS log does not show a clear peak. It increases to a maximum at 0.2 m BS and then steadily drops to the logs depth of 1.05 m BS (Figure 5.5). Given the poor core placement and non-descript MS log, this is not a good candidate for depth estimation. Depth estimates range greatly throughout all surveys, likely due to the noisy data (Figures 5.6 and 5.7). The majority of the estimates overestimate the maximum MS depth of 0.2 m, but using SI=2 with the G-858 data accurately estimates the depth to the MS peak. Although

this is not a clear feature location, the MS is of fairly high value at the maximum. Additional depth information is likely needed to make a more accurate assessment.

H) Feature H is more elliptical measuring approximately 1.75 x 2.5 m. The MS log does not show a clear peak. It rises in MS to it's maximum located at 0.26 m BS and then falls slightly to it's maximum depth at 1.12 m BS (Figure 5.5). This could be due to slight misplacement, but the maximum MS value is rather high. This feature is likely not a good candidate for depth estimation. Depth estimates do not appear consistent within or between sensors (Figures 5.6 and 5.7). The HW estimates are fair across both instruments and especially accurate for the G-858 using SI=2. It is particularly interesting the MH estimates with the G-858 data are wildly inaccurate and different from the HW estimates. No obvious data discrepancy or error is apparent, so this may warrant further investigation. Unfortunately, without a clearer MS log, an accurate depth comparison is not viable.

I) Feature I is a circular anomaly measuring approximately 1.25 m in diameter. It is possibly dipolar in nature. The SENSYS lower survey suffers from one line of erroneous data. The MS log for feature I is shaped like a curly bracket and shows a slight peak at 0.44 m BS coinciding with the maximum MS. A slightly smaller minor peak is at 0.79 m BS (Figure 5.5). The log is also placed on the edge of the magnetic anomaly, likely causing poor results. Although there is possible poor MS core placement, the magnetic anomaly is small and circular making this a good candidate for depth analysis. Overall, depth estimates are not consistent between instruments but the HW estimates appear fair to extremely accurate depending on the survey and SI used (Figure 5.6). MH estimates are good overall (Figure 5.7). The G-858 higher survey with SI=3 is extremely accurate, but other estimates at this SI are not. Using SI=2 is more consistent with all other surveys. The anomaly width is larger than the distance to the sensor for all surveys. However, the width is just barely larger than the distance to the sensor in the G-858 higher

survey. In the near-surface, the magnetic anomaly width is larger than the actual feature width. So, it is possible this depth estimate is accurate, because the feature width, which is an unknown, is actually smaller than the distance to the sensor. This is further substantiated because the G-858 higher HW with SI=2 greatly underestimates the depth to the feature, where the majority of estimates appear to overestimate the depth.

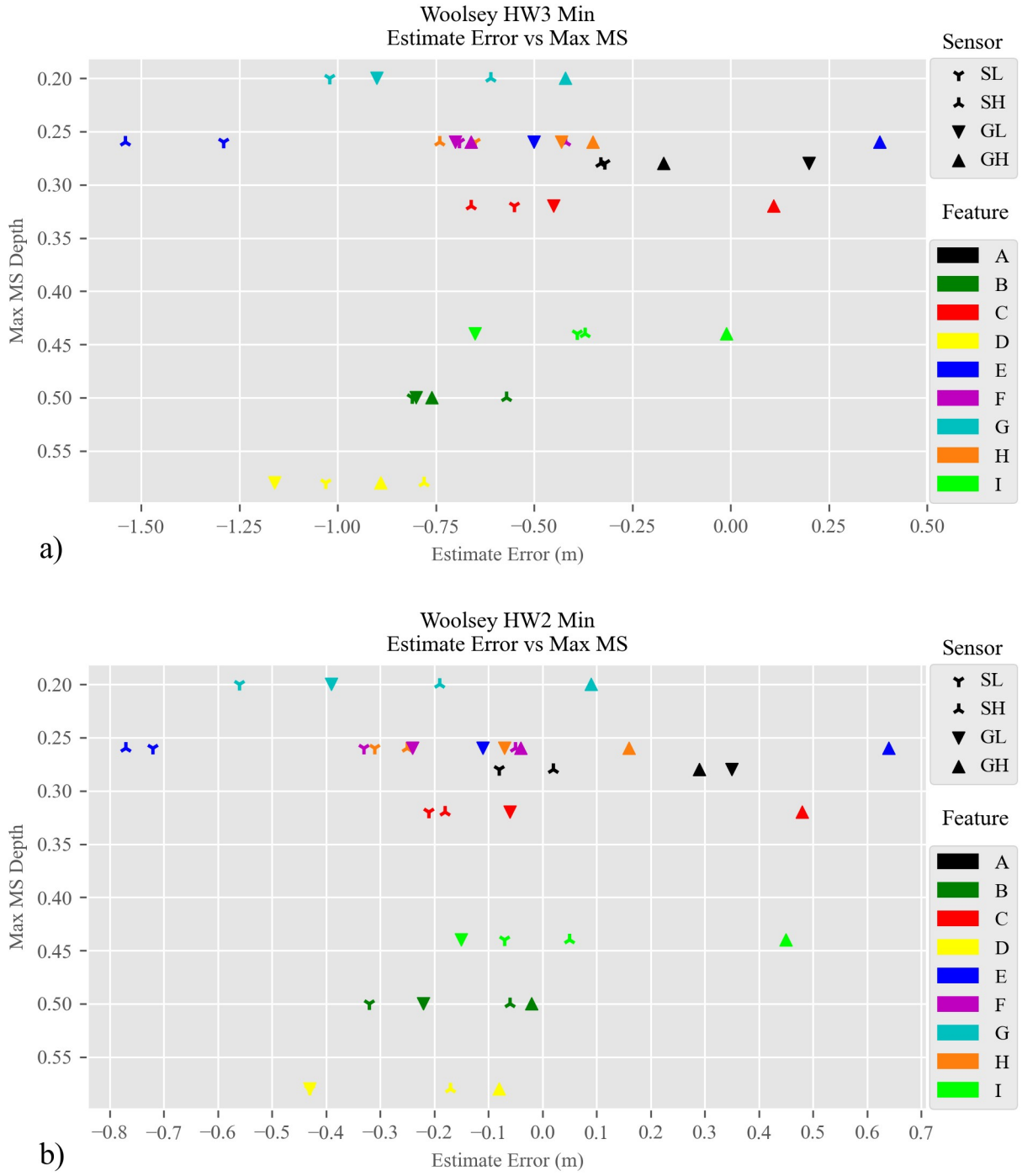

Figure 5.6. Woolsey Half Width Depth Estimates. The HW minimum depth estimate error (the difference between the HW estimate and the DHMS depth estimate) is plotted against the maximum MS depth for all features where a) is the SI=3 estimates and b) is the SI=2 estimates. Sensor labels are ‘S’ for SENSYS, ‘G’ for Geometrics, ‘L’ for lower height, and ‘H’ for higher height.

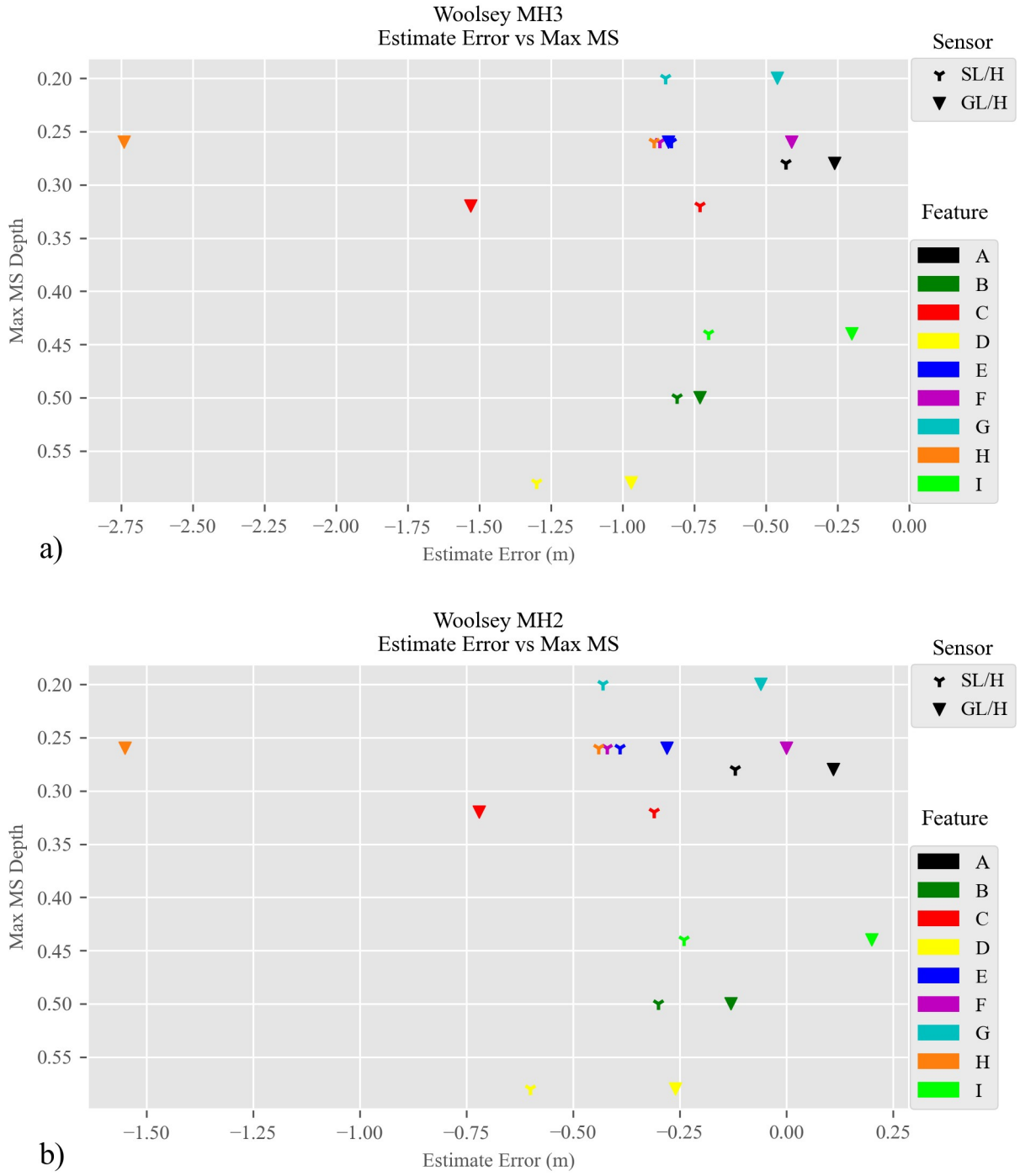

Figure 5.7. Woolsey Multi-height Depth Estimates. The MH depth estimate error (the difference between the MH estimate and the DHMS depth estimate) is plotted against the maximum MS depth for all features where a) is the SI=3 estimates and b) is the SI=2 estimates. Sensor labels are ‘S’ for SENSYS, ‘G’ for Geometrics, ‘L’ for lower height, and ‘H’ for higher height.

Site Summary

Of the nine features of interest, the author determined five would likely be good candidates for depth estimation while four would not. In almost all cases, the width of the magnetic anomaly was greater than the distance from the MS peak to the sensor. Fair depth estimates were made for all features except E, which suffered from poor data quality and MS core placement. Using SI=2 across all features yields the most consistently accurate depth estimates which fall within plus or minus 0.25 m.

A pattern of depth estimates decreasing with sensor height is seen for the majority of features. This furthers the idea that many of the features may be wider than the distance from the peak MS to the sensor. In the case of feature I, using SI=3 fits extremely well for the G-858 higher survey, while five other SI of two estimates fall within the 0.25 m range. The SENSYS HW SI of two estimates for this feature are around 0.05 m, which is extremely accurate. So, using either SI=3 or SI=2 can accurately estimate the depth the same feature based on the distance to the sensor.

Thus far, data suggest that when the width of certainly the source-body and possibly just the magnetic anomaly is greater than the distance to the sensor SI=2 is more appropriate. When this does not occur, SI=3 is more appropriate. The full anomaly width was used as a proxy for the width of the feature. The MH technique estimates skewed towards overestimation. The majority of the HW estimates were also overestimates, but generally the G-858 higher data underestimated the depths. HW estimates are more closely grouped by sensor height than by sensor type. The HW and MH techniques appear to have approximately the same percentage of estimations with the plus or minus 0.25 m range.

The features designated as likely point-sources (A-D) are more often accurately estimated with SI=3 and SI=2, depending on the height of the sensor. The features designated as more ‘pit’

like (E-H) appear to only be accurately estimated with SI=2. Feature I which is more pit like appears to be accurately estimated with either SI, depending on the distance to the sensor.

Pile Mound

Results at Pile Mound include magnetometry, down-hole MS, and depth estimation. Two different magnetometer systems were used at Pile Mound the Geometrics G-858 and SENSYS prototype. Five grid blocks of varying size were selected for survey. Unfortunately, the Geometrics system malfunctioned during this survey and data for Grid Block 1 (G1), lower, and Grid Blocks 3 and 4 (G3 and G4), lower and higher, were all corrupted making them unusable. Additionally, G3 and G4 were covered in high grass, approximately 1 to 1.5 m high, which resulted in very poor data quality for the SENSYS surveys. These grid blocks were excluded from data analysis leaving Grid Blocks one, two, and five (G1, G2, G5) for analysis. Nineteen anomalies of interest (A-S) were selected for depth estimation. Prior gradiometry survey data were used to guide data collection. A known GNSS datum was in place at the site before survey began allowed alignment between the prior and current gradiometer surveys.

Magnetometry

G1 encompasses an 11 x 10 m area at 0.2 x 0.1 and 0.25 x 0.1 m resolution for the SENSYS and G-858 data, respectively. The SENSYS prototype data appear of good quality with only minor noise in some areas (Figure 5.8a). Only the higher G-858 data are usable for analysis and appear of overall good quality (Appendix B.5). This area has three anomalies of interest (A-C). Features A and C are well-defined while feature B is harder to distinguish, especially in the G-858 data.

G2 measures 16 x 11 m and 15 x 11 m at 0.2 x 0.1 m and 0.25 x 0.1 m resolution in the prototype and G-858 data, respectively (Figure 5.8b). The difference is due to the fixed width of the prototype. Data from both instruments appear of good quality with little to no noise

(Appendix B.7 and B.8). Six anomalies of interest (D-I) are in this survey area. Feature I is a rather complex anomaly, described below, but otherwise no other issues arose in this area.

G5 measures 26 x 20 m and 25 x 20 m at 0.2 x 0.1 m and 0.25 x 0.1 m resolution in the prototype and G-858 data, respectively (Figure 5.9). The difference is due to the fixed width of the prototype. Overall data quality appears good (Appendix B.9 and B.10). The SENSYS surveys suffer from some minor noise and the higher survey has minor striping. The G-858 lower survey has some minor striping while the higher survey appears smooth. Ten anomalies of interest (J-S) are in this survey area.

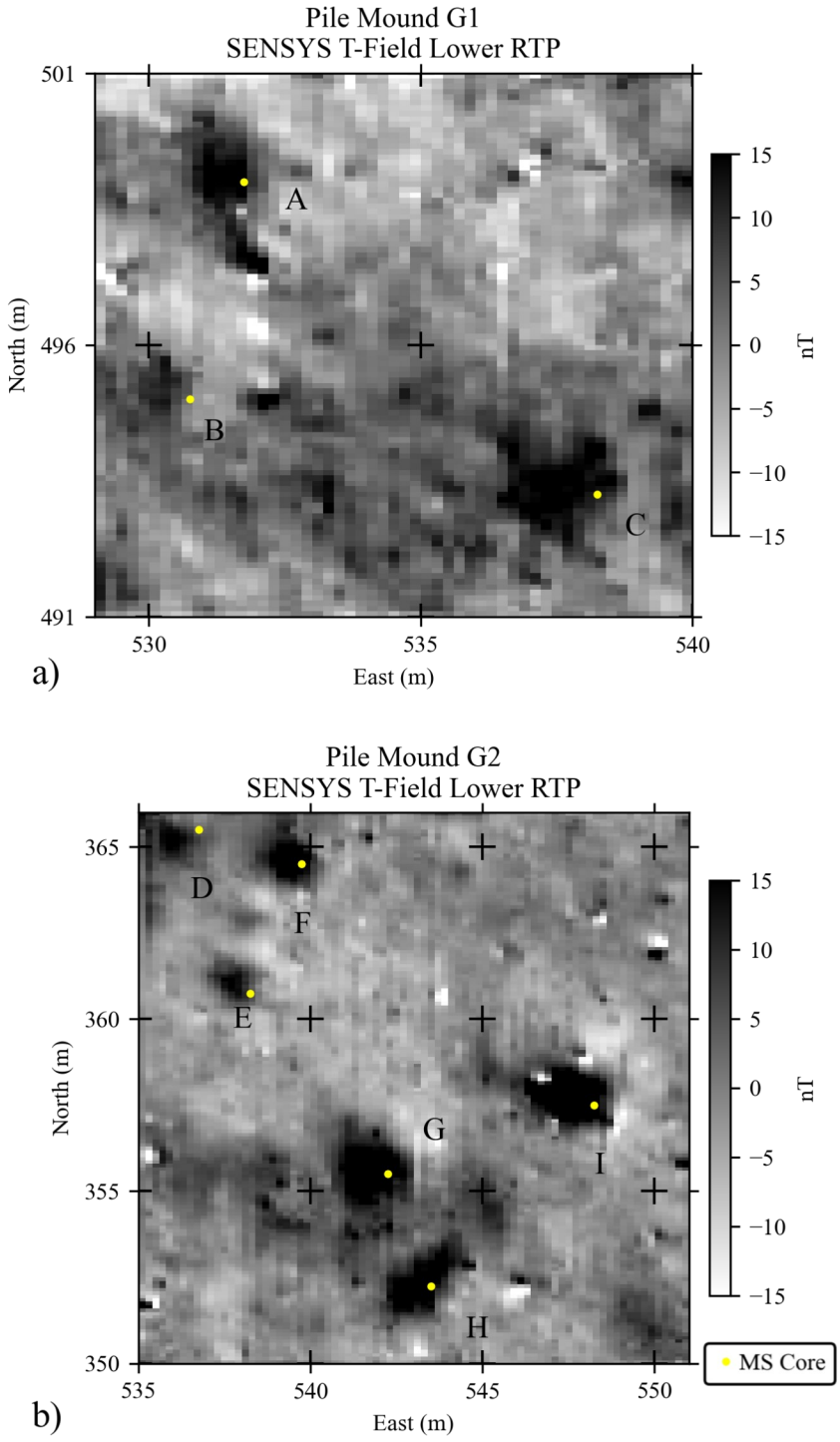

Figure 5.8. Pile Mound G1 and G2 SENSYS Lower Data. a) G1 processed data and b) G2 processed data. Both are in local grid coordinates.

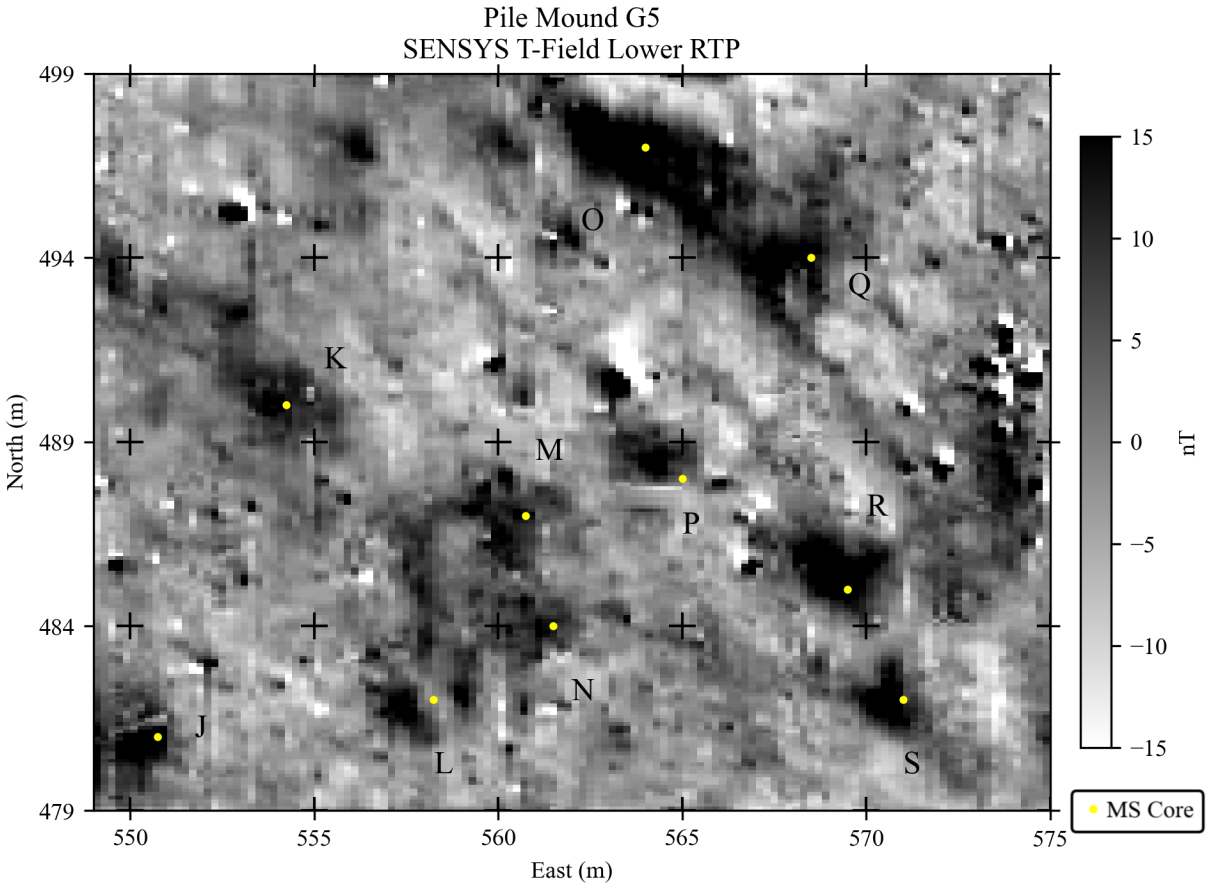

Figure 5.9. Pile Mound G5 SENSYS Lower Data. Processed data in local grid coordinates.

Down-hole MS

Nineteen magnetic anomalies were chosen for depth estimation testing, A-S, (Figures 5.10-13). The location of MS cores was based on the previously collected gradiometry data. The location of all MS cores appears slightly offset in the direction of grid East, thus making some not ideally located (see Appendix). This is due to a computer malfunction in the field, so the author had to "guestimate" the effects of RTP on the gradiometry data and sadly under-corrected. The MS core B misses the anomaly in all datasets. MS cores D and E are likely outside of the features of interest in all data sets. MS cores J and P are on the edge or slightly outside of the features. Anomaly L appears as one in the previously collected gradiometry data, however, in the higher resolution data it is clearly two different anomalies. Core L, therefore, is located in

between these two anomalies. The core is closer to the left anomaly and it is the larger of the two, so this was designated anomaly L for all testing. No other issues are present with the down-hole MS data. The MS data can be categorized into three types at this site: a well-defined single peak, a larger area of higher MS (pit), or top-skewed. Examples of the first two were found at Woolsey, while the third is new to Pile Mound.

Two logs (J and K) show clear data peaks and likely fit the point-source model (Figure 5.12) Seven logs (A, C, E, F-I) do not show a single small feature. These logs show a larger area of higher MS, similar to those at Woolsey. The MS steadily increases from the ground surface to about 0.15 m BS and then level off until the bottom, or near the bottom, of the log is reached. These likely correspond to a pit feature. MS log B appears not to exactly fit into this category. It is not as elongated as the others in the pit category, but it is suspected this is a shallow (in size) pit and therefore would likely behave magnetically similar to the large area pits.

Nine logs (D and L-S) are referred to as "Top-skewed." These logs increase in MS from the ground surface to about 0.15 m BS, similar to the pit like anomalies. The MS then increases slightly beyond this depth until reaching a peak. A steady decline in observed after the peak. These logs may best represent a shallow pit feature. In three cases (L, S, O) one or more minor peaks occurs at depth beyond this initial MS drop off. Although this new category has a larger area of MS than the single peak category, the majority of the MS is located at or near the MS maximum. This suggests that location may be an appropriate center location. In the case of logs with multiple peaks below the initial large one, an adjusted center depth may be more appropriate. The most similar computer model to this top-skewed category is the half-sphere, so SI=3 may be most appropriate. All the top-skewed features, except D, occur in G3. This suggests that there may be a geomorphological cause for this log type, which warrants future investigation. Also, peak magnetic susceptibilities throughout all logs are noticeably less than

those at Woolsey, suggesting less well developed magnetic features or less magnetically susceptible sediments (Figures 5.10-13).

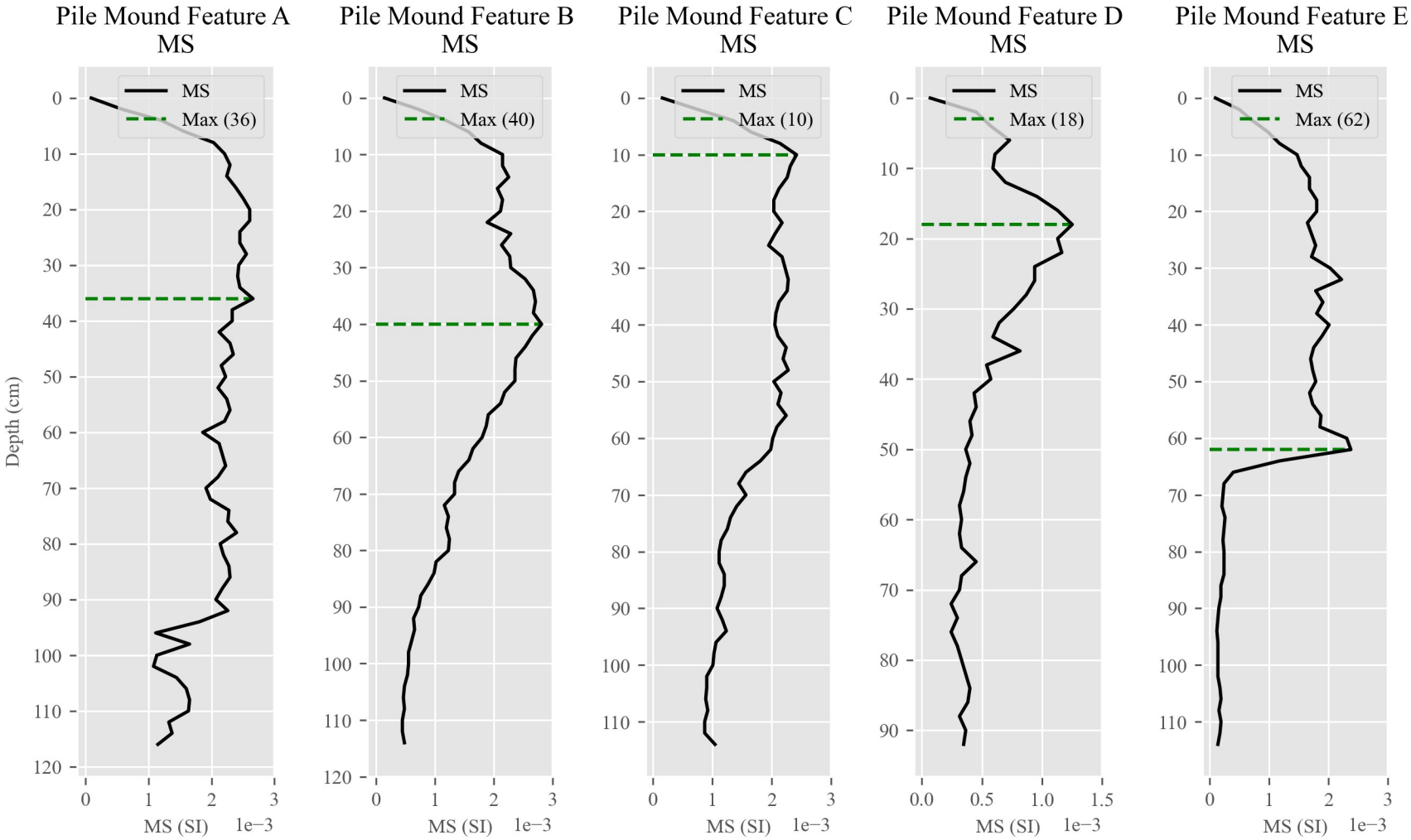

Figure 5.10. Pile Mound DHMS Logs of Features A-E. MS logs of features A-E with MS in the dimensionless SI units and log depth in cm below surface.

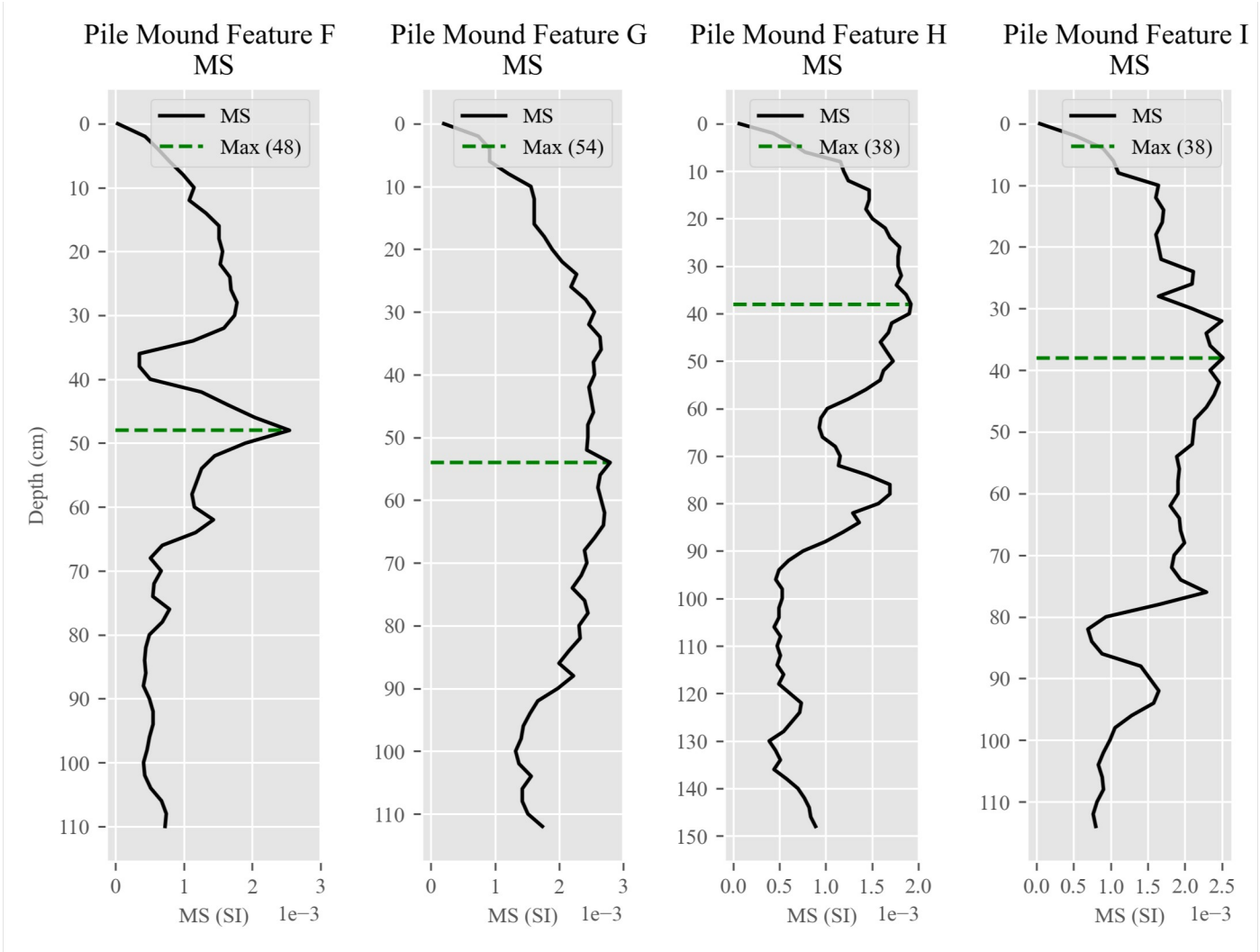

Figure 5.11. Pile Mound DHMS Logs of Features F-I. MS logs of features F-I with MS in the dimensionless SI units and log depth in cm below surface.

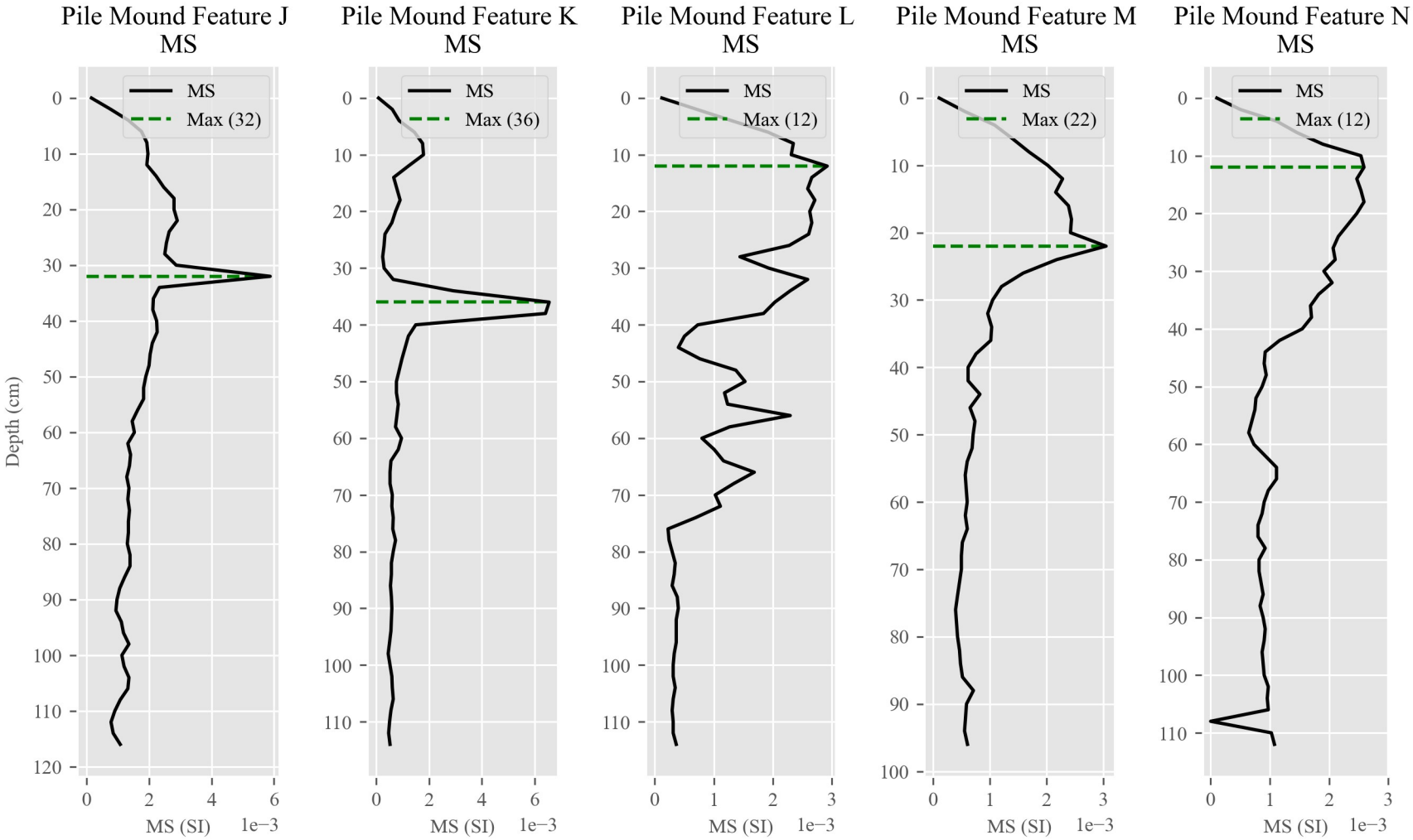

Figure 5.12. Pile Mound DHMS Logs of Features J-N. MS logs of features J-N with MS in the dimensionless SI units and log depth in cm below surface.

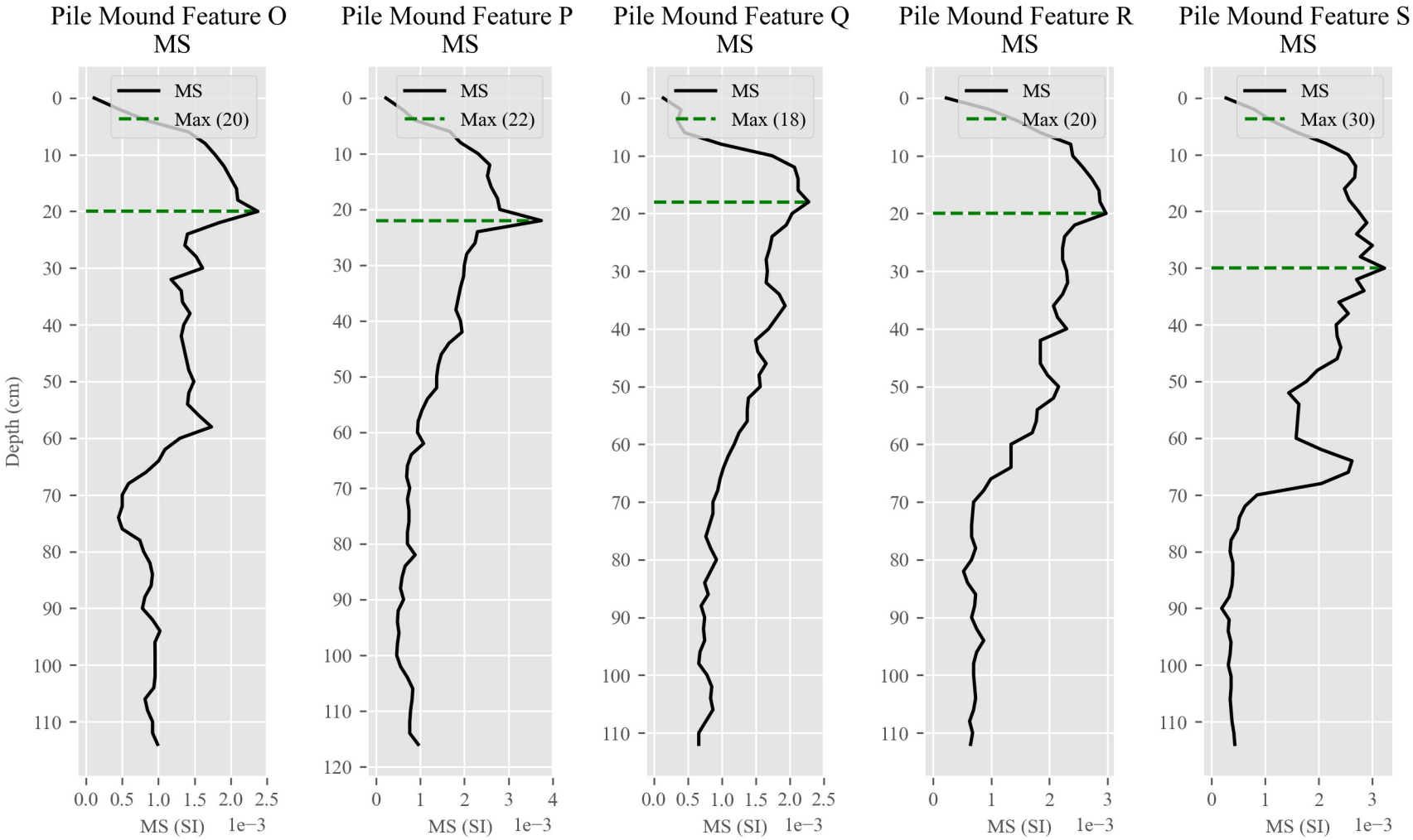

Figure 5.13. Pile Mound DHMS Logs of Features O-S. MS logs of features O-S with MS in the dimensionless SI units and log depth in cm below surface.

Depth Estimation of Features

Depth is estimated for all features at the site using each available survey. Due to equipment malfunction, features A-C have no G-858 lower HW or G-858 MH estimates. Excluding those three features, six depth estimates were made for SI=3 and SI=2 in the same manner as Woolsey. Two features (O and Q) are much broader and in the magnetic survey they tend to blend together (Appendix B.12 and B.13). When they are combined together, the resulting anomaly is rather long and so SI=1 was investigated as that may be more appropriate. Only HW minimum estimates are provided, as the others were less accurate. Due to the number of total features investigated, depth estimate graphics are separated into two sets, G1 and G2 together (Figures 5.14 and 5.15) and G3 by itself (Figures 5.16 and 5.17).

A) Feature A is a fairly defined circular anomaly measuring approximately 1.25 m in all data sets (Appendix B.8 and B.9). The MS core does not have a well-defined peak and its maximum MS occurs at 0.36 m BS (Figure 5.10). The MS rises steadily until approximately 0.1 m BS and then stays fairly similar until it decreases at a depth of 0.92 m. This fits the pit type of MS log. The distance from the MS peak to sensor is greater for both SENSYS surveys, but not the G-858 higher survey. Based on the magnetic survey, this feature would be a good candidate for depth estimation, but the lack of a definitive MS feature could make accessing accuracy difficult. Depth estimates are not consistent across the surveys (Figures 5.14 and 5.15). Overall using SI=2 is the most accurate for the SENSYS surveys while the G-858 higher survey consistently underestimates the feature. For only the G-858 the distance to the MS peak from the sensor is greater than the width of the anomaly. This should allow an accurate evaluation with SI=3, but this does not occur. It is unclear if the MS log is slightly misplaced or if the feature does span 0.8 m, a rather large and deep pit for the site. If this is the case, the SENSYS MH with SI=2 proves a good estimator followed by fair performance from the HW rules.

B) Feature B is moderately defined in the SENSYS data. It appears to be a somewhat circular anomaly measuring approximately 1.25 m in diameter in the SENSYS lower survey. In the SENSYS higher survey it appears almost square with dimensions of 1.5 m per side. Additionally, the anomaly is varied throughout the SENSYS data and not decreasing in strength from the center to the outside evenly. It is poorly defined in the G-858 higher survey, as the western side does not drop below the half-maximum value. What is surveyed appears elliptical measuring approximately 1.4 x 1.8 m (Appendix B.8). Unfortunately, this renders the G-858 survey unusable for depth estimation. The MS log shows a moderate peak with a maximum value at 0.4 m BS (Figure 5.10). The potential feature likely ranges from either 0.1 or 0.3 to 0.5 m BS. The core placement could be better, but overall this appears a good feature for depth analysis. The MH SI of three depth estimates appears quite accurate (Figures 5.14 and 5.15). Estimates with SI=2 perform worse than with three, but all three depth estimates consistently underestimate by approximately 0.25 m.

C) Feature C is very defined in all datasets. It is a slightly elliptical anomaly measuring approximately 1.4 x 2.2 m in all data (Appendix B.8 and B.9). The anomaly is somewhat dispersed internally in the SENSYS lower data. The MS log does not show a clear peak (Figure 5.10). The data rises to the maximum at 0.1 m BS and then stays consistent until beginning to decrease at approximately 0.55 m BS until the end of the log at 1.15 m BS. This would suggest either little to no feature is observed, or the feature spans from 0.1 to 0.7 m with a center at 0.35 m BS. Even with this estimated center, the magnetic anomaly is wider than the distance to sensors, making depth estimation with SI=3 unreliable. This feature is likely not a good candidate for depth estimation. Depth estimates are fairly consistent within the SENSYS surveys and the G-858 higher survey is relatively similar. Using the MS maximum, depth estimates with SI=3 and two severely overestimate to the potential feature (Figures 5.14 and 5.15). However, if

one differences the estimates to the adjusted possible feature center, the HW SI of two estimates are more reasonable, but are still greater than 0.25 m in error. This adjusted center is more likely the case, given 0.1 m is extremely shallow for an archaeological feature at the site. Additionally, the MS core placement on the edge of the anomaly may be the cause of a poor comparison.

D) Feature D is a well-defined circular to slightly elliptical anomaly measuring approximately 1 m in diameter in all datasets. In the G-858 higher data, the anomaly runs to the edge of the data window which causes error and is not usable for HW estimation (Appendix B.11). The MS core shows a clear peak from approximately 0.1 to 0.3 m with a maximum MS at 0.18 m BS (Figure 5.10). Even with the core placement to the northeastern edge of the anomaly, this appears a good candidate for depth analysis. Depth estimates are very consistent within the different estimation techniques (Figures 5.14 and 5.15). The HW estimates with SI=2 are mostly within reason. The difference in estimates to the MS log may be due to poor MS core placement.

E) The magnetic anomaly for feature E is a clearly defined and slightly elliptical in shape measuring approximately 1.6 x 2 m in the SENSYS lower and both G-858 surveys. In the SENSYS higher survey the anomaly is more circular measuring approximately 1.6 m in diameter (Appendix B.10). The MS log does not show a clear peak, but does show a clear area of higher MS ranging from approximately 0.15 to 0.62 m with the end coinciding with the MS maximum (Figure 5.10). Given the small anomaly size and clear area of increased MS, it is likely a good candidate for depth analysis. Depth estimates show considerable variability between the different height and instrument surveys (Figures 5.14 and 5.15). This feature is underestimated in most surveys, breaking the norm. A clear relationship to the sensor height is seen, as higher sensors increase the underestimate. The lowest sensor and sensor pair with SI=3 most accurately estimate the distance to the MS peak, however, a more appropriate feature center may be approximately 0.38 m BS. When using this adjusted center (a 0.24 m decrease in depth), the SI of three

estimates center around zero error and are fairly well placed. A clearer relationship between the distance from the source-body to the sensor is then seen and follows what is expected. One expects overestimation when the feature is wider than the distance to sensors.

F) Feature F shows good definition at its boundary and is a fairly circular anomaly measuring approximately 2 m in diameter in all datasets (Appendix B.10 and B.11). The MS log shows a clear peak with a maximum at 0.48 m BS. The peak ranges from approximately 0.36 to 0.6 m BS (Figure 5.11). The MS log also shows a clear area of increased MS shallower than the maximum peak. This appears an excellent candidate for analysis. Depth estimates are well clustered, especially the HW SI of three (Figures 5.14 and 5.15). However, these estimates with SI=3 consistently overestimate the depth to the center of the feature. HW estimates using SI=2 vary around the center distance, skewing towards underestimation. Additionally, the error appears to have a direct relationship to the height of the survey, e.g. the distance between the source and the sensor, with a greater distance more accurately estimating while using SI=3. Given the clear peak and well-defined magnetic anomaly, it is likely the SI of three estimates are off slightly because, the width is larger than the distance to sensors. Using the SI of two produces fairly accurate results and may be partly influenced by the shallower area of higher MS. When accounting for this shallow area of higher MS, the estimation should be more shallow which occurs in the SI of two estimates. SI of three estimates are likely more effected by the feature width being greater than the distance to the sensor. Given the multiple areas of high MS SI=2 may be more appropriate. Either case is plausible and more data is needed to better assess the situation.

G) Feature G is a well-defined fairly circular feature measuring approximately 2.5 m in diameter in all datasets (Appendix B.10 and B.11). The SENSYS lower survey has the most internal dispersion, but is still of good quality. The MS log does not show a clear peak, but is

shaped similar to a “curly bracket” and has a maximum MS at 0.54 m BS in the approximate center of this shape (Figure 5.11). Given the good magnetic anomaly and somewhat clear MS log, this is likely a good candidate for analysis. Depth estimates are relatively similar for all heights and instruments (Figures 5.14 and 5.15). Estimates for SI=3 and two consistently overestimate the depth of the feature. Although the MS log does not show a well-defined peak, the SI of three estimates are likely affected by the large width of the anomaly, especially the HW estimates. Using SI=2 across all techniques is very accurate with five estimates falling between zero and 0.25 m overestimation and one underestimating by only 0.02 m. We see an opposite pattern in the depth estimates (estimates increase with sensor distance) than features E and F, which suggests this feature is deeper (true assuming the adjusted center for feature E) and that SI=2 is likely more reasonable.

H) The magnetic anomaly for feature H is well-defined, elliptical in shape and measures approximately 1.7 x 3 m in all datasets, suggesting this feature is more linear in nature (Appendix B.10 and B.11). The SENSYS surveys appear more internally dispersed than the G-858 surveys, especially the SENSYS higher survey. The MS log appears bimodal with one shallower moderate peak from ground surface to 0.6 m with the MS maximum at 0.38 m BS and a second deeper well-defined peak at 0.76 m bounded at approximately 0.65 to 0.95 m BS (Figure 5.11). Given the bimodal nature of the MS log, this may not be a good candidate for depth analysis. Depth estimates between the SENSYS instrument do not relate well as both surveys appear to have internal dispersion. This is also likely the cause for the extremely erroneous MH estimates (Figures 5.15 and 5.15). In fact, when moving the MH estimate location one cell to the right, the error reduces to -0.63 and -0.22 m for SI of three and two respectively. The G-858 surveys have extremely similar depth results and the adjusted SENSYS estimates are close to these estimates. Depth estimates to the shallower peak appear over estimated across all

SIs while those to the deeper peak appear underestimated, note the SENSYS lower estimate is over-plotted by the G-858 estimates in figure 5.14. However, when using the center between the two MS peaks, approximately 0.57 m BS and using the adjusted SENSYS MH estimates, all, excluding the erroneous SENSYS higher estimate, of the SI of two estimates' error is plus or minus 0.1 m or less. It appears the center of the possibly two magnetic bodies is being estimated. This makes sense as the magnetic field detected at the sensors is a complex summation of all magnetic sources below it. Additionally, the depth estimates appear to increase with sensor distance. This developing pattern shows increased accuracy with SI=2.

I) Feature I appears to be a defined circular feature measuring approximately 2.1 m in diameter in the G-858 and higher SENSYS data (Appendix B.10 and B.11). The lower SENSYS data is actually comprised of two anomalies, a small dipolar anomaly to the northwest and a broader circular anomaly consistent with the other surveys. Given the high magnetic value of the small dipolar anomaly and its definitive presence only in the lowest survey, it is likely a small piece of metal which surely contributes to the broader anomaly in the other datasets. This makes the anomaly extremely complex and the RTP process introduces error at this location. The MS log, located on the southeastern side of the broader anomaly, does not show a definitive peak and has a MS maximum at 0.38 m BS (Figure 5.11). An area of high MS is present from 0.1 to 0.76 m BS, the center of which coincides roughly with the maximum MS location. Given the complex nature of this anomaly, it is likely not a good candidate for depth analysis. Unfortunately, the SENSYS lower and MH depth estimates are skewed by the presence of the likely metallic object. The HW depth results are not consistent across different heights of instruments (Figures 5.14 and 5.15). The G-858 and SENSYS higher depth estimates are fairly accurate with SI=2. Given the complexity of the anomaly, these fairly accurate estimates to the broader anomaly are surprising.

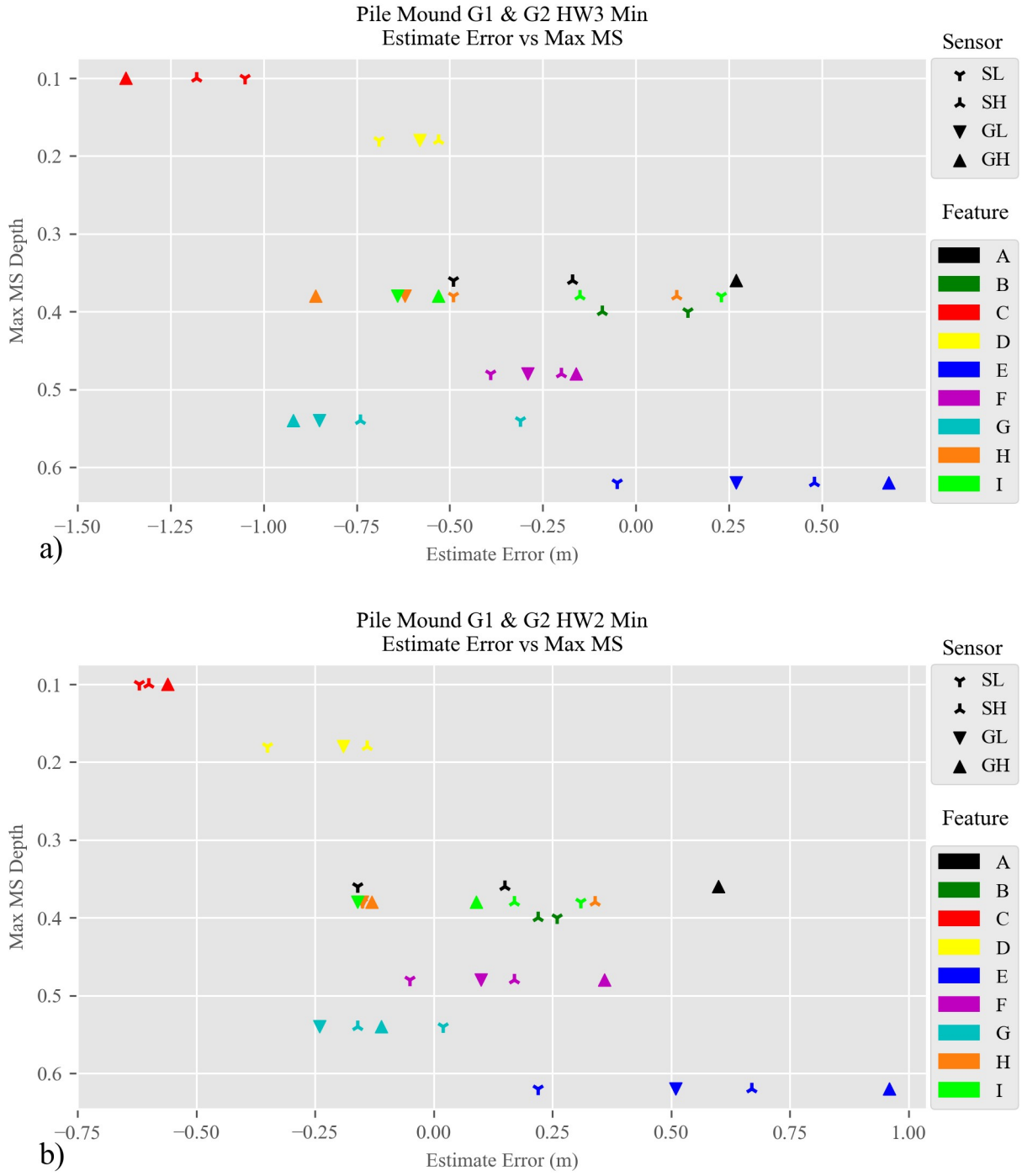

Figure 5.14. Pile Mound G1 and G2 Half-width Depth Estimates. The HW minimum depth estimate error is plotted against the maximum MS depth for all features where a) is the SI=3 estimates and b) is the SI=2 estimates. Sensor labels are 'S' for SENSYS, 'G' for Geometrics, 'L' for lower height, and 'H' for higher height.

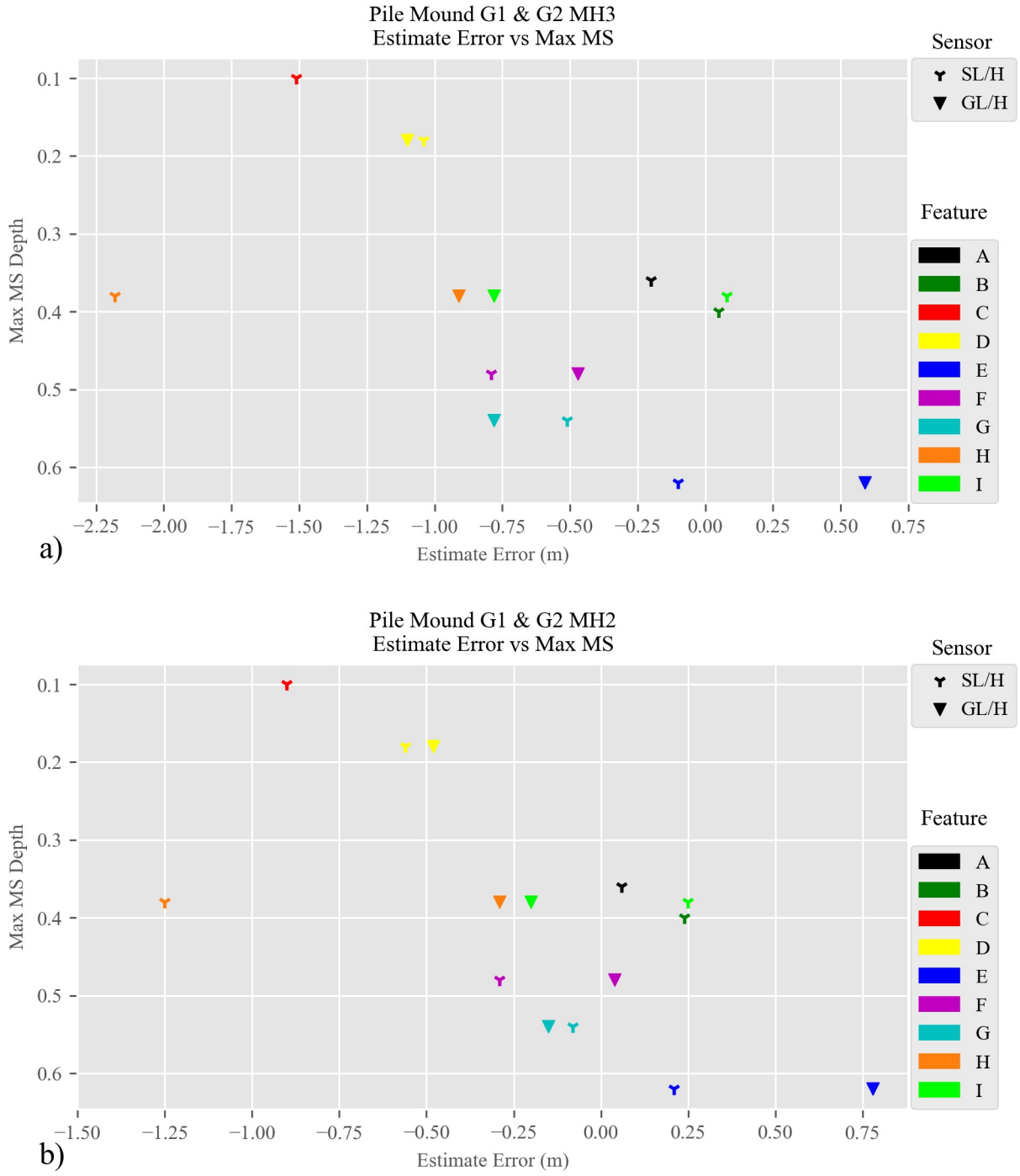

Figure 5.15. Pile Mound G1 and G2 Multi-height Depth Estimates. The MH depth estimate error is plotted against the maximum MS depth for all features where a) is the SI=3 estimates and b) is the SI=2 estimates. Sensor labels are 'S' for SENSYS, 'G' for Geometrics, 'L' for lower height, and 'H' for higher height.

J) Feature J is a well-defined elliptical, almost linear, anomaly measuring approximately 1.1 x 1.8 m in the SENSYS lower survey and is slightly broader in the higher survey. It is a fairly defined somewhat elliptical anomaly measuring approximately 2 x 2.2 m in the G-858 lower survey and is more circular with a diameter of approximately 2.5 m in the G-858 higher survey. However, the western edge of the anomaly is outside the survey boundary (Appendix B.13). The MS log shows a nicely defined single peak at 0.32 m BS, coinciding with the maximum MS (Figure 5.12). This would suggest the anomaly is a good candidate for depth analysis. The depth estimates are consistent between survey heights but not instruments (Figures 5.16 and 5.17). The SENSYS lower survey HW with SI=3 provides a very accurate estimate. Using SI=2 is more appropriate for all the estimates combined. This follows a growing pattern when error trends towards overestimation with increased sensor height. It is likely this feature is wider than the distance to sensors, making depth estimation unreliable with SI=3.

K) Feature K is a fairly well-defined somewhat circular anomaly measuring approximately 2.2 m in diameter in all the surveys. The SENSYS lower survey is the most internally dispersed while others do have some dispersion, but they are not of overall poor quality (Appendix B.12). The MS log shows a single well-defined peak from 0.32 to 0.4 m with the MS maximum at 0.36 m BS (Figure 5.12). Given the clear MS peak, this feature is likely a good candidate for depth analysis. The depth estimates are not particularly consistent between survey heights, but are relatively close for each sensor (Figures 5.16 and 5.17). The SI=3 uniformly overestimates the depth to the feature. The SENSYS SI=2 estimates are accurate, but the G-858 SI=2 estimates are certainly less accurate. Given the very well-defined peak, the feature is most likely point-source in nature and therefore it is likely this feature is wider than the distance to sensors, making depth estimation unreliable by these methods. It is odd that the SENSYS higher survey produces a

deeper estimate since it has a greater distance, but it is likely the HW estimate is effected by the internal dispersion of the magnetic anomaly.

L) Feature L appeared as a single source in the previous gradiometry data, but in all the current surveys it is clearly two different anomalies. The larger of the two anomalies is selected for testing. The anomaly is fairly defined and circular measuring approximately 1.5 m in diameter across all surveys. The SENSYS surveys suffer from internal dispersion (Appendix B.12). The MS log is rather complex with four peaks. The shallowest coinciding with the MS maximum at 0.12 m BS. Additional peaks occur at 0.32, 0.56, and 0.66 m BS (Figure 5.12). The center of all the peaks is at approximately 0.35 m BS. Due to the proximity of other anomalies, HW estimates were unattainable for the G-858 higher survey. Given the quality of the magnetic anomalies, the MS core placement, and the complexity of the MS log, this feature is likely not a good candidate for depth analysis. The depth estimates vary greatly between survey heights and instruments (Figures 5.16 and 5.17). If the adjusted center of the MS feature is considered, half of the estimates with SI=2 overestimate by approximately 0.1 m, and are the most accurate. The SENSYS estimates appear affected by the internal dispersion of the magnetic anomalies. Again, for a complex MS log the SI of two estimate appears accurate to an averaged center depth.

M) Feature M is not a very clearly defined anomaly. It appears cross like in shape and is internally dispersed in all surveys (Appendix B.12 and B.13). It measures roughly 2.8 x 2.8 m at the longest sections. In order for the SENSYS lower HW estimation process to be performed, the data window had to be smaller than the data window used for others urveys. The anomaly measures approximately 0.5 in diameter in this survey. The MS log shows a clear peak from 0.1 to 0.3 m with the maximum at 0.22 m BS (Figure 5.12). Given the low quality and odd shape of the magnetic anomaly, this is likely not a good candidate for depth estimation. Surprisingly the SENSYS SI of two depth estimates are fairly accurate while the G-858 estimates overestimate

the depth (Figures 5.16, and 5.17). Given the G-858 data are the smoothest and are comprised of larger anomalies, it is likely they are directly affected by the anomaly widths being larger than the distance to sensors. The SENSYS lower survey is the most accurate and also used a much smaller data window, due to the internal dispersion of the larger anomaly. The other discrepancies between these estimates are due to this dispersion.

N) Feature N is not well-defined and internally dispersed in the SENSYS data and is only moderately defined in the G-858 data. In the SENSYS data, the anomaly measures approximately 1 x 2 m. It measures approximately 2 x 2.3 m in the G-858 data and is not as internally dispersed, but still not of good quality (Appendix B.13). The MS log shows a slight peak from the ground surface to approximately 0.45 m with the maximum MS at 0.12 m BS (Figure 5.12). Given the poor magnetic data, it may not be a good candidate for depth analysis. The HW depth estimates vary greatly with either SI while the MH estimates are much more consistent (Figures 5.16 and 5.17). The G-858 HW estimates are likely effected by the larger anomaly widths. Although the SENSYS higher HW SI of two estimate is accurate, given the amount of internal dispersion and data quality, little confidence is placed in the accuracy.

O) Feature O is a fairly defined broad linear elliptically shaped anomaly measuring approximately 5.5 x 2.5 m in all surveys. The SENSYS data appear to have some ‘stripey’ sections, especially the higher survey. In the higher surveys, this anomaly starts to blend with the neighboring Feature Q on the southeastern side (Appendix B.12 and B.13). The MS log shows three peaks (Figure 5.13). The shallowest ranging from the ground surface to approximately 0.26 m with the MS maximum at 0.2 m BS. A second minor peak occurs directly after this from 0.28 to 0.32 m BS. The third smaller peak ranging from 0.5 to 0.7 m centered on 0.58 m BS. The complexity of the anomaly suggest it is likely not a good candidate for depth estimation. HW estimates, especially with SI of three, are very consistent between all the surveys (Figures 5.16

and 5.17). The MH estimates are grossly overestimated. When averaging the MS peaks to an adjusted center position of 0.42 m all surveys still overestimate the depth. Given the large anomaly size, SI=1 was also investigated as it potentially fits this type of feature better. All HW estimates overestimate the first peak, but are consistent with the average adjusted center depth. The MH estimates are considerably closer to zero error, estimating in between the first peak and adjusted center. The SI of one is likely more appropriate for this broad linear anomaly.

P) The magnetic anomaly for feature P is circular, measuring approximately 2 m in diameter in all surveys and clearly defined (Appendix B.12 and B.13). The MS log shows a definitive peak from 0.12 to 0.24 m with a MS maximum at 0.22 m BS (Figure 5.13). This is likely a good candidate for depth estimation analysis. Depth estimates are fairly consistent across survey heights and instruments (Figures 5.16 and 5.17). Estimates with SI=3 overestimate the depth considerably, potentially due to the anomaly diameter being larger than the distance to the from the source to sensors. The estimates with SI=2 are fairly accurate for all except the SENSYS MH.

Q) Feature Q is a somewhat elliptical to square anomaly measuring approximately 1.7 x 2.4 m and 2.5 x 3 m in the SENSYS and G-858 data, respectively. In the higher surveys, this anomaly blends with the large neighboring feature O. The SENSYS data is far more internally dispersed than the G-858 data (Appendix B.12 and B.13). The MS log shows two peaks. The first ranges from the ground surface to 0.24 m with a maximum MS at 0.18 m BS (Figure 5.13). The second smaller peak ranges from 0.32 to 0.42 m BS. These both are within 0.04 m from the peaks in feature O, showing similar depth results. This anomaly is likely not a good candidate for depth analysis. Due to the blending of anomalies with feature O, HW estimates from the G-858 higher survey were not possible. The other HW estimates overestimate and are similar to the neighboring feature O (Figures 5.16 and 5.17). Given this similarity, SI=1 was also investigated

for this feature. The SI of one estimates are certainly closer in accuracy to the average adjusted center, but not as accurate as the estimates for feature O. Given that the anomalies run together and the MS logs show similar depths it is possible these are the same or are at least related features.

R) Feature R is a well-defined somewhat elliptical anomaly measuring approximately 2 x 2.6 m in all surveys (Appendix B.12 and B.13). The MS log shows a peak ranging from 0.08 to 0.24 m with a MS maximum at 0.2 m BS (Figure 5.13). Minor peaks occur at 0.4 and 0.5 m BS as the MS slowly decreases to approximately 0.7 m BS. This is likely a fair candidate for depth analysis. Depth estimates are fairly consistent between the survey instruments and within different SIs (Figures 5.16 and 5.17). The SI of two estimates, especially HW, are the most accurate. At this feature accuracy directly increases with increased sensor height. This pattern has been observed with other features. Given the MS log, one could estimate an adjusted center depth at 0.4 m BS. If that depth is used, the SI of two estimates are much more accurate. However, the estimates to the MS maximum peak certainly suffer from the large anomaly width.

S) Feature S is a fairly circular anomaly measuring approximately 1.2 m in diameter (Appendix B.12 and B.13). The MS log shows two peaks (Figure 5.13). The shallower is saw-tooth in appearance and ranges from 0.1 to 0.46 m with a MS maximum at 0.3 m BS. The second well-defined peak occurs from 0.6 to 0.7 m with a central maximum at 0.65 m BS. Although the MS log is more complex, this is likely a good candidate for depth analysis. Using SI=3 overestimates both the MS maximum and second peak (Figures 5.16 and 5.17). The SI=2 estimates are fairly consistent across all techniques and accurate. Using an adjusted center depth of 0.4 m slightly increases the accuracy of the SI of two estimates. The SI of three estimates likely suffer the most from the anomaly width being greater than the distance from the source to the sensor.

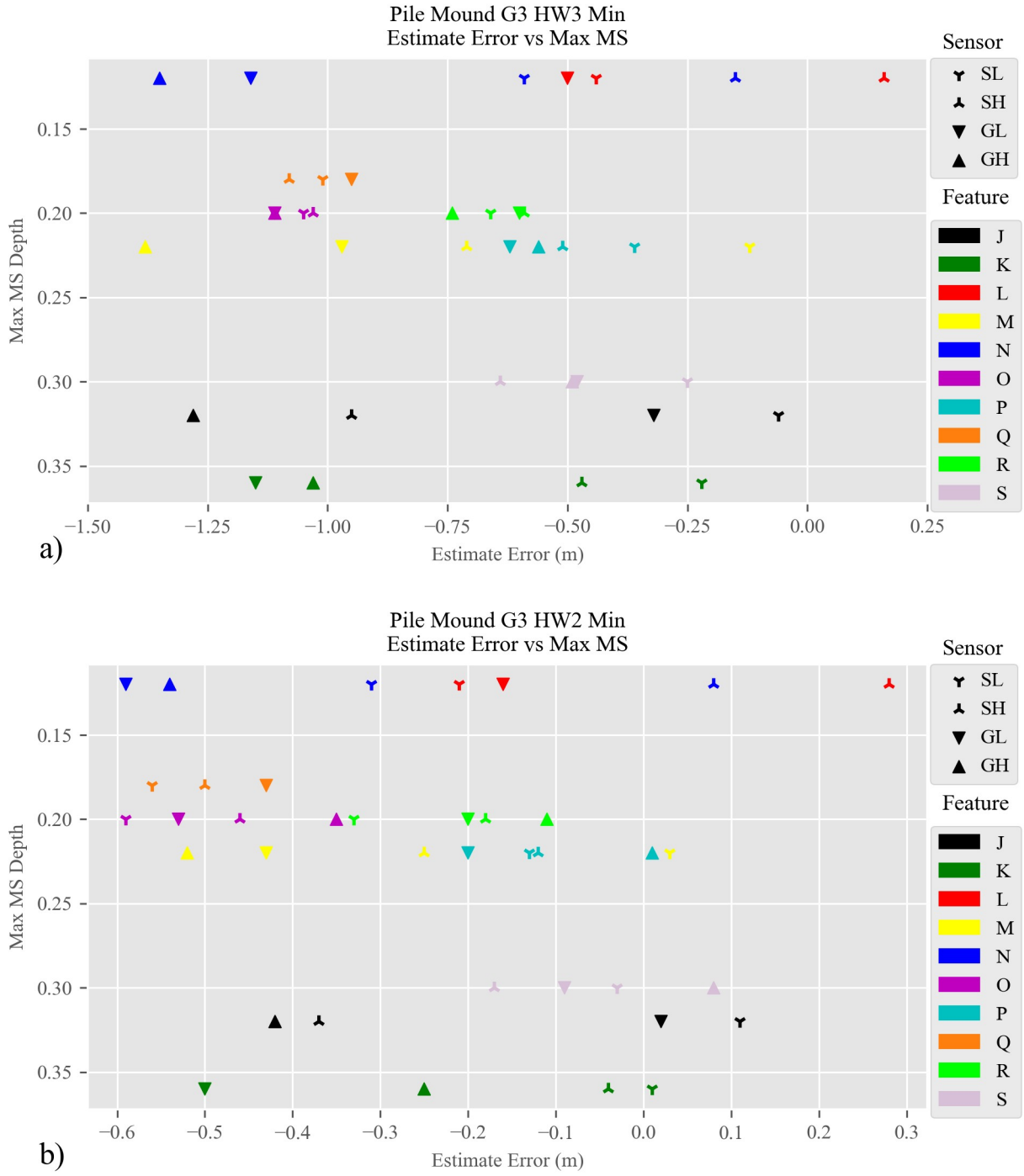

Figure 5.16. Pile Mound G3 Half-width Depth Estimates. The HW minimum depth estimate error is plotted against the maximum MS depth for all features where a) is the SI=3 and b) is the SI=2 estimates. Sensor labels are ‘S’ for SENSYS, ‘G’ for Geometrics, ‘L’ for lower height, and ‘H’ for higher height.

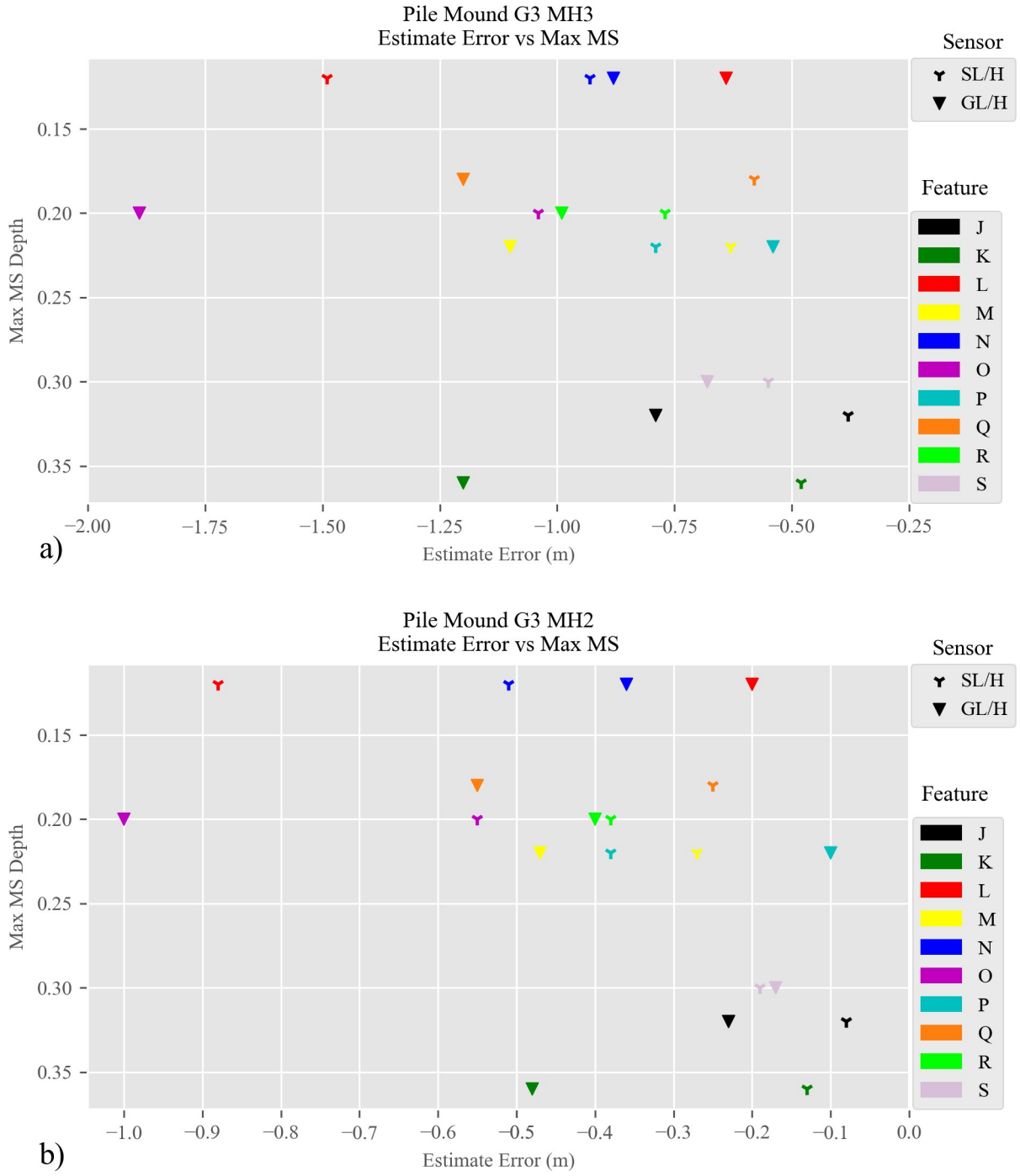

Figure 5.17. Pile Mound G3 Multi-height Depth Estimates. The MH depth estimate error is plotted against the maximum MS depth for all features where a) is the SI=3 estimates and b) is the SI=2 estimates. Sensor labels are 'S' for SENSYS, 'G' for Geometrics, 'L' for lower height, and 'H' for higher height.

Site Summary

Of the nineteen features of interest the author determined eleven would possibly be good candidates for depth analysis while the other eight would not. Similarly to the features at Woolsey, almost all magnetic anomaly widths were greater than the distance from the MS feature center depth to the sensor. When using SI=2, nine feature depths were correctly estimated by the majority of the depth estimation techniques. The only overwhelmingly accurate SI of three estimates were for feature B. Two features, O and Q, had much wider magnetic anomalies than the depth to the MS log's feature center and so SI=1 was employed in these cases. The SI of one proved the most accurate for these two features. Across all features at the site, SI=2 was generally the most consistently accurate within a plus or minus 0.25 m range.

As at Woolsey a pattern of estimates decreasing with increased sensor distance is observed (as seen for feature O). When this occurs, features appear to better fit a point-source model, but depth is overestimated due to the larger width of the feature. When the opposite pattern occurs (as seen for feature J), the estimation increases with sensor distance, SI=2 appears a better fit with very consistent and accurate estimates occurring. Again the MH estimates skew towards overestimation across the entire site while HW estimates are more centered about an error of zero.

Given results thus far, at Woolsey and Pile Mound, a clear pattern is evolving within the HW estimates. When depth estimates decrease with increased sensor distance, the higher survey is likely most accurate with SI=3. This is likely due in part to the increased feature width to sensor distance ratio. The width of the feature is less than or extremely close to the distance to the sensor. When this is not the case, or the direct opposite pattern (the estimate increases with increased sensor distance) is observed, SI=2 is more aptly applied to all survey heights.

Many features had an MS log type designated as large areas of high MS (pit) at Pile Mound. It is clear that in most cases the MS maximum is not a good feature center proxy for these log types. The author has combined visual analysis of the MS logs and simple calculations to create an "adjusted center-depth". In most cases this increases the center depth and increases the accuracy of the SI of three estimates. It does not always increase the accuracy of the SI of two estimates. In any case, it is clear that this is an area for further study and improvement in the future as this method is skewed by the author's visual interpretation of the MS log, and therefore it is not completely quantitative in nature.

Runion

Results in this section include magnetometry, down-hole MS, and depth estimation models. Two different magnetometer systems were used at Runion, the Geometrics G-858 and SENSYS prototype. Unfortunately, due to a combination of operator and instrument error the SENSYS prototype data were not recorded properly and are unusable for depth estimation. Three Grid Blocks (G1, G2, and G3) of varying size were selected for survey encompassing 15 magnetic anomalies of interest. The field vegetation was low and snow provided a smooth surface for the survey. Sixteen down-hole MS logs were taken, denoted as D-P with L having an additional 1-5 designation. Prior gradiometry survey data were used to guide data collection. A known GNSS datum was in place at the site before survey began which allowed alignment between prior data and the current survey.

Magnetometry

G1 encompasses a 25.5 x 25 m area at 0.25 x 0.1 m resolution (Figure 5.18). The data appear of good quality with some speckling in the lower dataset and minor noise in the higher dataset (Appendix B.14). The grid block has 10 anomalies of interest (A-J). Anomalies are generally distinct with no major data defects.

G2 encompasses an 8 x 8 m area at 0.25 m x 0.1 m resolution (Figure 5.19a). The data are of good quality with minor noise in the lower dataset. This grid block encompasses two anomalies of interest (K and L). Based on prior work at the site, feature L is a likely house floor and multiple MS cores were taken throughout this anomaly. This is different from any other features in all previous surveys.

G3 encompasses a 10 x 11 m area at 0.25 x 0.1 m resolution (Figure 5.19b). The data are devoid of any major errors and well represent four features of interest (M-P). Based on prior work at the site, these features likely all comprise part of a structure with possible internal archaeological features like a hearth or pit. The anomalies may represent, walls, the floor, pits, or hearths. This is different than features from previous surveys and is most similar to G2 feature L. These features do slightly differ from feature L however, as one or all of the G3 features may not be a floor.

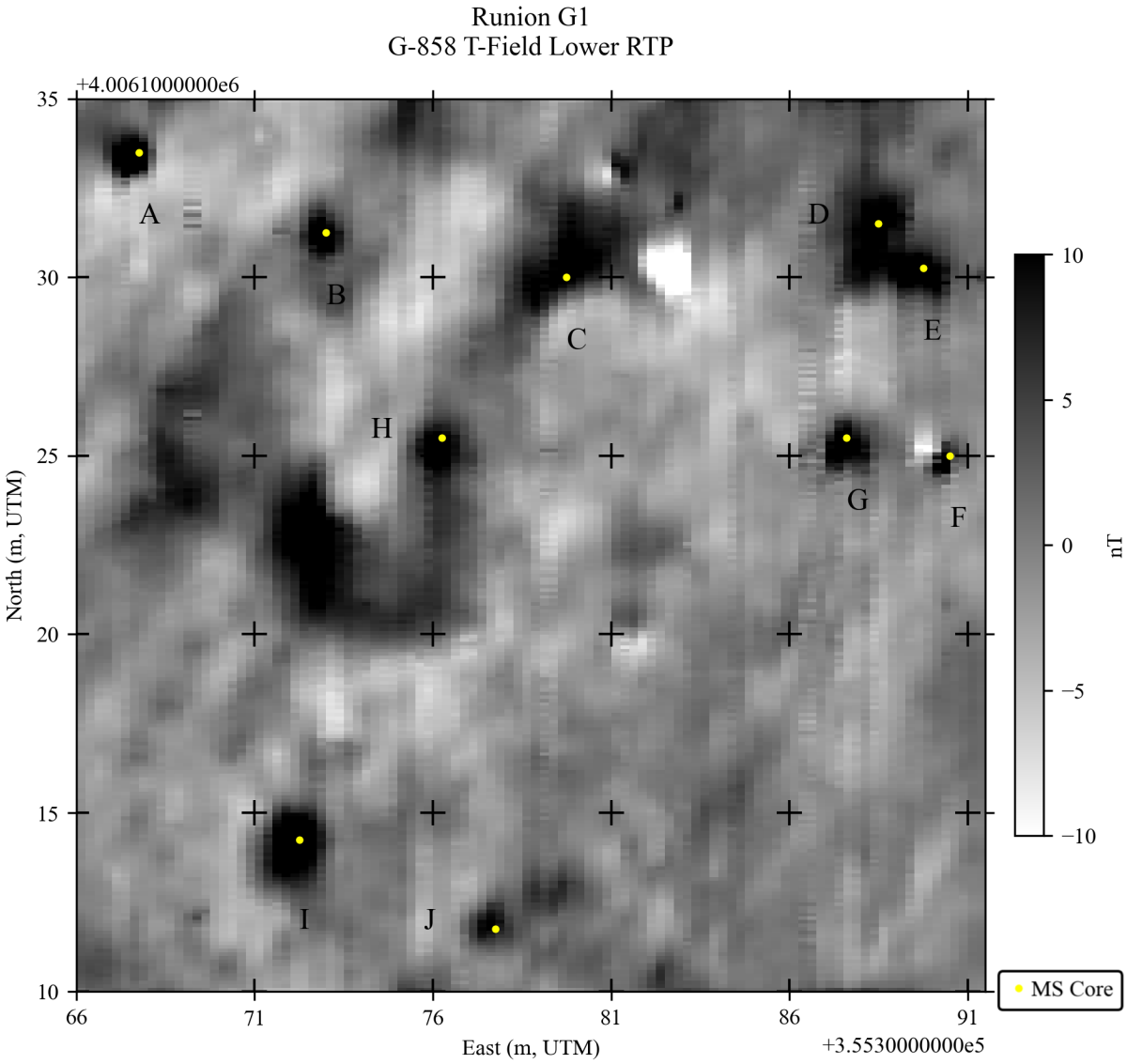

Figure 5.18. Runion G1 G-858. Processed lower data in UTM coordinates. Labels of features A-J with corresponding MS core locations in yellow.

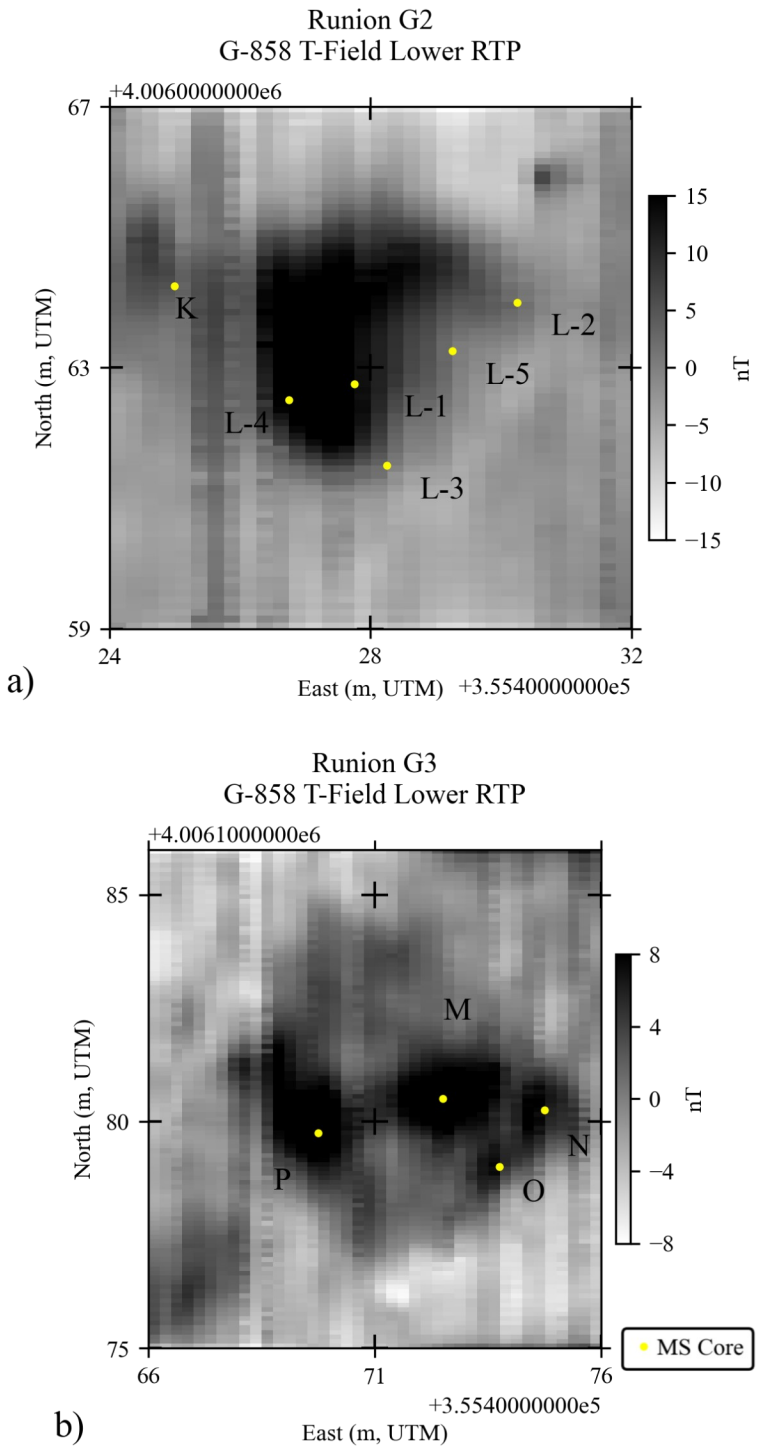

Figure 5.19. Runion G2 and G3 G-858. Processed lower data in UTM coordinates of lower. a) Grid block two. b) Grid block three. Labels of features K-P with corresponding MS core locations in yellow.

Down-hole MS

A total of twelve magnetic anomalies were investigated with DHMS. The locations of MS cores were based on the previously collected gradiometry data. Unfortunately, soil cores A, B, C, and H encountered rock at varying depths which prohibited DHMS over those features. Feature L is likely a structure floor and so five cores were placed throughout its area. This resulted in 16 MS logs (Figures 5.20-23). Cores appear fairly well placed for all anomalies in G1 and G3. The core locations of G2 are slightly misplaced compared to the new total field data. The five cores in feature L (L-1 through 5) could have been placed more to the west in order to better delineate the magnetic anomaly, as suspected structure floor. No other issues are present with the down-hole MS data. The MS logs from this site can be placed into five categories: a well-defined single peak, a larger area of higher MS (pit), top-skewed, likely floor, and small pit.

Five MS logs (G and M-P) are categorized as well-defined single peaks which are most relatable to point-sources. Log G is of particular note given its extremely high MS, the highest surveyed throughout the project. Logs M-O show peaks at similar depths and are related to a likely structure. They are not categorized as likely floors based on the magnetic anomalies at those locations. A magnetic floor anomaly would best be represented by one broad anomaly, where the anomalies associated with these logs are fairly separate. It is possible that they are in fact part of a floor. Log P is anomalous, as it is the deepest log collected throughout the project and contains the deepest MS peak. If the MS log is considered alone, one might suggest the feature is more geomorphic in nature given its depth, but the magnetic anomaly associated with this location is clearly archaeological in nature and so it is treated as such.

One log (L-5) is placed in the pit category. Although this core is likely part of a structure, it is not similar to the other L logs and is more similar to logs fitting a pit feature. It is quite

plausible that there is a pit inside the likely structure at the core location. For those reasons it is categorized differently than the other L logs.

Log J most closely fits the top-skewed category, but the top is shifted downward compared to the logs from Pile Mound.

Four logs (L-1-4) are categorized as likely floor. These logs show clear well-defined peaks, but given the site background and that all have peaks occurring at similar depths indicative of a floor layer, these are likely not point sources and so placed into a new category.

Five logs D-F, I, and K (small pits) are categorized differently as they do not clearly fall into the single peak or large area of high MS (pit) categories. In general, MS increases slightly from the ground surface to about 0.15 m BS. Then the log levels off for a distance before rapidly increasing in MS. A small area of high MS, roughly 0.1 m in length is observed before MS decreases again. This category contains the most variability between logs.

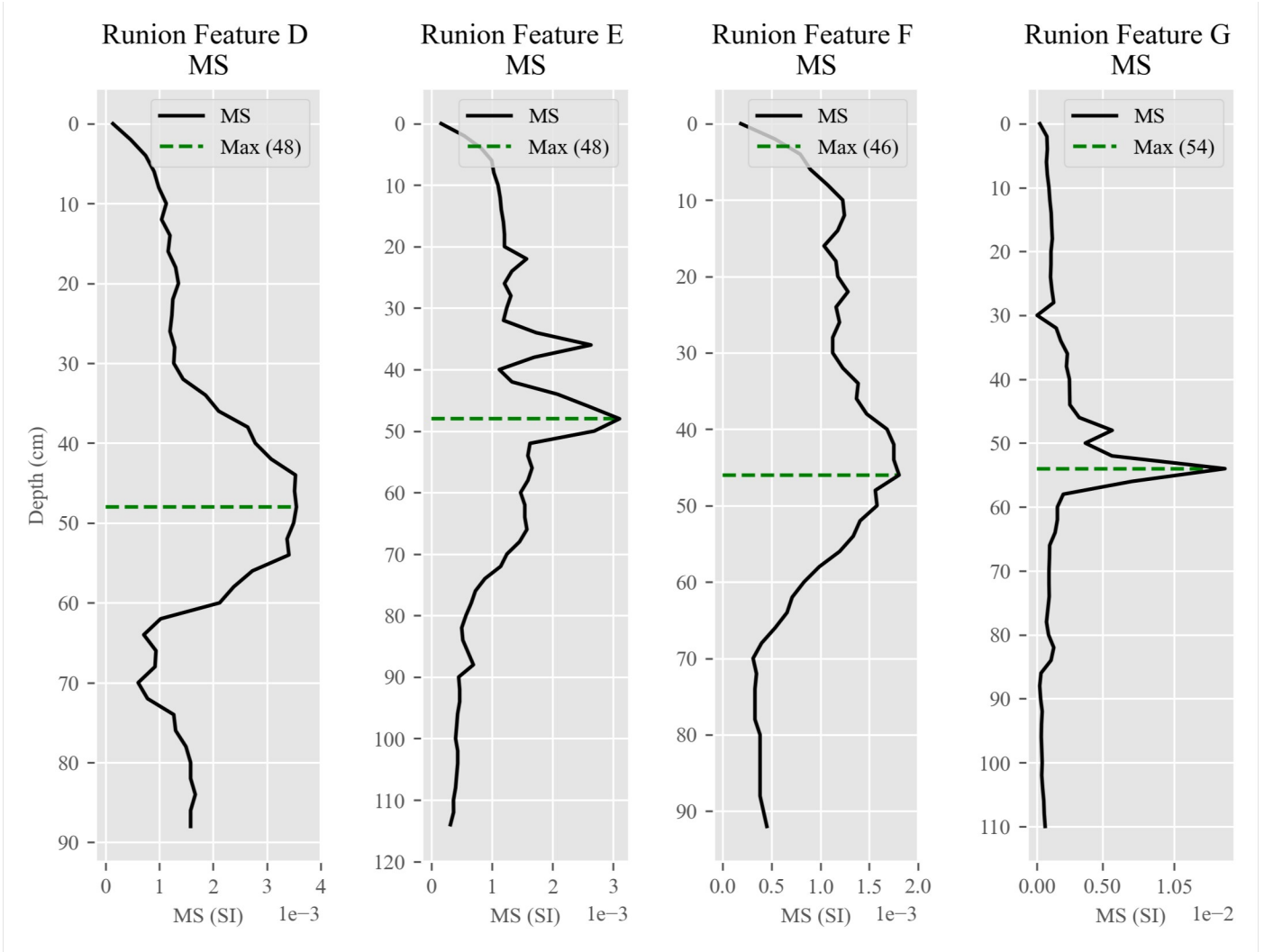

Figure 5.20. Runion DHMS Logs of Features D-G. MS logs of features D-G with MS in the dimensionless SI units and log depth in cm below surface.

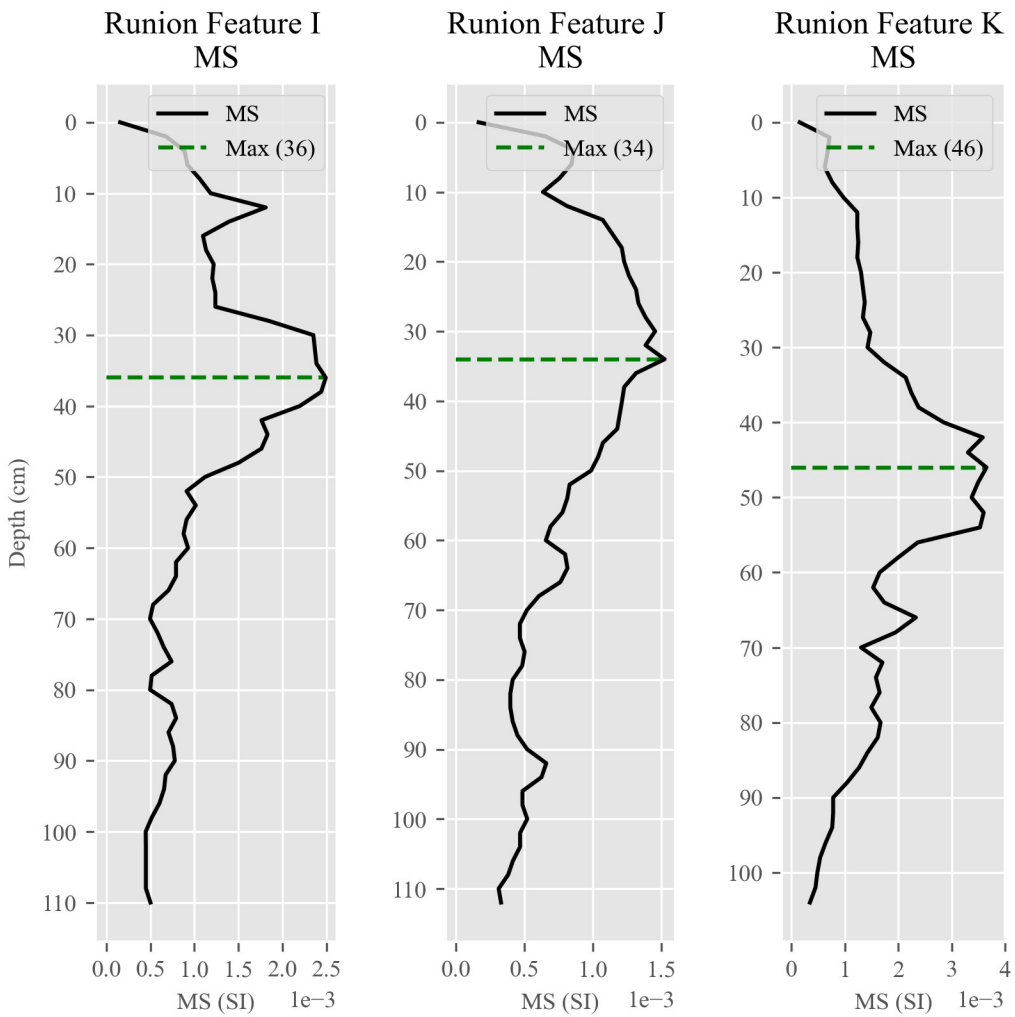

Figure 5.21. Runion DHMS Logs of Features I-K. MS logs of features I-K with MS in the dimensionless SI units and log depth in cm below surface.

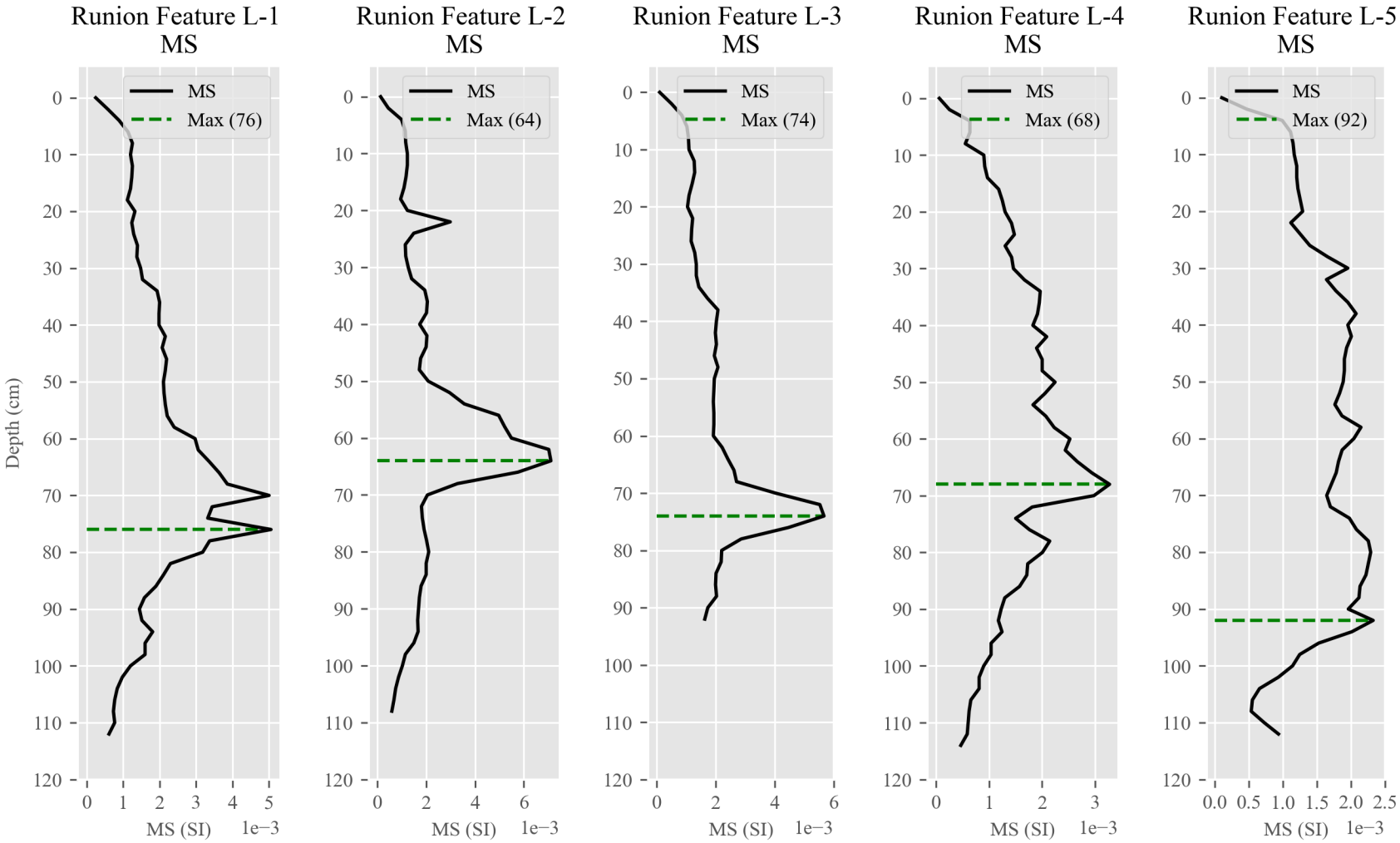

Figure 5.22. Runion DHMS Logs of Feature L. MS logs (1-5) of feature L with MS in the dimensionless SI units and log depth in cm below surface.

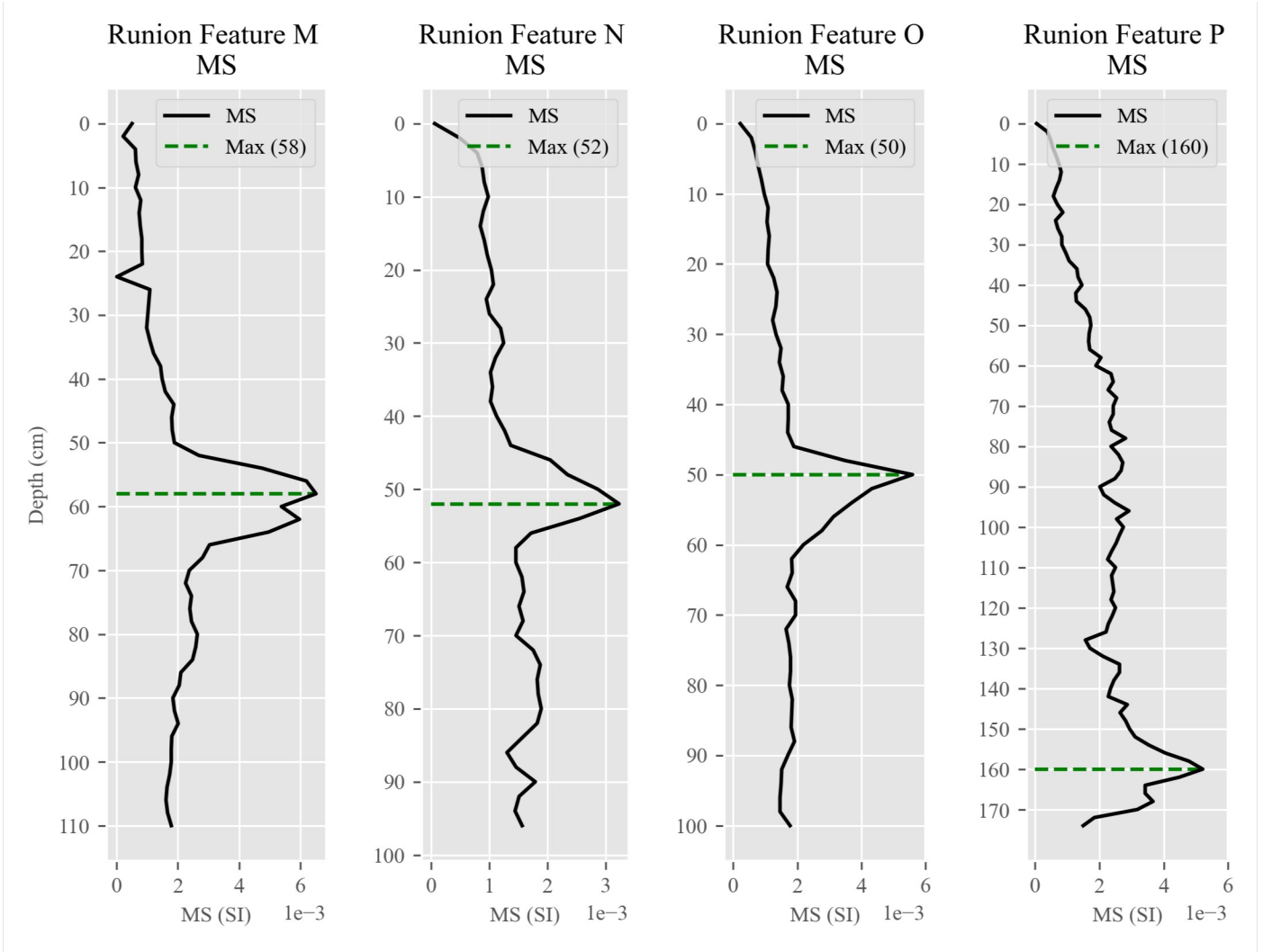

Figure 5.23. Runion DHMS Logs of Features M-P. MS logs of features M-P with MS in the dimensionless SI units and log depth in cm below surface.

Depth Estimation of Features

All sixteen magnetic anomalies of interest were chosen for depth estimation testing. Unfortunately, complete MS cores were not possible for features A, B, C, and H due to impenetrable ground (rocks). Multiple core holes in each anomaly were tried, but encountered rock in all. In these cases, the average depth to the rocks was taken and 0.1 m was added to it as a proxy feature depth. This was based on the median MS feature range of 0.2 m. Assuming the rocks as the top of the feature, adding one half of the median range to the rocks would emulate the potential center of a feature. The accuracy of these depth estimates is taken with caution. Multiple core holes were placed throughout feature L to better delineate the bounds of the likely structure floor. In some cases in G2 and G3, the SI of one was also investigated as this is theoretically more applicable to potential floor like source-bodies, but no figure is shown. For G1 only SI=3 and two was investigated as these all fit more of a point-source like model.

A) Feature A is a distinct circular anomaly measuring approximately 1.3 m in diameter in both surveys (Appendix B.14). No MS log was possible at this anomaly, but five core holes were attempted expanding from the center of the anomaly and all encountered rock. The core depths are 0.15, 0.22, 0.25, 0.25, and 0.32 m BS. An estimated center depth of 0.34 m BS was used for depth estimation testing. Disregarding the lack of MS data, this is a good candidate for depth analysis. Depth estimates differ between the two heights (Figure 5.24). The SI of three estimates all fall within a fair estimation range while using SI=2 increases overall error. Given the smaller anomaly diameter and likely rocks as the source-body, the SI of three makes theoretical sense. Without additional depth information no definitive comparison can be made.

B) Feature B is a well-defined circular anomaly measuring approximately 1.2 m in diameter in both surveys (Appendix B.14). Again, no MS log was possible at this anomaly. Five core holes expanding from the center were attempted, but all hit rock. The maximum depths of the holes

were 0.27, 0.32, 0.35, 0.4, and 0.42 m BS. An estimated center depth of 0.45 m BS was used for depth estimation testing. Barring the lack of MS data, this is a good candidate for depth estimation. All SI of three estimates appear fairly accurate and only slightly overestimate the depth to the feature (Figure 5.24). Error increases when using SI=2, where all techniques underestimate the depth. Given the similarity between the magnetic anomalies and the soil core information, this feature likely fits a point-source model, but without additional depth information a true depth is unclear. It is very possible the center of the feature is slightly deeper, increasing the accuracy of the SI of three estimates.

C) Feature C is clearly a more linear elliptical anomaly measuring approximately 1.8 x 3.8 m in both surveys (Appendix B.14). No MS log was possible for this feature due to rocky soil. Two core holes were attempted with bottom depths of 0.3 and 0.35 m BS. An estimated center depth of 0.43 was used for depth analysis. This anomaly is likely a good candidate for depth analysis even without the MS data. Depth estimates are fairly consistent between the techniques (Figure 5.24). Using SI=3, all estimates sufficiently overestimate the depth while using SI=2 produces quite accurate results. Although rock was encountered at a similar depth to features A and B, this magnetic anomaly is much larger and linear compared to A and B. This could be the reason SI=2 is more appropriate, but without additional depth information it is difficult to evaluate the depth estimates further.

D) In the previously collected gradiometry data, features D and E are definitively separate. However, in the current surveys their anomalies blend together (Appendix B.14). Due to this blending, the data subsets used for the depth estimation were somewhat oddly shaped in order to estimate depth for each feature separately. Feature D is a rectangular anomaly measuring approximately 2 x 2.8 m. The MS log shows a well-defined peak from 0.3 to 0.65 m with a MS maximum in the approximate middle at 0.48 m BS (Figure 5.20). Given the blending of

anomalies, this may not be a good candidate for depth analysis. Depth estimates between the two heights and the combined MH are fairly consistent across both SIs (Figure 5.24). In all cases, the depth is significantly overestimated. It is likely this feature is wider than the distance to sensors, making depth estimation unreliable by these methods. Also, the blending of this anomaly with E likely causes some discrepancy.

E) Feature E is a somewhat defined circular anomaly measuring approximately 1.5 m in diameter. The northwest side of the anomaly blends together with feature D, especially in the higher dataset (Appendix B.14). The MS log is comprised of two large peaks and one minor peak (Figure 5.20). The first minor peak occurs at 0.22 m BS. The second, larger peak occurs from 0.32 to 0.4 m with a center at 0.36 m BS. The third and largest peak occurs from 0.4 to 0.52 m with a data maximum at 0.48 m BS. Manual core interpretation showed layered burnt black and red soil resembling a hearth centered at 0.52 m BS. Due to anomaly blending, the higher survey was unusable for HW rule depth estimates. Even with the anomaly blending the anomaly is very clear in the lower survey and therefore is a good candidate for depth analysis. All the depth estimates are extremely consistent within each SI (Figure 5.24). Using SI=3, depth is fairly overestimated. When using SI=2, all three estimates are nearly the same and accurately estimate the depth. They have an under 0.1 m overestimation to the MS log maximum and are within 0.03 m to the burnt soil layers. Additionally, if one adjusts the center distance to average the second large peak, making the center shallower by 0.065 m, the SI of two estimates are even more accurate. It is possible that the SI of three estimates are skewed by the larger width than the distance to the sensors, but the author favors the consistency and accuracy of the SI two estimates. Given the lack of G-858 higher survey, no pattern relating to the estimate distance and sensor height is possible. If observed, the pattern may add credence to which SI is more appropriate.

F) Feature F is an elliptical dipolar anomaly measuring approximately 0.8 x 1 m. The dipolar nature and rapid decrease in maximum magnetism (roughly 26 to 2 nT) between the two surveys possibly suggest a metallic or point-source like object (Appendix B.14). The MS log shows one small and one larger peak (Figure 5.20). The smaller goes from the ground surface to 0.15 m with a peak at 0.1 m BS. The second larger peak ranges from 0.3 to 0.7 m with a MS maximum at 0.46 m BS. Overall, the magnetic susceptibility of the log appears low compared to the site average. Given the small size of the magnetic anomaly, it is likely a good candidate for depth analysis. The depth estimates all severely underestimate the second peak, this may be partially due to the drastically lower nT values in the higher survey (Figure 5.24). Some estimates to the first peak are plausible, but the MS at this peak seem quite low for the lower survey maximum nT value. A few things are potentially causing errors. Given the distinct dipolar nature of the anomaly and rapid magnetic fall off, a small piece of metal could be at or near the surface. This would certainly skew the magnetic map. It is possible that a different low magnetism feature is observed in the MS log. Additionally, given the clear dipolar nature of the anomaly after RTP, remanent magnetism is present and was not accounted for in the RTP process. This could be causing erroneous values in the data. More information is needed to make a concrete decision.

G) Feature G is a well-defined circular anomaly measuring approximately 1.4 m in diameter in both surveys (Appendix B.14). The MS log shows an extreme peak from 0.46 to 0.6 m with a MS maximum at 0.54 m BS (Figure 5.21). Given these details, this feature is the best case for a point-source model throughout the entire study. The SI of three accurately estimates the depth to the feature in all cases. This is a significant test case because of the overall accuracy and precision of the estimates, and because the MS for this feature is the highest throughout the entire project. This suggests the feature is the most magnetic and compact, well-fitting the point-

source model and offering a clear example of both depth estimation techniques working properly in this situation. Additionally, the MS core coincides with the maximum value in both the lower and higher surveys giving credence to the potential need for more accurately placed cores in other analyses.

H) Feature H is a distinct circular feature measuring approximately 1.6 m in diameter in both surveys (Appendix B.14). There is no MS log for this feature do to cores encountering rocks. Three cores were placed near the center of the anomaly with maximum depths of 0.6, 0.63, and 0.7 m BS. An estimated center depth of 0.74 was used for the depth analysis. Given the magnetic anomaly size and quality, this is likely a good candidate for depth analysis. The depth estimates are inconsistent between the different survey heights, but the lower HW and MH are very similar (Figure 5.24). An SI of three produced the most accurate results with the higher HW being extremely accurate This survey has an equal distance to the source from the sensor compared to the anomaly width. Since the feature is certainly less wide than the representative magnetic anomaly, the feature width should be less than the distance to the sensor. This further suggests the SI of three is appropriate. Estimates with SI=2 all underestimate the feature depth. The SI of three estimates are close to the rock depth, but this may be an inaccurate depth proxy and so more information is needed to make a proper assessment.

I) Feature I is a well-defined slightly elliptical anomaly measuring approximately 1.7 x 2.1 m in both surveys (Appendix B.14). The MS log shows two clear peaks (Figure 5.21). The shallower ranges from 0.1 to 0.16 m with at peak at 0.12 m BS. The second ranges from 0.26 to 0.52 m with a MS maximum at 0.36 m BS. This is likely a good candidate for depth estimation. The higher and lower HW estimates are not very similar while the MH estimate is close to the lower survey estimate (Figure 5.24). Using SI=3 overestimates with all three sensor configurations. The SI of two more accurately estimates the depth, however the estimates are

both under and over estimations. It is likely this feature is wider than the distance to sensors, making depth estimation unreliable by these methods.

J) Feature J is a fairly circular anomaly measuring approximately 1 m in diameter in the lower survey and is less well-defined in the higher survey (Appendix B.14). The MS log shows four peaks (Figure 5.21). The shallow peak ranging from the ground surface to 0.1 m centered at 0.05 m BS. The second most significant peak ranges from 0.1 to 0.6 m with a MS maximum at 0.34 m BS. The third and fourth peaks are minor and occur at 0.64 and 0.92 m BS, respectively. This feature is a good candidate for depth analysis. Depth estimates are fairly consistent within and between the surveys (Figure 5.24. Using the SI of three overestimates the depth to the second peak while using SI=2 equally underestimates the depth to the feature. The estimates decrease with sensor distance, fitting the observed pattern that suggests SI=3 is more appropriate. It is difficult to suggest more of a cause without additional details, because both SIs moderately estimate the depth to the source.

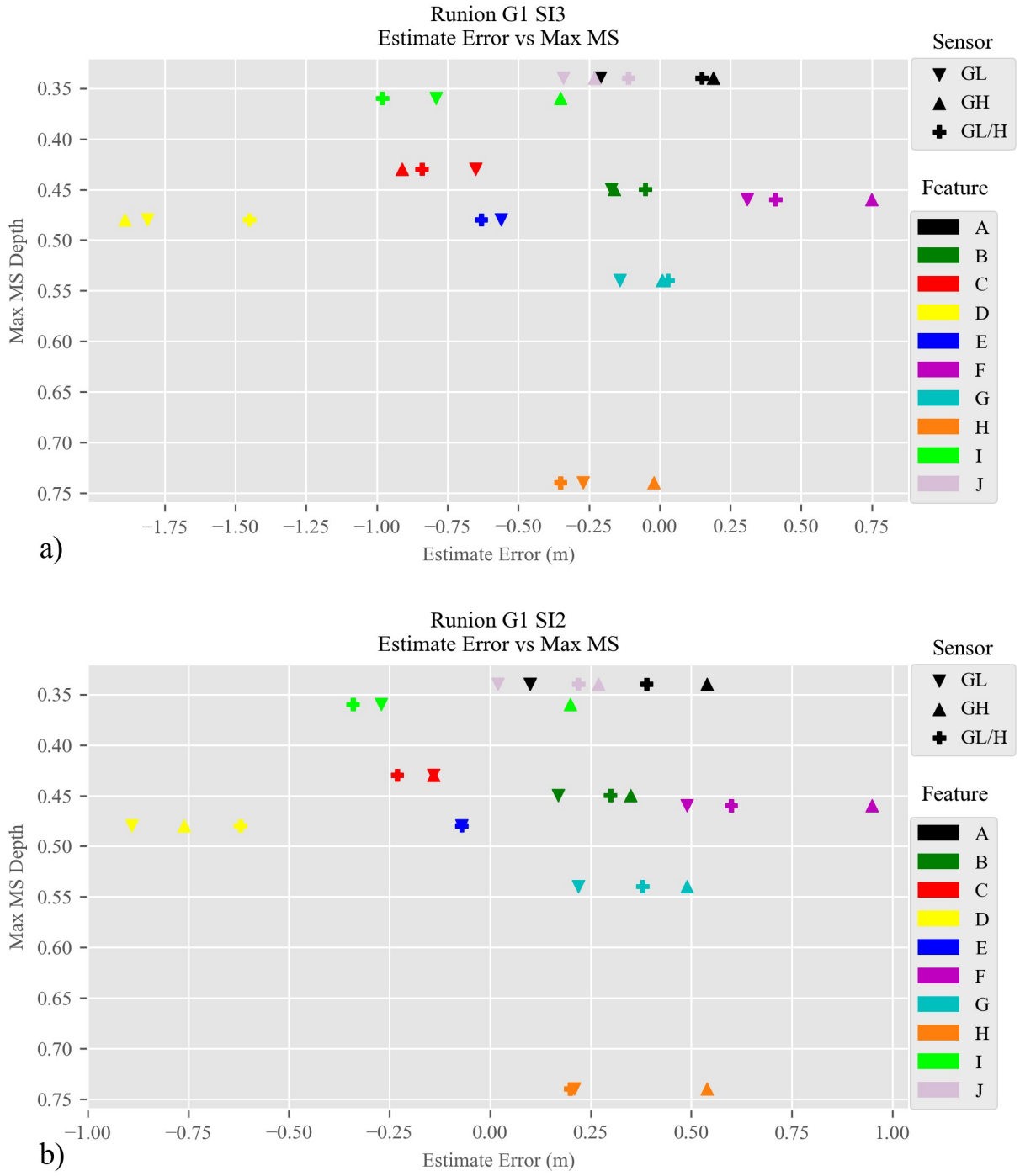

Figure 5.24. Runion G1 Depth Estimates. The HW minimum depth estimate and the MH error is plotted against the maximum MS depth for all features where a) is the SI=3 estimates and b) is the SI=2 estimates. Sensor labels are ‘G’ for Geometrics, ‘L’ for lower height, and ‘H’ for higher height.

K) Feature K is a fairly defined elliptical anomaly measuring approximately 0.75 x 1.8 m in both datasets. The higher data anomaly is less well-defined and slightly larger (Appendix B.15). The MS core is slightly offset to the southeast of the anomaly. The MS log shows a clear major peak from 0.3 to 0.6 m with a MS maximum at 0.46 m BS (Figure 5.21). A small secondary peak is at 0.66 m BS. This anomaly should be a good candidate for depth estimation. The depth estimates show fair consistency with SI=2 and are more dispersed with SI=3 (Figure 5.25). The SI of three lower survey HW estimate is extremely accurate and the MH estimate is fair. All three SI of two estimates are approximately a 0.25 m underestimate. Given the poorer quality of the higher survey, the well-defined MS log, and the excellent accuracy of the lower survey, the SI of three is preferred.

L) Feature L is likely a structure floor and so is different from other anomalies evaluated thus far. The anomaly is fairly well-defined and measures approximately 4.8 m square with the bulk of the magnetic anomaly on the western half. For these reasons, multiple cores were placed throughout the anomaly. MS log L-1 shows a double peak that ranges from 0.6 to 0.9 m with a MS maximum at 0.76 m BS (Figure 5.22). L-2 has two peaks, a minor peak is located at 0.22 m BS and the major peak ranges from 0.5 to 0.7 m with a MS maximum at 0.64 m BS. L-3 has one clear peak ranging from 0.6 to 0.8 m with a MS maximum at 0.74 m BS. L-4 has a single major peak that ranges from approximately 0.54 to 0.74 m with a MS maximum at 0.68 m BS. L-5 does not have a well-defined single peak, but it is also in the least magnetic portion of the anomaly. It has an area of increased MS from 0.3 to the MS maximum at 0.92 m BS (Figure 5.22). Since this log more aptly fits the pit model, it is likely not indicative of the floor and is a poor data point for comparison. This suggests the likely structure floor around 0.7 m BS with some variance. One depth estimation was used for the entire anomaly and compared to each MS log individually (Figure 5.25). Using SI=3, which is likely not the appropriate SI based on computer modeling,

significantly overestimates the depth to the floor. This is expected given the large anomaly width. The data show a trend of the depth estimate decreasing with a lower SI. An SI of two placed the majority of estimates within the plus or minus 0.25 m window. The trend continues when employing and SI of one, no figure shown as the estimates are worse. The most accurate SI is two with the majority of the data falling between plus or minus 0.25 m.

M) Feature M is a broader elliptical anomaly measuring roughly 2 x 2.5 m in both datasets (Appendix B.16). Given the anomaly is located inside a likely structure, it could be an internal pit or hearth feature, or possibly a portion of the floor. The MS log shows a clear peak ranging from 0.5 to 0.7 m with a MS maximum at 0.58 m BS (Figure 5.23). Given the magnetic data quality this is a good candidate for depth analysis. The depth estimates are fairly consistent within each SI (Figure 5.25). The SI of three severely overestimates the depth while using SI=2 is only marginally better. If the anomaly is treated as an internal structure feature, the depth estimation is likely affected by the greater width than distance to the sensor. If treated more like a floor, the SI of one would be most appropriate. When using SI=1, the HW estimates fall within plus or minus 0.2 m. This is in conflict to what we see when estimating the distance to a floor in feature L. It is possible this feature is not a floor and is much wider than the distance to sensors, making depth estimation unreliable by these methods.

N) Feature N is a somewhat defined slightly elliptical anomaly measuring approximately 1 x 1.5 m (Appendix B.16). It is possible this is a portion of the outer wall or floor of the structure. The MS log shows a clear peak ranging from 0.4 to 0.58 m with a MS maximum at 0.52 m BS (Figure 5.23). This is slightly shallower than the neighboring feature. It is unclear if this anomaly will be good for depth estimation. The lower HW and MH estimates are fairly consistent within each SI (Figure 5.25). The HW estimates are likely being affected by the proximity to the

neighboring feature, thus limiting the data subset being used for depth estimates and introducing error into the estimate. Overall, the SI of two appears the most accurate.

O) Feature O is a circular anomaly in the lower data measuring approximately 0.9 m in diameter and is not well represented in the higher survey (Appendix B.16). This anomaly is near features M and N and blends slightly into them. It is possibly part of an outer wall or floor of the structure. The MS log shows a clear peak ranging from 0.46 to 0.6 m with a MS maximum at 0.5 m BS (Figure 5.23). This is almost exactly the same as the nearby feature N. Due to the proximity to other anomalies and the lack of clear representation in the higher dataset, no HW estimates for the higher data were possible. The two possible depth estimates are fairly consistent and the SI of two accurately estimates the depth to the feature (Figure 5.25).

P) Feature P is a well-defined fairly circular anomaly measuring approximately 1.9 m in diameter (Appendix B.16). The anomaly is on the outer edge of the possible structure and appears similar to feature M. It is possibly a pit or hearth, or a portion of the outer wall or floor. The MS log shows a peak ranging from 1.5 to 1.7 m with the MS maximum at 1.6 m BS (Figure 5.23). This is much deeper than the previous features. Depth estimates show fair consistency within and between survey heights (Figure 5.25). The SI of two severely underestimates the depth while using SI=3 is accurate for all estimates. Given the much deeper feature and that the SI of three work well, this is possibly a deep internal storage pit. Also, the error is especially small given the total distance from the sensors to the feature.

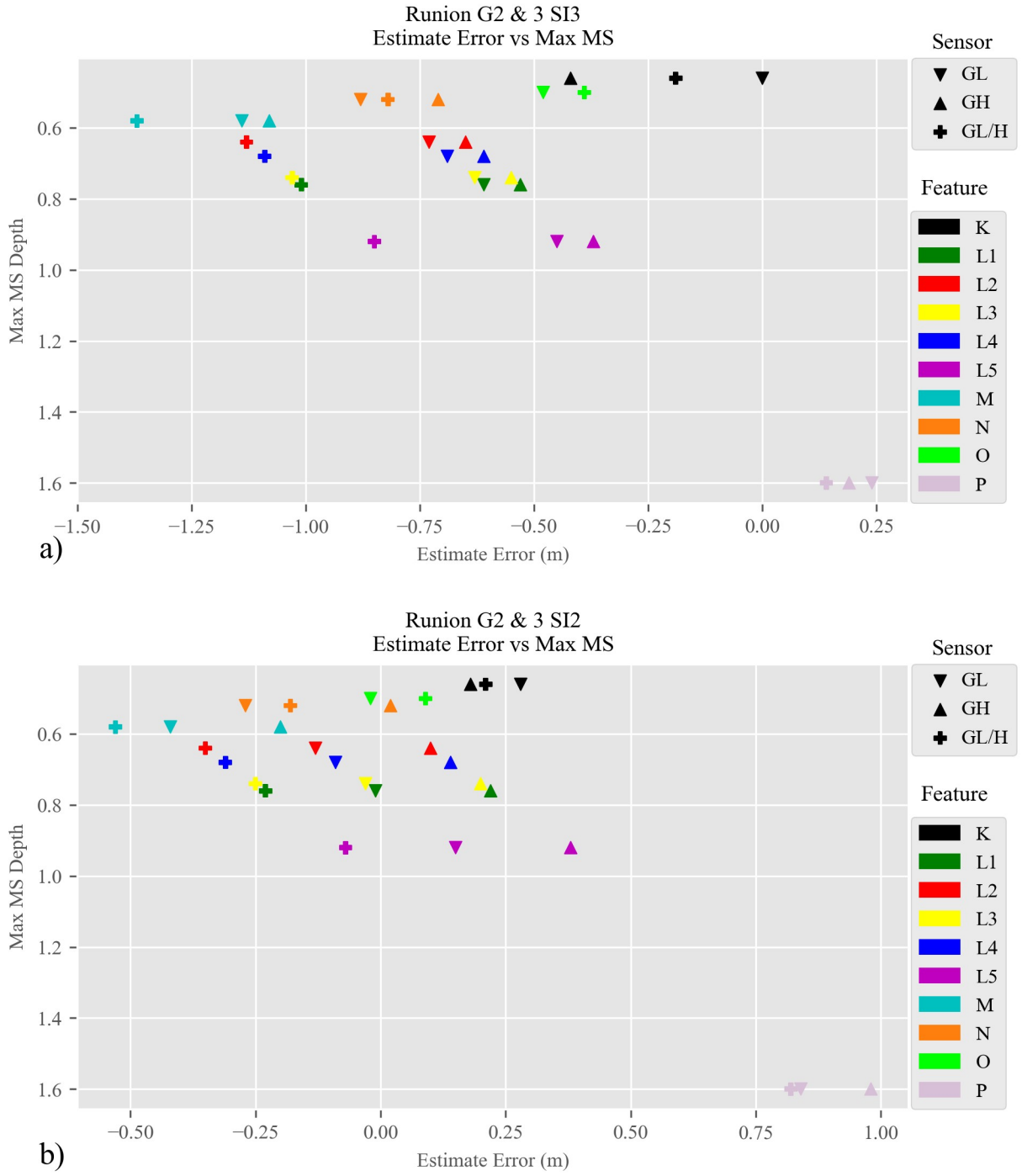

Figure 5.25. Runion G2 and G3 Depth Estimates. The HW minimum depth estimate and the MH error is plotted against the maximum MS depth for all features where a) is the SI=3 estimates and b) is the SI=2 estimates. Sensor labels are ‘G’ for Geometrics, ‘L’ for lower height, and ‘H’ for higher height.

Site Summary

Off the sixteen features of interest, the author determined eleven would likely be good candidates for depth estimation, one would not be a good candidate, and four were difficult to determine. These four are related to the two potential structures at the site in G2 and G3 and so are less understood. In the majority of the cases the width of the magnetic anomaly was greater than the distance to the sensor, but this site contained the most features that had almost equal width to distance ratios and in some cases the distance was clearly shorter than the width. This data is likely skewed in comparison to data from other sites in part by the lack of SENSYS data, as these surveys occur at lower heights. Fair estimates were made for all but two features (D and F). Across the entire site, SI=2 yielded the most consistently accurate results given an error range of plus or minus 0.25 m to the feature center depth.

Although this site did not benefit from the SENSYS survey, using only the G-858 data and therefore reducing the amount of data points for each feature, a pattern of decreased estimates with increased sensor distance is apparent. When this occurs SI=3 is likely more applicable, but often the width of the anomaly and likely the feature is greater than the distance to the sensor. This creates error which fits the error modeled in the computer simulations. When the opposite pattern occurs, SI=2 appears more reasonable.

Feature G is an exemplary case of the HW and MH techniques working properly. The magnetic anomaly is smaller in size and circular. The MS log shows a clear single peak of the highest magnetism compared to all others in this study. This is the most point-source like anomaly in the entire study. Using SI=3 correctly estimates the depth for this feature This shows clear proof of concept for the HW and MH techniques when dealing with a point-source.

Two likely structures were evaluated at this site. These types of sources were not encountered at other sites in the study. In these cases, SI=1 was also investigated as it would

theoretically be the more appropriate SI to use. Feature L, a clear structure floor, was more accurately estimated by using SI=2, however. The SI=1 produced considerably worse results. It is unclear if feature M is part of a floor or an internal feature of a structure, but using SI=1 was more accurate in this case. It appears more data is needed for these types of features to better understand the real-world relationship.

Results Summary

Forty-six features of interest were surveyed across the four sites. The majority of the features were surveyed with the SENSYS and G-858 instruments at two heights per instrument. The SENSYS surveys occurred at 0.0845 m (lower) and 0.3845 m (higher) above the ground surface. The G-858 surveys occurred at 0.35 m (lower) and 0.85 m (higher) above the surface. No SENSYS data were usable for the sixteen features at the Runion site, and some G-858 data were either not available or unusable for features at CATS, Pile Mound, and Runion. Although magnetometry data were collected at CATS, there is not sufficient depth information about the features that are suitable for depth estimation to accurately assess the estimation techniques. For this reason, CATS' data are not included in the following summary.

This summary is broken into three parts. First, the magnetic susceptibility data is reviewed to best categorize what types of features were detected in this study. The characteristics of those features are examined in the context of how they are relevant to depth estimation. Certainly, an entire study could be performed solely on the intricacies of the magnetic logs and corresponding soil characteristics, but that is outside the scope of this project. MS logs were evaluated specifically as an adequate proxy for the depth to magnetic source-bodies. The "center-depth" is of utmost concern in this regard, although future studies may benefit from evaluating depths to the tops or bottoms of magnetic source-bodies.

Next, the nature of the magnetic anomalies surveyed throughout this study are addressed. Different anomaly shapes and sizes can directly affect which depth estimation technique should be used and the accuracy of the techniques. This is most directly observed in HW estimates as anomaly shape and size changes the depth estimate.

The accuracy and effectiveness of the two depth estimation techniques, half-width and multi-height, performed in this study are evaluated. Data accuracy is evaluated for each MS feature log type (e.g. point-source, pit etc.), as this should correspond to the appropriate SI. Further, data trends are reiterated with a focus on the effects of larger feature widths.

MS Summary

Of the forty-six features selected for depth estimation only forty-two had MS logs. Four logs were not taken due to ground impediments, always rock, stopping the coring device. In these cases, depths to the top of the rocks plus 0.1 m were used as a proxy center depth of the feature. Additionally, one feature (a potential structure floor) had five logs taken. These two cases occurred at the Runion site. This amounts to forty-six MS logs and fifty total depth estimates. The MS logs were categorized into six descriptive categories (Figure 5.26a). These categories were an attempt to relate the MS logs to a potential magnetic source-body types and their archaeological equivalents.

- A ‘Single Peak’ was used to describe MS logs that had a sole well-defined MS peak. This log type is best associated with a point-source which theoretically should be estimated with SI=3. Archaeological features likely included in this category are hearths or very small pits. These were the most sought after feature type throughout the project and eleven occurred in the study areas.
- The most prominent MS log type ‘Pit’ has fourteen occurrences. This log type does not have a clearly defined peak and is most easily described as a single large area of high

MS. This is best modeled by a vertical cylinder source-body which has an associated theoretical SI of two.

- The third most prominent MS log type "Top-skewed" has ten occurrences, the majority of which are located at Pile Mound. In these logs, a smaller area of high MS is shallowly concentrated and then MS drops gradually with depth. This shape is most likely best categorized by the half-sphere model and should theoretically have an associated SI of three.
- A 'Small Pit' was used to describe MS logs that fit somewhere in between the Pit and Single Peak log types. In this category, MS logs slightly increase with depth for a variable distance and then increase rapidly, like a point-source, but plateau off for a sizable distance (approximately 0.2 m), before the MS rapidly decreases. This type occurred five times at the Runion site. No direct comparison to a theoretical source-body geometry can be made, but the author suggests SI=2 as the most applicable given the log types similarity to the Pit category.
- Four cores encompassed within Runion feature L are categorized as 'Floor'. This is because they are all within the bounds of a likely structure and have clear MS peaks at relatively the same depth. This is expected if they are in fact part of a structure floor. Although the MS logs look the same as the Single Peak category, their spatial proximity to each other and inclusion within one large magnetic anomaly exclude them from this category. Computer modeling results relating to this category were not overly definitive, but this feature type should be related to SI=1.

Since MS logs were collected at three different sites which varied greatly in geographic location, the soil environments encountered at each site are somewhat different. The sites all occur near a river or stream, so site geomorphology is not immensely different, but the change in

soil parent material creates differences in the potential MS of soils at the locations. This is directly observed in the overall low MS values at Pile Mound compared to Woolsey and Runion. The MS maximum value across all sites ranges from approximately 0.00125 SI to 0.014 SI, centered around 0.0025 SI (Figure 5.26b). This study is more concerned with the contrast difference between individual site background matrices and the sites respective archaeo-magnetic features, but there may be some relation between the maximum or peak MS values and the effectiveness of depth estimates. This potential relation is exemplified by the one major outlier, the study maximum which occurs at Runion, feature G. This feature is the most point-source like and the depth is extremely accurately estimated. This warrants future investigation.

In general, MS maximum values were used as a proxy for feature center depth. With the exception of one outlier all the MS maximums are shallower than 1 m BS (Figure 5.26c). This is shallower than the majority of the features tested in the computer models throughout Chapter 3. This shallow zone also has the most variability in depth estimates in the tests above. This means the real-world depth estimates tested in this project are likely to be more error prone than those in the modeling environment, an unfortunate occurrence.

Additionally, when using the SI of three for point-sources in the modeling environment, error was observed when the width of the feature was greater than the distance from the sensor to the center or top of the source-body. The error increased as more of the feature grew closer to the sensor, e.g. the source body center was shallower. The vast majority of the feature tops are 0.5 m BS or shallower (Figure 5.26d). Given many of the surveyed features are likely wider than 0.5 m, discussed more below, error is certainly being introduced for SI of three estimates.

Excluding the one outlier, all the feature bottoms occur above 1 m BS (Figure 5.26e). Combined with the feature top distance, the feature range (a proxy for thickness) is measured (Figure 5.26f). These measurements are especially useful when considering more complex

source-body models in potential future computer modeling. Currently, a small range is expected for point-source models. The majority of features studied have a range of approximately 0.2 m or less which may or may not fit into the point-source model. This data may be used in the future to better create archaeological source-body models.

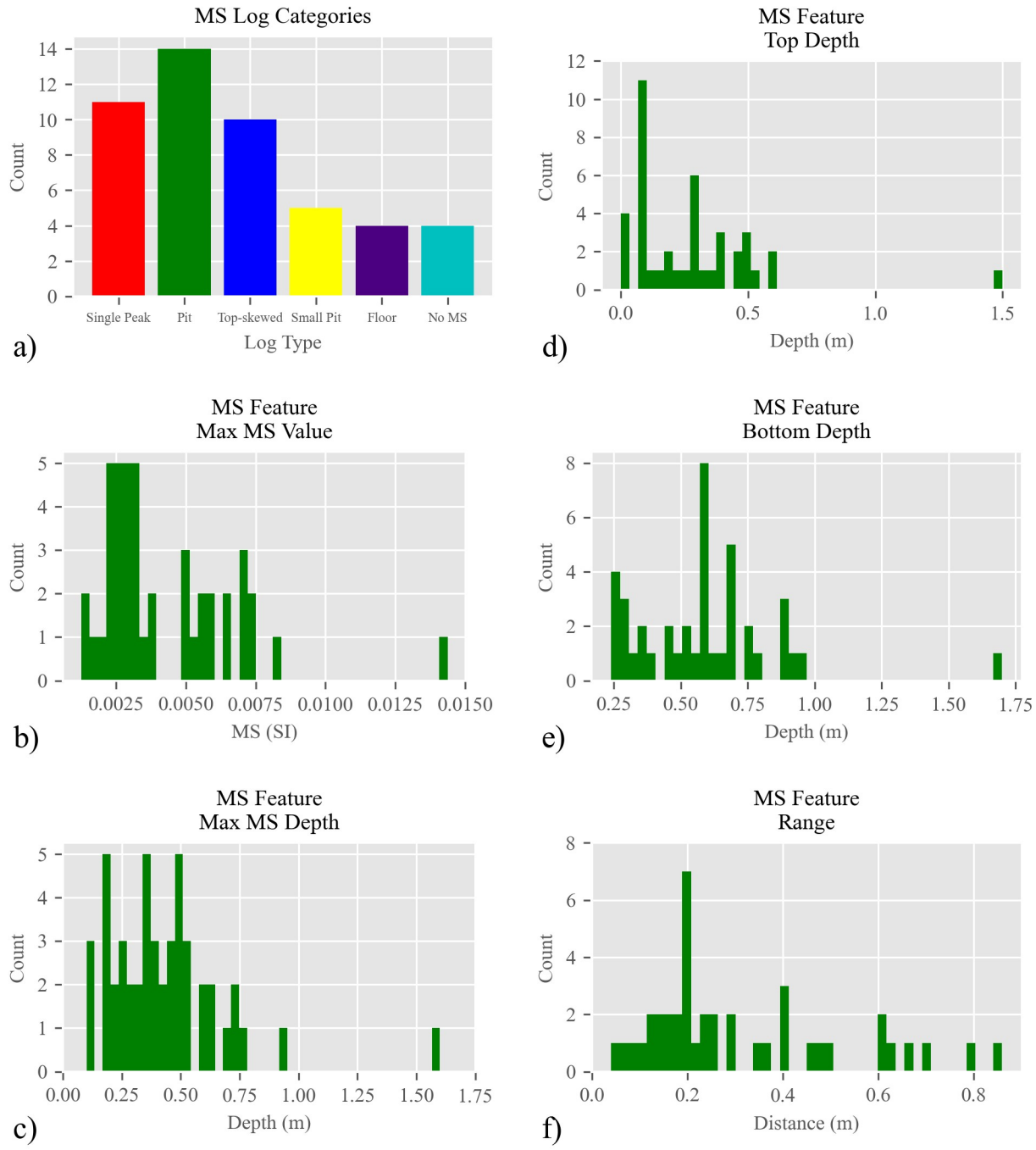

Figure 5.26. MS Features Summary. a) Graph of MS log categories. b) Histogram of MS logs maximum MS value. c) Histogram of the maximum MS value's depth. d) Histogram of top depth. e) Histogram of bottom depth. f) Histogram of the range of MS features, a proxy for thickness.

Magnetic Anomalies

The size and shape of magnetic anomalies can directly affect the depth estimates, especially the HW rules. The dimensions and shape also enlighten the observer on the possible type of source-body present, as per usual magnetic interpretation. For example, a large square anomaly would likely be related to a structure, perhaps walls or a floor. In contrast, a small circular anomaly may best represent a hearth or pit. These interpretations can lead to a better understanding of the likely source-body type and proper SI selection when evaluating the depth.

Circular anomalies are more likely to be considered point sources than elliptical anomalies as magnetism should emanate from a point source equally in all directions. Additionally, the size of the circle may warrant different interpretations. A medium size circle is likely not a hearth and may be better categorized as a pit or if a very large circle, a circular floor. Depending on the dimensions, elliptical anomalies can either be closer to a circle or more linear in nature. Linear anomalies would more appropriately fit a wall source-body model where more circular anomalies may better fit the point-source model. More elliptical anomalies may also more aptly be categorized as pit features, because hearths (fire pits) are circular more often than not. Rectangular anomalies suggest a potential wall or possibly floor, as pits and hearths are generally not rectangular in nature. By interpreting the different shapes and sizes of magnetic anomalies one may better select an appropriate structural index.

A major issue with these depth estimation techniques is their failure when a feature is wider than the distance from the from the source-body to the sensor. At present, there is not a definitive way to derive the actual feature width only from a magnetic map. So, the magnetic anomaly width has been used as a proxy knowing that the feature width is slightly smaller. Unfortunately, the majority of the magnetic anomalies in this study suffer from this condition (Figure 5.27). As one would expect, the lowest height survey, SENSYS lower at 0.0845 m,

suffers the most from this issue (Figure 5.27). As the sensor height increases, this issue diminishes and more anomaly widths are shorter than the distance to the sensor (Figure 5.27d). The obvious solution would be to survey at higher heights. However, surveying at such a height or higher imposes its own problems—features may not be detected at all. At the highest survey height (0.85 m) in this project, multiple features are barely detected or not detected at all.

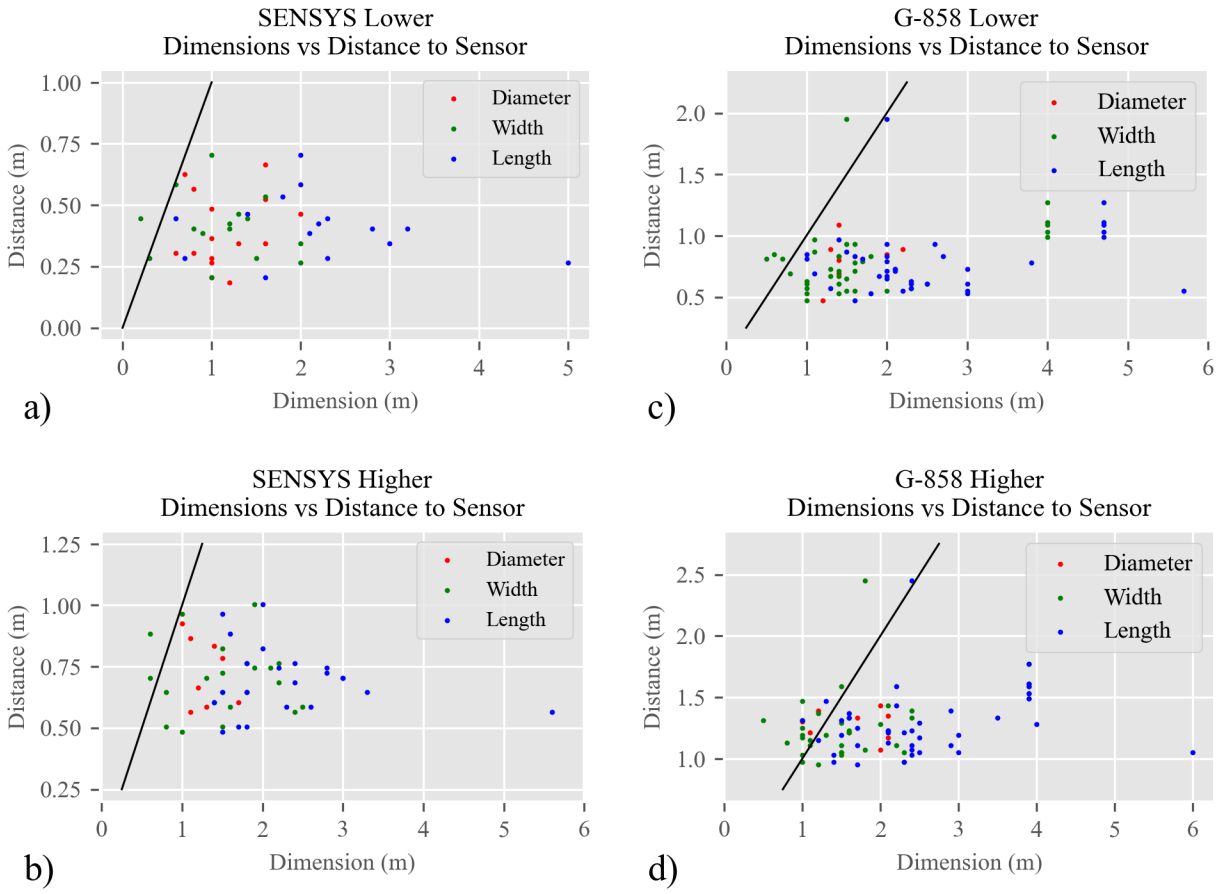

Figure 5.27. Magnetic Anomaly Dimensions Versus Distance. The dimensions of magnetic anomalies plotted against the distance from the MS maximum value to the sensor for the SENSYS lower, SENSYS higher, G-858 lower, and G-858 higher surveys (a-d). Data points above the black line are less than the distance to the sensor while those under the line are greater than the distance to the sensor.

Depth Estimates Summary

In total 432 depth estimates were made across three sites, Woolsey, Pile Mound, and Runion. These occurred at four heights: SENSYS lower (0.0845 m), SENSYS higher (0.3845

m), G-858 lower (0.35 m), and G-858 higher (0.85 m). With the exception of a few equipment malfunctions and magnetic anomaly blending, a half-width and multi-height estimate using each survey was made with SI=3 and SI=2. In a few circumstances SI=1 was used where it was likely more theoretically appropriate. These were performed when a much larger, in dimension, magnetic anomaly occurred. In general across all surveys and features, the HW method with SI=2 is the most consistently accurate within plus or minus 0.25 m. The accuracy of multi-height estimates using SI=2 were relatively similar to the HW estimates. In either technique, using SI=3 commonly overestimated the depth to features and had decreased overall accuracy. Additionally, higher surveys trended towards underestimation while lower surveys trend towards overestimation.

The MS logs are divided into five categories: Point-source, Pits, Top-skewed, Small pits, and Floor. Two graphics below show the aggregated depth estimates by MS log type (Figures 5.28 and 5.29). In some cases the estimates in these graphics have been adjusted from the raw estimates above. Where applicable the adjusted center-depths are used and the adjusted MH estimate of Pile Mound feature H is also used instead of the clearly erroneous estimate. The wildly inaccurate Woolsey feature H MH estimate was removed in order to better represent all other data. All other depth estimation data are as presented above.

Point-source models should be estimated with SI=3. In general, this SI overestimates the depth to features in this study (Figure 5.28a). Although there is clear error, it is likely caused by features being wider than the distance from the source-body to the sensor. The observed increased accuracy of the SI of two estimates may merely be a result of the lesser exponent used. If SI=1 were employed the estimates would decrease more. There are some notable accurate estimates in this category. Runion feature G is very accurately estimated and is the most point-source like of all the features studied. Woolsey feature I is also accurately estimated with SI=3.

In this instance, the source-body is likely not wider than the distance to the sensor. These results, coupled with the general trend of the data, suggest the depth estimation techniques are working as expected within their limits. An intriguing trend is observed in the HW estimates for this feature type. A clear trend of a decreased depth estimate with an increase in sensor height is observed. Further study of this pattern and sensor distance may be warranted to potentially improve the accuracy of these estimates.

The pit type MS logs were not examined in detail through computer modeling, but theoretically should have SI=2. The majority of the SI of two estimates fall within a 0.25 m error window with many more accurate estimates (Figure 5.28b). In this case, using SI=3 most often overestimates the depth to these features. The lower sensor heights, all but G-858 higher, appear to accurately estimate the depth to these features more commonly. The opposite of the pattern above is observed in the majority of the pit type data. In this instance, an increased depth estimate occurs with a decreased sensor height. Again, further study of this pattern and its relationship to the sensor distance may improve the overall effectiveness of the technique.

The cause of a top-skewed MS log was not studied in depth via computer modeling, but of the models studied thus far the half-sphere is most applicable. This would suggest three as the proper SI. Similarly to the point-source data, the SI of two appears to more commonly estimate the depth within a 0.25 m error window (Figure 5.29a). Estimates again decrease with increased distance between the source and sensor. As above, the SI of three overestimation is likely caused by the large width of the source-bodies and exceed the capabilities of the techniques.

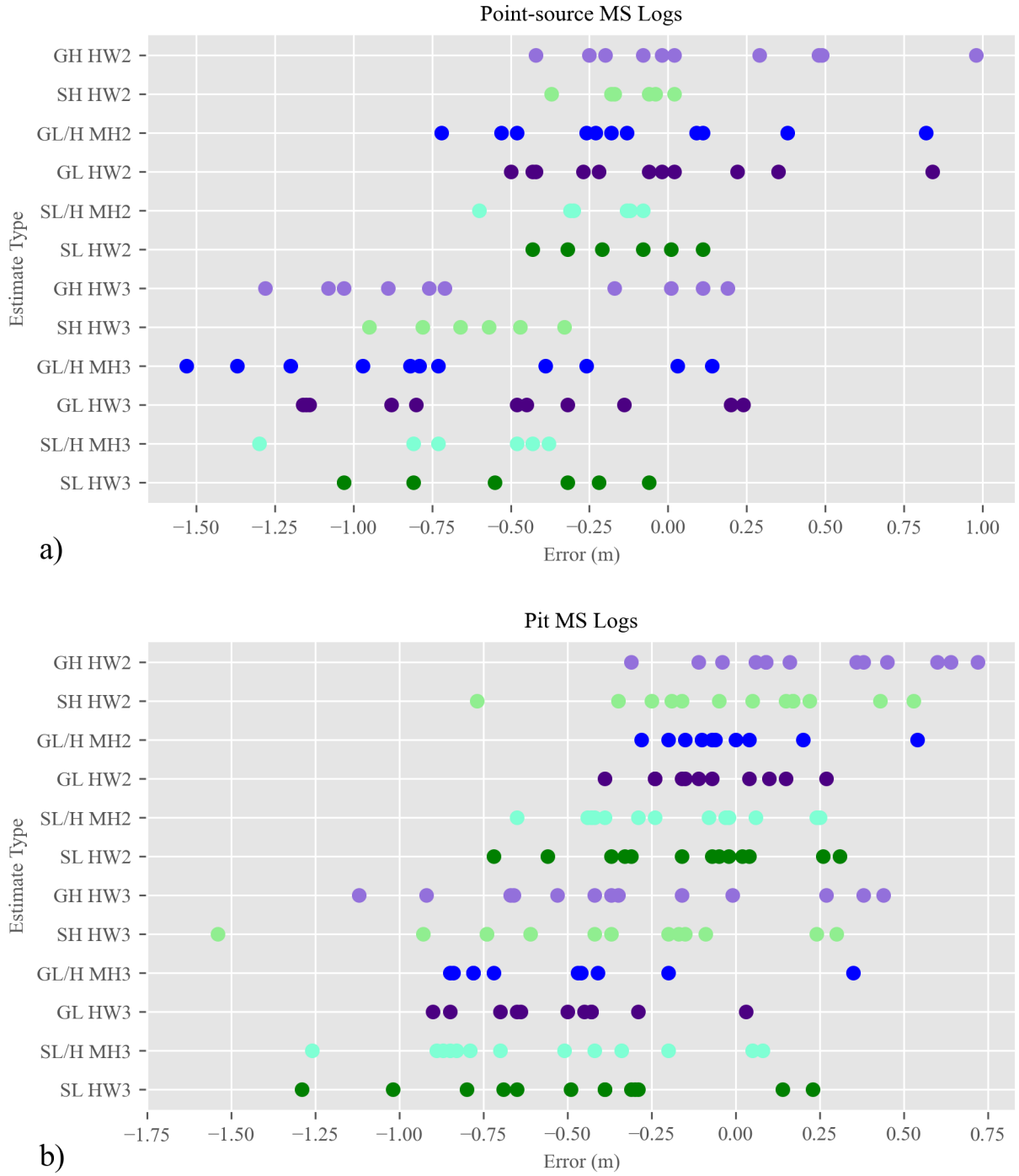

Figure 5.28. Depth Estimation Error for Point-source and Pit Log Types. Depth estimation errors for the point-source (a) and pit (b) MS log types. Sensor, survey, estimation technique, and SI are on the left. S (SENSYS), G (G-858), L (lower), H (higher), HW (half-width), MH (multi-height), number designates SI. Negative error is an overestimation.

A fourth category of MS logs is present at the Runion site, ‘Small Pit’. These features are roughly span 0.25 m in thickness and have well defined tops and bottoms. It is unclear which SI would be more theoretically appropriate for this source. This feature type unfortunately was not detected with the SENSYS instruments and so the depth estimates are more limited. This also reduces the variation in sensor height used to detect these features which detracts from a visible trend in the data. For the few data points SI=2 appears more accurate, but more data is likely needed to determine if this is the proper SI or a situation of the features being wider than the distance to the sensors (Figure 5.29b).

The floor category contains four logs all from the same structure compared to the same depth estimate. It is not shown here as figure 5.25 accurately depicts all of the data. In this case, SI=2 was more accurate than either SI=3 or the theoretically ideal value of one. All but a few data points fell outside a 0.25 m error window. More data over this feature type is likely needed to properly address depth estimates for the floor source-body.

Overall, the MH techniques appears trends towards overestimation compared to the HW rules. The height of the two data points used in the technique do appear to follow the same pattern observed in the HW estimates. Using two points at lower heights skews the estimates more towards overestimation. However, this also means that these estimates are more error prone when estimating to shallower source-source bodies. This is shown in the computer modeling data and therefore simply appears a limitation of the technique.

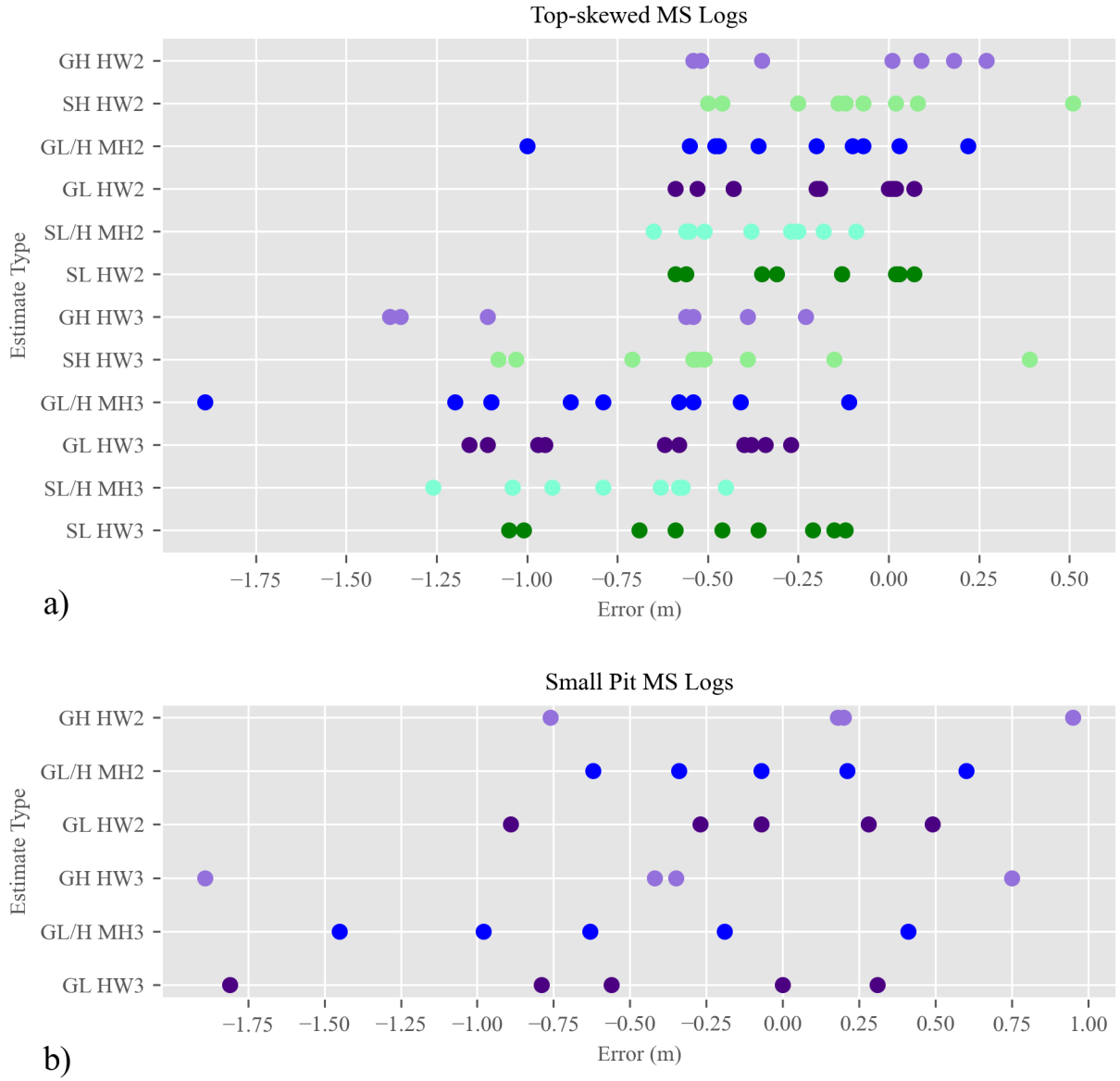

Figure 5.29. Depth Estimation Error for Top-skewed and Small Pit Log Types. Depth estimation errors for the top-skewed (a) and small pit (b) MS log types. Sensor, survey, estimation technique, and SI are on the left. S (SENSYS), G (G-858), L (lower), H (higher), HW (half-width), MH (multi-height), number designates SI. Negative error is an overestimation.

Chapter 6: Discussion

This chapter evaluates the results of the project, possible errors, and the potential for future improvements. Given the multitude of topics covered a concise overview of previous findings is first presented. Modeling results are then discussed with recommendations for future work in this area. The findings from each field site are summarized and issues that occurred at those sites are addressed with commentary on potential future solutions to those issues. Next, the findings from each sensor and from each height that was surveyed with are discussed. Any errors or revelations from these individual surveys is presented. Because the nature of magnetic anomalies examined directly effects the success and accuracy of depth estimates, the intricacies of the relationship between these two topics is addressed. The results from the two depth estimation techniques, half-width rules and multi-height techniques, are evaluated and an elaboration on their future use in archaeology is presented. Although discussed briefly throughout, potential "correction factors" are addressed more thoroughly with a focus on how these may be applied in the future. Finally, the original research questions from this study, found at the beginning of this document, are reiterated in short and are answered with the knowledge gained from this study.

Overview

The material presented thus far, covers a range of topics relating to archaeo-geophysics and depth-to-target investigations. Specifically, this project focuses on magnetic surveys and the estimation of depth in archaeological contexts. Current archaeo-geophysical practice generally dictates that magnetometry surveys be used only to produce 2D plan-view maps. However, magnetometry has the ability to estimate depth to source bodies, as revealed in deep geologic applications that produce 3D data. The advantages of magnetic 3D data over 2D data are immense.

In order to test the application of depth estimation techniques to archaeological features, computer modeling was first employed to better understand how these techniques could apply in an archaeological context. Then, multiple magnetometers and a down-hole magnetic susceptibility meter were utilized, permitting surveys at various heights, comparisons between data achieved through standard field practice and data needed for depth estimates, and a comparison between the resulting depth estimates and the proxy depth to features interpreted from the down-hole MS. Standard and specialized field equipment was employed to facilitate these surveys at four field sites. CATS is a constructed test site at the CERL facility (Isaacson et al. 1999). Woolsey, Pile Mound, and Runion are known archaeological sites in Arkansas and Tennessee with a variety of previous geophysical and excavation data (Menzer 2015; Mulvihill et al. 2019; Shreve et al. 2020).

Two magnetic-specific topics are integral to understanding and using depth estimation techniques. The reduction to the pole processing technique is rarely applied to archaeo-magnetic data, but is widely used in geologic applications. This method transforms magnetic data to appear as if it was collected at a geographic magnetic pole (Baranov 1957). It facilitates comparison of data collected at different magnetic latitudes and longitudes as the different magnetic inclinations and declinations that occur can make magnetic anomalies appear different, even if the source bodies are identical. By doing so, the magnetic anomaly is centered over the causative body and dipolar features are effectively reduced to monopoles. This is only performed properly when the source-body's direction of magnetization is known. For induced source-bodies, this is the ambient magnetic field's inclination and declination. For source-bodies with all or partial remanence, component directions are difficult to derive and this process is not commonly performed.

The structural index is inherent in all depth estimation techniques (Breiner 1999; Reid and Thurston 2014). It is a factor that attempts to account for the magnetic fall-off rate and geometry of a source-body. The complexity involved in calculating it means proper SIs are currently known only for simple geometries (e.g. spheres, cylinders). The SIs used are those that are closest in form to real-world source-bodies. This can introduce error given the complexity of real source-bodies.

A plethora of depth estimation techniques exist throughout the geophysical literature. This study focuses only on two of these techniques, half-width rules and a simple multi-height technique. HW rules are likely the oldest and simplest technique in the literature (Aspinall et al. 2008; Tite 1972). They work by measuring the linear distance in the horizontal plane from the anomaly maximum to the half-maximum value. Then, depending on the SI of the source-body, a scaling factor may be applied to the HW measurement. The proposed multi-height technique is a mere footnote in the literature (Breiner 1999; Weymouth 1976). This involves magnetic survey over an anomaly at two heights and using ratios between resultant measurements to determine depth to the source-body. To date, this project is the first to investigate this technique in-depth.

Modeling

Significant knowledge was gained through the use of computer modeling in this study. The open-source Python library ‘fatiando a terra’ was used to create simple and complex model source-bodies and their respective magnetic field models (Uieda et al. 2013). Simple shapes included spheres and rectilinear bodies similar to walls and floors. A complex model was used to create a half-sphere. The HW and MH techniques were then evaluated on magnetic models for different geometries: 566 spheres and half-spheres, 18,001 walls, and 3,020 floors. These source-bodies varied in their dimensions, magnetic strengths, and depths.

The HW and MH techniques with SI 3 most accurately estimated the center-depth of spheres. Almost all error was constrained within +/-0.05 m. The resolution limit of the techniques in their current implementation is +/-0.02 m. Few errors exceeded this bound, but some did by up to +/-0.08 m which occurred when values from the higher magnetic survey fell below 0.05 nT. This concretely shows for the first time the proposed multi-height technique is a theoretically viable depth estimator for point-sources.

Half-spheres were also well-estimated by both techniques with SI 3. When the diameter of source-bodies was less than the distance from source-body centers to the instrument sensor, depth estimates fell within +/-0.05 m. Error increased up to 0.2 m and 0.1 m for HW and MH techniques, respectively, as source-body diameters became larger than the distance from the sensor to the source-body center. Error is likely decreased in the MH method because it is not directly derived from the width of the magnetic anomaly. This source of error conforms with traditional wisdom where it has been noted that HW technique should estimate to whichever larger, the source-body width or the distance to source center (Aspinall et al. 2008; Tite 1972). However, in the present research, depth estimates fall between the distance to the source and the true diameter of the source –thus overestimating the distance to the source and underestimating the diameter of the source-body.

Wall model depth estimates provided the most intriguing results. SI of 2 was expected to provide the best results but, this was not the case. HW estimates to the center depth with SI 2 gave a +/-0.75 m range, centered on a 0.75 underestimate. Increasing the survey height only slightly decreased the error range and shifted the error's central tendency to a 1.25 m underestimate. HW SI 3 estimates to the center depth had a decreased error range, +/-0.5 to 0.25m for the lower and higher heights respectively. Both were centered about a 0.1 m overestimate. The HW SI 3 shows an overestimation from 0 to 1 m for the top depth of features.

Because the technique never underestimates the top depth in this case, a potential maximum top depth estimate is provided. With accurate source-body width, the top depth accuracy can potentially be increased through the application of a correction factor. MH estimates have error ranges similar to the HW estimates to the center depth, but the error does not follow a linear trend as the error follows a curve. MH with SI 3 shows greater accuracy and a smaller error range than SI 2. This result is similar to the HW estimates. Error ranges from +/-0.4 m centered on a 1.1 m overestimate. MH top depth estimates do not follow the same pattern as the HW estimates and are therefore likely not a useful estimator for the maximum top depth.

HW with SI 3 consistently overestimated distance in the top of wall models. These models provide a maximum distance to the top of source bodies with error ranging from a 0 to a 1 m overestimate. Used alone, this information is helpful because one can begin to constrain the depth to source-bodies. This error is in direct relation to the width of the source-body and therefore, with additional information about the dimensions of the body, one could better estimate the top distance. MH data also show a linear relationship to the bottom of wall models. Consistent estimates range by +/-0.6 m centered on an underestimate of 0.5 m.

At present, these techniques are not appropriate estimators to a wall in an archaeological context. The error ranges are much too great for archaeology, but since the error decreases with depth and geologic applications require less accuracy, the techniques may be more viable in that domain. With further examination, the methods' accuracy may improve enough to be applied in an archaeological context.

The HW technique does not provide good depth estimates to floors. Estimates scale directly with the width of the source-body. This is not unexpected as the estimate distance is a function of the width of the magnetic anomaly. If the width of the source-body is known prior to application, corrections could potentially be made. The MH technique is not a direct function of

the width of the magnetic anomaly, but given the half-sphere results estimates are certainly affected by the ratio of source body width to source distance. When applying the MH technique, SI of 1 gave the best results. Interestingly, the method provided reasonable estimates for data within the top 2 m and with widths greater than 5.5 m. In this case, the error ranges by +/-0.25 m. Data outside these constraints were erroneous, but much archaeological data falls within these bounds and therefore may prove a useful estimator under these constraints.

In general, model estimates are more accurate with increased depth where linear trends within the estimates are evident. These trends occur even in estimates that are not particularly accurate. In the modeling environment, point-sources are properly estimated by both techniques but accuracy varies for other source-bodies. Through additional modeling, correction factors could potentially be developed to increase the accuracy of the techniques. This is similar to correction factors for slope depth estimation methods, which would benefit from modern computer modeling as the slope correction factors were calculated prior to modern computing. (Nettleton 1976; Peters 1949; Skilbrei 1993).

There are some potential errors and areas of improvement within the scheme used. In order to test the theoretical applicability of the techniques, all models were noise free. Introducing random noise into the magnetic models would provide more realistic results. Furthermore, the half-sphere was the only complex source-body model used. Additional source bodies could be created with many small prisms in order to better represent the geometries of real archaeological features (Desvignes et al. 1999; Eder-Hinterleitner and Neubauer 2001). This would also create a more realistic magnetic fall-off rate. Archaeological bodies are generally compositions of soil, not solid source-bodies (e.g. rocks), though stone architecture does exist in the archaeological record, especially outside of North America. Using a combination of small prisms would especially improve the modeling of walls and floors in the North American

context, as walls are often the remnants of wooden posts that were created through wall trenches or single set-post construction. Also, floors are generally compacted clay layers which would likely act differently than a solid slab of stone depending on MS.

It is evident in the MS logs that a 'deep pit' model should be prioritized in future modeling applications. Increased understanding of this source-type would allow better delineation between the point-source features (hearths and small pits) and larger pits. This could best be tested with a complex source-body model, but a vertical cylinder would be a good simple model to begin investigations.

Most archaeological features are more shallow than many of the models used in this study. The current parameters show the applicability of the techniques outside of archaeology in other near-surface geophysical applications which may especially benefit from the current data trend showing increased accuracy with depth. But moving forward in an archaeological context, limiting the depth of feature bottoms to 2 to 3 m would reduce data complexity and computation time—thus facilitating more rapid in-depth study of only archaeological features.

Field Surveys

The four field sites investigated in this project introduced different field conditions and problems to over-come. Overall, these sites provided valuable information to the further study of depth estimation techniques. The main problems in regards to the surveys are examined further.

At CATS, unfortunately, only two relevant magnetic features were detected with enough accuracy to relate them to known buried features at the site. These two features also happen to have the least amount of documentation available and no concrete depth information is available for them. The well documented house complex was detected, but internal features were lacking definition and relating magnetic anomalies to known features was not possible. Without additional documentation or invasive techniques, the current study cannot garner more useful

information regarding depth estimates from CATS. Future studies at the site would benefit from attempting to relocate the original site datum, as this would facilitate greater accuracy, especially within the house complex. Furthermore, the mound at the site highlighted a problem with the current SENSYS prototype layout, as data quality were considerably lessened by the topographic effect of the mound. A slightly different sensor housing or narrower cart would greatly improve data quality in future similar situations.

Few problems were encountered at Woolsey. However, due to a combination of instrument and operator error, base station data was not collected with the SENSYS MagBase. The G-857 data were interpolated to the higher data sampling rate of the SENSYS system and used for differential correction. That no issues were detected with this method shows that the two instrument types can be used in conjunction with each other in future studies.

A few issues are evident in the Pile Mound survey. Due to instrument malfunction, multiple Grid Blocks of G-858 data were unusable. Additionally, the high vegetation over G3 and G4 caused poor data quality in the SENSYS prototype data. This is of no surprise as the vegetation was excessive, but it emphasizes the need for low vegetation with the instrument. Unfortunately, due to a computer malfunction, RTP was not performed on the magnetic data prior to the down-hole MS survey. The author attempted a ‘best guess’ for the appropriate data shift, but MS core locations were still poorly placed overall. This error detracted from the accuracy and confidence of the depth estimation analyses.

One major error occurred at the Runion site. Due to a combination of instrument and operator error, mainly due to the prototype nature of the SENSYS instrument, SENSYS data were not properly logged at the site. This made them unusable for analysis. This is extremely unfortunate as having the additional survey heights over the ‘Small Pit’ MS log type would improve the understanding of this feature type. Furthermore, no MS logs were acquired for four

features of interest. This was due to encountering rock at the core locations. These rocks are likely the full or partial cause of the magnetic anomalies and provide some insight to depth estimates at those locations. Without additional information, a more accurate assessment cannot be made for these features.

Generally speaking, the surveys at each site contributed extremely useful information to the further understanding of the depth estimation techniques investigated. One overall flaw of the study at all sites is the number of MS core logs taken. In future studies, the author would recommend the acquisition of significantly more MS logs throughout anomalous bodies. This would allow one to narrow down the exact depth and lateral geometries of source-bodies. With this additional information, a better understanding of the width of features and the distance to sensors could be garnered. It would also add confidence to the evaluation of the depth estimates. At present, one can say the feature of interest was possibly not detected properly in the only MS log. With more MS logs, one could definitively determine the source-body geometries and depth. A more costly option would be to fully excavate features of interest and systematically document the MS throughout the excavation.

Sensor Surveys

Two total field magnetometer systems were used throughout the project to survey magnetic anomalies of interest. A prototype magnetometer system was provided by SENSYS which used nine three-component fluxgate sensors which combined achieves total field measurements. These were in a rigid housing at fixed horizontal spacing of 0.2 m and a fixed height. This required the cart system to be reconfigured and a second pedestrian survey performed to acquire data at two heights. Four Geometrics G-858s were attached to a non-magnetic cart system at 0.25 m horizontal spacing and 0.5 m vertical spacing. This allowed for both a lower and higher survey height to be recorded at the same time which likely decreased

error between the two surveys and reduced total survey time, as only one pedestrian survey was required.

The SENSYS lower survey (0.0845 m above ground) data were affected the most by ground conditions due to the low survey height and the cart design. This introduced errors in some areas when tall vegetation or rising slopes rattled the sensors, but the low survey height also provided the highest detail of magnetic anomalies. This result far outweighed the errors introduced in the survey, which in some instances could be corrected in the future with an improved cart design. Additionally, in some cases the high resolution showed more internal anomaly detail which may have actually detracted from the HW depth estimates, discussed further below. In general, this survey shows the most consistently accurate depth estimates using SI 2 and the HW minimum and MH techniques. Only one anomaly had a larger width than distance to the sensor. Five others had near equal distances. Given modeling results, this is likely a cause of error in all estimates from survey at the lower height.

The SENSYS higher survey (0.3854 m above ground) data were less affected by ground conditions, but again due to the cart design some errors were introduced. In most cases, this survey showed about equal detail as the G-858 lower survey, this is not surprising as there is only a 0.0345 m difference in height between the two surveys, They both were less detailed than the SENSYS lower survey. The HW minimum with SI 2 yields the most consistently accurate depth estimates for the SENSYS higher survey. In all but two cases, the width or diameter of the magnetic anomalies are greater than the distance from the MS maximum value to the sensor. Four other anomalous bodies had almost equal distances. This likely influenced the results. By increasing the height of the sensor, magnetic anomalies generally increased in dimensions, but depth estimates decreased overall compared to the lower height SENSYS survey.

The G-858 lower survey (0.35 m above ground) data were less affected by ground conditions due to a different cart design and higher sensor placement. This survey offered detail similar to the SENSYS higher survey, given their similar heights. Overall SI 2 had the best results considering both the MH and HW minimum together. All but four anomalies have widths or diameters greater than the distance from the MS maximum value depth to the sensor. Another seven were almost equal distance. In the case of the greater widths, error is certainly introduced.

The G-858 higher survey (0.85 m above ground) was collected at a considerably higher height than all other surveys. Overall, this survey was the least detailed and in some cases no magnetic anomaly was detected over known features of interest. This certainly caused erroneous depth estimation results and in some cases no estimation was possible. When anomalies were detected, the higher height did produce the smoothest results (e.g. the least internal dispersion) which is beneficial for HW estimates. Again, the higher height generally produced lesser depth estimates than its lower height counterpart even though the anomaly dimensions were greater. Approximately one sixth of the anomaly dimensions were less than the distance from the sensor to the MS maximum values. This translated to the greatest underestimates of all the surveys. The HW minimum with SI 2 showed the most consistent and accurate results.

No issues arose from using the Bartington MS2H Sensor, as it performed well. However, overall proxy depth information would be greatly improved by the addition of more MS logs. Additional cores per anomaly would be helpful, but a good estimate require roughly four to five per square meter with focus on the maximum magnetic survey value. Core locations should also be based strictly on the magnetic survey data to be used for depth estimation as clear differences are evident between the different instrument types. This is particularly the case between vertical-gradient instruments and total field sensors.

The surveys would also benefit from a neutral MS log taken outside of any MS enhancement. By doing so, a better grasp of the background matrix's MS would occur. This can be compared to those at magnetic anomalies to potentially remove, or at least better understand, any background trends. This would likely better delineate where the tops and bottoms of magnetic features are located.

Lastly, a fundamental assumption in this survey was that depth estimates would be for MS maximum or some adjusted center-depth. These depth proxies take into account some of the variation in magnetism within the core log, but none of the variation in distance to the sensor. Because magnetism falls-off at an exponential rate, an area of high magnetism deep in a MS log would not be observed with as great a magnetic strength at the ground surface compared to an area of high magnetism closer to the surface. This is further exacerbated by adding more distance from the deeper magnetic source to the magnetometer sensor some height above the ground. This may further skew magnetic depth estimates to shallower targets in some cases (Desvignes et al. 1999). The author is not aware of an appropriate summation process that would account for this fall-off and not introduce bias through a user-defined fall-off rate.

The Nature of Magnetic Anomalies

Throughout this project it is clear that the amount of type of and amount of dispersion within a magnetic anomaly are of the utmost importance when it comes to depth estimation. Many things can detract from the accuracy of depth estimation. In a perfect world, magnetic anomalies would look like a smooth hill with the maximum value in the exact center and values steadily decreasing in all directions. In other words, a 'good' magnetic anomaly should have well-defined edges or boundaries, it should have a centered maximum value, and it should be smooth internally from the maximum value to minimum values in all directions.

A magnetic anomaly without well-defined edges can detract from the quality of estimates, especially HW estimates. In the example of a positive monopole, this is defined by having a clear and hopefully rapid change from high positive to near zero values. When this is not the case, extremely high or low HW estimates may occur. An example would be when magnetism rapidly decreases in one direction away from the anomaly center, but slowly decreases in the opposite direction. This type of problem is especially difficult to deal with when anomalies are close together and overlap. If a clear divide cannot be made between the anomalies, depth estimation may not be possible.

A similar error is encountered when the magnetic maximum is not centered within an anomaly. Being slightly offset from the center, HW values will vary greatly. Error is especially evident if the maximum value is at the edge of a magnetic anomaly. This greatly increases the variance within HW estimates and produces a likely erroneous HW minimum estimate. Correcting for this requires manual interpretation of multiple HW estimates of the same anomaly, a timely process.

Internal dispersion is referred to throughout the results section. This can best be characterized by imagining extremely complex topography, where there are many minor peaks and valleys throughout the landscape. When a magnetic anomaly fits this description, multiple errors can occur. This can increase the variance in HW estimates if half-maximum values are encountered multiple times along a single data line through an anomaly. For example, if moving away from the maximum value of ten, a line read eight, seven, five, four, eight, five. One would need to choose which occurrence of five is the appropriate half-maximum distance. Multi-height estimates can also detract when dispersion creates different spatial locations for the maximum magnetic value in the two different surveys. All this boils down to the fact that magnetic models

are based on simple geometric shapes. When the real world diverges from these shapes, large deficiencies arise in our models.

When magnetic maps are created, they are often scaled to a particular data range—usually plus and minus two standard deviations of the data set from zero. This can make anomalies visually look solid, but in actuality they are very internally dispersed. A potential automatic quantification of an anomaly's dispersion could be achieved by using a common raster GIS processing algorithm, such as Terrain Ruggedness Index (Riley et al. 1999), or something similar. Correcting for dispersion could possibly be done through smoothing filters like low pass filtering or possibly a more detailed interpolation scheme. Without further testing, it is unclear how these may effect depth estimates.

Complex anomalies overall are not good candidates for depth estimation. These occur when one or more source-bodies are extremely close to each other. This causes the magnetic anomaly to encompass the same area and it can be detrimental to MH estimations if some or all of the different source-bodies are detected at different heights. An example from this project is Pile Mound G2 Feature I. A very small dipolar anomaly was delineated with the lowest sensor, but not with higher sensors, so the lower surveys maximum value was in a different location than the respective higher survey.

Field Depth Estimations

It is clear that current limitations of the HW and MH techniques do not make them good depth estimators in all situations. If one can accept an approximate 0.25 m error window, then SI 2 should be applied blindly, but this is not recommended. When performing depth estimation, interpretation of a magnetic anomaly in question is crucial to selecting an appropriate SI and understanding the depth estimate from either proposed technique. Both techniques appear valid for point sources where distance to the source is greater than the source's width, but it appears

many features are wider than their depth which makes the techniques unsuitable. Through additional computer modeling and real-world survey, potential correction factors may be developed to rectify this issue. Also, few sources in this study likely fall outside of the point-source or pit types. More research therefore needs to be conducted on wall and floor types to make accurate assessments of the proposed techniques' accuracy in estimating their depth.

In this project, reduction to the pole is used to center the magnetic anomaly over the causative-body and transform the total field data as if all magnetization were vertical. Although this generally performed well, it is clear that multiple dipolar anomalies were not transformed properly. This is likely due to the presence of a remanent magnetic component in the source-bodies. In these situations, other techniques may be more appropriately applied to achieve a similar result. Calculation of the total gradient amplitude (TGA), also known as the 3D analytical signal, may offer a better solution (Roest et al. 1992; Tabbagh et al. 1997). It is not exactly clear how these processing techniques may affect the results of the two depth estimation techniques in this study and testing is required to more fully understand the situation.

A significant problem is that many archaeological features appear to be wider than their depth, thus skewing depth results. Yet "depth" does not refer to actual BS depth, but to distance below the sensor. An obvious solution is merely to raise sensor height. Yet, as has been shown, a great drawback is reduced sensitivity and blurred or degraded results. Further work is necessary to better understand this issue and develop a solution.

Although not a direct fix, a potential avenue to a solution would be to apply edge detection processes to the magnetic data. These should better delineate the true 'edge' of magnetic source-bodies which would allow one to determine if the source-body is in fact wider than the depth. There are multiple similar techniques to achieve this goal. The horizontal gradient of RTP data may offer a solution (Blakely and Simpson 1986). The 'tilt angle' may also prove an

effective solution (Salem et al. 2007). Cheyney et al. (2011) apply these techniques and additional similar and derivative techniques to archaeo-geophysical data with what appears good accuracy. The source-body tested in the above case is a well-defined rectangular structure's walls, and so it is unclear if the processes will work as effectively on circular or slightly elliptical anomalies. Any or all of the techniques introduced above may offer avenues to better estimate the depth with the proposed estimation techniques. Further study is warranted.

Half-width Technique

This study has shown that the HW minimum estimate is the most consistently accurate depth estimate within the HW rules (see Appendix C). The technique proves to be more effective than the 'rule-of-thumb' designation it commonly receives throughout the archaeo-geophysical literature (Aspinall et al. 2008). When feature width is not a major concern, this study shows the technique accurately estimates depth to various archaeological source bodies, point-sources and various types of pits. It certainly warrants more use than it currently receives in the field. With additional study and greater use of computer processing techniques to delineate the edges of source-bodies the accuracy of HW rules can likely be increased.

An unexpected benefit to the HW technique from the multi-height survey was observing the clear relationship of estimates either increasing or decreasing with sensor height. The presence of either of these these patterns within multiple HW depth estimates can assist in determining the proper SI to use and whether a feature is wider than depth. If estimates decrease with increased sensor distance, SI 3 is likely more appropriate and the source-body is more likely point-source in nature. When the estimates increase with decreased sensor distance, SI 2 appears more appropriate and a pit type source is likely observed. Overall, it appears the accuracy of HW rules is greatly improved by performing them at multiple survey heights.

Multi-height Technique

At present, the tested multi-height technique appears to accurately estimate depth to point sources when the distance from the sensor to the source-body is larger than the width of said source-body. But when this does not occur, the technique overestimates the depth. This technique will also likely benefit from the additional processing techniques proposed above. When dealing with pit type features, using SI 2 appears to estimate quite well the center-depth with only minor overestimation. The multi-height estimates are effected by the heights of the surveys used, but surveys at more heights with the same sensor type is likely needed to work out the intricacies of this pattern. Having different sensors detracted from the current studies ability to compare results from different heights. This is due to the minor differences in the sensors where they generally measure slightly different magnetic strengths. This is not particularly evident in visual inspection of processed magnetic maps, but when performing depth estimates, these minor differences are amplified.

Determining the accuracy of a multi-height estimate is also greatly benefited by performing the HW estimations in tandem. These estimates can be used to potentially better understand which SI to employ. Also when used in tandem, potential erroneous estimations can be accounted for if estimates are wildly different between the two techniques. As with other depth estimation techniques in the geologic literature, application of more than one at a time can help a researcher better understand the nature of the source-body in question and paint a clearer picture of what is below the ground surface.

Correction Factors

As noted above, other depth estimators use correction factors to increase the estimators' accuracy (Nettleton 1976; Peters 1949; Skilbrei 1993). This concept could certainly be applied to the two methods employed in this study. A correction factor would be either a constant value that

is mathematically applied to all estimates or a series of factors that would be applied depending on a specific situation, the width of a feature for example. The obvious case is to attempt to correct for the over-estimation occurring when feature width is greater than the distance from the source to the sensor. This factor would likely change depending on the width of the source body or possibly the width of the magnetic anomaly. In either case, through additional computer modeling a relationship between the width (of the source or magnetic anomaly) and the error in the depth estimate could be calculated. A suitable correction factor could then be applied to any depth estimate when the width is larger than the distance to the source from the sensor. This would certainly increase the accuracy of the depth estimators.

If one could get an estimate of the source body width through additional processing like those described in Cheyney et al. (2011), this would allow a direct relationship to be measured between the width of the feature and a depth estimator's error. This is likely preferred, but testing is needed to prove this. The other option would be to simply measure the width of the magnetic anomaly. The drawback to this is that similar magnetic anomalies can be created from various source-body geometries, so using only one magnetic map could be problematic. However, if multi-height methods are employed the potential error from this situation could be greatly reduced. This error reduction would occur because having two or more measures of the magnetic anomaly reduce the number of potential source body geometries that could cause the magnetic anomaly.

The structural index used also directly effects the depth estimate. Given that archaeological source-bodies may not be best categorized using the simple geometric models, using a different SI may be a potential solution. Reid and Thurston (2014) caution against this when using the Euler deconvolution depth estimator, but the proposed multi-height technique is based on different mathematical principles and therefore, should not be hindered by using a non-

integer SI. Measuring magnetic features at multiple heights may lead to a better way of determining the actual SI or fall-off rate of the magnetic feature of interest. If this is accomplished, using a measured SI would likely increase the accuracy of the depth estimators. Further research is certainly needed in this area.

Research Questions

Specific research questions were asked at the beginning of this document. These are reiterated here and a short answer is provided.

1) *How well do half-width rules work in a modeling environment?* They accurately estimate the depth to point sources when the anomalous body's width is less than the distance from the source body to the sensor. They perform more poorly when estimating to other source-body geometries and more research in these areas is likely needed.
2) *Can half-width rules provide adequate depth-estimations to actual archaeological features?* Yes, in the case of point-source and pit-like anomalies the HW rules can provide accurate depth information. Additional processing may increase the accuracy of these techniques.
3) *Do multi-height techniques work in a modeling environment?* Yes, they properly estimated depths to point sources when the width is less than the distance from the source body to the sensor. They are less affected by this phenomenon than HW rules. Depth estimates to other source-body geometries is less accurate and more research is needed in these areas.
4) *Can multi-height techniques provide adequate depth estimates to actual archaeological features?* Yes, like the HW rules, point-source and pit types are accurately estimated when the width is not greater than the depth. Additional processing may help improve this method.

5) *Do the half-width and multi-height techniques provide a consistent minimum or maximum estimate to points of interest?* Possibly, but computer modeling suggests there may be a methodological avenue to address this issue, but it is not completely clear at this time. The field results need further study to provide answers in either the case of minimum or maximum feature depth estimation.

Chapter 7: Conclusions

Overall, this project successfully showed that HW rules are more than mere 'rules-of-thumb' and that the proposed multi-height technique is certainly a viable depth estimator. Computer modeling was essential in understanding the nature of both depth estimation methods. This modeling showed when using the proper SI if feature width is greater than the distance from the source to the sensor, an inaccurate estimate would occur. This lead to a much better analysis and understanding of the field results. The modeling also showed the relationship to non-point-source bodies would be less accurate. The source-body models in this area of the study were extremely simple and future research would benefit from more complex source-body models using a combination of small prisms to create a pit, wall, or floor.

Both of these methods appear to work as expected on real point-source and pit-type features. As expected, when using the proper SI and feature width is not greater than the distance to the sensor, a majority of the data fall within a 0.25 m error window. This is not 'amazing' accuracy, but it is certainly better than no depth information. When the distance from the source body to the sensor is larger than the width of features, estimates decreased in accuracy. This is to be expected based on the computer modeling. In these cases, additional 'edge detection' processing techniques may provide an avenue to increase the accuracy. If the width of the feature can be accurately determined, or at minimum constrained, correction factors may be applied to increase the accuracy of the techniques. Computer modeling will be essential in calculating these correction factors.

The other feature types encountered in the project did not occur with enough frequency to accurately assess them. The current modeling suggests that the HW and multi-height techniques may not be well suited for estimating these source types. This certainly warrants further investigation, but estimates to these source types will likely be less accurate.

In all cases, this project would benefit from additional MS cores and a better understanding of the use of these techniques as a proxy for feature depth. This is especially needed for accuracy assessments of more complex magnetic feature types (e.g. pit). Determining the correct magnetic center of a feature is essential to accuracy assessments and to better understand how the depth estimators are performing. A major drawback to these techniques is the failure to properly estimate depth when the width of features is greater than distance from the sensor to the source. In future studies, many more cores should be taken from indicated anomalies. This would allow the magnetic spatial extent to be mapped with greater resolution and would assist in evaluating the accuracy of the proposed depth techniques. This would additionally allow for an accuracy assessment of the proposed 'edge detection' processing techniques. By doing so, fine tuning of any correction factors that may be created for the techniques may be possible..

With detailed analysis and experience these methods combined can lead to accurate depth assessments on an anomaly-by-anomaly basis, but in the present methodology they should not be used blindly across an entire survey. Additionally, using multiple heights, even for the HW rules, is crucial to understanding the nature of the magnetic source and making accurate assessments. This allows for patterns related to the distance of sensors to the source to be detected. Through this study, it appears when estimates decrease with increased sensor distance, SI=3 is more appropriate and the magnetic body is likely a point-source. When the opposite pattern occurs, estimates increase with decreased sensor distance, SI=2 is more likely correct and a pit type feature is possibly being encountered.

Neither technique is a one-size fits-all solution, but they do show accuracy when estimating to point-sources and pit-like features if the correct SI is applied. Additionally, applying SI=2 can be a fair indicator of the general depth of features across an archaeological

site. Even this general knowledge can be used to better understand the spatial layout of an archaeological site. Magnetometry is the most widely used geophysics technique in archaeology. Garnering depth information from this technique, even at a low accuracy, will greatly expand our knowledge of sites globally. Future research is certainly warranted, but this study definitively shows, for the first time, that multi-height techniques offer accurate depth estimators.

Works Cited

Aitken, Martin J.
1958 Magnetic Prospecting: The--Water Newton Survey. *Archaeometry* 1:24–29.

1961 *Physics and Archaeology*. 1st ed. Interscience Publishers Inc., New York and London.

1970 Magnetic Location. *Science in Archaeology*:681–694.

Åm, K.
1972 The arbitrarily magnetized dyke: Interpration by characteristics. *Geoexploration* 10(2):63–90.

Arkani-Hamed, J.
1988 Differential reduction-to-the-pole of regional magnetic anomalies. *Geophysics* 53(12):1592–1600.

Aspinall, Arnold, Chris Gaffney, and Armin Schmidt
2008 *Magnetometry for Archaeologists*. Vol. 2. Geophysical Methods for Archaeology. AltaMira Press.

Baranov, Vladimir
1957 A new method for interpretation of aeromagnetic maps: pseudo-gravimetric anomalies. *Geophysics* 22(2):359–382.

Baranov, Vladimir, and Henri Naudy
1964 Numerical calculation of the formula of reduction to the magnetic pole. *Geophysics* 29(1):67–79.

Barbosa, Valeria CF, Joao BC Silva, and Walter E. Medeiros
1999 Stability analysis and improvement of structural index estimation in Euler deconvolution. *Geophysics* 64(1):48–60.

Bartington Instruments
2010 Operation Manual for MS2 Mangetic Susceptibility System. Bartington Instruments Limited, England.

2014 Operation Manual for Grad601 Magnetic Gradiometer. Bartington Instruments Limited, England.

Bevan, Bruce W.
1998 *Geophysical Exploration for Archaeology: An Introduction to Geophysical Exploration*. United Stated Department of Interior, National Park Service, Midwest Archaeological Center Lincoln, Nebraska.

Bhattacharyya, B. K.
1964 Magnetic Anomalies Due to Prism-Shaped Bodies with Arbitrary Polarization. *GEOPHYSICS* 29(4):517–531.

1965 Two-dimensional harmonic analysis as a tool for magnetic interpretation. *Geophysics* 30(5):829–857.

Blakely, R. J.
1996 *Potential Theory in gravity and magnetic application*. Cambridge University Press.

Blakely, Richard J., and Robert W. Simpson
1986 Approximating edges of source bodies from magnetic or gravity anomalies. *Geophysics* 51(7):1494–1498.

Breiner, Sheldon
1999 Applications manual for portable magnetometers. Geometrics, San Jose California.

Burger, H. Robert, Anne F. Sheehan, and Craig H. Jones
2006 *Introduction to applied geophysics: Exploring the shallow subsurface*. W. W. Norton & Company, Inc., New York, NY.

Cheyney, S., I. Hill, and N. Linford
2011 Advantages to using the pseudogravity transformation to aid edge detection of total field archaeomagnetic datasets. *Archaeological Prospection* 18(2):81–93.

Conyers, Lawrence B.
2013 GROUND-PENETRATING RADAR STUDIES AT THE HAMMER TEST BED FACILITY, RICHLAND, WASHINGTON. *Journal of Northwest Anthropology* 47(2). accessed June 28, 2017.

Dalan, Rinita A.
2006 Magnetic Susceptibility. In *Remote Sensing in Archaeology: An Explicitly North American Perspective*, pp. 161–203.

Desvignes, Guy, Alain Tabbagh, and Christophe Benech
1999 The determination of the depth of magnetic anomaly sources. *Archaeological Prospection* 6(2):85–105.

Eder-Hinterleitner, Alois, and Wolfgang Neubauer
2001 Reconstructing neolithic ditches by magnetic modeling. In *Filtering, optimisation and modelling of geophysical data in archaeological prospecting*, edited by Mauro Cucarzi and Paola Conti, pp. 167–182. Fondazione Ing. Carlo Maurilio Lerici, Rome.

Ernenwein, Eileen G., and Jay D. Franklin
2017 Archaeological Geophysics at Runion, a Protohistoric Site on the Middle Nolichucky River. *30 Days of Tennessee Archaeology, Day 12*. https://tennesseearchaeologycouncil.wordpress.com/2017/09/12/archaeological-geophysics-at-runion-a-protohistoric-site-on-the-middle-nolichucky-river/, accessed February 10, 2020.

Evans, Michael E., and Friedrich Heller
2003 *Environmental Magnetism Principles and Applications of Enviromagnetics*. Academic Press.

Franklin, Jay
2018 Archaeological Testing at the Runion Site (40Wg20), a Protohistoric Town on the Middle Nolichucky River, Tennessee. *30 Days of Tennessee Archaeolog, Day 17*. https://tennesseearchaeologycouncil.wordpress.com/2018/09/17/archaeological-testing-at-the-runion-site-40wg20-a-protohistoric-town-on-the-middle-nolichucky-river-tennessee/, accessed February 10, 2020.

Gaffney, C.
2008 Detecting Trends in the Prediction of the Buried Past: A Review of Geophysical Techniques in Archaeology. *Archaeometry* 50(2):313–336. DOI:10.1111/j.1475-4754.2008.00388.x.

Geometrics, Inc.
2001 G-858 Magmapper: Operation Manual. Geometrics, San Jose California

2015 G-857 Memory-Mag TM Proton Precession Magnetometer: Operation Manual. Geometrics, San Jose California.

Gunn, P. J.
1975 Linear transformations of gravity and magnetic fields. *Geophysical Prospecting* 23(2):300–312.

Helbig, K.
1963 Some integrals of magnetic anomalies and their relation to the parameters of the disturbing body. *Zeitschrift fur Geophysik* 29:83–96.

House, John H.
1972 *Preliminary Reconnaissance of the Mulberry Creek basin Arkansas*. Arkansas Archeological Survey, Fayetteville, Arkansas.

Isaacson, John, R. Eric Hollinger, Darrell Gundrum, and Joyce Baird
1999 A Controlled Archaeological Test Site Facility in Illinois: Training and Research in Archaeogeophysics. *Journal of Field Archaeology* 26(2):227. DOI:10.2307/530663.

Kanasewich, E. R., and R. G. Agarwal
1970 Analysis of combined gravity and magnetic fields in wave number domain. *Journal of Geophysical Research* 75(29):5702–5712. DOI:10.1029/JB075i029p05702.

Kvamme, Kenneth L.
2006 Magnetometry: Nature's Gift to Archaeology. In *Remote Sensing in Archaeology: An Explicitly North American Perspective*, pp. 205–234.

Le Borgne, E
1955 Susceptibilite magnetique anomale du sol superficiel. *Annales de Geophysique* 11:399–419.

1960 Influence Du Feu Sur Les Proprietes Magnetiques Du Sol Et Sur Celles Du Schiste Et Du Granite. *Annales de Geophysique* 16:159–195.

Leica Geosystems
2012 Leica GS10/GS15: User Manual. Leica Geosystems AG, Switzerland.

Menzer, Jeremy G.
2015 Discovering Rock Features with Geophysical Exploration and Archaeological Testing at the Mississippian Pile Mound Site, Upper Cumberland Plateau, Tennessee. East Tennessee State University, Johnson City, Tennessee.

Mulvihill, Tim, Mary Brennan, Elizabeth Horton, Jami Lockhart, and George Sabo III
2019 Radiocarbon Dating of Two Pit Features from 3FR46. *Fiel Notes: newsletter of the Arkansas Archeological Society*, 2019.

Mushayandebvu, Martin F., P. Van Driel, Alan B. Reid, and James Derek Fairhead
2001 Magnetic source parameters of two-dimensional structures using extended Euler deconvolution. *Geophysics* 66(3):814–823.

Myer, William Edward
1924 Catalogue of Archaeological Remains in Tennessee. unpublished manuscript on file at Tennessee Division of Archaeology, Nashville.

Nettleton, L. I.
1976 *Gravity and Manetics in Oil Prospecting*. McGraw-Hill, Inc.

Neubauer, and Alois Eder-Hinterleitner
1997 3D-interpretation of postprocessed archaeological magnetic prospection data. *Archaeological Prospection* 4(4):191–205.

Neubauer, Wolfgang
2001 *Magnetische Prospektion in der Archäologie*. Vol. 44. Der Österreichischen Akademie Der Wissenschaften, Wien.

Oh, Jinyong, Tareq Abdallatif, and Mancheol Suh
2008 Magnetic and seismic investigations of historic features in the Suchon area, Kongju, Korea. *Archaeological Prospection* 15(3):227–238. DOI:10.1002/arp.336.

Pearson, William C., and Christopher M. Skinner
1982 Reduction-to-the-pole of low latitude magnetic anomalies. In *SEG Technical Program Expanded Abstracts*, pp. 356–358. Dallas.

Peters, Leo J.
1949 The direct approach to magnetic interpretation and its practical application. *Geophysics* 14(3):290–320.

Plouff, Donald
1976 Gravity and Magnetic Fields of Polygonal Prisms and Application to Magnetic Terrain Corrections. *GEOPHYSICS* 41(4):727–741.

Reid, Alan B., J. M. Allsop, H. Granser, A. J. Millett, and I. W. Somerton
1990 Magnetic interpretation in three dimensions using Euler deconvolution. *Geophysics* 55(1):80–91.

Reid, Alan B., Jörg Ebbing, and Susan J. Webb
2014 Avoidable Euler Errors - the use and abuse of Euler deconvolution applied to potential fields: Avoidable Euler Errors. *Geophysical Prospecting* 62(5):1162–1168. DOI:10.1111/1365-2478.12119.

Reid, Alan B., and Jeffrey B. Thurston
2014 The structural index in gravity and magnetic interpretation: Errors, uses, and abuses. *GEOPHYSICS* 79(4):J61–J66. DOI:10.1190/geo2013-0235.1.

Reynolds, John M.
2011 *An Introduction to Applied and Environmental Geophysics*. 2nd ed. Wiley-Blackwell.
Riley, Shawn J., Stephen Daniel Degloria, and Robert Elliot
1999 A Terrain Ruggedness Index that Quantifies Topographic Heterogeneity. *Intermountain Journal of Sciences* 5(1–4):23–27.

Roest, Walter R., Jacob Verhoef, and Mark Pilkington
1992 Magnetic interpretation using the 3-D analytic signal. *Geophysics* 57(1):116–125.

Salem, Ahmed, Simon Williams, J. Derek Fairhead, Dhananjay Ravat, and Richard Smith
2007 Tilt-depth method: A simple depth estimation method using first-order magnetic derivatives. *The Leading Edge* 26(12):1502–1505.

Scollar, Irwin
1969 A program for the simulation of magnetic anomalies of archaeological origin in a computer. *Prospezioni Archeologiche*(4):59–83.

SENSYS
2017 Handbuch: MAGNETO MXV3 Survey System. SENSYS, Sensorik & Systemtechnologie HmbH, Germany.

2018 Manual: MagBase. SENSYS, Sensorik & Systemtechnologie HmbH, Germany.

Shreve, Nathan K., Jay D. Franklin, Eileen G. Ernenwein, Maureen A. Hays, and Ilaria Patania
2020 An Arc of Interaction, a Flow of People, and Emergent Identity: Early Contact period Archaeology and Early European Interactions in the Middle Nolichucky Valley of Upper East Tennessee. In *Contact, Colonialism, and Native Communities in the Southeastern United States*, edited by Edmond A. III Boudreaux, Maureen Meyers, and Jay K. Johnson. 1st ed. Florida Museum of Natural History: Ripley P. Bullen Series. University Press of Florida, Gainesville.

Silva, Joao BC
1986 Reduction to the pole as an inverse problem and its application to low-latitude anomalies. *Geophysics* 51(2):369–382.

Skilbrei, Jan Reidar
1993 The straight-slope method for basement depth determination revisited. *GEOPHYSICS* 58(4):593–595.

Smellie, D. W.
1956 Elementary approximations in aeromagnetic interpretation. *Geophysics* 21(4):1021–1040.

Tabbagh, Alain, Guy Desvignes, and Michel Dabas
1997 Processing Z gradiometer magnetic data using linear transforms and analytical signal. *Archaeological Prospection* 4(1):1–13. DOI:10.1002/(SICI)1099-0763(199703)4:1<1::AID-ARP61>3.0.CO;2-5.

Tite, M. S.
1972 *Methods of Physical Examination in Archaeology*. Seminar Press.

Uieda, L., V. C. Oliveira Jr, and V. C. F. Barbosa
2013 Modeling the Earth with Fatiando a Terra. In , pp. 91–98.

Von Frese, Ralph R. B.
1984 Archaeomagnetic Anomalies of Midcontinental North American Archaeological Sites. *Historical Archaeology* 18(2):4–19.

Weston, D. G.
2002 Soil and Susceptibility: Aspects of Thermally Induced Magnetism within the Dynamic Pedological System. *Archaeological Prospection* 9(4):207–215. DOI:10.1002/arp.196.

Weymouth, John W.
1976 A Magnetic Survey of The Walth Bay Site (39WW203). *Midwest Archaeological Center*.

2000 On the Relationship Between the Profile of a Magnetic Anomaly and the Depth of the Source.

Witten, Alan J.
2006 *Handbook of Geophysics and Archaeology*. Equinox Publishing Ltd.

Appendix A: Acronyms

Table A.1. List of Acronyms.

Acronym	Meaning
2D	two-dimensional
3D	three-dimensional
AOI	area of interest
BS	below surface
CATS	controlled archaeological test site
CERL	construction engineering research laboratory
DHMS	down-hole magnetic susceptibility
EMI	electromagnetic induction
FFT	fast Fourier transform
FCR	fire-cracked rocked
FWHM	full-width half-maximum
GIS	geographic information system
GNSS	global navigation satellite system
GPR	ground penetrating radar
HW	half-width
IDW	inverse distance weighted
MS	magnetic susceptibility
Max	maximum
MPF	mean profile filter
Med	median
Min	minimum
MH	multi-height
UCP	upper Cumberland plateau
UTC	universal coordinated time
RTP	reduction to the pole
RTK	real-time kinematic
SI	structural index
ZMT	zero median traverse

Appendix B: Additional Magnetic Maps

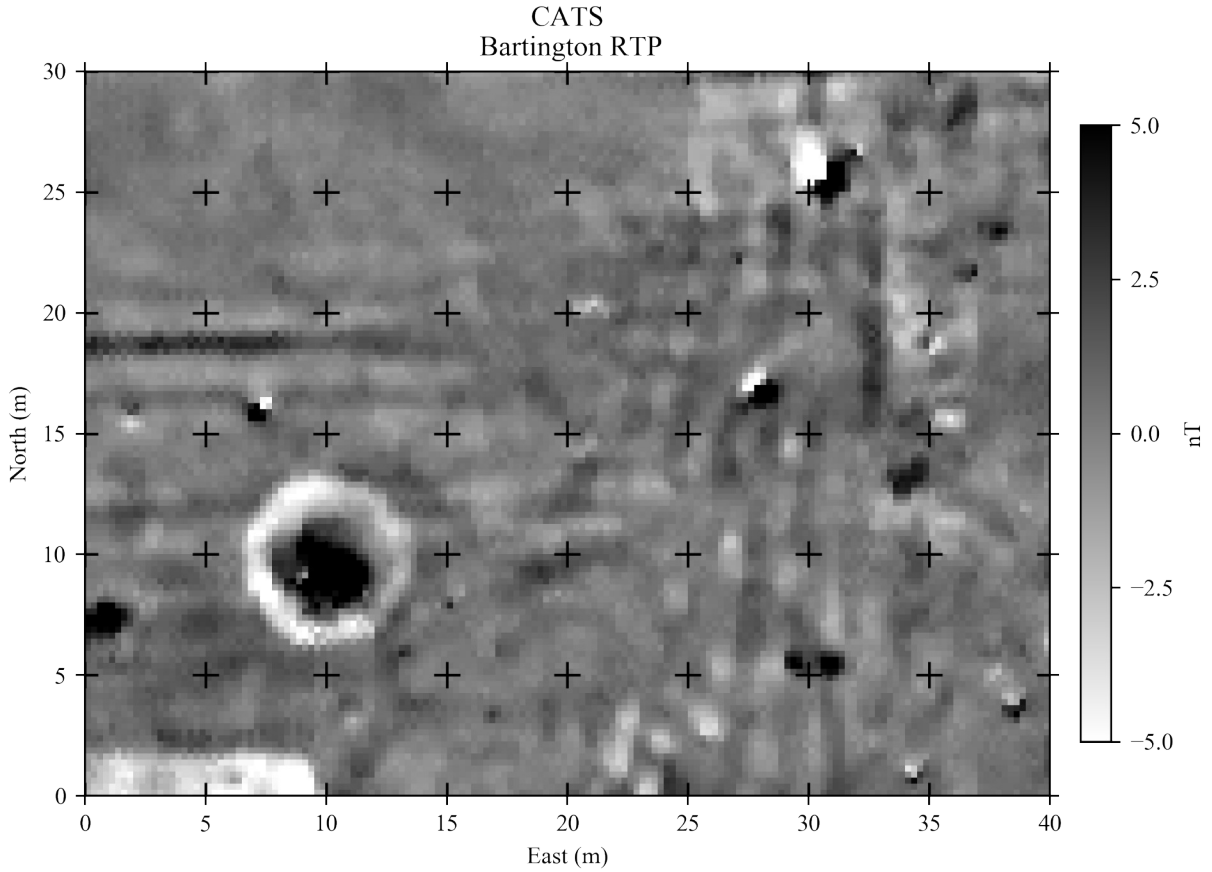

Figure B.1. CATS Bartington Data in local coordinates.

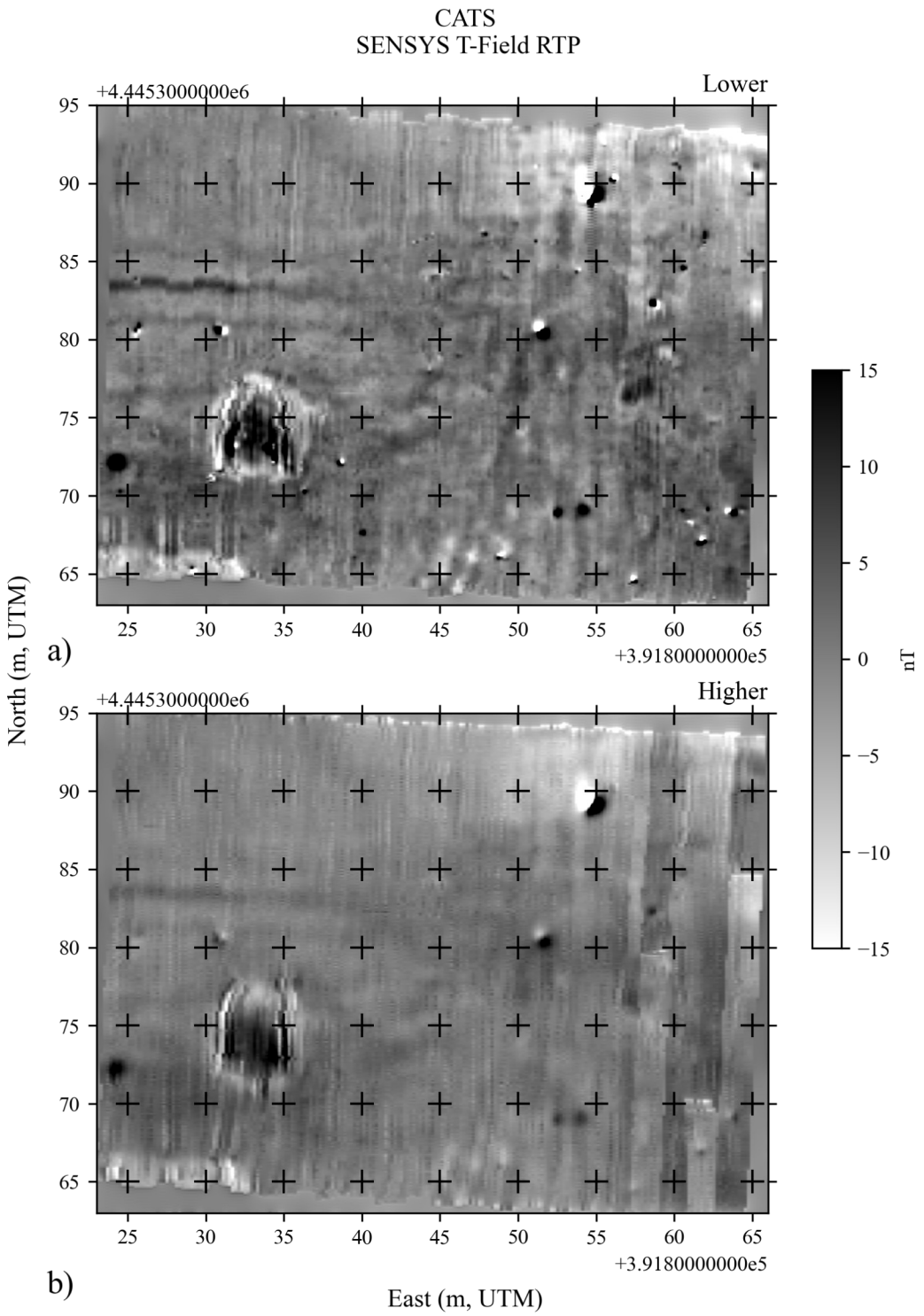

Figure B.2 CATS SENSYS Prototype data. a) Lower survey at 0.0845 m. b) Higher survey at 0.3845 m.

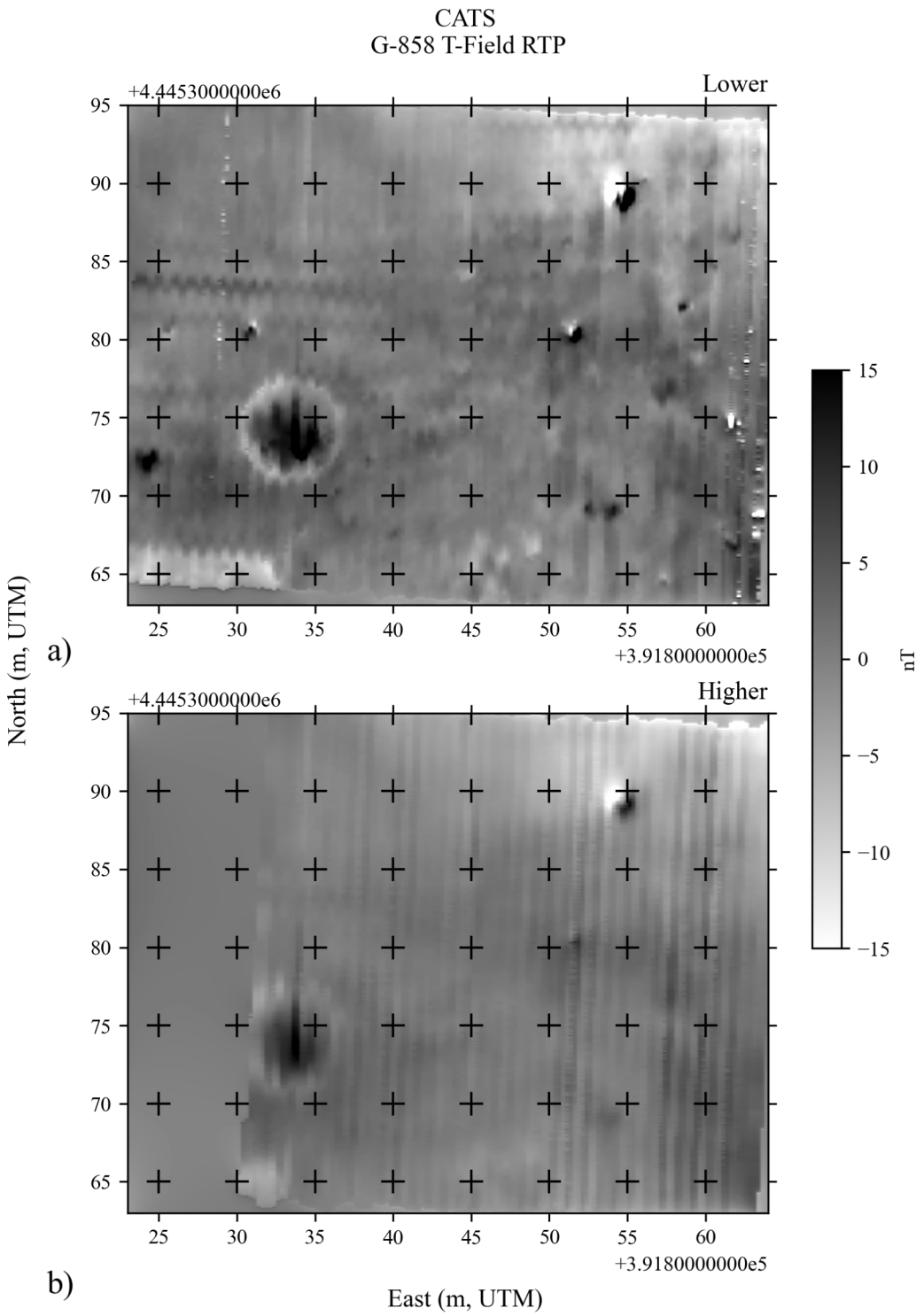

Figure B.3 CATS G-858 Data. a) Lower survey at 0.35 m. b) Higher survey at 0.85 m.

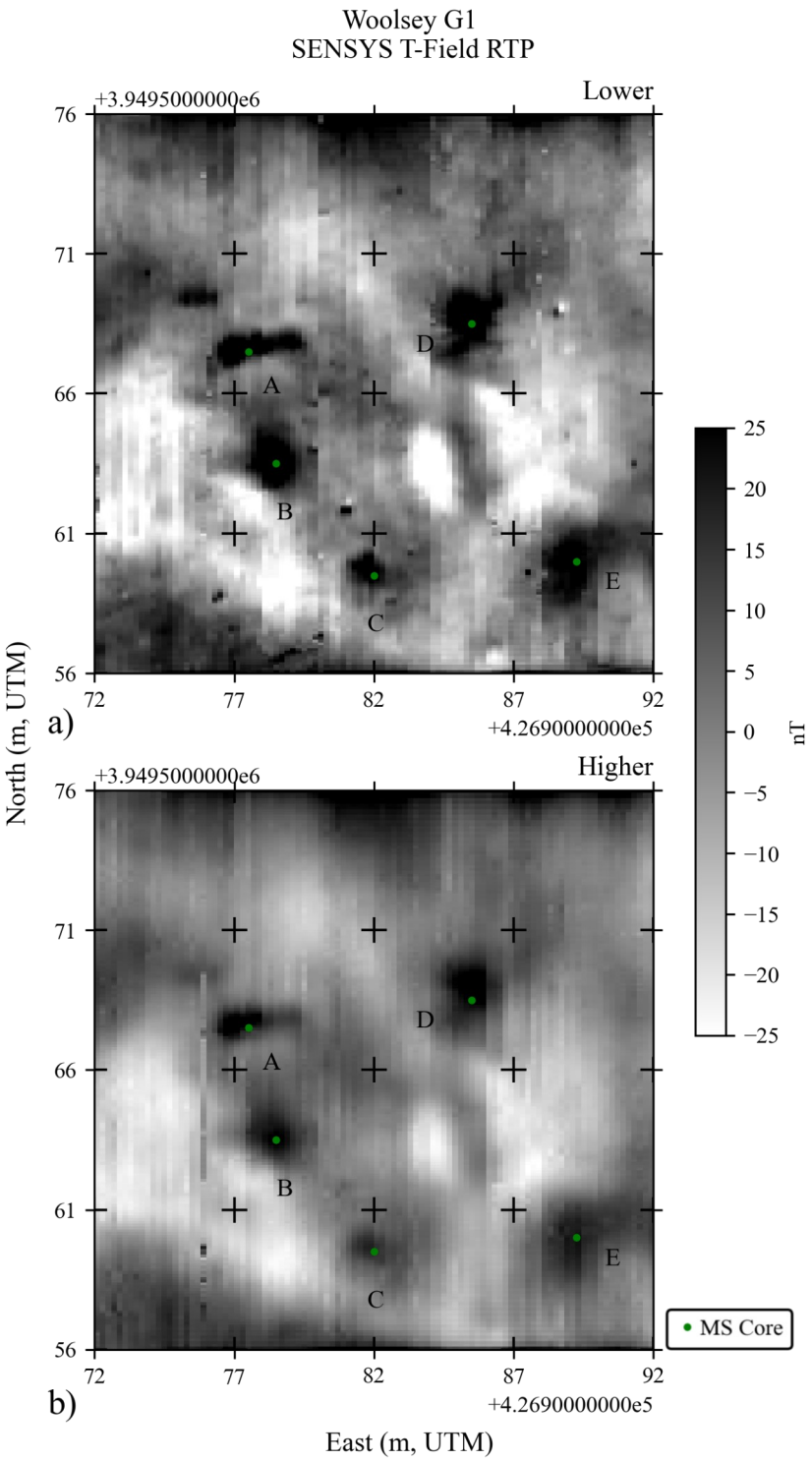

Figure B.4 Woolsey G1 SENSYS Data. a) Lower survey at 0.0845 m. b) Higher survey at 0.3845 m

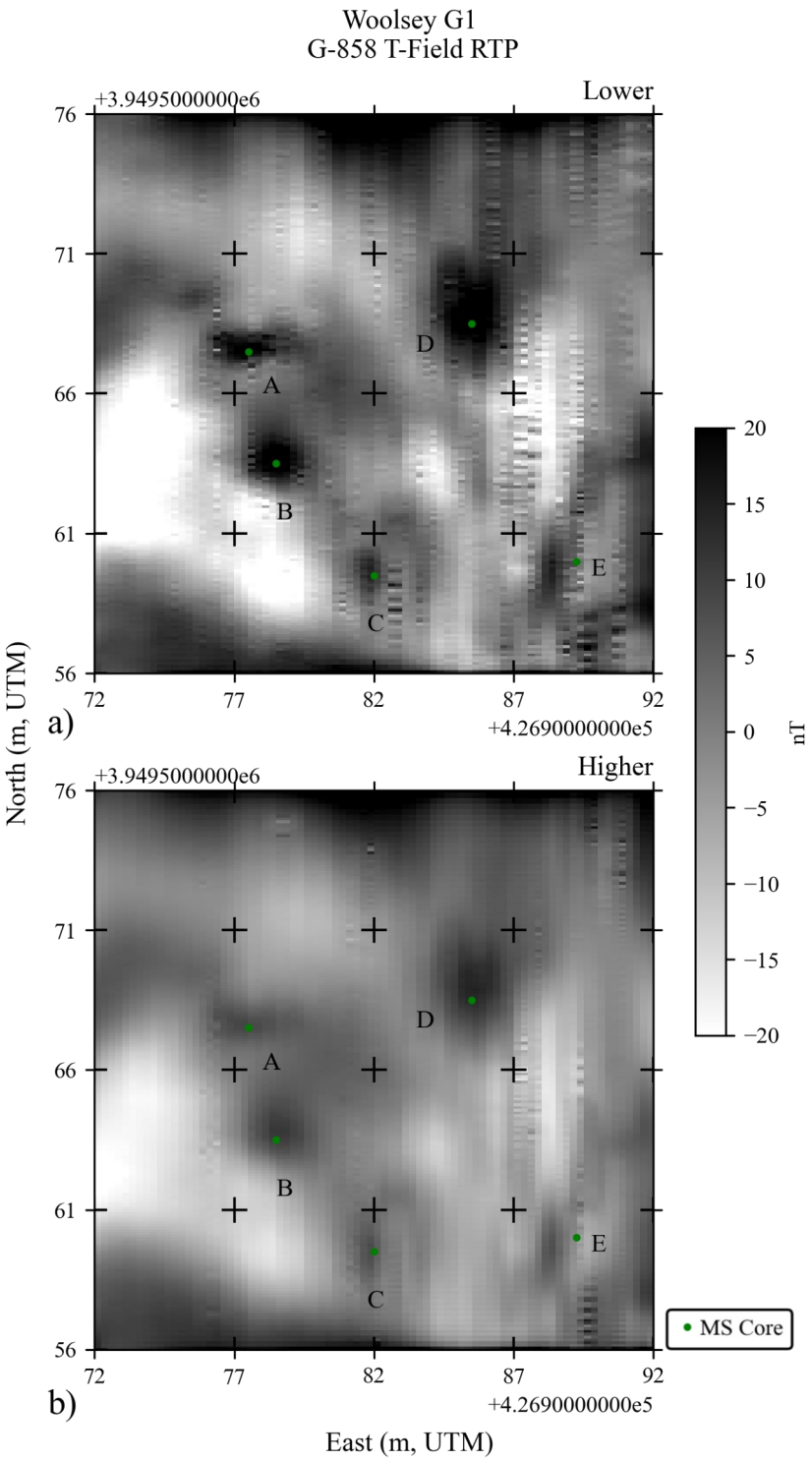

Figure B.5 Woolsey G1 G-858 Data. a) Lower survey at 0.35 m. b) Higher survey at 0.85 m.

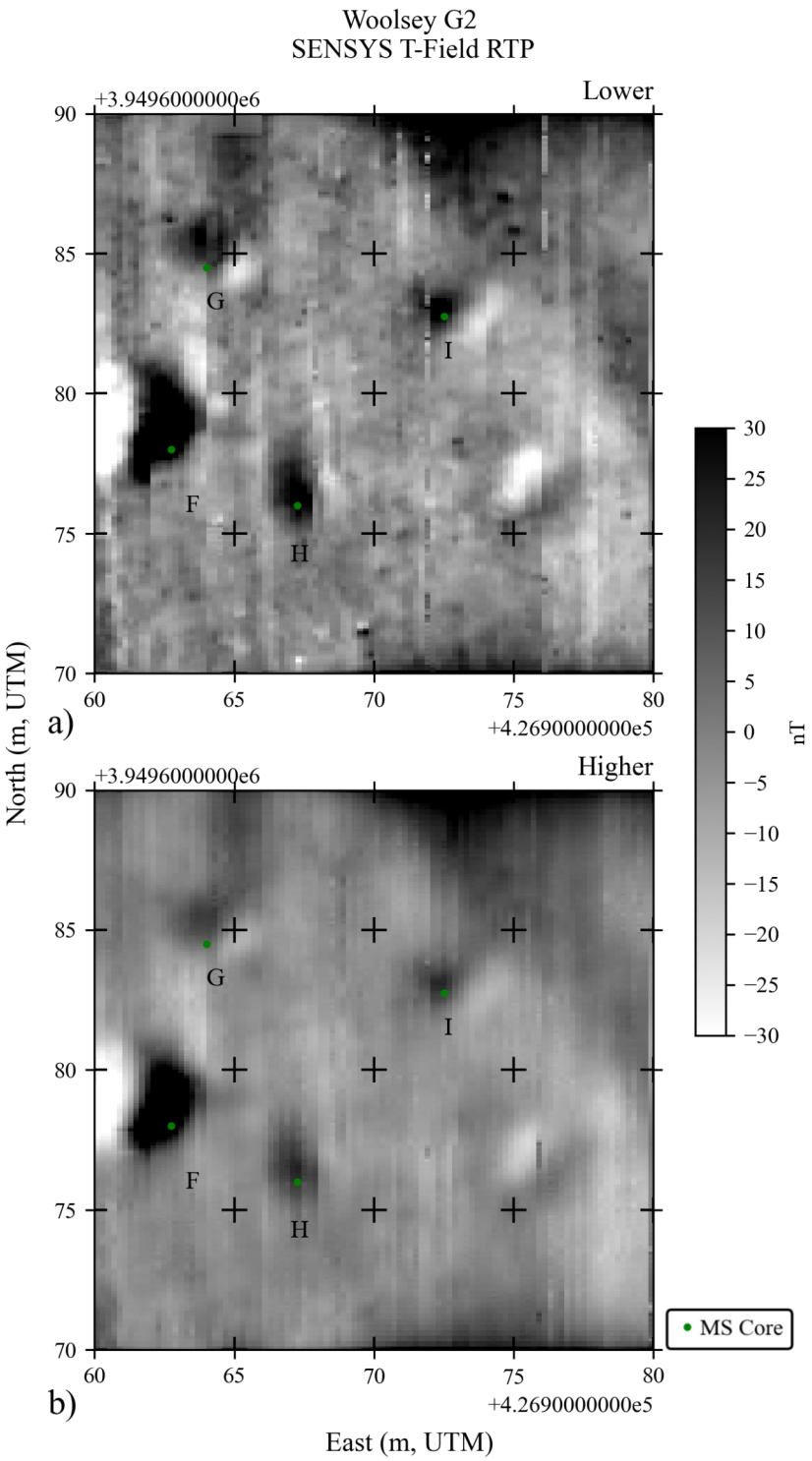

Figure B.6 Woolsey G2 SENSYS Data. a) Lower survey at 0.0845 m. b) Higher survey at 0.3845 m.

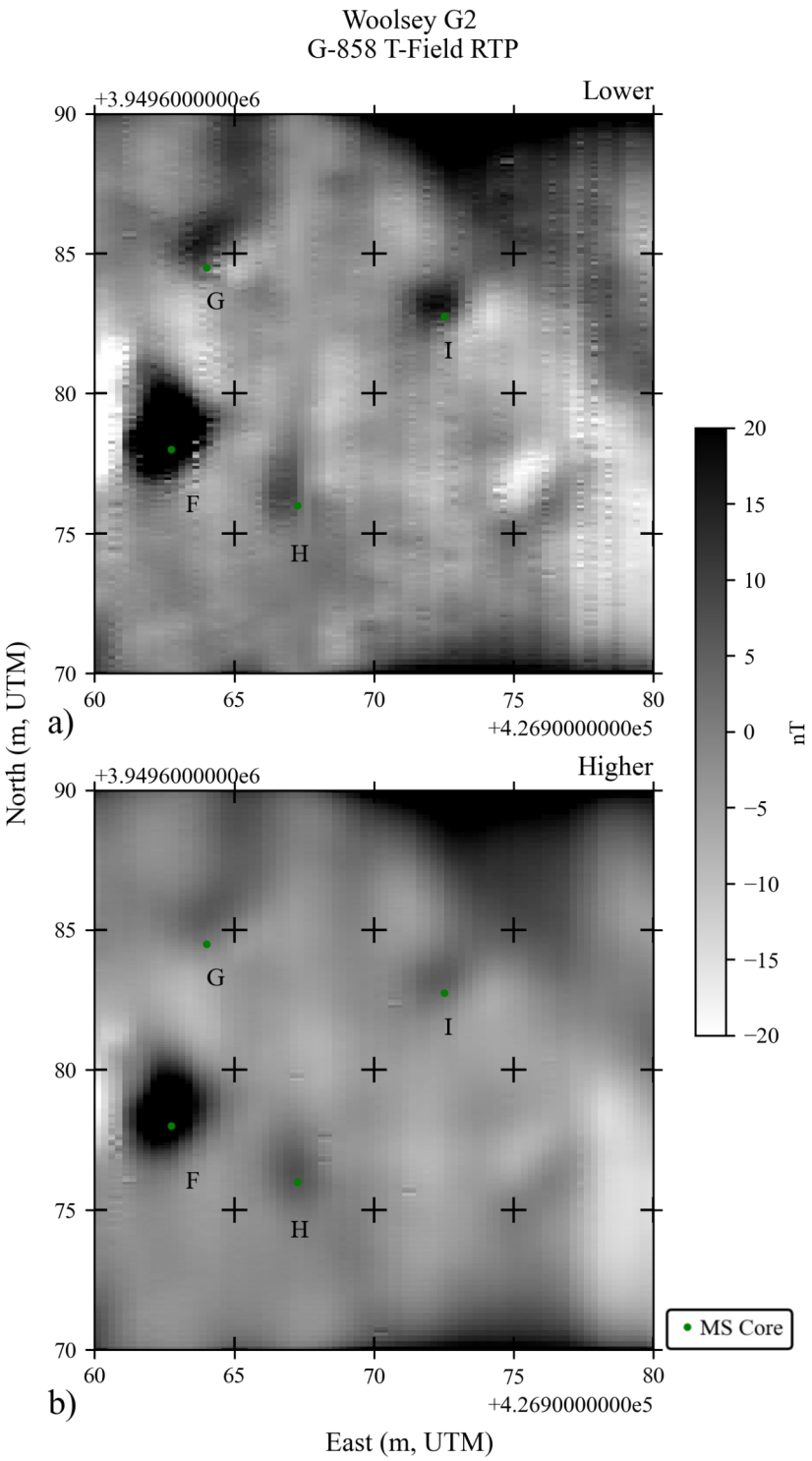

Figure B.7 Woolsey G2 G-858 Data. a) Lower survey at 0.35 m. b) Higher survey at 0.85 m.

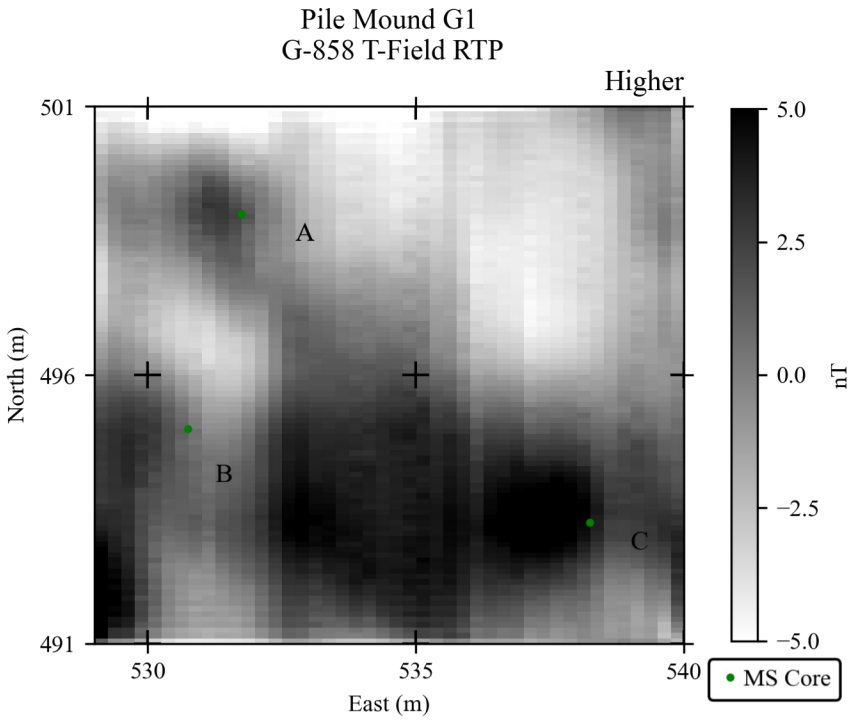

Figure B.8 Pile Mound G1 G-858 Higher Data. Survey height at 0.85 m.

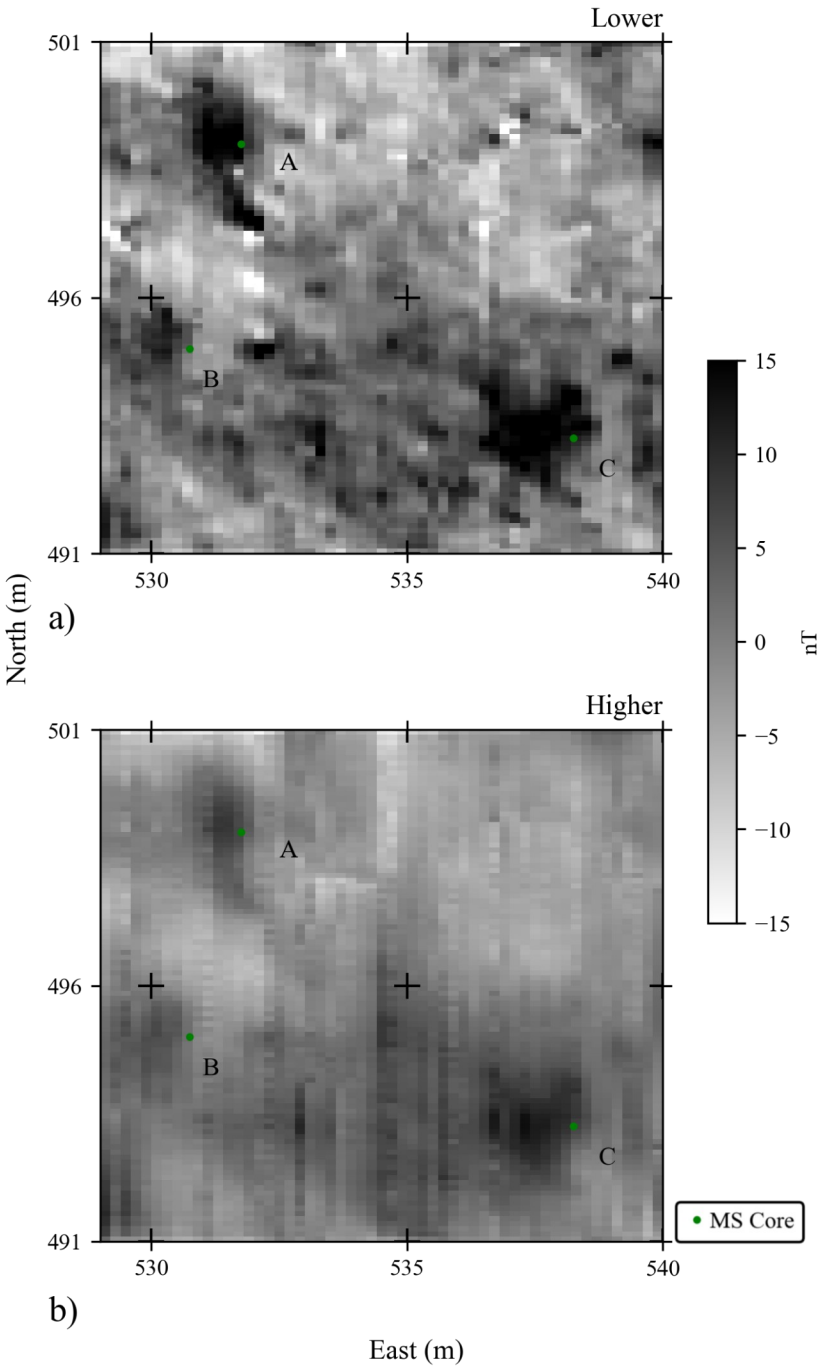

Figure B.9 Pile Mound G1 SENSYS Data. a) Lower survey at 0.0845 m. b) Higher survey at 0.3845 m.

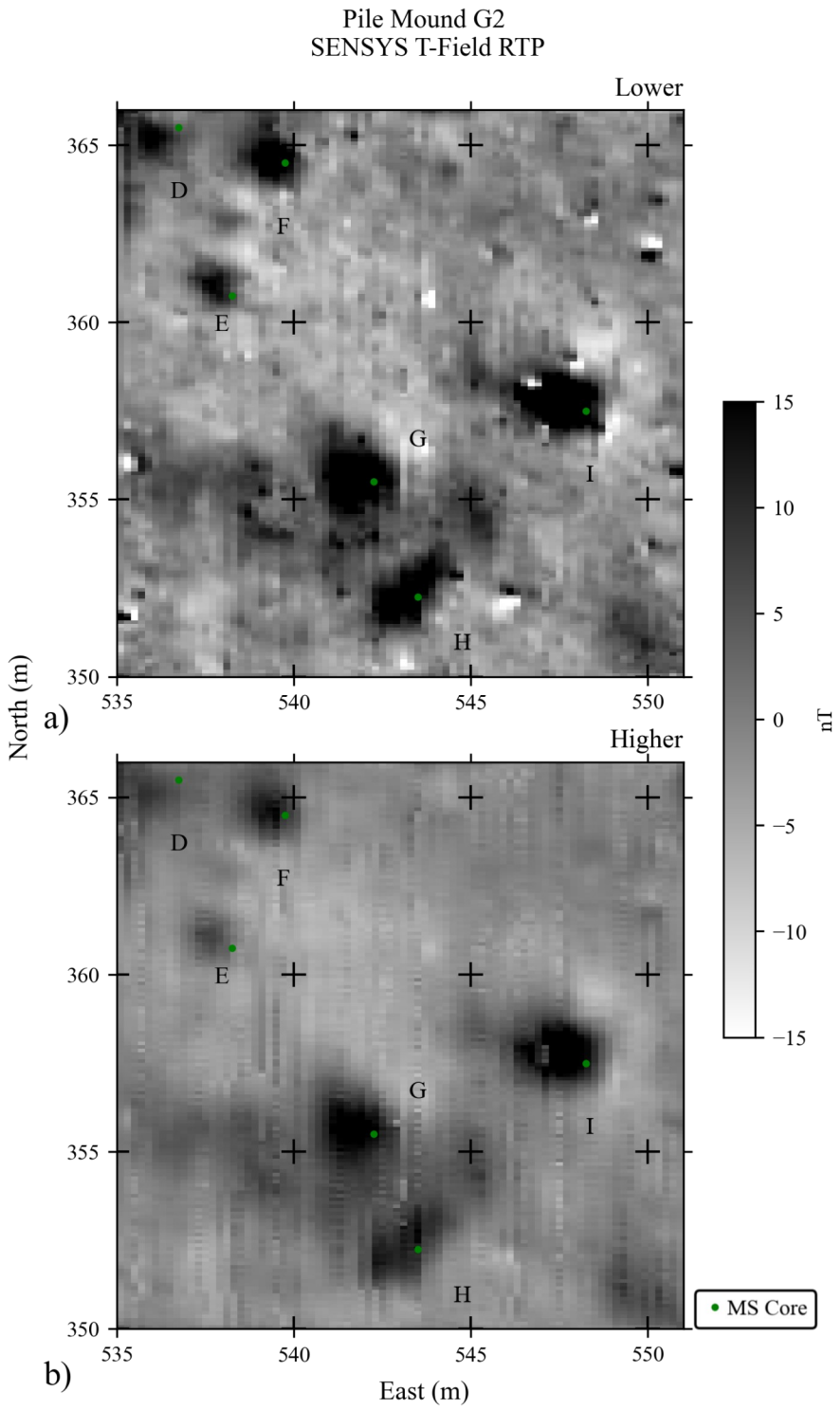

Figure B.10 Pile Mound G2 SENSYS Data. a) Lower survey at 0.0845 m. b) Higher survey at 0.3845 m.

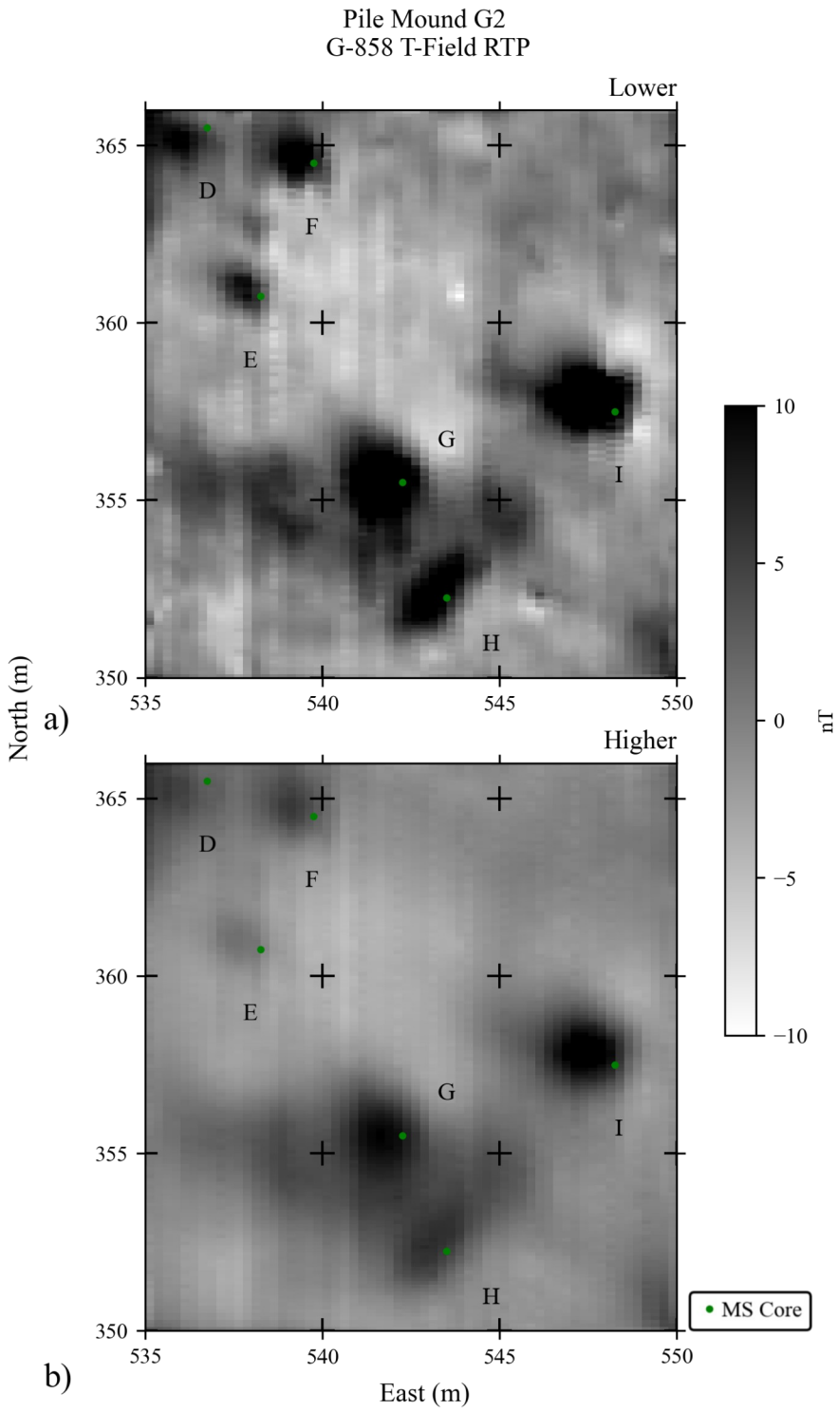

Figure B.11 Pile Mound G2 G-858 Data. a) Lower survey at 0.35 m. b) Higher survey at 0.85 m.

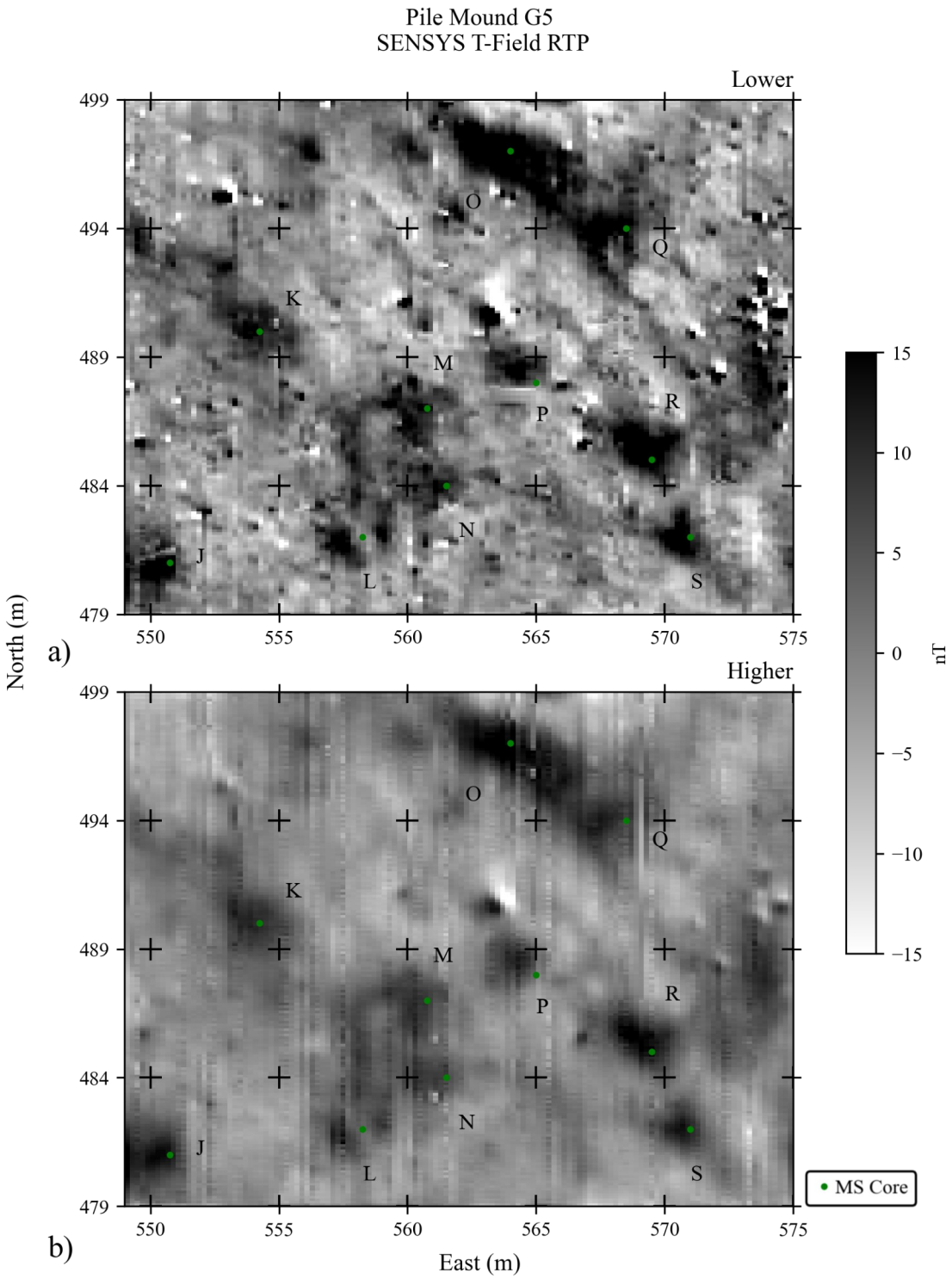

Figure B.12 Pile Mound G5 SENSYS Data. a) Lower survey at 0.0845 m. b) Higher survey at 0.3845 m.

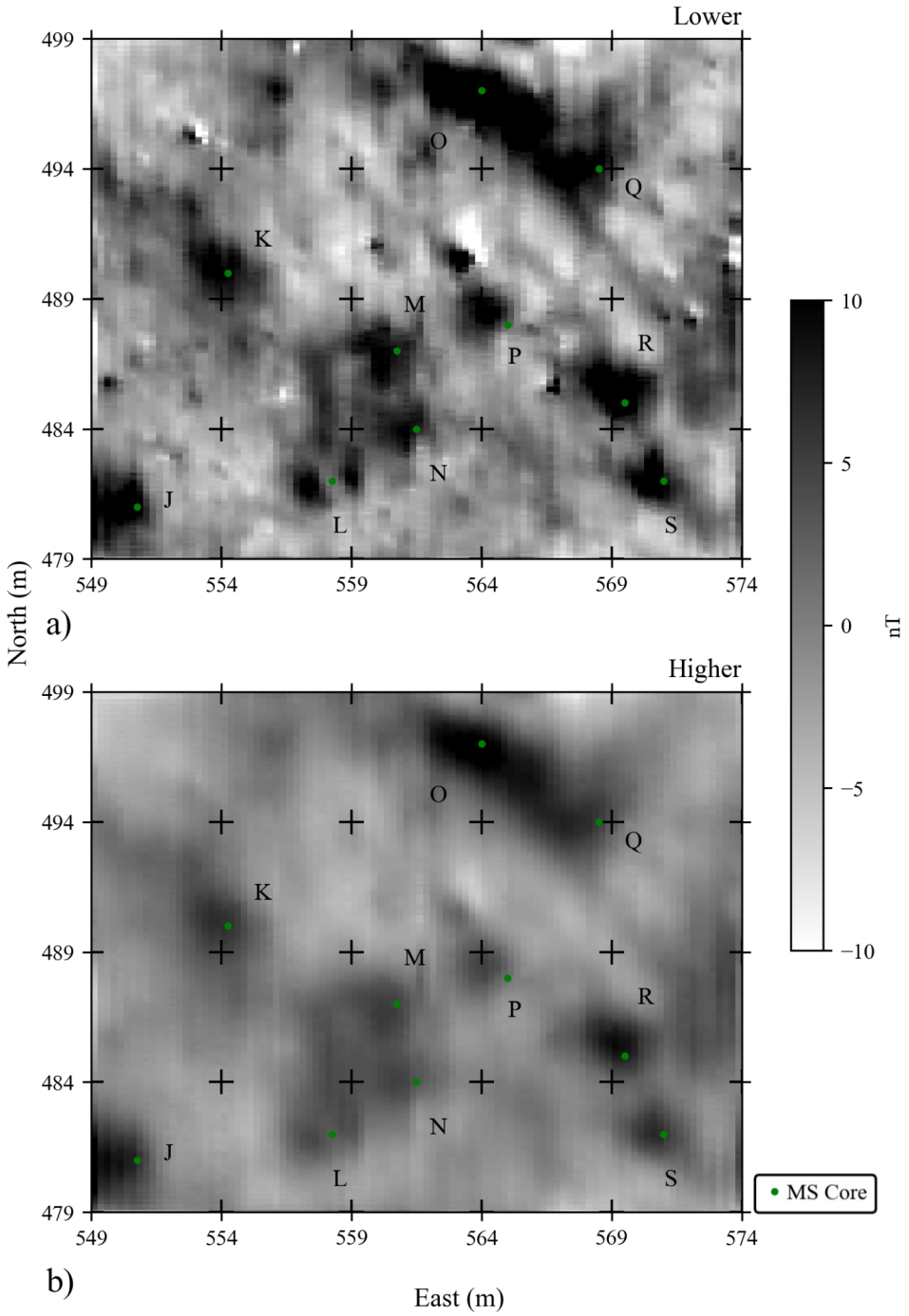

Figure B.13 Pile Mound G5 G-858 Data. a) Lower survey at 0.35 m. b) Higher survey at 0.85 m.

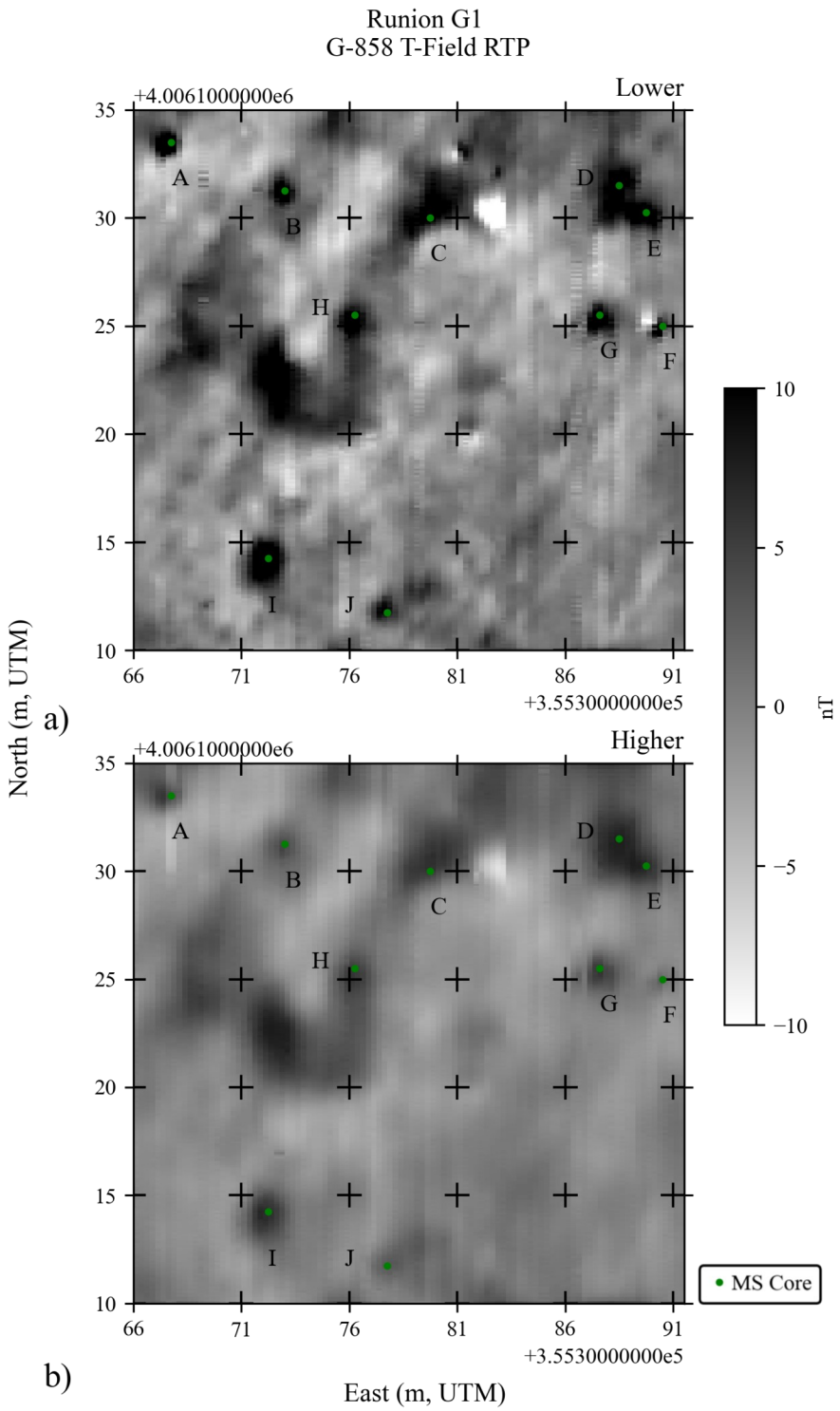

Figure B.14 Runion G1 G-858 Data. a) Lower survey at 0.35 m. b) Higher survey at 0.85 m.

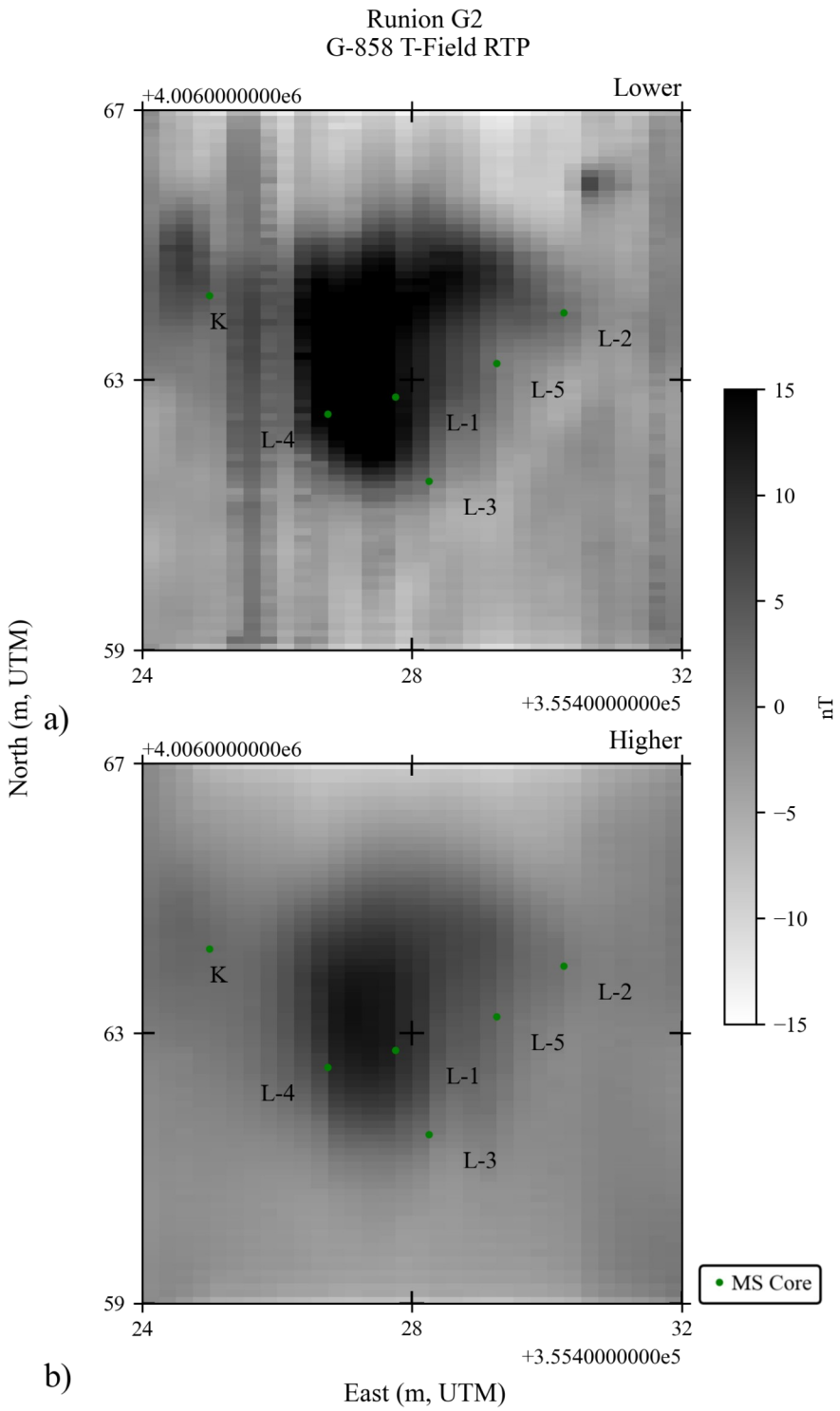

Figure B.15 Runion G2 G-858 Data. a) Lower survey at 0.35 m. b) Higher survey at 0.85 m.

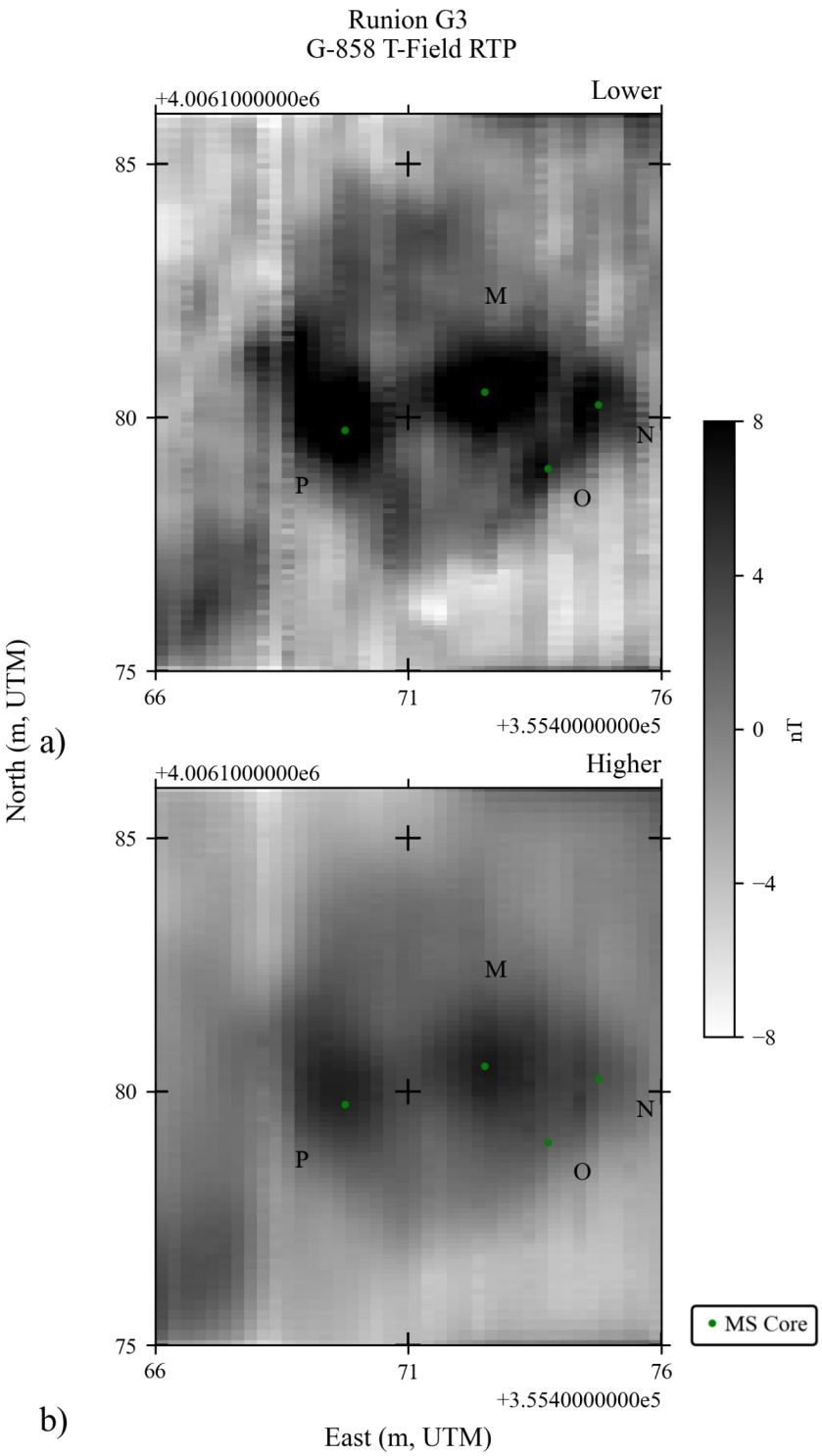

Figure B.16 Runion G3 G-858 Data. a) Lower survey at 0.35 m. b) Higher survey at 0.85 m.

Appendix C: Survey Statistics

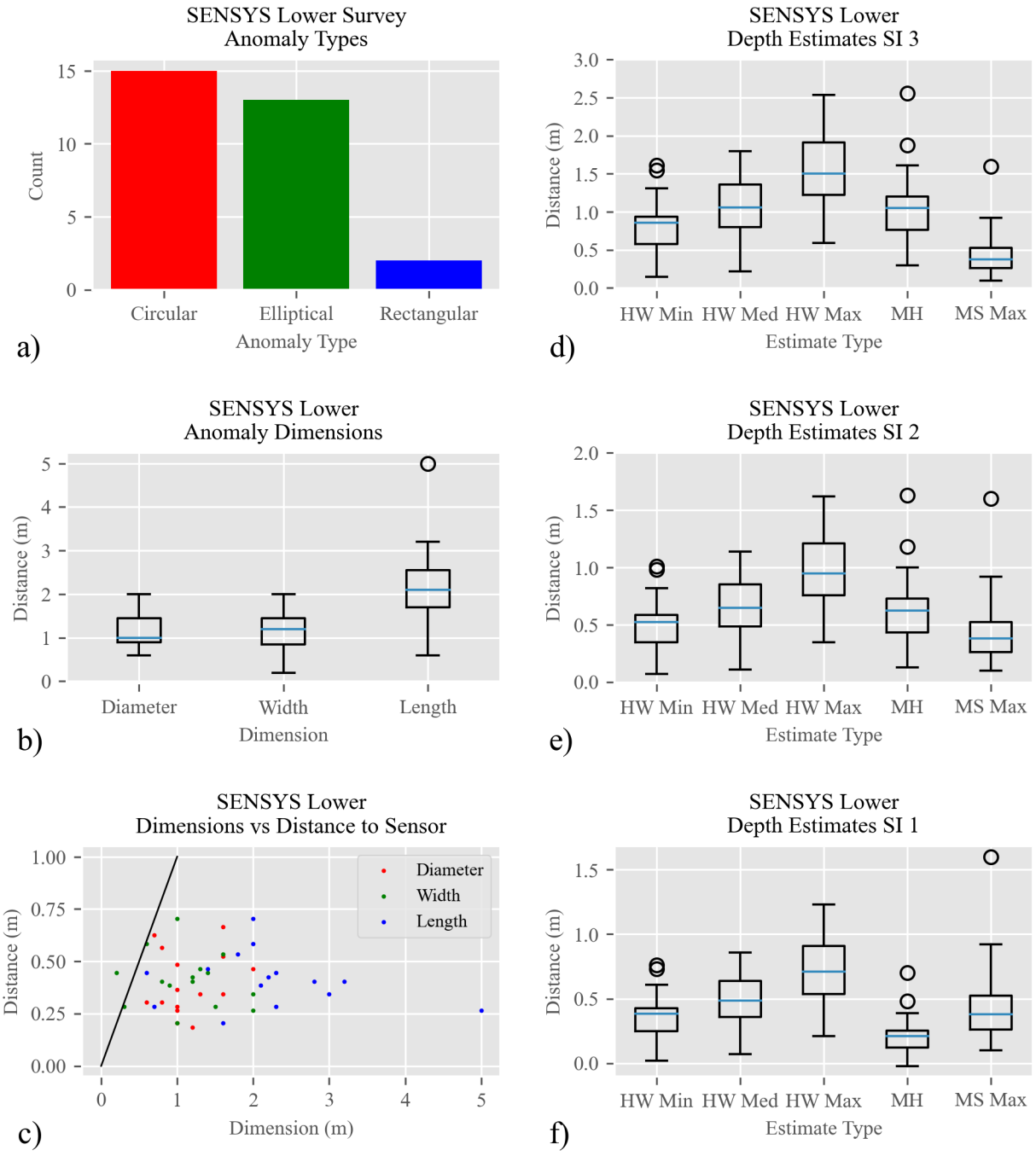

Figure C.1 SENSYS Lower Survey Statistics.

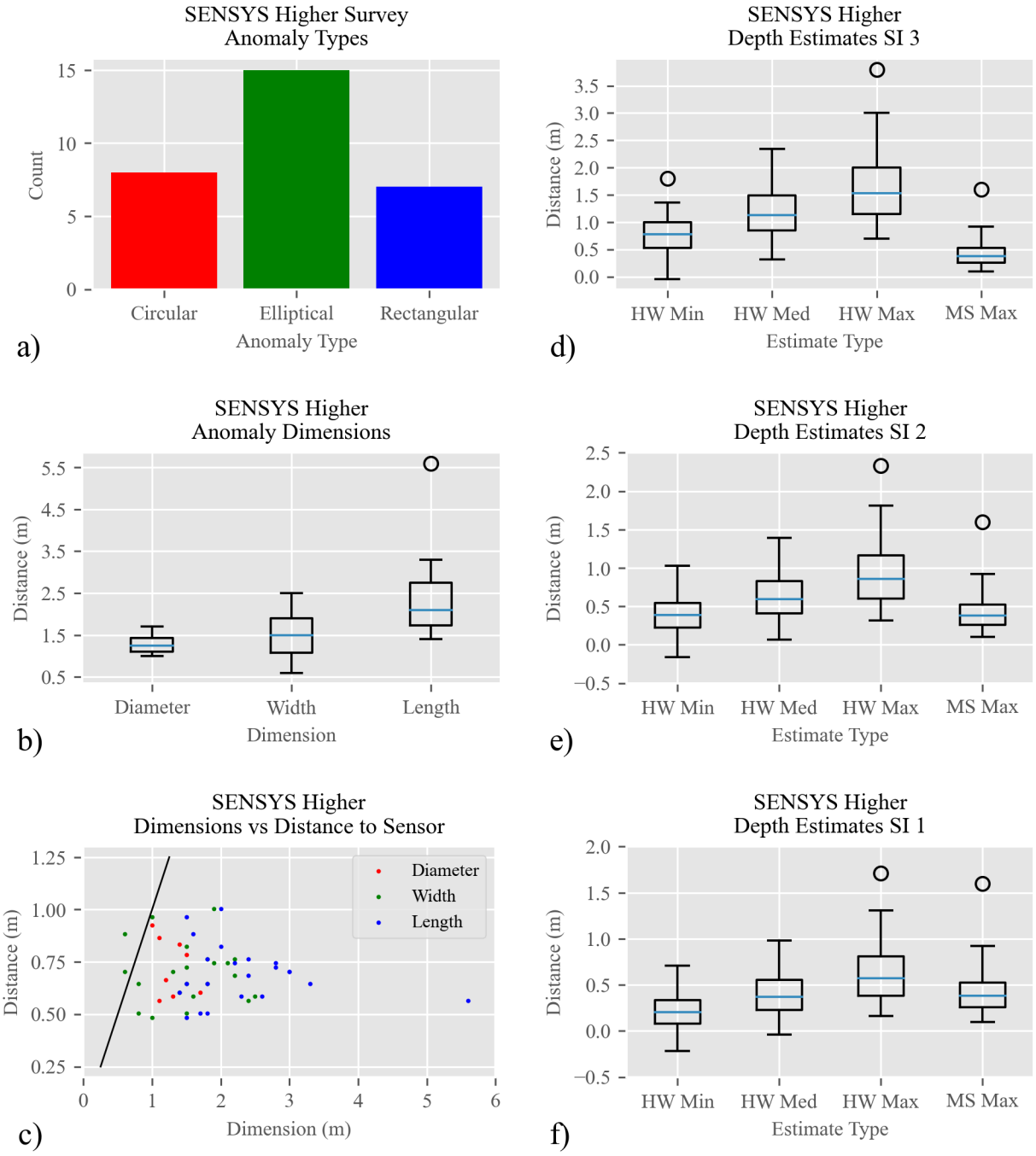

Figure C.2 SENSYS Higher Survey Statistics.

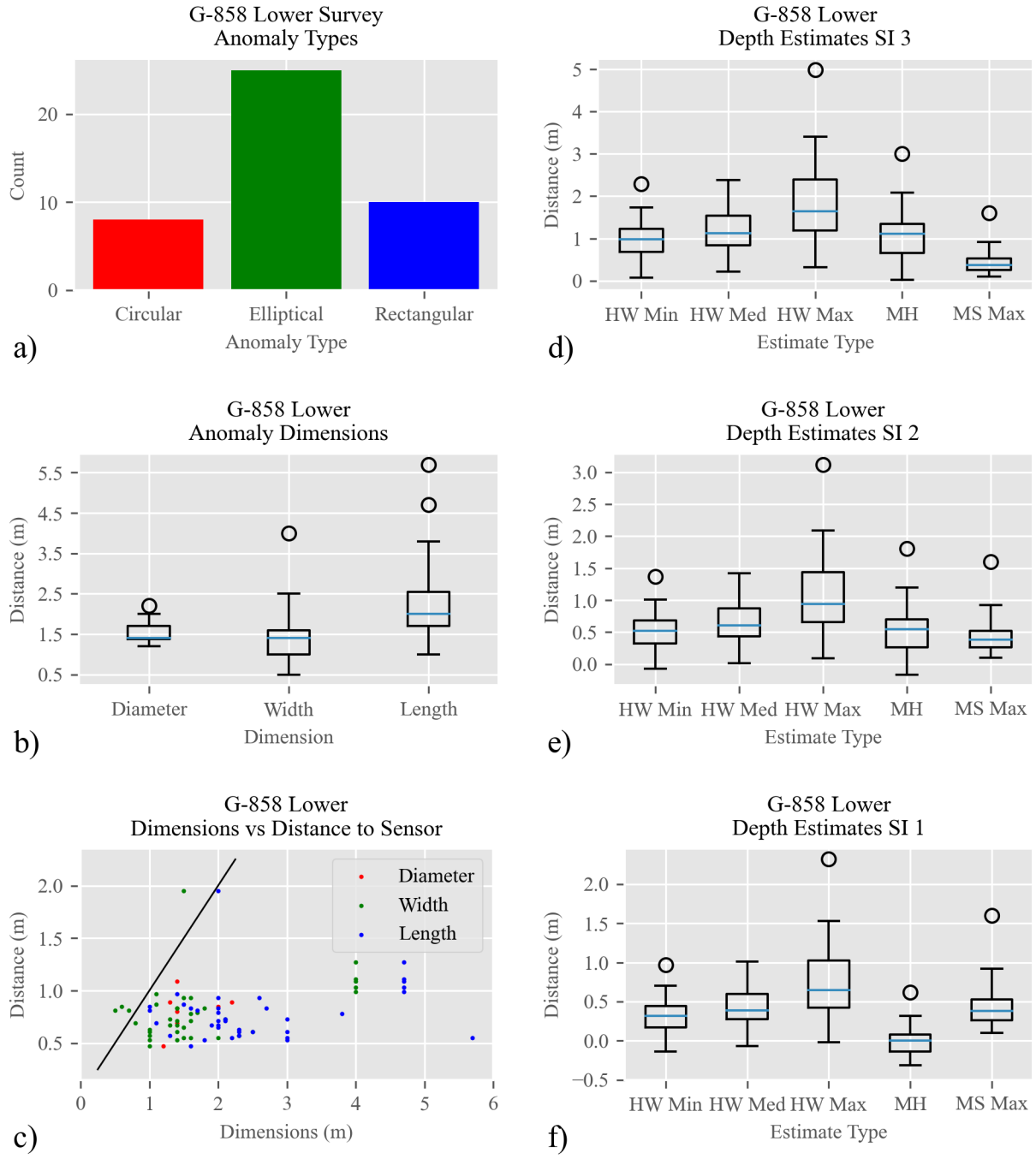

Figure C.3 G-858 Lower Survey Statistics.

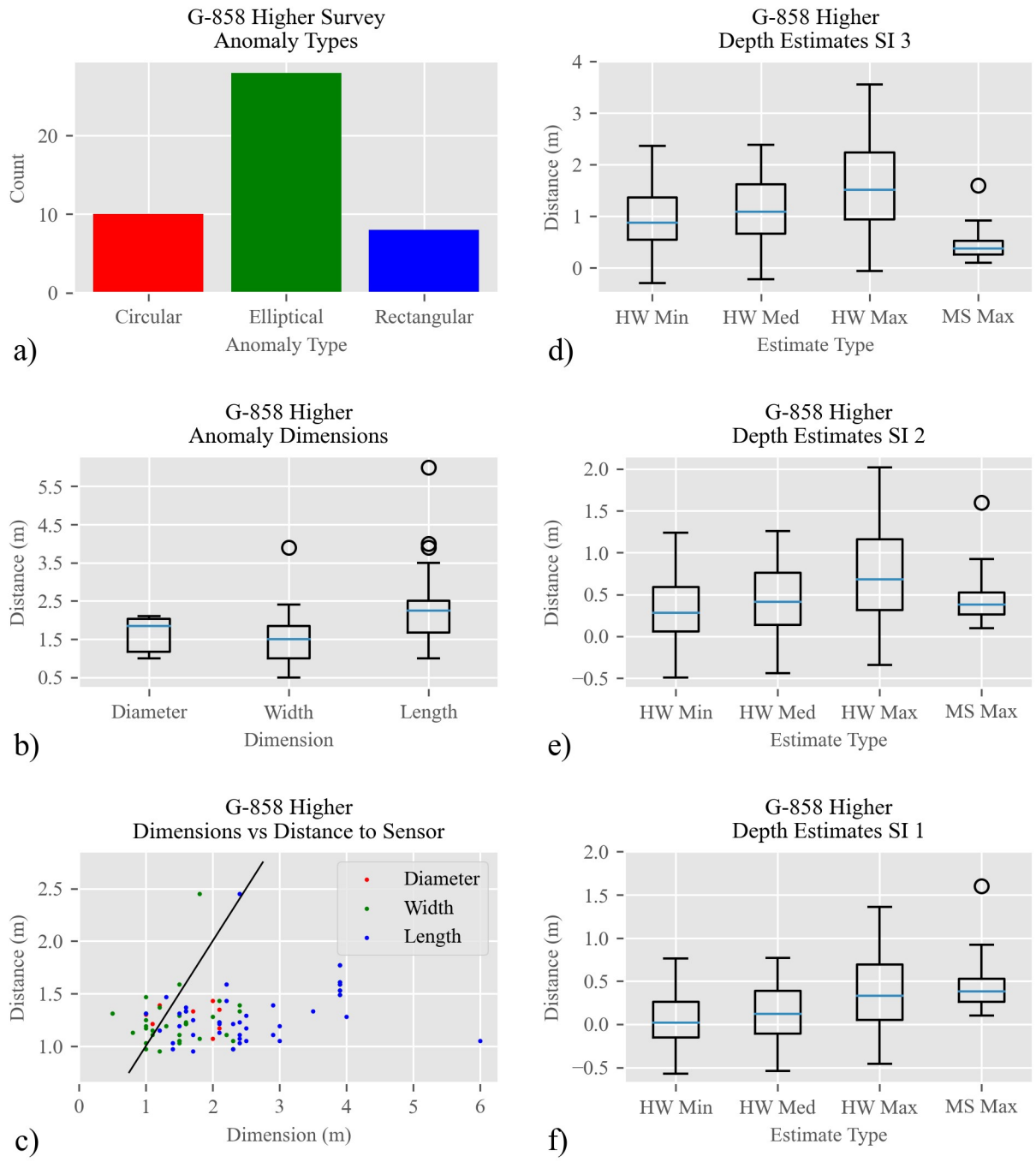

Figure C.4 G-858 Higher Survey Statistics.

Appendix D: Additional MS Log Information

Table D.1. Additional Magnetic Data. The maximum magnetic values and the magnetic susceptibility information for each feature. Site codes are W for Woolsey, PM for Pile Mound, and R for Runion. Magnetic survey codes are S for SENSYS, G for G-858, L for lower, and H for higher. Max stands for maximum value. X and Y are the locations of the MS core log. Z is the depth below surface where the maximum MS value occurs in the corresponding MS log. The MS maximum value of each core log is also provided.

Site	Grid	Feature	SL Max (nT)	SH Max (nT)	GL Max (nT)	GH Max (nT)	X (m)	Y (m)	Z (m)	MS Max Value (SI)
W	1	a	87.5	33.81	27.51	9.02	426977.5	3949567.5	0.28	0.005026
W	1	b	47.35	26.34	24.85	11.15	426978.5	3949563.5	0.5	0.007342
W	1	c	37.93	18.74	15.18	8.22	42682	3949559.5	0.32	0.005057
W	1	d	43.92	30	28.54	14.58	426985.5	3949568.5	0.58	0.008274
W	1	e	36.57	22.22	16.58	7.5	426989.25	3949560	0.26	0.0028.6
W	2	f	219.6	122.7	105.5	44.18	426962.75	3949678	0.26	0.007193
W	2	g	31.25	16.85	17.54	6.18	426964	3949684.5	0.2	0.005878
W	2	h	37.82	21.68	10.01	7.17	426967.25	3949676	0.26	0.007378
W	2	i	38.64	21.16	18.98	5.62	426972.5	3949682.75	0.44	0.007113
PM	1	a	19.41	8.72	n/a	2.96	531.75	499	0.36	0.002661
PM	1	b	13.31	6.6	n/a	3.5	530.75	495	0.4	0.002812
PM	1	c	21.58	13.35	n/a	6.22	538.25	493.25	0.1	0.002417
PM	2	d	16.76	9.21	11.14	5.71	536.75	365.5	0.18	0.001252
PM	2	e	18.02	7.38	9.35	1.21	538.25	360.75	0.62	0.002377
PM	2	f	28.69	15.73	14.25	5.62	539.75	364.5	0.48	0.002544
PM	2	g	30.18	18.22	20.46	9.88	542.25	355.5	0.54	0.002795
PM	2	h	21.12	15.3	13.23	6.66	543.5	352.25	0.38	0.001922
PM	2	i	78.4	27.4	18.89	5.62	548.25	357.5	0.38	0.002515
PM	5	j	37	14.36	17.29	8.76	550.75	481	0.32	0.005878
PM	5	k	23.18	12.29	12.42	6.59	554.25	490	0.36	0.006556
PM	5	l	20.8	14.79	12.78	4.45	558.25	482	0.12	0.002922
PM	5	m	20.7	10.9	11.84	5.44	560.75	487	0.22	0.003049
PM	5	n	17.38	10.46	11	4.95	561.5	484	0.12	0.002591
PM	5	o	27.58	17.68	19.82	11.34	564	497	0.2	0.002376
PM	5	p	25.2	12.24	12.87	4.91	565	488	0.22	0.003739

Table D.1 (Cont.)

Site	Grid	Feature	SL Max (nT)	SH Max (nT)	GL Max (nT)	GH Max (nT)	X (m)	Y (m)	Z (m)	MS Max Value (SI)
PM	5	q	23.74	12.64	14.76	7.85	568.5	494	0.18	0.002278
PM	5	r	34.64	16.37	19.46	9.39	569.5	485	0.2	0.002974
PM	5	s	23.99	13.6	17.47	6.82	571	482	0.3	0.003228
R	1	a			29.75	5.69	355367.75	4006133.5	n/a	n/a
R	1	b			18.04	4.61	355373	4006131.25	n/a	n/a
R	1	c			14.12	6.44	355379.75	4006130	n/a	n/a
R	1	d			13.08	7.58	355388.5	4006131.5	0.48	0.003548
R	1	e			16.71	7.7	355389.75	4006130.25	0.48	0.003102
R	1	f			25.83	2.27	355390.5	4006125	0.46	0.001805
R	1	g			21.3	6.23	355387.6	4006125.5	0.54	0.014376
R	1	h			14.22	5.83	355376.25	4006125.5	n/a	n/a
R	1	i			15.14	6.95	355372.25	4006114.25	0.36	0.002492
R	1	j			11.59	3.11	355377.75	4006111.75	0.34	0.001523
R	2	k			8.39	3.13	355425	4006064.25	0.46	0.003652
R	2	l1			23.65	12.92	355427.75	4006062.75	0.76	0.005061
R	2	l2			“	“	355430.25	4006064	0.64	0.007107
R	2	l3			“	“	355428.25	4006061.5	0.74	0.005664
R	2	l4			“	“	355426.75	4006062.5	0.68	0.003276
R	2	l5			“	“	355429.25	4006063.25	0.92	0.002325
R	3	m			11.37	6.51	355472.25	4006180.44	0.58	0.006516
R	3	n			8.97	4.58	355474.75	4006180.25	0.52	0.003229
R	3	o			7.65	4.44	355473.75	4006179	0.5	0.005594
R	3	p			12.5	6.07	355469.75	4006179.75	1.6	0.005215

Appendix E: Python Code

The magnetic modeling in this project was performed in Python 2.8 with the "fatiando a terra" package. This Python library is now depreciated, but it can still be found at https://legacy.fatiando.org/api/fatiando.html. The fatiando project is currently working on developing new code for the same tasks in Python 3. This new library can be found at https://www.fatiando.org/.

Python code is provided that was developed for this project due to the lack of available software (commercial or open-source) that could perform the depth estimation techniques used in this study. The code will also be housed at https://github.com/jgmenzer/archaeo-mag. This repository will be updated with better documentation and additional functions in the future. A brief overview of the current code is provided here.

The functions below perform two main tasks, either processing of magnetic data or performing depth estimation. In order to use the below code, one must first install Python 3.8 or greater. After installing, the user will need to load in their magnetic data. Depending on the instrument used formats vary, but you should easily be able to load any ascii format with the numpy or pandas libraries. If you need to perform additional processing outside of Python, do this before loading into Python. Next the user should cut the data around specific anomalies of interest—there should only be one magnetic anomaly in any single dataset. The user will then pass any data subsets to the depth estimation functions.

The "clip base", "med despike", and "thresh despike" functions could be used to process any base station data. These functions are used to remove erroneous data or smooth large data spikes. The "notch filter" is used to remove 60 Hz data which can occur from ambient power lines and other electrical devices. The "pd mad" and "pd hampel" filter work together to perform a hampel filter. This is used to remove data spikes and smooth magnetic data. The "make grid"

and “idw” functions can be used in conjunction to interpolate data onto a regular grid system—thus creating a raster dataset from GNSS data. The “UTM to local” function transforms data from the UTM coordinate system to a local grid coordinate system. Local grids are commonly used on archaeological sites. The “save surfer” function exports data to the surfer ascii format so that one could view the data outside of Python. “Cut Grid” selects a subset of data from a raster and creates a new smaller raster. This is used to select the magnetic data of individual features. The smaller datasets are used in depth estimation processes. The “MPF” function performs a Mean Profile Filter on 2D raster data. See Chapter 4 for additional information on the processing technique.

The “half max all dir” function performs the HW rule depth estimations. A series of subroutines are used within this function to complete the task. The magnetic data for individual features should be cut out before passing data into this function. It will output the HW estimates for SI=3, 2, and 1. The “multi height profile” function performs the multi-height depth estimation. Again, this should be used on magnetic data of individual features. It will provide depth estimates for SI=3, 2, and 1. Note that before performing depth estimations, total field data should be differentially corrected and processed for any data striping.

```
# -*- coding: utf-8 -*-
"""
Created on Tue Aug 31 11:24:41 2021

@author: jer
"""
# a master list of python 3.8 functions

# dependencies,
```

```
import numpy as np
import scipy as sp
from scipy import ndimage as ip
from scipy import interpolate as interp
import pandas as pd
# the fatiando project has since divided into multiple packages
# the easiest solution is to simply copy the functions below
# and add them to this file
from fatiando.gridder import regular, profile, interp_at, extrapolate_nans
import 'the file with these functions' as am


#
def clip_base(basedata, n):
    # this clips off the start and end of a file by n number
            # this is used when basedata have erroneous data at the
            # beginning and end of a survey due to the user being nearby
            # basedata is a numpy array, n is the number of data point
            # to remove
    tmp = len(basedata)-n
    tmp = basedata[n:tmp]
    return tmp


def med_despike(data, r, threshold, data_sign):
    # data is the data to be despiked, data_sign either '+' or '-'
            # data is a  numpy array
    # is if the data is positve or negative, insert data_sign=''
    # is a range factor, eg is data >/< median + range
    # threshold is the number to cut data off at, if its above/below its bad data
```

```
    if data_sign == '+':
        tmp_goodlocs = np.where(data>threshold)
        tmp_median = np.median(data.iloc[tmp_goodlocs])
        new_data = np.where(data < tmp_median-r, tmp_median, data) #for erroneous data insert the good data median
    if data_sign == '-':
        tmp_goodlocs = np.where(data<threshold)
        tmp_median = np.median(data.iloc[tmp_goodlocs]) #for erroneous data insert the good data median
        new_data = np.where(data > tmp_median+r, tmp_median, data)
    return new_data


def thres_despike(data, threshold, threshsign):
    # data is the data to be despiked, threshold is the data value cutoff, threshsign either '>' or '<'
            # data is a numpy array
    # is if you want data above or below the threshold, need to write threshsign=''
    if threshsign == '>':
        tmp_goodlocs = np.where(data>threshold)
        tmp_median = np.median(data[tmp_goodlocs])
        new_data = np.where(data < threshold, tmp_median, data) #for erroneous data insert the good data median
    if threshsign == '<':
        tmp_goodlocs = np.where(data<threshold)
        tmp_median = np.median(data[tmp_goodlocs]) #for erroneous data insert the good data median
        new_data = np.where(data > threshold, tmp_median, data)
    return new_data


def notch_filter(data, f_notch, fs, Q):
    # an iir notch filter, input data is data to be filtered as a numpy array
    # f_notch is the desired notch frequency in Hz,
    # fs is the data frequency in Hz and Q the quality factor/bandwith factor a
```

```
    # higher factor decreases the bandwidth, recommend 30>
    b_notch, a_notch = sp.signal.iirnotch(f_notch, Q, fs=fs)
    filtered = sp.signal.filtfilt(b_notch, a_notch, data)
    return filtered

def pd_mad(data, window_size):
        # median absolute deviation filter in pandas dataframe format
        # data is the pandas series
    data= data
    tmp = data.rolling(window=window_size, min_periods=1, center=True).median()
    tmp2 = np.absolute(data-tmp)
    tmp_mad = tmp2.rolling(window=window_size, min_periods=1, center=True).median()
    # return the moving mad data and the moving median data
    return tmp_mad, tmp

def pd_hampel(data, mad_data, median_data, nd):
    # data to be filtered, a pandas series
        # nd = number of deviations equivalent to standard deviations
    new_data = data.copy()
    k=1.4826
    outlier_locs = np.where(np.absolute(new_data-median_data) >= nd*k*mad_data)
    new_data.iloc[outlier_locs] = median_data.iloc[outlier_locs]

    return new_data

def make_grid(xmin, xmax, ymin, ymax, xspacing, yspacing, rounding):
    # note - this should be at cell centers
        # makes a grid of evenly spaced data in numpy 1D arrays
```

```
    x = np.arange((xmin+(xspacing/2.)), (xmax+(xspacing/2.)), xspacing)
    y = np.arange((ymin+(yspacing/2.)), (ymax+(yspacing/2.)), yspacing)
    gx, gy = np.round(np.meshgrid(x,y),rounding)
    gx = gx.ravel()
    gy = gy.ravel()
    return gx, gy



def idw(xz, yz, zz, x, y, p, xs, ys):
            # perform an inverse distance weighted interpolation
            # xz is original x values, yz is original y values, zz is original z values
            # all are in numpy 1d arrays. x and y are the new data locations in numpy 1d
            # arrays. p is power of interpolation, xs, and ys are the search window dimensions
            # returns a numpy 1d array of the new interpolated z values

    zfinal = []
    for ix, iy in zip(x, y):



        ellipse = np.where(((((xz-ix)**2)/(xs**2)) + (((yz-iy)**2)/ys**2)) <=1 )
        ellipse_dists = ((((xz[ellipse]-ix)**2)/(xs**2)) + (((yz[ellipse]-iy)**2)/ys**2))



        weights = (1./ellipse_dists)**2
        w_sum = np.sum(weights)
        weights = weights/w_sum
        z_ellipse = zz[ellipse]*weights
        zfinal.append(np.sum(z_ellipse))
```

```
    zfinal = np.asarray(zfinal)
    return zfinal


def utm_to_local(utmx, utmy, utmxyA, utmxyB, localxyA, localxyB):
    # transformation of utm to local data using a line AB
        # utmx and utmy inputs are numpy 1d arrays of original data
        # utmxyA and utmxyB are a,y coords of the two reference points in UTM
    # localxyA and localxyB are the coords of the two reference points in local coords

    #transform equations/scaling
    utmscale = np.sqrt(((utmxyB[0]-utmxyA[0])**2)+((utmxyB[1]-utmxyA[1])**2))
    localscale = np.sqrt(((localxyB[0]-localxyA[0])**2)+((localxyB[1]-localxyA[1])**2))
    # rotation note - np should give result in radians
    utmtheta = np.arccos((utmxyB[0]-utmxyA[0])/utmscale)
    localtheta = np.arccos((localxyB[0]-localxyA[0])/localscale)
    theta = utmtheta-localtheta
    # translation
    tmp = np.sqrt((utmxyA[0]**2)+(utmxyA[1]**2))
    transtheta = np.arctan(utmxyA[1]/utmxyA[0])
    transtheta = transtheta-theta
    tx = localxyA[0]-tmp*np.cos(transtheta)
    ty = localxyA[1]-tmp*np.sin(transtheta)
    tmp1 = np.cos(theta)
    tmp2 = np.sin(theta)
    localx = tx+(utmx*tmp1)+(utmy*tmp2)
    localy = ty-(utmx*tmp2)+(utmy*tmp1)
```

```
    return localx, localy


def save_surfer(fname, data, shape, area):
#set header variables, note all variables are switched to x horizontal and y vertical to fit with surfer terminology
#also z values are set to a max of 5 decimal places to save on space in ascii format
#this was chosen because this is just slightly above most field equipment's level of precision



#required inputs are a file name (fname) and the data (data) to be exported
#also need data shape and area which should already be created from fatiando
    ncols = int(shape[1])
    nrows = int(shape[0])
    xmin = area[2]
    xmax = area[3]
    ymin = area[0]
    ymax = area[1]
    datamin = round(np.amin(data), 5)
    datamax = round(np.amax(data), 5)
    header = ('DSAA'+'\n'+' '+str(ncols)+' '+str(nrows)+'\n'+' '+str(xmin)+' '+str(xmax)
            +'\n'+' '+str(ymin)+' '+str(ymax)+'\n'+' '+str(datamin)+' '+str(datamax))
#make 2d array
    tmp = np.array(data).reshape(ncols,nrows)
    np.savetxt('%s.grd' % (fname),tmp, fmt='%.5f', delimiter=' ', header=(header), comments = '')


def cut_grid(x,y,z,area, resolution):
            # x,y,z are numpy 1d arrays, areas is bounding coords, resolution is x,y
    # area must be evenly divisible by resolution due to floating point rounding
    # eg if res is 0.2 must use n.6 not n.5
```

```
    xmin, xmax, ymin, ymax = area
    if len(x)!= len(y):
        raise ValueError('x and y must be the same length dummy')
    tmp = np.where((x>=xmin) & (x<=xmax) & (y>=ymin) & (y<=ymax))
    newx = x[tmp]
    newy = y[tmp]
    newz = z[tmp]
    xshape = round((xmax-xmin)/resolution[0]) # note was int()
    yshape = round((ymax-ymin)/resolution[1]) # note was int()
    newshape = [xshape,yshape]

    return newx, newy, newz, newshape

## raster data processing e.g. 2d arrays

def mpf(data,lp,hp):
    # data is a 2d numpy array in the shape of your survey
    # eg what you would input to imshow
    #lp = low pass window size
    #hp = high pass window size
    #NOTE- this is currently a vertical only filter
    tmpl=ip.uniform_filter(data, size=(lp,1))
    tmph=ip.uniform_filter(tmpl, size=(1,hp))
    tmp=tmpl-tmph
    mpf=data-tmp
    return mpf
```

```
# depth estimation stuff
#####################################################

def half_max_all_dir(x, y, z, sampling):
        # note this returns data that still needs the sensor height subtracted
        # computes the HW in 360 degrees of the maximum z value in a data window
        # x, y, z are 1d numpy arrays of data
        # sampling is the line interpolation spacing, or number of values to interp
        # between the current data resolution.

    lines = make_all_direction_profiles(x, y, z)
    iterator =  np.arange(0,180,1)
    hm_data = []
    for i in iterator:
        samples = find_samples_pdist((lines[0][i],lines[1][i]), (lines[2][i],lines[3][i]), sampling)
        profile = extract_profile(x, y, z, (lines[0][i],lines[1][i]), (lines[2][i],lines[3][i]), samples)
        tmplocs = np.where(~np.isnan(profile[3]))
        newz = profile[3][tmplocs]
        tmpdist = profile[2][tmplocs]
        length = len(tmpdist)
        newdist = np.arange(0,length,(1./sampling))
        hm_tmp = calc_half_max(newdist, newz)
        hm_data.append(hm_tmp)

    hm_data = np.asarray(hm_data)

    fwhm = hm_data[:,0]
    hm_n2 = hm_data[:,1]
```

```
    hm = hm_data[:,2]


    return fwhm, hm_n2, hm


def make_all_direction_profiles(x, y, z):
            # makes 180 lines (360 deg) around the max z value
    xmin = np.min(x)
    xmax = np.max(x)
    ymin = np.min(y)
    ymax = np.max(y)
    zmax = np.max(z)
    zmaxi = np.where(z==zmax)
    if len(zmaxi) > 1:
       zmaxi = zmaxi[0]
    xp = x[zmaxi]
    xp = xp[0]
    yp = y[zmaxi]
    yp = yp[0]


    topdist = ymax-yp
    rightdist = xmax-xp
    bottomdist = yp-ymin
    leftdist = xp-xmin


    length = np.sqrt((((xmax-xmin)**2)+(ymax-ymin)**2))
    deg = np.arange(0,180,1)


    northy = []
```

```
    northx = []
    southy = []
    southx = []

    for d in deg:

        northy.append(yp+(length * np.sin(np.deg2rad(d))))
        northx.append(xp+(length * np.cos(np.deg2rad(d))))
        southy.append(yp-(length * np.sin(np.deg2rad(d))))
        southx.append(xp-(length * np.cos(np.deg2rad(d))))

    return northx, northy, southx, southy



def find_samples_pdist(point1, point2, sampling):
    # points are in x, y, samping is # per unit
    dist = np.sqrt(((point2[0]-point1[0])**2)+((point2[1]-point1[1])**2))
    samples = np.round((dist*sampling),0)
    samples = samples.astype(int)

    return samples


def calc_half_max(profile_dist, profile_data):
            # note this returns data that still needs the sensor height subtracted
    hm_locs = find_half_max_locs2(profile_data)
    if np.isnan(hm_locs[0][0])== True or np.isnan(hm_locs[0][1])==True:
        fwhm=np.nan
        hm=np.nan
```

```
        hm_n2=np.nan
    else:
        fwhm = np.abs(profile_dist[hm_locs[1][0]]-profile_dist[hm_locs[1][1]])
        hm = fwhm/2.
        hm_n2 = hm*1.3

    return fwhm, hm_n2, hm

def find_half_max_locs2(data):
    max_data = np.max(data)
    half_max_data = max_data/2.
    max_index = np.where(data == max_data)
    max_index = int(max_index[0])

    #tmp = find_points_along_slope(data[:max_index], half_max_data)

    L_nearest, L_index = find_points_left_slope(data[:max_index], half_max_data)
    R_nearest, R_index = find_points_right_slope(data[max_index:], half_max_data)

    R_index +=max_index

    indexes = (L_index, R_index)
    nearest = (L_nearest, R_nearest)

    return nearest, indexes

def find_points_left_slope(data, point):
    tmp = np.where(data <= point)
```

```
    tmp=np.squeeze(tmp, axis=(0))
    if len(tmp) > 0: # note work with 1
        tmp = np.max(tmp)
        nearest = data[tmp]
        index = tmp
    else:
        #tmp = np.min(data)
        nearest = np.nan
        index = np.nan
    return nearest, index


def find_points_right_slope(data, point):
    tmp = np.where(data <= point)
    tmp=np.squeeze(tmp, axis=(0))
    if len(tmp) > 0:
        tmp = np.min(tmp)
        nearest = data[tmp]
        index = tmp
    else:
        nearest = np.nan
        index = np.nan
    return nearest, index


def multi_height_profile(profile_1, profile_2, h_1, h_2):
            # calculates the multi-height depth estimate
            # h_1 and h_2 are the survey heights (lower and higher)
            # profile 1 and 2 are numpy 1d arrays of profile (could also be a grid)
            #returns estimates with SI = 3, 2.5, 2, 1
```

```
max_1 = np.max(profile_1)

max_1_index = np.where(profile_1 == max_1)

max_2 = profile_2[max_1_index] # use exact location above lower profile max point


#calculate the distance estimations for all 3 structural indexes

depth_est_n3 = (h_2 - h_1 * (max_1/max_2)**(1./3.))/((max_1/max_2)**(1./3.)-1.)

depth_est_n25 = (h_2 - h_1 * (max_1/max_2)**(1./2.5))/((max_1/max_2)**(1./2.5)-1.)

depth_est_n2 = (h_2 - h_1 * (max_1/max_2)**(1./2.))/((max_1/max_2)**(1./2.)-1.)

depth_est_n1 = (h_2 - h_1 * (max_1/max_2)**(1./1.))/((max_1/max_2)**(1./1.)-1.)

####NOTE these return the depth below surface


return depth_est_n3, depth_est_n25, depth_est_n2, depth_est_n1
```